Dissecting the Role of ZAKβ in Skeletal Muscle Using Zebrafish as a Model Organism

Alexander John Russell

PhD

University of York

Biology

January 2023

Abstract

Congenital myopathies are a group of inherited, heterogenous, rare muscle diseases, associated with progressive muscle wasting, chronic disability and a reduced quality of life. Inheritance of mutations in *ZAK*, a gene encoding a MAP triple kinase, has been identified as a novel cause of congenital myopathy in humans. This thesis utilises zebrafish to model the impacts of absence of ZAK on skeletal muscle, with investigations ranging from development studies to the analysis of the aging process of muscle in adult zebrafish. In contrast to other vertebrates, where the two isoforms are achieved through differential splicing of a single gene (to produce ZAKα and ZAKβ), in zebrafish the two isoforms exist as different genes on separate chromosomes, simplifying efforts to target each isoform.

ZAKβ is shown to be the isoform expressed in zebrafish skeletal muscle, and CRISPR-Cas9 gene editing was used to create mutations in each *ZAK* isoform and raise lines of zebrafish lacking either individual or both isoforms. Sequencing of the mRNA transcript and qRT-PCR confirmed mutations to each isoform result in a premature stop codon, and that there was a significant reduction in transcript levels.

Breeding the ZAK$\beta^{-/-}$ line into transgenic reporter lines allowed the assessment of the structure of developing skeletal muscle, and the immune response of neutrophils following wounding in larval zebrafish, using confocal imaging. Individual muscle fibre area was significantly reduced in ZAK$\beta^{-/-}$ embryos at two and five days of development, compared to wild type, potentially indicating growth defects in the skeletal muscle.

Aged ZAK$\beta^{-/-}$ zebrafish (35-months-old) show significantly decreased swimming capabilities, as well as abnormalities in the ultrastructure absent in age-matched wild type controls, suggesting a potential accelerated aging process in skeletal muscle with loss of ZAKβ. Thus, ZAKβ signalling may represent a promising target for developing novel therapies for the treatment of sarcopenia.

List of Contents

List of Tables

List of Figures

List of Appendices

Acknowledgments

First of all, I would like to extend a big thank you to my Supervisors, Betsy Pownall and Gonzalo Blanco for all they have helped me with over the last 4 years. You have always made time for me and helped me whenever I needed it, as well as provided me with unlimited lagers at the summer BBQ! Thank you to my TAP member, Chris MacDonald for all the helpful advice and support provided in bi-annual TAP meetings. I would also like to thank all lab members past and present for all their help, support and general friendliness. A big thank you goes out to Laura, who started at the same time as me and has always been extremely helpful and a great source of entertainment after a pint of cider! I am extremely grateful for the help of the BSF in keeping the fish alive on days off!

I would like to thank Mr Alistair McCleary for his assistance in getting me the surgery that allowed me to continue with my PhD, as well as some entertaining conversations on the operating table. A big thank you to the nurses at York hospital, who provided the morphine to help me to write my thesis when I fractured my spine.

I am extremely grateful for the unwavering support that my family provided throughout my PhD; always being there, putting up with my rants and making sure I was well fed! Thank you also to my friends for keeping me sane during lockdown and always being there for me when I needed it.

Lastly, my biggest thank you goes to my partner, Gaby Turvey, who I could not have done this without. From being excellent company during lockdown, to putting up with multiple trips to A&E as well as always being a rock for me to lean on. You've kept me calm and composed when I have needed it and always made sure I have had a great time along the way! I can't wait to see what the next chapter brings. A massive thank you to the Turvey-Barber's for welcoming me into their family and being so kind to me, as well as providing much-needed support.

Declaration

I declare that this thesis is a presentation of original work and I am the sole author. This work has not previously been presented for a degree or other qualification at this University or elsewhere. All sources are acknowledged as references.

Signed……

1. Introduction

1.1. Overview

Skeletal muscle is the most abundant tissue in the human body comprising between 40-50% of the body mass of adults (Karagounis and Hawley, 2010). Skeletal muscle is connected to bones through tendons, allowing the voluntary movements essential for everyday life. Different types of skeletal muscle serve different purposes, ranging from general posture and support against gravity, to muscles that produce the more 'explosive' force required to lift heavy items or escape danger (Paillard, 2017; Serrano *et al.*, 2019). Another feature of skeletal muscle is its ability to regenerate following damage or injury. A dedicated population of resident stem cells (satellite cells) are the basis of the muscle's remarkable capacity for tissue repair. Furthermore, skeletal muscle can exhibit lifelong plasticity to respond to stimuli, such as endurance exercise or weight lifting, where skeletal muscle can respond, remodel and grow (Flück and Hoppeler, 2003). The importance of skeletal muscle can be highlighted by the severity of certain neuromuscular diseases associated with mutations in key genes. This thesis is concerned with mutations in the MAP triple kinase, ZAK, which has been identified as a novel cause of a congenital myopathy; typically presenting with a slow, progressive muscle weakness and decreased vital capacity (Vasli *et al.*, 2017). There is a need for greater understanding into the molecular pathogenesis of these skeletal muscle diseases, so that better support and treatments can potentially be identified in order to improve the quality of life of patients with these diseases (Wang *et al.*, 2012).

This chapter will commence by describing the three different types of muscle before detailing how skeletal muscle is formed as well as its ultrastructure. The process of skeletal muscle contraction at a molecular level will then be discussed, before outlining the different types of skeletal muscle, and how they differ to each other. There will then be a transition into current knowledge of complications that can arise with mutations to genes coding for key proteins, namely with respect to congenital myopathies. This thesis documents the use of zebrafish to model the impacts that absence of ZAK may have on skeletal muscle. There is, therefore, a discussion into the current knowledge of both ZAK isoforms, as well as the use of animal models, namely zebrafish, in researching neuromuscular diseases.

1.1.1 Different Types of Muscle

There are three main types of muscle:

- Smooth muscle is non-striated muscle that lines blood vessels, airways, urogenital tract, and digestive tract. Smooth muscle is part of the autonomic nervous system (ANS) and contraction is involuntary. Example roles of smooth muscle include peristalsis of food during digestion; vasodilation and vasoconstriction in response to temperature; and airway contraction/relaxation depending on rest or exercise status.
- Cardiac muscle is striated muscle – the contraction of which, is required for the circulation of blood throughout the body. Cardiac muscle is rather unique in its ability to rhythmically control the rate of contraction and relaxation by electrical impulses that arise from the sinoatrial node. Heart rate can be further modified by the ANS when needed, for example, when exercising.
- Skeletal muscle is striated muscle that is connected to bones (the skeleton) by tendons, hence, its name. It is under voluntary control and underpins all movement and fine motor control.

This thesis is predominantly concerned with skeletal muscle. Figure 1.1. represents the overarching organisation of muscle, with each muscle being comprised of many bundles (fascicles) of muscle fibres (Wilson, 2014). Each individual muscle fibre within a fasciculus is comprised of many myofibrils. Myofibrils are composed of a repeating individual contractile unit, called the sarcomere (Wilson, 2014), which is represented in figure 1.2.

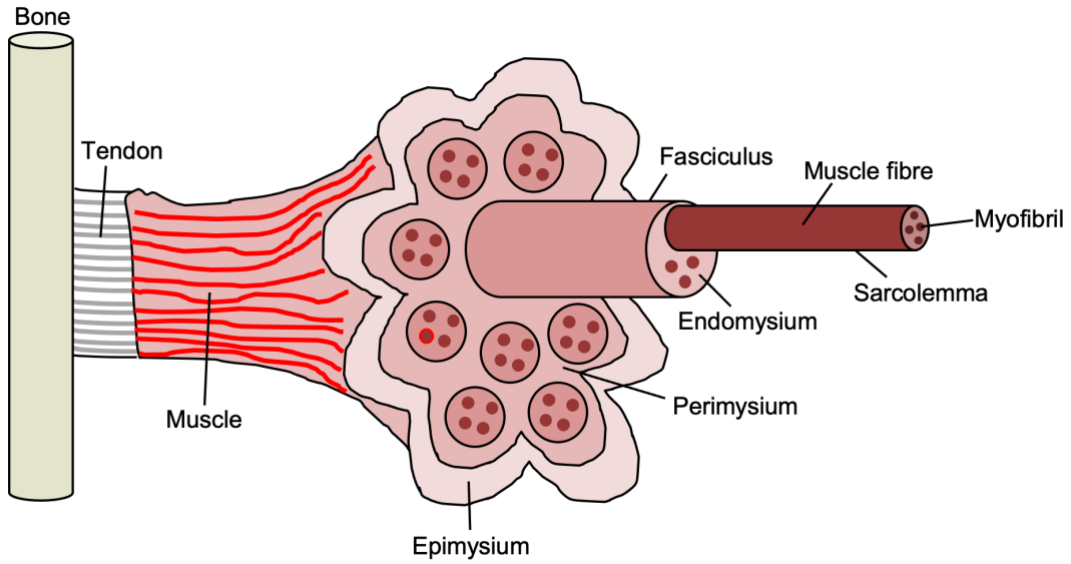

Figure 1.1. Organisation of Skeletal muscle.
Skeletal muscle is attached to bone through tendons. Within the skeletal muscle, there are many bundles of muscle fibres are called fascicles. Each individual muscle fibre is comprised of many myofibrils, which contain the repeating contractile unit, called the sarcomere. The organisation of the connective tissue is also shown, with epimysium encasing the entire muscle; perimysium surrounding the fascicle, and endomysium surrounding and connecting individual muscle fibres within a fascicle. Figure made using Microsoft PowerPoint.

1.1.2. Organisation of Skeletal Muscle Fibres

As seen in figure 1.1, there are three layers of connective tissue in skeletal muscle:

1. Endomysium is a proteoglycan matrix located between individual muscle fibres within a fascicle and form a 3D structure that links the individual muscle fibres (Purslow, 2020; Schleip *et al.*, 2021). The endomysium is mainly composed of collagen fibres and acts as a continuum between the basement membranes of individual muscle fibres (Purslow, 2020; Schmalbruch, 1974).
2. Perimysium is a highly organised chiasmic lattice of proteoglycan matrix that surrounds and connects fascicles within the muscle (Purslow, 2020; Schleip *et al.*, 2021).
3. Epimysium is the connective tissue composed of coarse collagen fibres in a proteoglycan matrix that surrounds and encases the entire muscle (Purslow, 2020; Velleman and McFarland, 2015). The arrangement of the collagen can vary between different muscles (Purslow, 2020).

Prefixing ‘sarco’ before the name of the organelle is common in muscle nomenclature, for example, sarcoplasm is the cytoplasm and sarcoplasmic reticulum is the endoplasmic reticulum in muscle cells. The sarcolemma is the plasma membrane of individual skeletal muscle fibres and acts as the interface between the muscle and the extracellular matrix.

1.2. Myogenesis

Myogenesis is the name given to the process of muscle formation. Skeletal muscles originate from somites, which are derived from the paraxial mesoderm (Christ and Ordahl, 1995). Initially in mice, embryonic myoblasts fuse to form the early multinucleated myotubes, in a process known as primary myogenesis, (Kahane *et al.*, 1998). These primary myotubes act as a scaffold on which myoblasts can proliferate and fuse in a process known as secondary, or foetal myogenesis (Kahane *et al.*, 1998; Matsakas *et al.*, 2010). A further wave of differentiation produces paired box 7 $(PAX7)^{+}$ and, sometimes $PAX7^{+}PAX3^{+}$ satellite cells, which are required for the hypertrophic muscle growth of newborns (White *et al.*, 2010). A subset of $PAX7^{+}$ satellite cells enter quiescence and remain located between the basal lamina and sarcolemma to form the stem cells that allow skeletal muscle plasticity throughout life (Schultz *et al.*, 1978; Hernández-Hernández *et al.*, 2017). Adult myogenesis and the role of satellite cells are discussed in greater detail in section 1.2.2.

Simplistically the stages of myogenesis can be broken into three distinct sections: i) there is an initial cell commitment to a myogenic lineage. ii) Precursor cells become activated and proliferate before terminal differentiation into post-mitotic myocytes. iii) Differentiated myocytes can then fuse to become multinucleated myotubes, that are capable of contraction (Sabourin and Rudnicki, 2000). PAX3 is the first myogenic transcription factor to be expressed in paraxial mesoderm, and is important in specifying the cell towards a myogenic lineage (Williams and Ordahl, 1994). PAX7 is important for the postnatal myogenesis achieved through satellite cells and does not appear to be essential for embryonic or foetal myogenesis in mice (Seale *et al.*, 2000; Kuang *et al.*, 2006).

The myogenic regulatory factors (MRF) are a family of basic helix loop helix (bHLH) transcription factors that are critical for myogenesis (Mary Elizabeth Pownall *et al.*, 2002; Asfour *et al.*, 2018). There are four members of the MRF family that all regulate different stages of myogenesis: myogenic factor 5 (Myf5), Myogenic differentiation factor (MyoD), myogenin and myogenic regulatory factor 4 (Mrf4) (Braun *et al.*, 1989; Davis *et al.*, 1987; Wright *et al.*, 1989; Rhodes and Konieczny, 1989). In mice, Myf5 is the first MRF to be expressed and along with MyoD and Mrf4 is important in specification (Ott *et al.*, 1991; Kassar-Duchossoy *et al.*, 2004). MyoD and Myf5 can compensate for the absence of the other protein, resulting in normal formation of skeletal muscle in mice lacking either MyoD or Myf5 (Rudnicki *et al.*, 1992; Braun *et al.*, 1994); however, genetic depletion of both genes in mice resulted in complete absence of skeletal muscle and postnatal lethality (Rudnicki *et al.*, 1993), albeit there was some compensation when mrf4 was still present in the double MyoD, myf5 mutant (Kassar-Duchossoy *et al.*, 2004). MyoD is also required for terminal differentiation of the proliferating myoblasts and muscle regeneration is compromised in MyoD$^{-/-}$ mice (Rawls *et al.*, 1998; Yablonka-Reuveni *et al.*, 1999).

Absence of myogenin in mice results in death shortly after birth as a result of severely disrupted muscle formation, with myoblasts formed, but they are unable to undergo terminal differentiation and fusion (Hasty *et al.*, 1993; Nabeshima *et al.*, 1993). Zebrafish lacking myogenin are viable, however, there is almost complete absence of fusion in embryos suggesting an essential role for myogenin for fusion (Ganassi *et al.*, 2018). Isolated muscle progenitor cells (MPC) from the myogenin null zebrafish also showed defective fusion, however, the mutants strikingly showed no defects in terminal differentiation, compared to siblings (Ganassi *et al.*, 2018). The role of myogenin in zebrafish fusion is discussed in greater detail in section 1.2.1. As well as a reduced body and myofibre size, adult zebrafish lacking myogenin show a 10-fold increase in satellite cell numbers, that are abnormally located and fail to enter full quiescence (Ganassi *et al.*, 2020).

Mrf4 is the least well understood MRF, with expression early in embryonic commitment, alongside myf5, as well as appearing later post-differentiation (Hinterberger *et al.*, 1991; Kassar-Duchossoy *et al.*, 2004). Mrf4 has been shown to be a regulator of muscle growth in adult muscle with miRNA inhibition promoting hypertrophy in mice, likely by preventing Mrf4 from repressing MEF2 (Moretti *et al.*, 2016). Mrf4 has also been suggested as having a role in preventing the premature differentiation of satellite cells (Lazure *et al.*, 2020).

1.2.1. Myoblast Fusion

Myoblast fusion is a process whereby differentiated cells migrate until finding the respective fusing partner, where there is then adherence and alignment of membrane proteins, such as integrins and cadherins (Kaufmann *et al.*, 1999; Schwander *et al.*, 2003). Once adhered, there is hemifusion (merging of the membranes and lipid mixing), followed by pore formation allowing the contents of the two cells to mix (Leikina *et al.*, 2018). Lastly, the pores expand, resulting in the breakdown of the membrane and integration of the intracellular components (Rochlin *et al.*, 2010).

In zebrafish, myogenin is essential for the vast majority of fusion, through increasing the expression of fusogenic proteins, such as myomaker and myomerger (also known as myomixer) (Ganassi *et al.*, 2018). Mice lacking myogenin die shortly after birth, as a consequence of severe muscle disruption (Hasty *et al.*, 1993). Myomaker and myomerger are membrane proteins and are both essential for fusion (Millay *et al.*, 2013; Bi *et al.*, 2017). Myomaker is required for hemifusion, whereas myomerger is required for the pore formation and drives completion of myoblast fusion (Leikina *et al.*, 2018). Inhibition of actin polymerisation resulted in failure of cells to fuse, despite the presence of myomaker and myomerger in the cell membrane (Millay *et al.*, 2013; Zhang *et al.*, 2017). Actin cytoskeletal remodelling has been proposed as producing invasive membrane protrusions that are essential in myoblast fusion (Shilagardi *et al.*, 2013). Myomaker and myomerger have been proposed as regulating the actin cytoskeletal reorganisation, however, the extracellular location of the c-terminus of myomerger weakens this theory (Leikina *et al.*, 2018).

Transforming growth factor (TGF)-β signalling has recently been identified as a molecular brake in muscle fusion, where the process of myoblast fusion allows TGFβR1-TGFβR2 dimerisation and activation of the downstream signalling pathway (Melendez *et al.*, 2021; Girardi *et al.*, 2021). The induced SMAD signalling temporarily inhibits further fusion until RAB-dependent receptor internalisation and degradation occurs and fusion is again possible (Melendez *et al.*, 2021; Girardi *et al.*, 2021). The process is proposed to fine-tune growth and prevent hyperfusion.

1.2.2. Adult Myogenesis and the Role of Satellite Cells

Myogenesis occurs throughout life, allowing for muscle repair and maintenance, and the process of adult myogenesis is similar to embryonic myogenesis (Wang and Conboy, 2010). In muscle regeneration or response to increasing load, satellite cells are responsible for adaptation. Satellite cells are PAX7 expressing, muscle-resident small quiescent stem cells, that ordinarily lie in between the basement membrane and the sarcolemma (Mauro, 1961; Seale *et al.*, 2000). They respond to a change in homeostasis, such as, growth factors or muscle damage, becoming activated and undergo the processes of myogenesis discussed above (Charge and Rudnicki, 2004). The majority of satellite cells either bind to each other to form new muscle fibres during regeneration, or they can fuse to existing muscle fibres, increasing the size (Schmalbruch, 1976; Snijders *et al.*, 2015). Satellite cells can also self-renew, producing further quiescent cells that could respond to future damage (Schmalbruch, 1976; Collins *et al.*, 2005).

The importance of satellite cells is emphasised by failure of skeletal muscle to regenerate following injury, when satellite cells are genetically ablated in mice (Murphy *et al.*, 2011; Sambasivan *et al.*, 2011). Whilst undoubtably essential for regeneration, the importance of satellite cells for hypertrophy has been the subject of debate. γ-irradiation treatment to remove satellite cells in mice resulted in failure of muscle growth (Rosenblatt and Parry, 1992); however, the lack of specificity of the irradiation has been levelled as a criticism and mice with PAX7 ablation have demonstrated a comparable adaptation to load compared to wild type, following two weeks of exercise (McCarthy *et al.*, 2011). More recent research in mice has demonstrated satellite cells to be essential for hypertrophy and adaptations to long-term/sustained physical activity (Englund *et al.*, 2020). The term 'satellite cell-opathy' has recently been coined for neuromuscular diseases where the mutated gene directly affects the function of satellite cells, for example, PAX7 and myomaker in humans (Ganassi et al., 2022). Moreover, there is a decline in satellite cells with aging, that is correlated with an increase in atrophy, particularly in fast-twitch fibres, in a process known as sarcopenia (Verdijk et al., 2007).

1.3. Organisation of the sarcomere

Cardiac and skeletal muscle are both striated muscles and these striations can be visualised using electron microscopy (see figure 1.2 (a)) and are known as the sarcomere. The sarcomere is the individual contractile unit of striated muscle and is comprised of thin and thick filaments. The thin filaments are composed of mainly filamentous (F)-actin, tropomyosin and troponin. The thick filament is the myosin filament. The sarcomere can be subdivided into zones depending on the composition of F-actin and/or myosin (figure 1.2(b)). The anisotropic (A)-band encompasses the length of myosin, and the isotropic (I)-band encompasses the length where there is no myosin, between adjacent sarcomeres. The H-zone is the region in the centre of the sarcomere where there is only myosin present (no thin filaments). The M-band is located in the centre of the H-zone. The Z-discs represent the boundaries of the sarcomere, located centrally in the I-band.

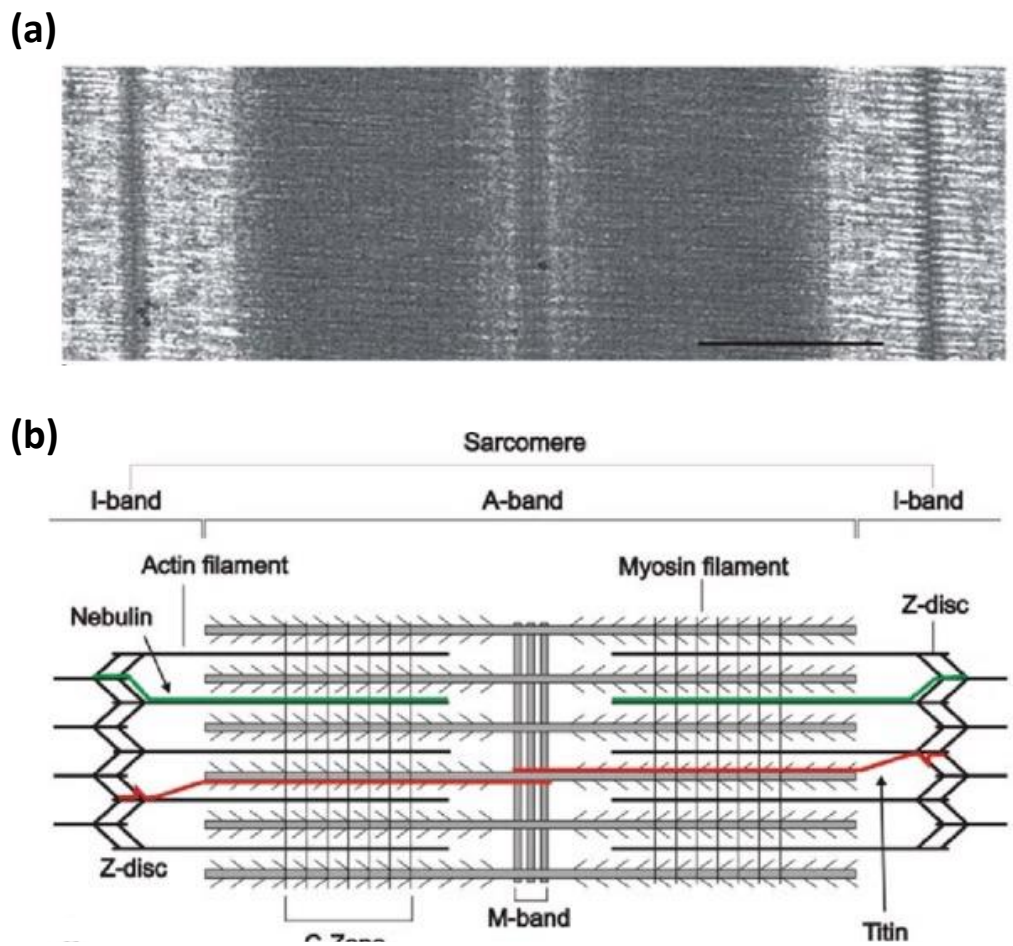

Figure 1.2. Ultrastructure of skeletal muscle.
(a) TEM image of an individual sarcomere showing the distinct regions/zones of striated muscle. Black scale bar = 500 nm (b) Cartoon depicting the individual components of the sarcomere as well as the distinct zones, based on the presence of actin and myosin. The distinct zones of the sarcomere line up with the TEM image above. The I bands are lighter, and the A band is darker in appearance. Image was modified from (Luther, 2009).

Being the contractile unit of skeletal muscle, the sarcomere is subject to a great deal of regulation to ensure it forms correctly and muscle can contract effectively.

Titin, also known as connectin, is the largest known protein in humans (~4.2 MDa), spanning half of the sarcomere, from the Z-disc to the M-line, and regulates the assembly and length of the thick filament (Fürst *et al.*, 1988; Labeit *et al.*, 1992; Tonino *et al.*, 2017). Titin is often, therefore referred to as a 'molecular ruler' (Bennett *et al.*, 2020). Titin is important for elasticity and 'passive force', with immunoglobulin (Ig) domains capable of unfolding and refolding, aiding the stretching and shortening of the sarcomere upon muscle relaxation and contraction (Rief *et al.*, 1997; Tskhovrebova *et al.*, 1997; Kellermayer *et al.*, 1997; Rivas-Pardo *et al.*, 2016). Titin also has important roles in cell signalling (Kravchenko *et al.*, 2015), and mechanotransduction (sensing a physical change and converting it into a discernible biochemical signal) (van der Pijl *et al.*, 2018; Ibata and Terentjev, 2021). The importance of Titin is emphasised by mutations in the gene (*TTN*) encoding Titin resulting in human myopathy and muscular dystrophy (Ceyhan-Birsoy *et al.*, 2013; Hackman *et al.*, 2008; Oates *et al.*, 2018).

Nebulin is another giant protein (>700 kDa), thought to also play an important role in regulating the length and integrity of the sarcomere (Yuen and Ottenheijm, 2020). Nebulin is anchored at the Z-disc and is proposed to bind to the full length of the thin filament (Wang and Williamson, 1980; Wang and Wright, 1988; Wang *et al.*, 2022). Two nebulin proteins bind to one thin filament and are essential for mediating the length and the integrity of the thin filaments (Wang *et al.*, 2022). Nebulin has also been proposed as important in Z-disc structure and regulation of width, binding to proteins such as α-actinin, as well as aberrant Z-disc widths occurring in the absence of nebulin in humans and mice (Nave *et al.*, 1990; Ottenheijm *et al.*, 2009; Tonino *et al.*, 2010; Yuen and Ottenheijm, 2020). The elasticity of nebulin may provide resistance to force/stress placed upon thin filaments (Yadavalli *et al.*, 2009). Mutations in the gene coding for nebulin (*NEB*) are associated with human myopathy, with at least 50% of cases of nemaline myopathy arising from mutations to *NEB* (Telfer *et al.*, 2012; Scoto *et al.*, 2013; Laitila *et al.*, 2020).

Z-discs form the boundaries of each individual sarcomere and serve three main functions: to stabilise the F-actin thin filaments, transmit force and for signalling (mechanotransduction) (Geach *et al.*, 2015). The Z-disc is made up of layers of cross-linked actin filaments from adjacent sarcomeres (Luther *et al.*, 2002). α-actinin is involved in crosslinking the antiparallel actin thin filaments, forming the characteristic zigzag pattern associated with the Z-disc (Takahashi and Hattori, 1989; Luther *et al.*, 2002). In addition to the structural role of providing stability to the sarcomere, proteins of the Z-disc are involved in signalling and mechanosensation (Frank *et al.*, 2006; Knöll *et al.*, 2011). Further to force being transmitted longitudinally, which is discussed in greater detail in section 1.1.3, force can also be transferred laterally to the ECM through costameres (Street, 1983; Ramaswamy *et al.*, 2011). Costameres are protein complexes that link Z-discs to the sarcolemma/extra-cellular matrix (ECM) (Peter *et al.*, 2011; Andresen *et al.*, 2022). The two major protein complexes of the costamere are the integrin-vinculin-talin complex and the dystrophin-glycoprotein complex (DCG) (Peter *et al.*, 2011). Proteins that form part of the costameres are also important for signalling and mechanotransduction (Mathes *et al.*, 2019). Mutations in genes encoding for many of the proteins found at the Z-disc and/or costameres are associated with human myopathies/muscular dystrophies, emphasising the importance of the Z-disc for normal muscle structure/function (Monaco *et al.*, 1986; Knöll *et al.*, 2011; Jaka *et al.*, 2015).

The M-band is located in the centre of the sarcomere and is important for the structural integrity of the thick filaments, as well as for cross linking of the myosin (Agarkova *et al.*, 2003; Lange *et al.*, 2005). The M-band is composed mainly of myomesin proteins, of which there are three forms, differentially expressed depending on the muscle-type (Grove *et al.*, 1984; Obermann *et al.*, 1996; Schoenauer *et al.*, 2008). The elasticity of the myomesin domains allows it to function like a ‘molecular spring’ upon muscle contraction, in a similar way to titin (Schoenauer *et al.*, 2005). Obscurin and titin also form part of the complex at the M-band (Obermann *et al.*, 1996; Young *et al.*, 2001).

1.4. Mechanism of Contraction

Skeletal muscle is innervated by motor neurones, responsible for voluntary (and involuntary) control of movement. Simplistically, there are two types of motor neurone: upper motor neurones that originate from the cerebral cortex and descend down the spinal column; and lower motor neurones, that originate from the spinal column and are responsible for transmitting signal from the upper motor neurones, sensory neurones and interneurons (Zayia and Tadi, 2022). These motor neurones differ with the excitatory neurotransmitter used, with upper motor neurones using glutamate and lower motor neurones using acetylcholine in mammals (Zayia and Tadi, 2022; Stifani, 2014a). Lower motor neurones can be further subdivided into three categories, depending on target: branchial for skeletal muscle of the face (Chandrasekhar, 2004); visceral for the control of smooth muscle as part of the ANS (Stifani, 2014b); and somatic motor neurones for innervation of skeletal muscles required for movement (Rexed, 1954; Stifani, 2014b). Movement can be thought of as a complex process requiring the co-ordinated control (either inhibition or contraction) of multiple different muscle groups (Granzow and Kristan, 1986; Zayia and Tadi, 2022). A motor unit encompasses all the muscle fibres innervated by the branches of a single motor neurone.

The synapse between the motor neurone and the effector muscles is termed the neuromuscular junction. An action potential travelling down the motor neurone terminates at the presynaptic terminal, where the depolarisation results in the activation of the voltage-gated calcium channels to open (Sam and Bordoni, 2022). The presence of calcium in the cytosol results in the soluble N-ethylmaleimide-sensitive fusion protein attachment protein receptor (SNARE)-dependent exocytosis of vesicles containing acetylcholine (Söllner *et al.*, 1993; Schiavo *et al.*, 2000; Nishimune and Shigemoto, 2018). The acetylcholine diffuses across the synapse and binds to the nicotinic acetylcholine receptors (nAChRs) on the sarcolemma of the muscle fibre. Acetylcholine remains in the synaptic cleft, until removal through passive diffusion, or degradation by the enzyme acetylcholinesterase.

The sarcolemma of the post synaptic muscle fibre is a complex structure, with folding at the neuromuscular junction to increase the surface area for acetylcholine to bind to the nAChR (Salpeter and Harris, 1983; Slater, 2017). The sarcolemma has deep invaginations known as transverse tubules (t-tubules) (Porter and Palade, 1957). T-tubules are surrounded by two terminal cisternae of the sarcoplasmic reticulum to form the triad (Al-Qusairi and Laporte, 2011). The sarcoplasmic reticulum stores the majority of the calcium in the muscle fibre. The binding of acetylcholine to the nAChRs results in the opening of sodium channels and an influx of sodium. The resulting depolarisation travels down t-tubules, resulting in a conformational change in the dihydropyridine receptor (DHPR) (Rios and Brum, 1987). The DHPR interacts with the ryanodine calcium receptors (RyR1 in skeletal muscle) on the sarcoplasmic reticulum, and the conformational change opens the RyR1 receptor, causing calcium ions to flood into the cytosol and the muscle contraction to occur (Schneider and Chandler, 1973; Anthony Lai *et al.*, 1988; Dayal *et al.*, 2017). This mechanism is commonly referred to as excitation-contraction (e-c) coupling.

The release of calcium ions results in the sliding filament theory of muscle contraction, which was first described in 1954 by (Huxley and Niedergerke, 1954) and (Huxley and Hanson, 1954) and still remains the best mechanism to describe muscle contractions to date. The mechanics of myosin binding to actin and excitation-coupled contraction that are about to be discussed as part of the sliding filament theory of muscle contraction, mainly come from (Hynes *et al.*, 1987) and reviewed (Spudich, 2001). Following depolarisation, the influx of calcium ions in the sarcoplasm will bind to troponin C, which is a part of the complex on the thin filament, causing a conformational change leading to the movement of tropomyosin and freeing the myosin binding site (Lehman *et al.*, 1994). The subfragment 1 (S1) domain on globular head of myosin can then bind to the nearest myosin binding site on the actin filament (Toyoshima *et al.*, 1987). Prior to binding actin, the ATPase on the myosin hydrolyses ATP into ADP and Pi leaving it in a ‘primed’ high-energy state, where it is ‘cocked’. Myosin binding and forming a cross-bridge with actin results in the release of the inorganic phosphate, the energy of which causes the myosin to contract (known as the power stroke) and pull the actin filament across myosin towards the M-band, shortening the sarcomere. The myosin, now in a low-energy state, (Spudich, 2001) releases the ADP and binds ATP, breaking the cross-bridge. The myosin hydrolyses the ATP

into ADP and Pi re-positioning the myosin S1 domain further along the actin filament, ready for the next power stroke, to contract the sarcomere further. This occurs as a cycle and will continue until there is no longer calcium present in the sarcoplasm, at which point tropomyosin will block the myosin binding site and myosin will remain in the ‘primed’ position, ready for the next action potential.

1.5. Types of Skeletal Muscle

Two major forms of skeletal muscle exist: slow-twitch (type 1) and fast-twitch (type 2) fibres. Fast-twitch fibres can be further subdivided into type 2A (fast-twitch oxidative glycolytic), and 2X (fast-twitch glycolytic) in humans (Pette and Staron, 2000; Talbot and Maves, 2016). All of these fibres differ in the isoform of myosin heavy chain expressed (Ennion *et al.*, 1995).

The myosin heavy chain in slow-twitch fibres is typically slow to contract, hence, the name (Larsson and Moss, 1993). These fibres are fatigue-resistant, and abundant in mitochondria and vascularisation for oxidative metabolism (Andersen, 1975; Mishra *et al.*, 2015). The slow myosin heavy chain has the lowest levels of ATPase activity (Taylor. *et al.*, 1974; Scott *et al.*, 2001). Type 2A fibres are also referred to as intermediate fibres as they predominantly use oxidative phosphorylation but can still use glycolytic metabolism (Talbot and Maves, 2016). The speed of contraction is in-between that of type 1 and type 2X fibres (Larsson and Moss, 1993). Type 2X fibres are the fastest to contract with the greatest ATPase activity, chiefly using glycolytic metabolism, and fatigue quickly (Peter *et al.*, 1972; Larsson *et al.*, 1991; Larsson and Moss, 1993). Both forms of fast-twitch fibres contain higher levels of glycolytic enzymes and reduced numbers of mitochondria than slow-twitch fibres (Peter *et al.*, 1972; Mishra *et al.*, 2015).

The properties of slow-twitch fibres make them important for low levels of sustained contraction, for example, the postural muscles that keep an organism upright (Paillard, 2017). Fast-twitch muscles are suited for short periods of strong contraction, for example lifting heavy items (Serrano *et al.*, 2019).

1.6. Congenital Myopathies: Prevalence, Aetiology and Current Understanding

'Myopathy' is the collective term that describes all forms of muscle diseases, including muscular dystrophies. There are many causes of myopathies including: autoimmune conditions (McGrath *et al.*, 2018); nutritional deficiency in vitamins, such as Vitamin D (Rasheed *et al.*, 2013); mitochondrial and metabolic myopathies (Cohen, 2019); infection with a pathogen that attacks or causes sustained inflammation in muscle fibres, e.g. HIV and *Toxoplasma gondii* (Attarian and Azulay, 2001); and myotoxic drugs, that can cause damage to the muscle fibres or muscle organelles, e.g. statins and corticosteroids (Dalakas, 2009; Valiyil and Christopher-Stine, 2010).

This thesis is interested in congenital myopathies. Congenital myopathies are the collective term for a heterogeneous group of rare muscle diseases with a genetic basis, associated with (of varying severity) muscle wasting and reduced quality of life (Nance *et al.*, 2012). Congenital myopathies are often distinguished from the muscular dystrophies by genetic defects that affect the contractile apparatus of muscle fibres (Cardamone *et al.*, 2008). Muscular dystrophies, however, are the result of genetic defects in the muscle membranes or associated proteins (Cardamone *et al.*, 2008). Muscular dystrophies can be distinguished by the presence of necrosis of muscle fibres not usually seen in congenital myopathies (Cornelio and Dones, 1984).

The rarity of congenital myopathies, coupled with the varying severity of phenotypes, make it difficult to accurately estimate the prevalence of congenital myopathies. Meta-analysis from 11 studies investigating prevalence across European, Asian, Oceanian and North American populations estimated a prevalence of 1.62 cases per 100,000 across all age groups (Huang *et al.*, 2021). The prevalence of congenital myopathies is greater in children (2.62 per 100,000) and the incidence in men and women is typically similar (excluding X-linked myotubular myopathy) (Huang *et al.*, 2021; Theadom *et al.*, 2019). Despite the term "congenital" in congenital myopathies, often diagnosis and/or phenotype may not become apparent until late adolescence or adulthood - termed late-onset (Papadimas *et al.*, 2020).

Congenital myopathies can be sub-divided into five main classifications: nemaline myopathy, centronuclear myopathy, congenital fibre type disproportion (CFTD), core myopathy and myosin storage deficiency.

1.6.1. Nemaline Myopathy:

First identified as a classification of congenital myopathy by (Shy *et al.*, 1963). Nemaline myopathy is also called rod myopathy, due to the presence of rod-like structures in myofibrils named 'nemaline bodies' that are easily visualised following Gomori trichrome staining (Shy *et al.*, 1963; Laitila and Wallgren-Pettersson, 2021). The prevalence of nemaline myopathies is estimated to be 1:500,000 for all age groups (Huang *et al.*, 2021).

The severity of nemaline myopathies is highly variable, ranging from premature death in infancy, to a more mild muscle weakness, which becomes identifiable during early childhood (Laitila and Wallgren-Pettersson, 2021). A severe phenotype is rare and can manifest with respiratory issues (often the cause of mortality in infancy) and dilated cardiomyopathy (Wallgren-Pettersson and Laing, 2000; Ryan *et al.*, 2001). The 'typical' presentation includes neonatal hypotonia, progressive weakness and difficulties feeding (Ryan *et al.*, 2001; Shimomura and Nonaka, 1989; Sanoudou and Beggs, 2001).

12 genes have been implicated as the cause of nemaline myopathies, with mutations in nebulin (Scoto *et al.*, 2013) and skeletal muscle α-actin (Nowak *et al.*, 1999) being the most common causes. All the genes implicated have either a structural or regulatory role of the thin filaments of the sarcomere (Laitila and Wallgren-Pettersson, 2021). Nemaline bodies are thought to derive from z-discs because they appear to overlap between them; contain several proteins also found in z-discs, such as α-actinin, and have a similar lattice structure when visualised with electron microscopy (EM) (North *et al.*, 1997; Sewry *et al.*, 2019). It is still not clear how nemaline bodies form, however, it is thought that they can be a secondary aspect of metabolic stress (Sewry *et al.*, 2019). Nemaline bodies are located throughout the myofiber, especially around the sarcolemma and the nuclei or, rarely, intranuclearly (North *et al.*, 1997; Sanoudou and Beggs, 2001).

Haematoxylin and eosin (H&E) staining on patients' biopsies sometimes can appear normal, however, there is typically a predominance of type 1 fibres and fibre size can be smaller (Sanoudou and Beggs, 2001). Looking at biopsies under

EM showed a deficiency in contractile material and an excess formation of thin filaments (North *et al.*, 1997). Widened z-discs or z-disc streaming, which is a sign of myofibrillar disruptions, can also be seen in some patients with nemaline myopathy (Sanoudou and Beggs, 2001). Fatty infiltration in muscle fibres can be seen in more progressed cases, however, signs of regeneration and necrosis are highly uncommon (North *et al.*, 1997).

The difficulty in diagnosing the phenotype nemaline myopathy comes from overlapping features associated with other congenital myopathies, in some patients, for example fibre-type disproportion and cores (Sewry *et al.*, 2019).

1.6.2. Centronuclear Myopathy:

Centronuclear myopathies, are named after the presence of the nuclei in the centre of the muscle fibre, rather than the normal location of the periphery, which gives them the appearance of an myotube (Jungbluth *et al.*, 2008). Centronuclear myopathy was first identified as a classification of congenital myopathy by (Spiro *et al.*, 1966) who termed it “myotubular myopathy”. Centronuclear myopathies have a low prevalence of 0.08 cases per 100,000 in all age groups (Huang *et al.*, 2021). The prevalence is considerably greater in the paediatric population with 0.44 cases per 100,000 (Huang *et al.*, 2021). This is because of infant mortality in the severe cases – for example, the overall median life expectancy in 2001 of boys with X-linked myotubular myopathy (XMTM) was 29 months (McEntagart *et al.*, 2002). A more recent, but smaller, study does, however show 67% of patients (mean age of 10) to be alive at the end of the study, and a median age of death to be just under 7 years for those deceased (Amburgey *et al.*, 2017).

At least eight genes with mutations have been identified as causes of centronuclear myopathy, with the most common variants being in dynamin 2 (*DNM2*) in 50% of patients; (Catteruccia *et al.*, 2013); Myotubularin (*MTM1*) in XMTM (Laporte *et al.*, 1996); Amphiphysin 2 (*BIN1*) (Nicot *et al.*, 2007); Ryanodine receptor 1 (*RYR1*) (Abath Neto *et al.*, 2017); and *TTN* (Ceyhan-Birsoy *et al.*, 2013). There are at least three other less common gene variants that cause centronuclear myopathy (Reumers *et al.*, 2021).

The severity of centronuclear myopathy partly depends on the affected gene. For example, mutations in the autosomal dominant *DNM2* are generally milder and have later-onset than *MTM1* and *BIN1* mutations, but can still follow a severe course (Catteruccia *et al.*, 2013). The more severe cases tend to be with XMTM, with up to 85% of cases requiring ventilation from birth (McEntagart *et al.*, 2002); along with severe hypotonia and weakness (Barth and Dubowitz, 1998). The severity has been shown to extend to the ability to recognise the condition prenatally, by reduced foetal movement (Tanner *et al.*, 1998). There are moderate and mild forms of XMTM and other centronuclear myopathy variants, however, with patients that can live to adulthood and present with a milder phenotype that can include hypotonia, general weakness and possible minor respiratory insufficiency (Barth and Dubowitz, 1998). EM on muscle biopsies has also revealed a decrease in acetylcholine receptors (Bergen *et al.*, 1980; Jungbluth *et al.*, 2008).

It is not believed that the severity of the histopathology equates to the severity of the centronuclear myopathy, for example, there is no link between the number of centralised nuclei and clinical outcome (Lawlor *et al.*, 2016). The mean percentage of fibres with centralised nuclei can range between 5% (Pierson *et al.*, 2007) to > 50% (Shichiji *et al.*, 2013) in a patient. A correlation has been observed of poorer prognosis for patients with smaller myofiber size (Pierson *et al.*, 2007). Further to the centralised nuclei, the histology of the milder forms show fibre size variability (from hypotrophic and hypertrophic fibres) and fatty and/or connective tissue infiltration of muscle (De Angelis *et al.*, 1991; Reumers *et al.*, 2021). Atrophy and a predominance of type 1 fibres has been noted in patients (Böhm *et al.*, 2012).

As the name suggests, the presence of the nuclei at the centre of the fibre, rather than the periphery of fibres, in histopathology, is used for the diagnosis of centronuclear myopathy (Jungbluth *et al.*, 2008). In addition to sequencing for the implicated genes discussed above, an elongated head circumference and neonatal hypotonia are further signs of centronuclear myopathy (Joseph *et al.*, 1995). Muscle MRI can also be used to aid differential diagnosis of centronuclear myopathy (Schessl *et al.*, 2007; Klein *et al.*, 2011; Bugiardini *et al.*, 2018).

1.6.3. Congenital Fibre-type Disproportion (CFTD):

The classification of congenital fibre-type disproportion (CFTD) is named after the histopathological abnormality with a predominance of type 1 fibres, that are small and hypotrophic in comparison to type 2 fibres, which are normal sized or hypertrophic (Claeys, 2020), by Brooke and Engel in 1969 (Brooke and Engel, 1969). To be classified as small, type 1 fibres must be at least 12% smaller than type 2 fibres (Na *et al.*, 2006). The estimated prevalence of CFTD is estimated to be just under 1:400,000 (Huang *et al.*, 2021).

Multiple genes are implicated as a cause of CFTD, with the majority of cases arising from mutations in tropomyosin 3 (*TPM3*) (Clarke *et al.*, 2008) (Lawlor *et al.*, 2010); *RYR1* (Clarke *et al.*, 2010); skeletal alpha actin 1 (*ACTA1*) (Laing *et al.*, 2004), and Selenoprotein N (*SEPN1*) (Clarke *et al.*, 2006). There has also been one identified CFTD case with a mutation in myosin light chain 2 (*MYL2*), however the gene panel also revealed a heterozygous mutation in *NEB* also predicted as potentially pathogenic, complicating the association of just *MYL2* (Marttila *et al.*, 2019). Patients with mutations in the *MYH7* gene, encoding slow/β-cardiac myosin heavy chain, (MyHC1) present with a CFTD phenotype in early stages, however, in later stages, the phenotype can resemble more of a myosin storage myopathy (Ortolano *et al.*, 2011).

Mutations in *SEPN1* (Clarke *et al.*, 2006) and *RYR1* (Clarke *et al.*, 2010) are associated with autosomal recessive inheritance. Most *ACTA1* mutations are autosomal dominant (Laing *et al.*, 2004), and the inheritance pattern of TPM3 is varied between autosomal recessive, autosomal dominant and *de novo* (dominant) (Lawlor *et al.*, 2010). There has been one case of an X-linked mode of inheritance of CFTD (Clarke *et al.*, 2005).

The severity of CFTD can range from mild to severe, with more severe cases typically presenting with a greater percentage decrease in the size of type 1 fibres relative to type 2 fibres (Clarke and North, 2003; Lawlor *et al.*, 2010). Further to the common symptom of smaller and more numerous type 1 fibres, the clinical presentations are highly variable with elongated face and a high arched palate, common, and the more severe presentation involving severe limb weakness and respiratory insufficiency (Clarke and North, 2003). Mutations in the rod region of MYH7 can result in a ‘Laing distal myopathy’ phenotype with a distal weakness affecting ankle dorsiflexors and finger extensors (Ortolano *et al.*, 2011; Ruggiero

et al., 2015; Yu *et al.*, 2020). Heart complications are sometimes also present with mutations in *MYH7* gene site of the distal rod of the protein, with some patients presenting with non-compaction cardiomyopathy (Ruggiero *et al.*, 2015); and with MYL2, with infantile-onset cardiomyopathy (Marttila *et al.*, 2019).

Using CFTD as a classification for diagnosis of myopathy is made more complex by fibre type disproportions being a feature of other classifications of myopathy. There is also the further complication of fibre type disproportions also being present in non-congenital myopathies, such as metabolic or neurological disorders (Dehkharghani *et al.*, 1981; Iannaccone *et al.*, 1987). CFTD is typically a diagnosis when there is the fibre-type disproportions, without any of the other histopathological hallmarks of other myopathies, and where other classifications have been ruled out first (Clarke and North, 2003; Clarke, 2011). The 12% threshold decrease is also controversial, with debate around raising the threshold to 25% to reduce non-specific diagnosis (Clarke and North, 2003).

1.6.4. Core Myopathy:

Core myopathies are the most prevalent myopathy class and include central core disease (CCD) and multi-minicore disease (MmD). The prevalence of core myopathies has been estimated at just under 1:300,000 for all age groups (Huang *et al.*, 2021). Core myopathies were first described by (Magee and Shy, 1956), in what was the first paper to distinguish congenital myopathies as we now know them, based on the histopathology or structural abnormalities of skeletal muscle (Topaloglu, 2020). The name ‘central core disease’ first coined in 1958 (Greenfield *et al.*, 1958) and a family with multiple small cores in a muscle biopsy, lead to the classification of MmD in 1971 (Engel *et al.*, 1971). These ‘cores’ are regions of myofibrillar disruption, visualised by absence of oxidative enzyme activity, resulting from depletion of mitochondria (Jungbluth *et al.*, 2011; Claeys, 2020).

The most common cause of CCD are mutations in the *RYR1* gene (Huang *et al.*, 2021). Mutations in the N-terminus or central region of the of *RYR1* typically result in an increase in susceptibility to malignant hyperthermia (Sei *et al.*, 2004); whereas mutations in the C-terminus typically result in CCD (Tilgen *et al.*, 2001; Davis *et al.*, 2003). A study in Japan estimates that as many as 90% of CCD are the result of a mutation in the *RYR1* gene (Wu *et al.*, 2006). At least nine genes have been identified with mutations that result in MmD, including *RYR1*, *SEPN1*, *TTN* and *ACTA1* (Zhou *et al.*, 2007; Ferreiro *et al.*, 2002b; Ge *et al.*, 2019; Kaindl *et al.*, 2004). The inheritance pattern is typically dominant missense mutation in *RYR1* for CCD (Wu *et al.*, 2006). The inheritance pattern for MmD is more variable, with autosomal recessive mutations in *SEPN1* and *RYR1* common (Ferreiro *et al.*, 2002b; Ferreiro *et al.*, 2002a; Jungbluth *et al.*, 2005).

The severity of the condition is variable, ranging from mild to severe, with presentation typically occurring during early infancy (Quinlivan *et al.*, 2003; Ferreiro *et al.*, 2000). CCD can range from no observable symptoms to a lack of independent ambulation however, the phenotype of CCD is ordinarily mild and non-progressive/slowly progressive, with mild hypotonia, weakness in proximal muscles and facial muscle and motor developmental delays (Quinlivan *et al.*, 2003). There have been rare cases of severe CCD cases, for example foetal akinesia during pregnancy and severe hypotonia and respiratory insufficiency at birth (Romero *et al.*, 2003). Interestingly, 5 out of the 6 unrelated families in this study had a pattern of inheritance that strongly suggested autosomal recessive, which is unusual for CCD, and has been previously associated with a more aggressive phenotype (Manzur *et al.*, 1998). MmD typically presents with a ‘classic’ phenotype that is non-progressive or slow-progressive, with mild proximal weakness, hypotonia, motor developmental delays and scoliosis (Ferreiro *et al.*, 2000; Jungbluth *et al.*, 2000). There are rare cases where MmD can present with ophthalmoplegia, affecting the extra-ocular muscles (Jungbluth *et al.*, 2005).

The main diagnostic criteria is the presence of these white core regions, or multiple cores, with no enzymatic activity, following nicotinamide adenine dinucleotide tetrazolium reductase (NADH-TR) oxidative enzymatic staining of muscle biopsy samples (Dubowitz and Pearse, 1960; Wu *et al.*, 2006). Myofibrillar disruption can be seen when a patients muscle is visualised using EM (Claeys, 2020). The cores are almost exclusively seen in type 1 fibres (Wu *et al.*, 2006), as well as a predominance and hypotrophy of type 1 fibres (Ferreiro *et al.*, 2000). Centralised nuclei was sometimes present in histological samples in MmD, as was a mild fatty infiltration and Z-disc streaming (Jungbluth *et al.*, 2000). Fatty infiltration and z-disc streaming has also seen for CCD (Quinlivan *et al.*, 2003; Isaacs *et al.*, 1975).

The complexity of the histology and unusual core myopathies has led to the classification of dusty core disease (DuCD), characterised by irregular areas of myofibrillar disorganisation, with reddish/green material deposition and uneven oxidative stain (Garibaldi *et al.*, 2019). There is also the presence of centralised nuclei, type 1 fibres and is typically more severe than other forms of core myopathy and can be thought of as the hallmark of the recessive *RYR1* recessive form of core myopathy (Garibaldi *et al.*, 2019). There are also a small subset of patients that have both cores and rods, seen in nemaline myopathy, further complicating the distinct classification of core-rod myopathy (Romero *et al.*, 2009; Garibaldi *et al.*, 2018; Scacheri *et al.*, 2000).

1.6.5. Myosin Storage:

Myosin storage myopathy, or hyaline body myopathy, like the name suggests is a disease with hyaline-like protein aggregates of myosin in the muscle (Yüceyar *et al.*, 2015). The first case can be seen in 1971 by (Cancilla *et al.*, 1971) in a family with ‘finely granular material’ that disrupts myofibrillar organisation. The term ‘myosin storage myopathy’ was not coined until 2003 by (Tajsharghi *et al.*, 2003) following identification of heterozygous missense mutations in the *MYH7* gene. The prevalence of myosin storage myopathy is harder to estimate than other myopathy classifications, with only (Pagola-Lorz *et al.*, 2019) estimating the prevalence to be just over 1:200,000 in children, in Northern Spain.

The mutation implicated is in the gene *MYH7*, with mutations in this gene also resulting in Laing distal myopathy (Meredith *et al.*, 2004), CFTD (Muelas *et al.*, 2010) and MmD (Cullup *et al.*, 2012), as well as dilated and hypertrophic cardiomyopathies (Fiorillo *et al.*, 2016). There are over 500 identified disease-causing mutations in this gene (Colegrave and Peckham, 2014). The pattern of inheritance is usually autosomal dominant (Tajsharghi *et al.*, 2003; Bohlega *et al.*, 2004; Masuzugawa *et al.*, 1997), but three recessive cases have been recorded to date (Tajsharghi *et al.*, 2007; Yüceyar *et al.*, 2015; Beecroft *et al.*, 2019). The *MYH7* gene codes for the β-cardiac and slow-twitch muscle specific myosin heavy chain (MyHC), with mutations in the rod region of MyHC typically resulting in skeletal myopathies and/or cardiomyopathies (Tajsharghi *et al.*, 2003; Fiorillo *et al.*, 2016). Mutations in the very distal (C-terminus) of the rod region (exons 37-40) result in myosin storage myopathy (Fiorillo *et al.*, 2016). Mutations in the head region ordinarily result in cardiomyopathies without skeletal muscle myopathies (Tanjore *et al.*, 2010), however that has been one reported case of a mutation in the head region resulting in myosin storage myopathy (Beecroft *et al.*, 2019).

Diagnosis typically occurs in infancy (Tajsharghi *et al.*, 2003; Cancilla *et al.*, 1971), however, there are cases of adult diagnosis (Tajsharghi *et al.*, 2003; Rafay *et al.*, 2005). The severity and phenotype are heterogenous, with hypotonia occurring; a severe course can include diffuse weakness and muscle wasting, respiratory insufficiency and progressive scoliosis (Fiorillo *et al.*, 2016). Cardiac manifestations typically occur sometime after diagnosis of skeletal muscle myopathy phenotype, usually in adulthood (Fiorillo *et al.*, 2016).

The main histologic abnormality is the presence of the sub-sarcolemmal hyaline bodies in slow-twitch muscle fibres that disrupt the myofibrillar organisation and have ATPase activity (Shingde *et al.*, 2006; Viswanathan *et al.*, 2017). Hyaline bodies have a “glassy” or translucent appearance (Shingde *et al.*, 2006). A predominance of type 1 fibres in some patients with myosin storage myopathy has been noted (Barohn *et al.*, 1994; Tajsharghi *et al.*, 2003; Yüceyar *et al.*, 2015).

1.6.6. Potential for Future Therapies for congenital myopathies

Congenital myopathies are complex to research for various reasons. Firstly, congenital myopathies are rare, with a limited number of cases to compare and analyse (Huang *et al.*, 2021). Secondly, the clinical phenotype can overlap between classifications, so it can be difficult to decide on the most appropriate classification. Lastly, mutations in the same gene can result in a differing presentation (genetic heterogeneity), even within families with the same mutation (Lawlor *et al.*, 2010; Attali *et al.*, 2013; Liewluck *et al.*, 2017). An example of the genetic heterogeneity is demonstrated by mutations in the *RYR1* gene, which is implicated in several different classifications of congenital myopathy (Abath Neto *et al.*, 2017; Lawal *et al.*, 2018). Simply using sequencing techniques is not sufficient to provide full diagnosis (North *et al.*, 2014).

Despite advancements in genetic screening of patients, there is still a subset of patients with an undiagnosed genetic/molecular basis for disease. For example, one study in Denmark estimates that the causative gene remains to be identified in approximately 43% of children over the age of 5 with a congenital myopathy (Witting *et al.*, 2017). Approximately 20 – 40% of centronuclear myopathy genes remain to be discovered (Agrawal *et al.*, 2014; Ravenscroft *et al.*, 2018).

Genetic counselling is offered to patients diagnosed with these conditions, but with limited knowledge of the causative gene which can indicate the molecular basis of their disease, and with no effective treatments, there are limitations in the effectiveness of the support provided (Wang *et al.*, 2012). Nevertheless, regular appointments can help monitor disease progression, and physiotherapy can help maintain strength and joint flexibility (Vry *et al.*, 2016). Whilst there are treatments in clinical trials, there are currently no approved treatments for congenital myopathies (Gineste and Laporte, 2023). Gene editing/therapy presents an exciting potential therapeutic option, with promising results in human cell lines and animal models of neuromuscular disease. Examples of this include: *MTM1* in myotubular myopathy (Childers *et al.*, 2014) and *DNM2* in centronuclear myopathy in cells from human patients (Rabai *et al.*, 2019).

1.7. Sterile Alpha Motif and Leucine zipper Containing Kinase ZAK

The ZAK kinase, MAP triple kinase 20, is known by names including MAP3K20, MLTK, MLK7 and MRK due to its discovery by four independent groups (Liu *et al.*, 2000; Bloem *et al.*, 2001; Gotoh *et al.*, 2001; Gross *et al.*, 2002). The gene coding for *ZAK* is alternatively spliced to give rise to two distinct isoforms in humans (Vasli *et al.*, 2017), mice (Gotoh *et al.*, 2001) and *Xenopus* (Suzuki *et al.*, 2012). The alternative splicing after exon 11 can result in either the longer isoform, *ZAKα*, consisting of 20 exons, coding for 800 amino acids or the shorter isoform, *ZAKβ*, consisting of 12 exons, coding for 455 amino acids (Gross *et al.*, 2002). Note, that the first 331 amino acids, which contain the serine-threonine kinase domain and the leucine zipper, are identical in both isoforms. The leucine zipper has been shown to be important in the dimeristation of ZAK (Huang *et al.*, 2004a). The unique C-terminus of ZAKα contains a sterile alpha motif (SAM) domain, along with two partially redundant ribosome binding domains (Liu *et al.*, 2000; Vind *et al.*, 2020). The unique C-terminus of ZAKβ contains a stress fibre binding domain (SFBD), discussed in greater detail further in section 1.7.2 (Nordgaard *et al.*, 2022). Activation of ZAK is through autophosphorylation at key residues Thr161, Thr162, and Ser165, following dimerisation (Tosti *et al.*, 2004; Huang *et al.*, 2004a).

ZAK is a mitogen-activated protein (MAP) triple kinase (MAP3K) and is, thus, a component of the MAP kinase pathway (Gross *et al.*, 2002), often initiated through activation of a receptor tyrosine kinase (RTK) in the presence of a signal, such as a growth factor (e.g. FGF, IGF and EGF), cytokine or stress (Katz *et al.*, 2007; Kim and Choi, 2010). Figure 1.3 is a demonstrates the traditional MAPK signalling pathway, simplistically: The MAP3K (or MAPKKK) is activated by a stimulus, phosphorylating and activating a MAP double kinase (MAP2K or MAPKK), that in turn phosphorylates and activates the MAP kinase (MAPK), of which there are more than a dozen, but the most characterised include: ERK (1 and 2); P38 (α, β, γ and δ); c-Jun N-terminal kinase (JNK) and ERK5 (Cargnello and Roux, 2011). MAPK can phosphorylate a variety of proteins, modulating their activities and influencing cell differentiation, apoptosis and stress-induced responses (Cargnello and Roux, 2011; Pearson *et al.*, 2001). ZAK has been

shown to preferentially activate P38 (especially P38γ) and JNK via MKK3/6 and MKK4/7, respectively (Liu *et al.*, 2000; Gross *et al.*, 2002).

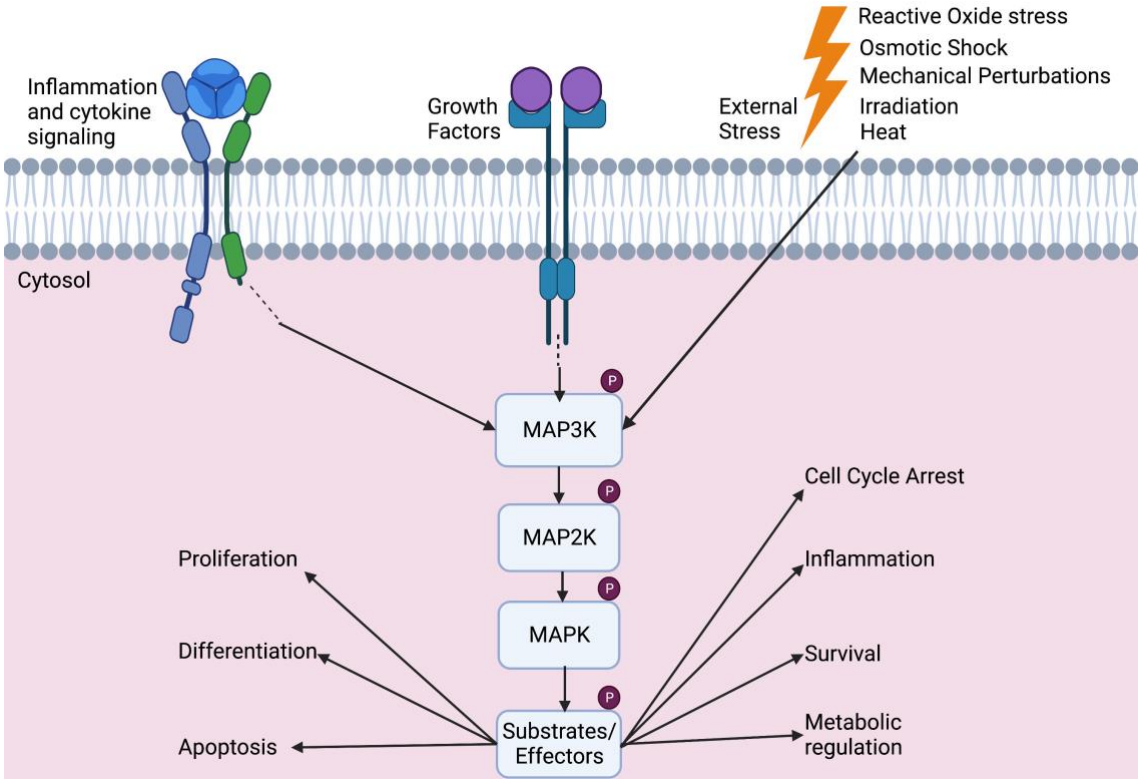

Figure 1.3. MAPK Signalling Pathway
MAPK signalling pathways can be activated by multiple stimuli, for example, cytokines, growth factors and various types of external stress. The common consequence will be activation of a signalling cascade, which includes the phosphorylation and activation of a MAP3K, which can then phosphorylate and activate a MAP2K, which in turn can then phosphorylate and activate a MAPK. The activated MAPK will then interact with and phosphorylate substrates, resulting in a range of downstream physiological effects. Dotted lines indicate further signalling proteins that have been omitted for simplicity. Figure was inspired by (Vind *et al.*, 2020). Figure created using BioRender (biorender.com).

1.7.1. Existing Knowledge of ZAKα

A potential role for ZAKα as a MAP3K involved in the ribosomal stress response was first described by (Wang *et al.*, 2005b), where inhibition of ZAKα prevented anisomycin-induced P38 and JNK activation. There are two main pathways of ribosomal surveillance for ensuring ribosomal function is correct: the ribosome-associated quality control (RQC) and the lesser-researched ribosomal stress response (RSR) (Brandman and Hegde, 2016; Iordanov *et al.*, 1997). More recently, ZAKα has been shown to contain two partially redundant ribosomal sensing domains in the in the unique C-terminal region (named S and CTD domain) (Vind *et al.*, 2020). A proposed mechanism was put forward, whereby

ZAKα uses these domains to bind and surveil ribosomes (Vind *et al.*, 2020). Upon ribotoxic stress and stalled ribosomes, ZAKα autophosphorylates, becoming active, where it dissociates from the ribosome, resulting in P38 and JNK signalling as well as inflammation (Vind *et al.*, 2020). ZAKα has also been proposed as a sensor for excessive levels of colliding ribosomes, that exceed the capacity for the RQC components (Wu *et al.*, 2020). Activated ZAKα results in RSR signalling with P38 and JNK as well as in blocking translation initiation through general control nonderepressible 2 (GCN2) signalling (Wu *et al.*, 2020). Moreover, upon UVB treatment and the consequential ribosomal stalling ribonucleic acid (RNA) photo-lesions, ZAKα has been shown to phosphorylate and activate P38, which along with ZAKα, phosphorylates the linker region of the inflammasome protein NOD-like receptor family pyrin domain-containing 1 (NLRP1) (Robinson *et al.*, 2022). The activated NLRP1 can then activate caspase-1 leading to pyroptosis and release of the pro-inflammatory cytokine interleukin (IL)-1β, which can then mediate a wound-response (Hu *et al.*, 2010; Robinson *et al.*, 2022). ZAKα and the ribosomal stress response have also shown to be activated by amino acid starvation, resulting in activation of AMPK (Snieckute *et al.*, 2022).

In 2016, two families with split-foot malformation and polydactyl were found to have mutations in the *ZAK* gene, specifically within the SAM domain, which is unique to *ZAKα* (Spielmann *et al.*, 2016). Deleting the SAM domain in mice led to a similar phenotype. (Spielmann *et al.*, 2016) attempted to knockout both ZAK isoforms using CRISPR/Cas9 with a guide strand designed against exon 2 of ZAK. Surprisingly, the mutation resulted in embryonic lethality at E9.5, with severe growth abnormalities and cardiac oedema. This contradicts other research as other ZAK knockout mice do not result in embryonic lethality and lack such developmental defects (Jandhyala *et al.*, 2016; Nordgaard *et al.*, 2022). Embryonic lethality and severe developmental disruption also contradict the human pathology of ZAK absence (Vasli *et al.*, 2017). (Vind *et al.*, 2020) found by rescuing a ZAK knockout CRISPR cell line with ZAKα containing the mutated SAM domain (F368C), resulted in constitutive activation of ZAKα activity. The activity of ZAKα could not be further increased with anisomycin (inducer of RSR signalling) and there was a decreased affinity for ZAKα for the ribosomes, suggesting the potential pathogenicity of the mutation.

1.7.2. Existing Knowledge of ZAKβ and its Role in Skeletal Muscle

Recent research by (Lin *et al.*, 2022) has shown a role for ZAKβ in reducing apoptosis caused by oxidised low-density lipoproteins (oxLDL). LDLs are a form of cholesterol, prone to oxidation, which can result in increased apoptosis and inflammation, and is a risk factor for atherosclerosis (Poznyak *et al.*, 2020). ZAKβ also reduced the expression of B-type natriuretic peptide (BNP), which reduces blood pressure and is a biomarker for congestive heart failure (Okamoto *et al.*, 2019; Lin *et al.*, 2022). The protective effects of ZAKβ are through inhibition of apoptosis-inducing caspase-3 activity, as well as increasing activated phosphatidyl isolsitol-3 kinase (PI3K), B cell lymphoma-extra-large (Bcl-xL) and super oxide dismutase-2 (SOD2) (Lin *et al.*, 2022).

In humans and mice, ZAKβ is the predominant isoform with expression levels approximately 10-fold greater than ZAKα (Gross *et al.*, 2002; Nordgaard *et al.*, 2022). ZAKβ is the isoform exclusively expressed in the skeletal muscle of humans and mice (Gross *et al.*, 2002; Vasli *et al.*, 2017; Nordgaard *et al.*, 2022). ZAKβ has been shown to interact as part of a protein complex at the Z-disc of skeletal muscle, along with proteins such as Kyphoscoliosis peptidase (KY) and filamin C (FLNC), mutations in which are implicated in human myopathy (Beatham *et al.*, 2004; Shatunov *et al.*, 2009; Baker *et al.*, 2010; Ehsani *et al.*, 2022). The role of ZAKβ in skeletal muscle has been, until recently, poorly described. Research by (Nordgaard *et al.*, 2022) has demonstrated a potential role for ZAKβ as a protein that recognises muscle contraction and mechanical load, transducing this into a discernible biochemical signal. These stresses activate ZAKβ, localised to the Z-disc in skeletal muscle using the stress fibre binding domain (SFBD) in the unique c-terminus of the shorter isoform. (Nordgaard *et al.*, 2022) therefore propose a model whereby Z-disc-localised ZAKβ is activated by muscle contraction and can result in P38 and JNK activation.

There are still areas of ZAKβ knowledge that need further investigation. The ubiquitous expression of ZAKβ across many tissues (GTEx Portal), as well as the ability for ZAK to recognise other stresses, such as osmotic shock, suggests a role as a compression or osmotic cell sensor for cell types (Nordgaard *et al.*, 2022). Further research will be required into the exact process in other tissues. With regards to the muscle-specific role of ZAKβ, the protein that ZAKβ binds to at the Z-disc using the SFBD, remains to be discovered (Nordgaard *et al.*, 2022).

1.7.3. ZAK in Myopathy

Exome sequencing on patients with congenital myopathies (Vasli *et al.*, 2017) first identified mutations in ZAK as a novel cause of congenital myopathy in 6 individuals from 3 families of different ethnic backgrounds. Transcript analysis suggest the pathogenesis is absence of ZAK, through nonsense-mediated messenger RNA (mRNA decay) (Vasli *et al.*, 2017). Patients commonly presented with a slow, progressive muscle degeneration and decreased vital capacity. In addition, haematoxylin and eosin (H&E) staining of skeletal muscle biopsies in $ZAK^{-/-}$ mice showed fibre size variation along with centralised nuclei and predominance of type 1 (slow-twitch) muscle fibres (Nordgaard *et al.*, 2022), reminiscent of the muscle degeneration seen in humans lacking ZAK. Due to the ZAKβ isoform being exclusively expressed in skeletal muscle, it is absence of this isoform that is implicated as driving myopathy (GTEx portal) (Vasli *et al.*, 2017). Myopathy-causing mutations in ZAK are called centronuclear myopathy-6 with a fibre type disproportion. A novel frameshift mutation in a further 7 individuals from a family in Pakistan was identified in 2022 (Ahmad *et al.*, 2022). These patients presented with a large degree of phenotypic overlap as in (Vasli *et al.*, 2017), such as calf hypertrophy, winged scapula and scoliosis. On the other hand, there was an additional, unique phenotype of a quadrupedal locomotion. Moreover, four of the patients died in early infancy, however, the exact cause of death is not determined (Ahmad *et al.*, 2022).

$ZAK^{-/-}$ mice demonstrate that slow-twitch muscles are more prone to the deleterious effects caused by absence of ZAKβ, likely coming from the constitutive contraction of slow-twitch fibres to provide support against gravity (Nordgaard *et al.*, 2022).

1.8. Animal Models of Myopathy

Human congenital myopathies are rare diseases, estimated to affect 1.62 out of 100,000 people, across all age groups in European, Asian, Oceanian and North American populations (Huang *et al.*, 2021). Animal models of neuromuscular diseases are, therefore, immensely useful for understanding these conditions in greater detail.

The most widely used model organism to study muscle diseases is the murine model. Mice have the advantage of being small and relatively cheap to maintain in comparison to larger model organisms; mice can be easily genetically manipulated and they have a short gestational period/lifespan (van Putten *et al.*, 2020). Most human congenital muscular dystrophies and myopathies have a genetic mouse model to further understand the function of the mutated gene (Sztretye *et al.*, 2020). The best known murine neuromuscular disease model is the *mdx* model for Duchenne muscular dystrophy. Duchenne muscular dystrophy is a severe X-linked condition, arising from mutations in the gene coding dystrophin (*DMD*), presenting with a severe progressive wasting of muscle and death between the ages of 20-40, usually as a result of respiratory or cardiac failure (Mercuri *et al.*, 2019; Duan *et al.*, 2021). The *mdx* mice have a nonsense mutation in exon 23 of the dystrophin gene, producing a truncated dystrophin protein and presenting with several similar phenotypic changes to humans with DMD, such as: centralised nuclei, infiltration of immunological cells, some disintegration of myofibrils and loss of Z-discs, as well as increased creatine kinase levels (Bulfield *et al.*, 1984; Sicinski *et al.*, 1989). Use of *mdx* mice is limited by the milder phenotype exhibited as well as the fairly normal lifespan (Bulfield *et al.*, 1984; DiMario *et al.*, 1991; Yucel *et al.*, 2018). Indeed, as discussed in section 1.7.3, there is a mouse model for absence of ZAK that presents in a similar way to humans lacking ZAK (Vasli *et al.*, 2017; Nordgaard *et al.*, 2022; Ahmad *et al.*, 2022). The shared pathological features include a progressive muscle deterioration, presence of centralised nuclei, predominance of slow-twitch muscle fibres and evidence of slow-twitch and fast-twitch fibre atrophy (Vasli *et al.*, 2017; Nordgaard *et al.*, 2022). Whilst the small size and short lifespan are advantageous with respect to the cost and time studying the animals, these features often limit the consistency between humans and mice (Collins and Morgan, 2003).

The canine model of human muscle diseases is another useful animal model. Dogs are closer than mice to humans in size, weight, and complexity of organ systems and, therefore, are used to further understand neuromuscular diseases (Story *et al.*, 2020). As of 2019, there were 21 mutations in dogs presenting with neuromuscular diseases also seen in humans (Barthélémy *et al.*, 2019). The most researched and best characterised example is the DMD model in golden retrievers (Sharp *et al.*, 1992; Kornegay, 2017). The mutation results in a phenotype that more closely resembles the human pathology than mice (Sharp *et al.*, 1992; Collins and Morgan, 2003). Recently, the same R465W missense mutation in the *DNM2* gene (encoding dynamin 2) present in humans with centronuclear myopathy was identified in a Border Collie, resulting in a similar phenotype to that observed in humans (Kim *et al.*, 2022). Reducing dynamin 2 levels through antisense oligonucleotides in mice was shown to improve the phenotype, as evidenced by the ultrastructure of the mutant muscle looking similar to wild type (Buono *et al.*, 2018). Confirming this finding in another model organism would strengthen the case for testing potential therapeutics targeting *DNM2* to treat this form of centronuclear myopathy. However, this is harder to do in dogs, given their larger size; in addition, their longer lifespan makes them more expensive to maintain, which in turn means there will be fewer biological repeats in an experiment, limiting statistical power of results obtained.

Pigs are a useful model organism for research, on account of the similar size, anatomy, metabolism and pathology to humans (Aigner *et al.*, 2010). Duchenne muscular dystrophy (DMD) has been successfully modelled in pigs, with targeted deletion of exon 52 using modified bacterial artificial chromosomes (BAC) where exon 52 has been replaced with neomycin, causing a frameshift mutation (Klymiuk *et al.*, 2013). These pigs are deficient in the protein dystrophin, following a frameshift mutation in exon 52 of *DMD* and display a similar phenotype to humans, with progressive muscle weakness and elevated creatine kinase (CK) levels (Klymiuk *et al.*, 2013). Further similarities in the porcine model were signs of inflammation and fibrosis, cycles of degeneration and regeneration as well as a marked locomotion impairment (Klymiuk *et al.*, 2013). Gene therapy was successful in ameliorating the phenotype, through restoring a truncated, but functional, form of dystrophin (Moretti *et al.*, 2020). There was an improvement in the muscle structure and function, a reduction in fatal heart arrhythmias and an

increase in the expected lifespan (Moretti *et al.*, 2020). The large size and cost of maintenance is a limitation for using pigs for research (Aigner *et al.*, 2010).

1.8.1. Zebrafish as models of human muscle disease

This thesis presents a study using the model organism, zebrafish (*Danio rerio*) to model how absence of ZAK might affect the development and maintenance of skeletal muscle.

Danio rerio are small fish belong to the Teleostei infraclass and are considerably distanced from humans, from an evolutionary perspective, compared to mice, for example (Woods *et al.*, 2000; Adamson *et al.*, 2018). Nevertheless there are many aspects of zebrafish that make them an attractive model organism, for instance: their small size, high fecundity of transparent embryos that develop externally and can be easily genetically manipulated as well as having a relatively short lifespan (Zang *et al.*, 2022). The transparency of the zebrafish embryos allows for live imaging of transgenic, fluorescently tagged proteins within certain cell types or tissues (Kaveh *et al.*, 2020). Approximately 70% of all human genes and 82% of disease-causing genes have an orthologue in zebrafish (Howe *et al.*, 2013).

As a result of these advantages, zebrafish have been used to model multiple human pathologies, such as: neurological conditions (Hughes *et al.*, 2020), inflammation and immunity (Levraud *et al.*, 2022), cancer (Miao *et al.*, 2021), behaviour (James *et al.*, 2021), and neuromuscular diseases (Bassett and Currie, 2003; Lieschke and Currie, 2007). A further benefit of establishing a zebrafish model organism is that zebrafish can go through high-throughput screening for therapeutics that might help. The *sapje* mutant for *DMD* has had over 1000 potential therapeutics assessed, as of 2016 (Kawahara *et al.*, 2011; Widrick *et al.*, 2016).

The most abundant tissue in zebrafish is skeletal muscle (Roy *et al.*, 2001), which is highly similar to humans on a cell and molecular, as well as a structural level (Daya *et al.*, 2020). Like mammals, zebrafish have both slow and fast-twitch muscle fibres (Jackson and Ingham, 2013).

Zebrafish myogenesis occurs as follows: Presomitic/paraxial mesoderm cells are located next to the notochord and express the bHLH transcription factors, committing them to a myogenic lineage (Weinberg *et al.*, 1996; Keenan and Currie, 2019). The notochord secretes sonic hedgehog (shh), the signalling of which in paraxial mesoderm cells results in expression of BLIMP1 (also known as PRDM1) (Blagden *et al.*, 1997; Baxendale *et al.*, 2004) (Keenan and Currie, 2019). BLIMP1 is a potent inhibitor of the fast-twitch lineage, resulting in the paraxial mesoderm cells becoming committed to being slow-twitch progenitors (Blagden *et al.*, 1997; Baxendale *et al.*, 2004). Following segmentation into somites, the majority of these cells, known as adaxial cells migrate laterally to the surface of the embryo, forming the superficial slow fibres (SSF), which remain mononucleated through early development (Jackson and Ingham, 2013; Keenan and Currie, 2019).

Fast-twitch fibres arise from non-adaxial cells in the paraxial mesoderm (Keenan and Currie, 2019). The majority of these fast-twitch fibres (lateral fast-twitch fibres) are specified by retinoic acid through fgf8 signalling, rather than shh (Hamade *et al.*, 2006). This results in the expression of the myogenic bHLH genes, a mechanism used to specify the muscle lineage in all vertebrates (Mary Elizabeth Pownall *et al.*, 2002), as well as fast myosin heavy chains, resulting in the formation of the lateral fast-twitch muscle fibres (Groves *et al.*, 2005; Hamade *et al.*, 2006; Keenan and Currie, 2019). Fast-twitch fibres can also form from a subset of cells named medial fast fibres (MFF) that are located and encompass the notochord in embryos and adults (Wolff *et al.*, 2003; Keenan and Currie, 2019). The lateral fast-twitch fibres are the predominant fast-twitch fibres (Keenan and Currie, 2019). Myogenin is essential in zebrafish for the fusion of fast-twitch fibres, with absence of myogenin resulting in failure of most fibres to fuse (Ganassi *et al.*, 2018). There small amount of residual fusion occurred as a result of shh signalling, confirming a second fusion pathway (Ganassi *et al.*, 2018). The bulk of the musculature in zebrafish is comprised of fast-twitch muscle fibres (van Raamsdonk *et al.*, 1982).

The distinct separation of muscle fibres that begins in embryogenesis and remains in adulthood is novel for fish (Keenan and Currie, 2019). Typically mammalian muscles contain a mixture of slow and fast-twitch fibres, therefore,

zebrafish are a useful tool for studying these fibre-types separately (Jackson and Ingham, 2013).

Somites begin to form after around just 10.5 hours post fertilisation (hpf), with further somites forming in an anterior to posterior direction (Stickney *et al.*, 2000). A characteristic of fish musculature is the chevron that separates individual somites, appearing as early as 1 dpf (Bassett and Currie, 2003). This is better known as the vertical myoseptum; is composed of dense collagen and can be thought of as the fish equivalent of a tendon (Kudo *et al.*, 2004; Hall *et al.*, 2007b). This connective tissue remains in adult fish, separating the individual myomeres (Kudo *et al.*, 2004).

Table 1.1. outlines the wide range of genes with skeletal muscle disease-causing mutations in zebrafish that also are associated with human congenital myopathies or muscular dystrophies. The mutations arise from either spontaneous mutations or have been generated using N-ethyl-N-nitrosourea (ENU) mutagenesis, transcriptional activator-like effector nucleases (TALEN), Zinc Finger Nucleases (ZFN) or clustered regularly interspaced short palindromic repeats (CRISPR)-Cas9. The phenotypes range from mild (sometimes due to the upregulation of compensatory genes), to severe, resulting in embryonic lethality and/or immobility. Further review of genetic-targeting methods is 3.1.3.

Gene	Human Disease	Features of mutation	Reference
BAG3	Dilated Cardiomyopathy and myofibrillar myopathy	Genetic compensation through upregulation of BAG2 in absence of BAG3. Inhibition of NMD process and, thus, genetic compensation led to an increase in skeletal muscle ultrastructure disruption and reduced cardiac function. Morpholino knock downs of *BAG2* led to a disruption to skeletal muscle and cardiac function	(Diofano *et al.*, 2020)
cdipt	Centronuclear myopathy	Reduced area of T-tubule, terminal cisternae and gap-width distance. Decreased locomotor performance	(Smith *et al.*, 2020)
COL6A1	Bethlem Myopathy/Ullrich Congenital Muscular Dystrophy	Reduced embryo length. detached myofibers upon methylcellulose stress. Impaired locomotion. Slow-twitch muscles greater affected than fast-twitch fibres. Reduced motor axon extension. Impaired autophagy. Disordered sarcomeres, abnormal mitochondria, and fibrotic signs. Phenotype persisted from embryos to adulthood, worsening with age. Phenotype improved with salbutamol treatment.	(Radev *et al.*, 2015) (Tonelotto *et al.*, 2022)
DAG1	Dystroglycanopathy	Muscle degeneration (reduced birefringence). Slower swimming and reduced distance. Destabilises toe dystroglycanopathy complex (DGC). Thickened myosepta and detached fibres from the myoseptum. Abnormal triad formation and ocular defects.	(Gupta *et al.*, 2011)
DMD (sapje or Sapje-like)	Duchenne or Becker Muscular Dystrophy	Fibre detachment from the basement membrane, from muscle contraction. Sarcolemmas are damaged from the detachment. Fibre detachment is accompanied by cell death. Ultrastructurally, sarcomeres are absent or collapsed. Atrophy of myofibers. Infiltration of immunological cells, such as neutrophils. Similar regeneration pattern to mammals.	(Bassett *et al.*, 2003) (Guyon *et al.*, 2009) (Berger *et al.*, 2010)
fkrp	Congenital Muscular Dystrophy	Defective basement membrane and fibre detachment. Failure to effectively form the fibronectin-collagen connection. Reduced maximum force of contraction	(Wood *et al.*, 2021)
FLNC (sot)	Myofibrillar myopathy	FLNC is duplicated in zebrafish: only FLNCB is mutated, producing a temporary disruption to the slow-twitch fibres that resolves with age. Targeting FLNCA with morpholino led to a similar mild phenotype, however, targeting both led to a severe phenotype of severe slow and fast-twitch muscle fibre disruption and aggregates containing myosin and desmin. These aggregates resemble myofibrillar myopathy.	(Ruparelia *et al.*, 2012)
GNE	GNE Myopathy	Embryonic lethal by 10 days post fertilisation (dpf). Reduced movement, severe myofibre disorganisation, reduced heart rate and increased body axis formation	(Livne *et al.*, 2022)
KY	Kyphoscoliosis	Upregulation of Chaperone Assisted Selected Autophagy (CASA) Components	(Jokl *et al.*, 2018a)
LAMA2 (candyfloss)	Congenital Muscular Dystrophy	Detachment of both slow-twitch and fast-twitch muscle fibres from the vertical myoseptum from as early as 36 hpf, brought about by movement and muscle contraction. The detachment of fibres is not associated with a loss of sarcolemmal integrity. Signs of fibrosis in the myoseptum. Most embryos die by 16 dpf. Can be rescued with injection of wild type *LAMA2* mRNA. Reduced muscle, brain and eye size.	(Hall *et al.*, 2007a) (Gupta *et al.*, 2012)

lamb2 (softy)	Congenital Muscular Dystrophy	High levels of muscle disruption occurring from fibres detaching from the basement membrane, from as early as 3 dpf. Sarcolemma damage. Abnormal ultrastructural appearance of the myotendinous junction (MTJ). Surprisingly not embryonic lethal.	(Jacoby *et al.*, 2009)
LMNA	Striated laminopathies	Damage to slow-twitch muscle fibres. Impaired larval locomotion. Abnormal expression of MAPK members, including upregulation of phosphorylated ERK. Also a downregulation of *Nfkb2* expression. Mild cardiac phenotype of decreased fractional shortening at 3 and 4 dpf.	(Nicolas *et al.*, 2022)
mbnl1	Myotonic dystrophy	Reduced adult body length. Impaired locomotion. Aberrant alternative splicing of genes, such as RyR1, implicated in disease.	(Hinman *et al.*, 2021)
MTM1	Myotubular Myopathy	Abnormal pectoral fin development. Embryonic lethal by 9 dpf. Substantially impaired locomotion and abnormal triad formation, lacking SR and fragmented t-tubules. Improvement of phenotype with PI3K inhibitors.	(Sabha *et al.*, 2016)
MYMK	Carey-Fineman-Zeiter Syndrome	Fast-twitch muscle fibres failed to fuse. Reduced size and weight of adult zebrafish and craniofacial Cartlidge deformities. Fast twitch fibres showed hypotrophy and fatty infiltration	(Di Gioia *et al.*, 2017)
MYO18B (fro)	Nemaline myopathy	Complete immobilisation of embryo. Disruption of myofibrillogenesis and fast-twitch fibre sarcomeric organisation. Loss of force generation in fast-twitch fibres and reduced force in slow-twitch fibres. Cardiac phenotype was mild with some sarcomeric organisation present, although cardiac oedemas did occur. Phalangeal Cartlidge was abnormal	(Berger *et al.*, 2017) (Gurung *et al.*, 2017)
neb	Nemaline myopathy	Reduced embryo length and thinner, bent tails. Severe locomotion defects at 48 hpf including reduced force. Muscle structure was highly disrupted (birefringence). Cardiac abnormalities, such as cardiac oedema. Ultrastructural abnormalities, such as reduced length of thin filament. Presence of nemaline bodies, demonstrating nemaline myopathy.	(Telfer *et al.*, 2012)
RyR1	MmD; centronuclear myopathy; core myopathy and CFTD	Impaired swimming response at 2 dpf. RyR1a and RyRb have fibre-type specific roles. No defects in the central nervous system or neuromuscular junction. Decreased calcium transients in fast-twitch fibres and DHPRs at t-tubule/SR junctions. Small cores and defects to the SR were also observed.	(Hirata *et al.*, 2007a) (Dowling *et al.*, 2012) (Chagovetz *et al.*, 2019)
SPEG	Centronuclear myopathy	Embryonic lethal by 11 dpf. Disrupted triad formation and reduced triad numbers. Impaired swimming ability and upregulation of dynamin 2 (*DNM2*) and desmin	(Espinosa *et al.*, 2022)
TTN (ruz)	Dilated Cardiomyopathy and skeletal myopathy	Phenotype was more severe when mutations were in the C-terminal region of TTN. Impaired cardiac contractility and sarcomere disorganisation. Sarcomeric proteins were aberrantly localised.	(Steffen *et al.*, 2007) (Zou *et al.*, 2015)

Table 1.1. Genetic zebrafish models of human skeletal muscle disease-causing gene mutations. Column 1 is the gene implicated and in brackets is the name given to the zebrafish mutant for this gene. Column 2 details the human muscle disease/s associated with mutations to the gene. Column 3 is the phenotype of the zebrafish with mutations in the gene and column 4 is the reference. Only genetically targeted zebrafish have been included, not morpholino knockdowns.

1.9. Thesis Aims

The aims of my thesis can be broken down into two distinct parts. Firstly, to characterise the expression of *ZAK* isoforms in embryonic and adult zebrafish and use CRISPR-Cas9 gene-targeting to mutate both isoforms. Secondly, to investigate any impact that the loss of ZAK has to the phenotype of zebrafish embryos and adults, including aged zebrafish.

- Characterise expression of both *ZAK* isoforms in zebrafish and compare to the expression profile in humans and mice.
- Genetically target *ZAK*α and *ZAK*β, and breed to create mutant lines lacking each isoform and both.
- Validate *ZAK* mutants, by measuring levels of each respective transcript using quantitative reverse transcriptase polymerase chain reaction (qRT-PCR)
- Investigate changes in the activation of prospective downstream MAPK proteins in the absence of ZAK, using western blots. Also investigate changes in the expression of other signalling pathways at the transcript level using qRT-PCR.
- Investigate muscle function by measuring key swimming attributes in *ZAK*β mutant zebrafish at a variety of different ages, through computational video analysis. The strength of muscle contractions in early zebrafish embryos will also be assessed using a tactile strength assay
- Assess the heart rate for any variability in the ZAK$\beta^{-/-}$ mutant.
- Analyse any changes to the fibre size or ability to repair wounds using confocal imaging of reporter lines. To do this ZAK$\beta^{-/-}$ mutants will be crossed into transgenic lines, allowing for high resolution imaging of skeletal muscle and macrophages.
- Assess for any abnormalities in the ultrastructure of old-aged ZAK$\beta^{-/-}$ skeletal muscle, compared to age-matched wild type, using transmission electron microscopy (TEM).

2. Materials and Methodology

2.1. Ethics

The experimental procedures performed as part of this thesis are carried out in accordance with the United Kingdom Home office Animals (Scientific Procedures) Act (ASPA) 1986 under project licence PPL POF245295 held by Professor Betsy Pownall and Personal Licence PIL I0EE85C59 held by Alexander Russell

2.2. Zebrafish Husbandry

Zebrafish are kept in 14-hour day and 10-hour night cycles as adults on an Aquatics Habitats Z-Hab system. Larval zebrafish (up to 5 days post fertilisation (dpf)) are kept in 28ºC incubators in E3 media (5mM NaCl, 0.17mM KCl, 0.33mM $CaCl_2$, 0.33mM $MgSO_4$, 0.1% methylene blue), except for when they are removed for use in experiments or cleaned. Zebrafish are fed twice a day: Morning feed is brine shrimp artemia cysts (ZMsystems). Afternoon feed is a dry formulation (Zeigler adult 1 mm pellet, 500-800 micron golden pearl, 300-500 micron golden pearl, freeze dried rotifers and spirulina flakes) The zebrafish tank water is automatically heated to 28ºC and buffered by the control system to ensure a pH range of 7.20-7.60 and a conductivity range of 750-850µs.

Anaesthesia was performed by transferring zebrafish into 250ml buffered-tank water containing 0.1% w/v MS-222 (tricaine) (Sigma; A5040-25G). Schedule 1 euthanasia was performed by overdose in benzocaine and confirmation of death by destruction of the brain, in accordance with UK ASPA Act 1986. Surplus zebrafish embryos are humanely discarded by euthanasia in 1% sodium hypochlorite.

2.3. CRISPR Genome Editing

2.3.1. ZAKα CRISPR Guide Strand Design

Single guide (sg)RNA against *ZAKα* was designed using the software 'CHOPCHOP'. This software identified regions within exon 2 of ZAKα with appropriate protospacer adjacent motif (PAM) against which complementary sequences CRISPR RNA (crRNA) can be designed to guide the Cas9 endonuclease to the correct region of deoxyribonucleic acid (DNA), for effective cleavage. In addition to the target sequence, which will be used to synthesise the guide strand RNA, a T7 promoter region (GCAGCTAATACGACTCACTATAGG) was also incorporated at the 5' end of the primer allowing for transcription of the guide strand using T7 RNA polymerase (Nakayama *et al.*, 2014). To the 3' end of the primer, part of the conserved transactivating CRISPR RNA (tracrRNA) motif was added (GTTTTAGAGCTAGAAATA), to bind to the Cas9 endonuclease, allowing the crRNA region to guide the complex to the target region of DNA, where Cas9 cause the double stranded DNA (dsDNA) breaks and the error prone repair to occur (Santos *et al.*, 2016b; Liao and Beisel, 2021). The reverse primer was used for both guide strands and is the remainder of the conserved tracrRNA motif sequence in reverse complement (Nakayama *et al.*, 2014; Santos *et al.*, 2016b). See table 2.1 for primer sequences.

Primer	**Sequence**
ZAKα CRISPR Guide Strand 1	GCAGCTAATACGACTCACTATAGGTTCTGGAAGC GCCCAATTATGTTTTAGAGCTAGAAATA
ZAKα CRISPR Guide Strand 2	GCAGCTAATACGACTCACTATAGGTTTTGAGCGT TCTCAGTCATGTTTTAGAGCTAGAAATA
CRISPR Reverse Primer	AAAAGCACCGACTCGGTGCCACTTTTTCAAGTTG ATAACGGACTAGCCTTATTTTAACTTGCTATTTCT AGCTCTAAAAC

Table 2.1. Sequence of primers used to produce sgRNA.
The sequence of primers used to synthesise ZAKα guide strands 1 and 2, as well as the universal reverse strand. Highlighted in yellow is the crRNA target sequence.

2.3.2. Guide RNA Transcription

Initially polymerase chain reaction (PCR) was performed to amplify the sgRNA. 1 μM forward primer (respective ZAKα CRISPR guide strand) and 1 μM reverse primer was combined with 27 μl of nuclease free water, 0.1 μM mixed deoxyribonucleotide triphosphates (dNTPs) (ThermoFisher; RO181) and 1X HF buffer. The PCR was set up for an initial hold at 98°C for 30 seconds before adding 2 units Phusion polymerase (New England Biolabs; M0530). The PCR settings were as follows for 35 cycles: 98°C for 10 seconds; 60°C for 30 seconds; 72°C for 15 seconds. There was a 10-minute final extension at 72°C. Confirmation of successful amplification was confirmed through presence of the correct sized amplicon on a 2% Tris-acetate-EDTA (TAE)-agarose gel run at 160V for 15 min.

Using the amplicon from the previous PCR reaction, a transcription reaction was set up using the MEGAshortscript™ T7 transcription kit (Invitrogen; AM1354M). A reaction was set up for each of the guide strands (3 μl) containing: 2 μl adenosine triphosphate (ATP), 2 μl cytidine triphosphate (CTP), 2 μl uridine triphosphate (UTP), 2 μl guanosine triphosphate (GTP), 5 μl water, 4 μl of DNA template and 4 μl 10X enzyme mix. The transcription reaction was incubated at 37°C overnight. The synthesised gRNA was analysed on a 2% TAE-agarose gel to ensure transcription had taken place effectively. 1 μl of Turbo DNase (Part of MEGAshortscript™ T7 transcription kit) was added to each sample and incubated at 37°C for 15 minutes, in order to remove residual DNA, leaving just guide RNA. To purify the gRNA, 40 μl 5 M ammonium acetate stop solution was added to each sample along with 340 μl of nuclease free water and then 400 μl phenol chloroform. Following a thorough vortex and a five-minute centrifugation at 13,000 rpm, 300 μl aqueous phase was transferred to a clean tube and 300 μl chloroform:isoamyl alcohol was added. A further, thorough vortex was followed by centrifugation at 13,000 rpm for five minutes. The aqueous phase was transferred to 800 μl 100% ethanol and left to precipitate at -20°C overnight. The samples were centrifuged at 13,000 rpm for 15 minutes, the supernatant discarded, and the pellet washed with 120 μl ice-cold 70% ethanol. The samples were centrifuged at 13,000 rpm for 5 minutes. The pellet was then dried by vacuum desiccation for 20 minutes and resuspended in 20 μl nuclease free water. The purified sgRNAs were validated by running on a 2% TAE-agarose gel at

150V for 15 minutes. Using the nanodrop ND1000, the absorbance at 260nm was also used to determine the concentration of guide RNA.

2.3.3. Microinjections

Male and female zebrafish were set up to mate during the afternoon/early evening in specialised breeding tanks (Aquatics Habitats), containing dividers to separate the male and female. The dividers were removed the following morning, shortly after the lights automatically turn on, and the zebrafish were allowed to mate undisturbed for 30 minutes. The embryos were then collected and stored in E3 media until injected. 1 nl containing 300 pg of each ZAK guide strands (co-injected both sgRNAs), 1 ng Cas9 endonuclease (in a buffer consisting of 20 mM tris, 200 mM KCl, 10 mM $MgCl_2$, pH 7.5) and 83 mM KCl was injected into the yolk of zebrafish embryos at the 1 - 4 cell stage, close to the cell body. Embryos were then grown as normal in fresh E3 media at 28^{o}C up until 5 dpf. Embryos that died during the procedure were removed and fresh E3 was provided daily. A microinjector (PM1000 Cell Microinjector, MDI) and foot pedestal were used for microinjections and all injections performed used borosilicate glass capillaries (Narishige; G-1). Injections were performed using a micromanipulator (Prion).

2.3.4. Heteroduplex Assay

The heteroduplex assay for screening mutants/genotyping is adapted from (Zhu *et al.*, 2014). Different sequences in a PCR product can bind to each other. Mismatches of bases, insertions or deletions can result in structural abnormalities in the DNA and slower migration during polyacrylamide gel electrophoresis.

2.3.4.1. DNA Extraction

ZAKα F0 zebrafish were raised to sexual maturity and then outcrossed with wild-type zebrafish to generate F1 heterozygotes. The potentially heterozygote embryos are collected and have their DNA extracted: Individual embryos are added to 50 µl lysis buffer (10 mM Tris; 10 mM ethylenediaminetetraacetic acid (EDTA); 200 mM NaCl; 0.5% sodium dodecyl sulphate (SDS); 200 µg/ml proteinase K) and heated at 55^{o}C for 3 hours with a vortex after 90 minutes and 150 minutes. The DNA is precipitated in 200 µl 100% ethanol for 30 minutes at 4^{o}C, before centrifuging at 13,000 rpm for 10 minutes. The pellet is washed with 200 µl 70% ethanol and centrifuged at 13,000 rpm for 2 minutes. The pellet is dried by vacuum desiccation before resuspending in 20 µl nuclease free water.

DNA can also be extracted from dissected adult zebrafish fin clips, allowing adults from a mixed tank to be genotyped. The same protocol is followed, however, 200 µl lysis buffer is used for the heating stage, the DNA is precipitated in 1 ml 100% ethanol and the final DNA pellet is resuspended in a greater volume of nuclease free water (typically 50 µl).

2.3.4.2. PCR Amplification

Primers were designed using sequences in flanking introns that were around 250 base pairs upstream (forward) and downstream (reverse) of the target sequence, and a PCR reaction was performed to amplify this region. 12.5 µl 2X Taq PCR mastermix (Promega; M7502); 1 µl forward primer (0.4 µM); 1µl reverse primer (0.4 µM); 1µl DNA and 9.5µl nuclease free water is added for each reaction. PCR reactions were typically run for 30 cycles, unless otherwise specified, with an initial denaturing step of 98ºC for 90 seconds. Denaturing and annealing times were always 30 seconds for genotyping PCR reactions. The annealing temperature and extension time can be seen in table 2.2. The extension temperature was 72ºC and the final extension time was always 10 minutes. Table 2.2 shows genotyping primer pair sequences.

2.3.4.3. Heteroduplex Mobility Assay

Heteroduplex mobility assays are used as a pre-sequencing screening tool to identify changes to the DNA sequence. The amplicon is run on a 12% resolving gel (12% acrylamide, 10 µg/ml ammonium persulphate (APS), 1.2 µg/µl tetramethylethylenediamine (TEMED), 1X Tris-Borate-EDTA buffer (TBE) buffer (0.1 M Tris base, 0.1 M Boric acid, 2 µM EDTA)) for 3 hours at 150V. The running buffer is 1X TBE. The gel is then stained using 1 µg/ml ethidium bromide in 1X TBE for 30 minutes and then de-stained for 2 hours in deionised water.

Heteroduplexes (2 different DNA strands that have annealed during PCR) migrate at a different rate to homoduplexes (2 identical DNA strands - wildtype or homozygous mutant DNA), allowing heterozygotes to be detected (Zhu *et al.*, 2014). Also, large insertions and deletions (INDELs) will be identified by bands running at different heights. PCR products that migrate abnormally or show additional bands are sequenced to identify the nature of the mutation.

2.3.5. Sequencing

Amplified DNA was purified using monarch DNA Extraction kit (New England Biolabs; T1020S) as per the protocol, prior to sequencing. The purified amplicon was either diluted to an appropriate concentration (dependent on Eurofins optimum specification for the amplicon size, subject to change) along with 5 µl of 5 µg/µl forward primer or was ligated into pGEM-T Easy plasmids (Promega; A1360) to sequence individual PCR fragments.

For the specific sequencing of suspected heterozygotes, ligating into pGEM-T Easy plasmids and transforming competent *E. coli* cells (New England Biolabs; C2925L) is the most beneficial method, as both alleles can be detected in different fragments. To do this 3 µl amplicon is added to 1 µl DNA Ligase; 1 µl pGEM-T easy vector and 5 µl 2X ligation buffer. A control with 3 µl nuclease free water insert of PCR product was set up. The ligations are stored at 4^{o}C overnight. 25 µl Competent *E. coli* cells were transformed by addition of 5 µl ligated plasmid and leaving on ice for 30 min. The cells were then subject to heat shock at 40^{o}C for 90 seconds before leaving on ice for a 5 min recovery. 1 ml lysogeny broth (LB) broth (10g/L Sodium Chloride; 10g/L Tryptone; 5g/L Yeast Extract) was then added and the cells were incubated with agitation at 37^{o}C for 1 hour. The cells were then plated on LB agar (10 g/L Sodium Chloride; 10 g/L Tryptone; 5 g/L Yeast Extract; 15 g/L Agar - supplemented with 100 µg/ml ampicillin (Scientific Laboratory Supplies; A9518)) and left at 37^{o}C overnight. Individual colonies were first screened using PCR: 2 µl of nuclease free water was added to a single colony, which was then mixed by pipetting. The 2 µl colony was then added to a clean PCR tube containing 10 µl Promega PCR master mix; 1 µl SP6 primer, 1 µl T7 primer and 6 µl nuclease free water. See table 2.2 for details of the parameters and primers. Primers were designed using the sequences for the SP6 and T7 sites on the p-GEM-T Easy plasmid, as these flank either side of the insert site, allowing for the potential insert to be checked. The presence of amplicon was checked on a 1.3% TAE agarose gel. The respective pipette tip used to mix and transfer the colonies to the PCR tubes was placed in a tube containing 3 ml LB broth (containing 300 µg ampicillin). Any colonies identified as having the amplicon inserted are then cultured overnight at 37^{o}C with agitation. The plasmids are extracted and purified using the QIAprep spin miniprep (Qiagen; 27104) clean up kit protocol.

The purified plasmids are then diluted to 80-100 µg/µl and sent for analysis by Sanger sequencing (Eurofins) using a 1 µg/µl SP6 primer.

Target	**Forward primer**	**Reverse Primer**	**Annealing temperature**	**Extension time**
ZAKα	TGGTGCTCT GTCAAAAAT AAATAA	TAAACAGAC CCTGTGGAC	59^{o}C	40 Seconds
ZAKβ	TCATGGCCT CAGACAGCA AA	TGCAGCTTT TGGGTGACG TA	62^{o}C	40 Seconds
KY	AGCCACCAA TCAGAAGAA GCA	GTGTTAGCA CAGAGTGCA CAA	62^{o}C	40 Seconds
SP6	AGGTGACAC TATAGAATAC TCAAG	N/A. Used alongside T7 primer	50^{o}C	Dependent on size of amplicon ligated into pGEM plasmid (35 seconds per 500 base pair insert).
T7	GTAATACGA CTCACTATA GGCG	N/A. Used alongside SP6 primer	50^{o}C	Dependent on size of amplicon ligated into pGEM plasmid (35 seconds per 500 base pair insert).

Table 2.2. Primers and PCR conditions for genotyping zebrafish.
The Annealing temperature and extension time are detailed as well as the sequence of the forward and reverse *ZAKα*, *ZAKβ* and *KY* genotyping primers. pGEM *SP6* and *T7* sequences are also included for amplifying the insert in pGEM plasmids following ligation and also for sequencing plasmids.

2.4. Quantitative Reverse Transcriptase (qRT) – PCR

2.4.1. RNA Extraction

The RNA extraction protocol was the same regardless of whether the samples were embryos or adult tissue. For embryos, a minimum of 5 embryos from a single mating were removed from the chorion (if younger than 3 dpf) and flash frozen using liquid nitrogen. Adult tissues were dissected from culled zebrafish (overdosed in benzocaine) and rinsed in 1X phosphate buffered saline (PBS (140 mM NaCl; 2.7 mM KCl; 10 mM Na_2HPO_4; 1.8 mM KH_2PO_4;) before being immediately flash frozen in liquid nitrogen.

The flash frozen embryos/tissues were defrosted and immediately homogenised in 1 ml TRI reagent (Sigma; T9424) before centrifuging at 12,000g for 10 minutes at 4^{o}C. The supernatant was transferred to a fresh Eppendorf and left to settle at room temperature for 5 minutes. 200 µl chloroform was added and the samples shaken thoroughly for 15 seconds and left to settle at room temperature for 10 minutes. The samples were centrifuged at 12,000 g for 15 minutes at 4^{o}C and the aqueous layer transferred to a fresh tube; 500 µl isopropanol was added and incubated at room temperature for 10 minutes. The samples were centrifuged at 12,000 g for 10 minutes. The pellet was washed three times with 1 ml 70% ethanol and spun down at 12,000 g for 5 minutes at 4^{o}C, after each addition of 70% ethanol. The pellet was dried by vacuum desiccation and resuspended in 40 µl molecular grade water. The pellet of RNA extracted from embryos or the heart was resuspended in 20 µl nuclease free water because of the low RNA concentration recovered.

The RNA is run on a 1.3% TAE agarose gel and the concentration is measured by spectrophotometry on the Nanodrop ND1000 (Thermo Scientific) to check for good quality. The RNA on the gel should have two major bands (28S:18S ribosomal (rRNA)) with roughly a 2:1 ratio and minimal degradation. The 260/280 and the 260/230 ratio also should be ~2.0 for the RNA to be used in qPCR.

ZYMO RNA Clean and Concentrator -5 (ZYMO Research; Cat #R1013 & R1014) protocol was used to purify and concentrate the RNA. 5µl DNAse and 5µl digestion buffer was transferred to the RNA and left for 15 min at room temperature. The Zymo clean and concentrator-5 protocol was then followed.

2.4.2. cDNA Synthesis

500 ng RNA was mixed with 0.7 µM dNTP (ThermoFisher; RO181), 3.6 µM random hexamer primers (ThermoFisher; SO142) and nuclease-free water to a final volume of 18 µl. The RNA was then incubated at 65^{o}C for 5 minutes, followed by a brief cooling on ice. 1X SSIV buffer; 17mM Dithiothreitol (DTT) and SSIV reverse transcriptase (RT) (200U) (all components part of SSIV Reverse Transcriptase kit (ThermoFisher; 18090010) was added to the RNA to a total volume of 25 µl. The RNA was then incubated at 23^{o}C for 10 min, 55^{o}C for 10 min before a final 80^{o}C heating stage for 10 min to inactivate the RT.

2.4.3. qRT-PCR

The NCBI primer basic local alignment search tool (BLAST) software was used to design qRT-PCR primers with minimal off-target regions (https://www.ncbi.nlm.nih.gov/tools/primer-blast/). There were set parameters (discussed below) used, so that all primers had similar conditions and could be used on the same qRT-PCR plate, with the same conditions. Primers with low levels of self-complementarity and no predicted off-target effects were selected. Primers that produced an amplicon of 75 – 200 base pairs were designed. A primer test was always performed to check the that the primer efficiency was between 90-110% following a set of known dilutions of complementary DNA (cDNA). The absence of primer dimers or abnormalities on the melt curve were also assessed. The primer test ensures that the primer is efficient at the concentrations of RNA that will be used in the relative expression experiments. See table 2.3 for the sequence of all primer pairs to be used in qRT-PCR.

For RNA that will also be used in qRT-PCR, the cDNA was diluted with 50 µl nuclease free water to allow for enough cDNA for the entire plate. 3 µl of cDNA is added to the respective well along with 10 µl SYBR Green Fast master mix (ThermoFisher; 4385612). 0.5 µl forward primer (10 µM); 0.5 µl (10 µM) reverse primer and 6 µl nuclease free water and mixed thoroughly. The PCR was immediately run to avoid the loss of the fluorescent signal intensity.

All primers were designed to have a melting temperature of between 57-63ºC, with an optimal temperature of 60ºC and a maximum 2ºC difference in the primer pair. All primers were designed to be between 75-200 base pairs. Consequently, all qPCR programmes were run with the same parameters:

- Initial 1X 95ºC: 30 Seconds
    - 95ºC: 1 Second
    - 60ºC: 20 Seconds
    - Following the initial 95ºC for 30 Seconds, the next 2 steps were repeated for 40 cycles

Technical triplicates of the same sample were performed to minimise pipetting error or anomalies from skewing data. At least biological triplicates were performed to increase the statistical power and avoid biological anomalies from skewing data. qPCR was performed using the QuantStudio 3 (Admiral; A28567) and the Livak method (Livak and Schmittgen, 2001) of $2^{-\Delta\Delta CT}$ was used for analysis. ΔCT was calculated by subtracting the cycle threshold (CT) value of *EF1*α (housekeeping gene) from the CT value of a target gene. The ΔCT of a reference gene is then subtracted from the average ΔCT of a target gene, from which the relative fold change difference for (ΔΔCT) (for example the ΔCT for wild type would be subtracted from the ΔCT of the mutant). $2^{-\Delta\Delta CT}$ was then used to calculate the fold change in expression. All statistical tests are performed on the untransformed ΔCT values.

Gene	Forward Primer	Reverse Primer
ZAKα	GGCACAGGACAAAAGGACTG	ATGTACGCTATCGCCACCTC
ZAKβ	CCGATCCTGCACTCCTCTGT	CCTCAGAGCTGTTGCTCTCC
Ef1α	TTGAGAAGAAAATCGGTGGT GCTG	GGAACGGTGTGATTGAGGGA AATTC
Myl1	CCCACCGCTGATGATATG GTA	CGAATACACGCAGACCCTCA
sMyHC	CAGGCTCCCAGAATG AGATTGAAG	AGCTTCATTCCTGCTGCGAG
Myogenin	ACTCAACCAGCAGGAGCA TGA	GTCGTCGTTCAGCAGATCCTC GT
Myomaker	GTCACGCTACTGGCGCTTG	CCCAGTCGGTCCTGGTAAATC
RUNX1	CGTCTTCACAAACCCTCCTCA	TAACGCGCCTGGCTTTACTG
KY	TGACCCTCATACATCCCAAGC	GAGCTCCTGTCTGGGGATCA
FLNCA	CCTTCGTGGGTCAGAAGAAC	GGAGTTCTAGGACCGTGGAC
FLNCB	GGCCCTACAAAGTGGACATC	CTTCAAACCAGGCCCATAAG
Bag3	TGCCCATTCAGATTCAACAG	GGCTGCTGTGTAGGTTGTTG

Table 2.3. qRT-PCR Primer sequences.

2.5. *In Situ* Hybridisation

In situ hybridisation (ISH) allows for tissue-specific expression of genes to be identified. Anti-sense RNA probes are generated, which incorporate Digoxigenin (DIG-UTP). These are hybridised to zebrafish embryos and the presence of DIG is detected using anti-DIG antibodies coupled with the enzyme alkaline phosphatase (AP). The AP is then provided with the substrate BM purple, where it catalyses the production of a permanent dark purple band allowing the mRNA location to be visualised.

2.5.1. Probe Synthesis

Primers used to make ISH probes were designed using NCBI Primer BLAST to ensure primer specificity (https://www.ncbi.nlm.nih.gov/tools/primer-blast/). The probes were designed to be between 300 – 700 base pairs and the amplicon sequence was subject to nucleotide blast (NCBI; Blastn) to avoid regions that could potentially bind to non-specific mRNA transcript in the embryo. See table 2.4 for details of the primers used to make the probes and the PCR conditions required.

cDNA was made from RNA extracted from 3 dpf wild type zebrafish embryos as per section 2.4.2. The PCR parameters in table 2.4 were followed generate the amplicon against which the probe is synthesised. The denaturing step was 98^{o}C for all PCR reactions and the final extension was for 10 minutes at 72^{o}C. The PCR was set up with 10 μl Promega 2X Taq mastermix; 1 μl forward primer (10 μM); 1 μl forward primer (10 μM); 7 μl nuclease-free water and 1 μl cDNA. All PCR reactions were run for 30 cycles. The presence of taq polymerase ensures a 3' adenine overhang, allowing the amplicon to be ligated into pGEM t-easy Vectors. 3 µl amplicon, 1 µl DNA Ligase; 1 µl PGEM t-easy vector and 5 µl 2X ligation buffer were gently mixed by pipetting and stored at 4^{o}C overnight. The same protocol for transformation of *E. coli* and miniprep seen in section '2.3.5 sequencing', and the orientation of the amplicon insert was checked by sequencing with the SP6 primer (table 2.2).

The plasmids were linearized with an appropriate restriction enzyme (see table 2.4). 3 µg of plasmid was added to 10 µl 10X restriction buffer (Buffer H (Roche; 11417991001)) for *NdeI* and rCutSmart buffer (New England biolabs; B6004S) for *NcoI*), 1 µl respective restriction enzyme and nuclease free water to a final volume of 100µl. The digestion time was 2 hours at 37^{o}C.

The linearized plasmid was made to 400 µl with addition of 310 µl nuclease free water. The diluted, linearised plasmid was purified using phenol chloroform extraction: an equal volume of phenol chloroform was added followed by centrifugation at 13,000 rpm for 5 minutes. The aqueous phase was transferred to an equal volume of chloroform, followed by centrifugation at 13,000 rpm. The aqueous phase was again transferred to a solution of 10% sodium acetate, 2.5X the existing volumes worth ethanol and precipitated at -20^{o}C overnight. The sample was spun at 13,000 rpm for 20 minutes before washing discarding the supernatant and washing the pellet with 200 µl 70% ethanol. The plasmid was spun again at 13,000 rpm for 5 minutes before discarding the supernatant and drying the pellet by vacuum desiccation. The pellet was resuspended in 25 µl molecular grade, nuclease free water.

The probes were synthesised using 1 µg clean linearised plasmid, 2 µl 10X transcription buffer (buffer H – unless the restriction enzyme is *NcoI*, where it is buffer tango), 10 mM Dithiothreitol (DTT), 1 µl correct RNA polymerase, DIG RNA labelling mix (Roche; 11277073910) and nuclease free water to a final volume of 20 µl. The transcription reaction was overnight at 37^{o}C. Following the transcription, the probes were precipitated by adding 300 µl 100% ethanol, 50 µl ammonium acetate and 50 µl nuclease free water and incubating overnight at -20^{o}C. The sample was then centrifuged at 13,000rpm for 30 minutes, followed by addition of 100 µl 70% ethanol, and centrifuging at 13,000rpm for 15 minutes. The probe was then vacuum desiccated to dry and remove residual ethanol before re-suspending in 50 µl deionised water ready for use in the ISH procedure.

Probe	Forward Primer	Reverse Primer	PCR parameters.	Restriction Enzyme	RNA Polymerase
ZAKα	GAGACCTGCGACACCTTCTC	GTCTTGCTCCAGTCCTCGTC	60^{o}C annealing temperature. 40 second extension	*NdeI* (NEB; RO111S)	T7 (Thermo Fisher; EP0112)
ZAKβ	TTTGCAGACCTGATGAGACG	CTTCTTGGCTTGCATGTTGA	60^{o}C annealing temperature. 1 minute extension	*NdeI* (NEB; 93193S)	T7
sMyHC	CAGGCTCCCAGAATGAGATTGAAG	AGCTTCATTCCTGCTGCGAG	60^{o}C annealing temperature. 40 second extension	*NcoI*	SP6 (Thermo Fisher; EP0131)
Myogenin	GCTTTTCGAGACCAACCCCT	GGACGACACCCCAGTATGTG	59^{o}C annealing temperature. 40 second extension	*NdeI*	T7
Myomaker	CCGACTGGGCTACGGCATTTACTC	CATCATACACAGCAGCAGAGGGT	56^{o}C annealing temperature. 30 second extension	*NdeI*	T7
SOX6	TACCTCGACCCCTGATGGAG	CATGGTGGAGAGTTGTCGCT	55^{o}C annealing temperature. 30 second extension	*NdeI*	SP6

Table 2.4. Forward and reverse primers, and PCR conditions used to generate probes for ISH.
Also detailed are the PCR parameters used to produce the amplicon, the restriction enzyme to linearise the plasmid and the RNA polymerase used to synthesise the probe.

2.5.2. ISH Procedure

Embryos from a lay were grown in zebrafish E3 media (5mM NaCl; 0.17 mM KCl; 0.33 mM $CaCl_2$; 0.33 mM $MgSO_4$ and 0.0001% Methylene Blue), supplemented with 0.6 g/L PTU, which is known to inhibit the melanisation of embryos post 24 hpf (Karlsson *et al.*, 2001), making the imaging considerably easier further downstream. Embryos were transferred to a dish containing fresh media and PTU daily. At the appropriate day of development, up to 60 embryos were placed in a glass vial containing 15 ml MEMFA (0.1 M MOPS, 2 mM EGTA, 1 mM magnesium sulphate, 10% formaldehyde) to fix through rolling for one hour, before removal of the liquid and replacement with 15 ml methanol. The embryos were rolled for 15 minutes before replacement with fresh methanol and storing at -20^{o}C until used in the protocol.

The embryos were gradually re-hydrated in PBST (140 mM NaCl; 2.7 mM KCl; 10 mM Na_2HPO_4; 1.8 mM KH_2PO_4; 0.01% Tween20), using initially 25% PBST in methanol and rolling the embryos for 10 minutes. 15 ml of 50% PBST in methanol replaced the previous solution and the embryos were again rolled for 10 minutes. The embryos were then subject to 3X 5 minute washes in PBST to remove excess methanol. Proteinase K was used to make the membrane of the embryo more permeable allowing the probe to pass more readily into the embryo. Proteinase K was added to 10 ml PBST to produce a final concentration of 10 µg/ml followed by gentle agitation for up to 10 minutes per day post fertilisation (dpf). The embryos were acetylated by subsequent washes of 5 ml 0.1 M triethylamine, followed by 2.5% acetic anhydride in 5 ml 0.1 M triethylamine and finally 5% acetic anhydride in 5 ml 0.1 M triethylamine. A buffer exchange into PBST (2 washes) was performed prior to re-fixing in 10% formaldehyde in PBST and leaving to fix for 20 minutes on a roller at room temperature. A further buffer exchange back into PBST was performed (5 washes). Embryos were heated at 60^{o}C for 2 hours in 1 ml Hybridisation buffer (100 µg/ml heparin; 10 mM EDTA; 0.1 CHAPS; 0.1% Tween20; 50% Formamide; 5X SSC buffer; 1X denharts) supplemented with 2% yeast RNA (pre-boiled at 80^{o}C) in a 1.5 ml eppendorf. Hybridisation buffer containing 4% v/v of pre-heated probe (probe was heated at 80^{o}C for 3 minutes before use in hybridisation buffer) replaced the existing buffer and the embryos were left to incubate overnight at 60^{o}C at a gentle agitation.

Excess probe was washed off by 2X 10-minute washes in 1 ml hybridisation buffer at 60^{o}C before 3X 20-minute washes in 1 ml 2X saline sodium citrate (SSC) buffer (Sigma; S6639 - supplemented with 0.1% tween) at 60^{o}C. 3X 30-minute washes in 1 ml 0.2X SSC (0.1% Tween) at 60^{o}C before washing twice with 1 ml MABT buffer (0.05 M maleic acid; 0.07 M sodium chloride; 0.1% v/v Tween 20) at room temperature with gentle agitation. A pre-incubation solution containing 2.5% BMB; 20% heat-treated lamb serum; 1X MAB was made and the embryos were incubated in 1 ml of pre-incubation solution for 2 hours. 0.5 μl anti-digoxigenin-AP fragmented antibodies (Roche; 11093274910) was added to 1 ml of fresh pre-incubation buffer (forming incubation solution) and was added to the embryos following 2 hours of pre-incubation. The embryos were incubated with the incubation solution overnight at 4^{o}C with gentle rolling to keep the embryos from clumping together and the pre-incubation solution mixed.

The incubation solution was removed from the embryos by 3X 5-minute washes in MABT before transferring to a 6 well plate. The embryos were then subject to 3X 1-hour washes in MABT with gentle agitation. The embryos were then washed in 10 ml alkaline phosphatase (AP) buffer (100 mM tris base; 100mM NaCl; 50 mM $MgCl_2$; 0.1% Tween 20) for 3 minutes and then a further 15 minutes with fresh AP buffer. AP buffer was removed by aspiration and fresh 1 ml BM purple substrate (Roche; 11442074001) was then added and the embryos were left to develop. Once regions of high mRNA expression have been identified by comparatively deeper colour change, the colorimetric reaction is terminated by 2X 10-minute washes in 10 ml PBST before re-fixing the embryos by rolling in 10 ml MEMFA in a fresh glass vial for 1 hour and then storing in fresh MEMFA until imaged.

Images were captured using Spot Insight Firewire camera (Diagnostic Instruments inc., 239037), which was magnified using a microscope (Leica; MZ75).

2.6. Western Blot

2.6.1. Protein Extraction

The samples were prepared differently depending on the size of the tissues. All samples (embryos and adult tissue) were homogenised on ice with glass borosilicate homogenisers (Fisherscientific; 11522443), using Phosphosafe extraction buffer (Novagen; 71296-3) until homogenous and there was minimal debris present. It should be noted that skeletal muscle and heart require substantial homogenisation for effective protein extraction. The following volumes of Phosphosafe were added to each sample:

- Zebrafish embryos (5 embryos per sample): 100 μl Phosphosafe
- Adult Heart: 100 μl Phosphosafe
- Adult skeletal muscle: 200 μl Phosphosafe

The lysates were centrifuged at 13,000 rpm for 7 minutes before transferring supernatant to a fresh tube. An equal volume of 2X sample buffer (150 mM tris; 20% Glycerol; 4% SDS; 10% β-mercaptoethanol) was added to each sample, followed by heating at 95^{o}C for 5 minutes.

2.6.2. SDS Polyacrylamide Gel Electrophoresis (PAGE)

The samples were briefly centrifuged at 13,000 rpm for 1 minute before loading onto the SDS Polyacrylamide gel (PAGE). An appropriate amount of sample was added following an initial test and ponceau (Sigma; P7170) stain of the membrane prior to performing the experiment. 10 μl of Pageruler Plus Protein ladder (Thermofisher; 26619) was added per gel to allow for an estimation of the molecular weight of the protein. The gel was comprised of two layers: a 12% resolving gel (0.5 M tris (pH 8.8); 0.1% SDS; 5 mg/ml APS; 0.3 mg/ml TEMED; 12% acrylamide) and a 4% stacking gel above (125 mM tris; 0.1% SDS; 5 mg/ml APS; 0.3 mg/ml TEMED; 4% acrylamide). When making the resolving gel, water saturated butanol was added on top of the gel, to ensure no bubbles and that the gel is flat at the top. The water saturated butanol was removed prior to addition of the stacking layer.

Running buffer (3g/L Tris base; 14.4g/L glycine and 0.1% v/v SDS) was added to the tank and the SDS PAGE was run at 180V for one hour (or until sufficient

ladder had run off, if resolution/separation of 2 proteins of similar-size molecular weight is required).

2.6.3. Protein Transfer

Polyvinylidene difluoride (PVDF) membrane (Millipore; IPVH00010) was activated in methanol for 15 seconds before rinsing with water and transferring to the transfer buffer (3g/L Tris base; 14.4g/L glycine; 10% v/v methanol) for 5-15 minutes. Foam pads and filter paper (Whatman; 10426981) were also pre-soaked in transfer buffer prior to transfer. Once the ladder on the SDS PAGE gel had run to a sufficient level, the electrophoresis was terminated, and the gel was soaked in transfer buffer for at least 10 minutes. The transfer was set up with filter paper on the outside of the gel and membrane, and foam squares flanking the filter paper.

A wet protein transfer was performed to transfer the migrated proteins from the SDS gel to a membrane: The protein from the SDS PAGE gel was transferred to the membrane using a current of 85V of current for two hours in transfer buffer. Ice packs were used to keep the transfer buffer cool and were routinely changed every 30 minutes.

2.6.4. Probing Membrane

Following the transfer of proteins from the membrane, it was blocked in 5% w/v milk powder (Marvel) in PBST (0.137 M NaCl; 0.0027 M KCl; 0.01 M Na_2HPO_4; 0.0018 M KH_2PO_4; 0.1% Tween20) for one hour at room temperature. The primary antibody was diluted appropriately in 5/10 ml fresh blocking solution (see table 2.5), the membrane added and left rolling overnight at 4^{o}C. The membrane was washed in 200 ml PBST 6 times, with fresh PBST added after each 15 minutes. The membrane was blocked for 45 minutes at room temperature before adding appropriately diluted secondary antibody (see table 2.5) in fresh blocking solution and leaving for one hour, rolling, at room temperature. The membrane was then subject to 6X 15 min washes with PBST before adding chemiluminescence substrate (Merck; WBKL50100) and exposing on photography film (Insight Biotechnology; sc-201696) using the XOgraph (Konica Minolta Medical and Graphical, inc.; SRX-101A) to develop the photography film. Figures were made by cropping scanned photography film using Adobe Photoshop CS3.

Antibody and type	Species Raised	Dilution	Manufacturer Details
Dp-ERK 1 and 2 (primary)	Mouse	1:4,000	Sigma (M9692)
Total ERK (primary)	Rabbit	1:100,000	Sigma (M5670)
p-P38 (primary)	Rabbit	1:2,000	Cell Signalling Technologies (9211)
p-AKT (primary)	Rabbit	1:2,000	Cell Signalling Technologies (9271S)
Anti-mouse horseradish peroxidase (HRP)-conjugated (secondary)	Goat	1:10,000	Jackson laboratories (115-035-174)
Anti-rabbit HRP-conjugated (secondary)	Donkey	1:2,000	Cell Signalling Technologies (7074)

Table 2.5. Antibodies used in western blot experiments.
Also detailed are the species they were raised in, the dilution of antibody and manufacturer details. There is also mention of whether the antibody is a primary or a secondary antibody.

2.7. Methylcellulose Stress Treatment of Zebrafish Embryos

Zebrafish are raised, as normal, in E3 media until 5 dpf, when zebrafish larvae are transferred to 0.6% or 1% methylcellulose supplemented E3 media. The larvae are collected at 8 dpf, as per the optimised protocol to damage defective muscle (Hall *et al.*, 2007b; Ganassi *et al.*, 2018). A maximum of 30 embryos per methylcellulose dish allows sufficient space for larval zebrafish to swim. At 8 dpf the larval zebrafish are either immediately fixed in 4% Paraformaldehyde (PFA) for analysis on confocal microscopy (see section 2.9) or flash frozen in liquid nitrogen and stored at -80^{o}C for use in qRT-PCR and western blot for analysis of transcription and protein expression changes, respectively.

2.8. cDNA Sequencing

Zebrafish are known to have nonsense-mediated decay (NMD)-evasion mechanisms including exon skipping, cryptic splice sites and intron inclusion (Anderson *et al.*, 2017). This is discussed in greater detail in chapter three. Consequently, whilst there is a premature stop codon at the genomic level, it is important to assess that the mRNA is transcribed as predicted and it does not evade NMD by one of the mechanisms discussed. To do this, primers in exon 1 (prior to the CRISPR target region in exon 2) and exon 12 for both ZAKα and ZAKβ were designed. See table 2.6 for primer sequences. The cDNA was amplified using these primers with a large extension time, to ensure that any small introns included could be detected.

RNA was extracted from 3 and 6 dpf embryos from the respective single mutant line and cDNA was synthesised. Using the respective primers and PCR conditions in table 2.6, the cDNA was amplified. The PCR product was then ligated into pGEM t-easy plasmid (see 2.3.5. for further details) and *E. coli* was transformed. Individual colonies were selected for overnight culture and the plasmids were extracted and purified using the Qiagen DNA miniprep kit as per manufacturers protocol (Qiagen). The plasmids were then sent for sequencing using SP6 primer (table 2.2) and the sequence was analysed against the predicted mutant genomic sequence.

Gene	Forward Primer	Reverse Primer	PCR Conditions
ZAKα	ATGGCATCTC TGGGCAGCTC	CTTCAAAGATCT GCTCCATCCAG	Denaturing temp: 95^{o}C Annealing temp: 53^{o}C Extension time: 90 seconds Cycles: 30
ZAKβ	ATGACTGGGA TTGTTCATAG	CTAATCGCTGT CGTCGTCAGAC	Denaturing temp: 95^{o}C Annealing temp: 56^{o}C Extension time: 110 seconds Cycles: 30

Table 2.6. Forward and reverse primers used for amplification of *ZAKα* and *ZAKβ* cDNA. The PCR conditions for each primer pair is also included.

2.9. Confocal microscopy and Image Acquisition

ZAKβ$^{-/-}$ zebrafish were successfully crossed into a range of transgenic lines (see table 2.7).

Transgenic Line	Phenotype	Reference
Tg (Acta1:Lifeact-GFP; mCherry(CAAX))	Lifeact-GFP is a 17 amino acid actin-binding peptide fused with a green fluorescent protein (GFP) tag, that allows the location of actin to be visualised (Riedl *et al.*, 2008). mCherry(CAAX) allows visualisation of the sarcolemma through the CAAX tag. Both fluorescent tags are under the Acta1 promoter.	(Berger *et al.*, 2014)
Tg (mpx:GFP)	Myeloperoxidase (also known as MPO or MPX) is an enzyme primarily expressed in neutrophils (polynuclear granulocytes that form part of the innate immune response). Expression of the MPX gene is restricted to neutrophil and neutrophil precursors (Bennett *et al.*, 2001). The mpx:GFP transgenic line express GFP under this promoter.	(Renshaw *et al.*, 2006)

Table 2.7. Transgenic lines crossed with ZAKβ$^{-/-}$ zebrafish.
Details of the accompanying phenotype of the transgenic line has also been included, along with details of the Lab who created the Transgenic zebrafish line.

The transgenic zebrafish embryos following the appropriate condition or dpf are fixed for one hour by rolling in 4% PFA. The embryos are then transferred to a fresh glass vial containing 10ml PBST and 10 μg/ml Hoechst H33258 (Sigma; B2883) and incubated, whilst rolling, at 4^{o}C overnight to allow sufficient time for penetration of the nuclei stain. The fixed and stained embryos are placed on a glass coverslip and mounted in 0.8% low melting temperature agarose (LMA) (Promega; V2111), positioned on the side, with the dorsal side facing north and the anterior end facing west, ready for imaging. The coverslip is added to a glass slide along with two layers of 0.36mm double sided secure seal adhesive sheets (Sigma; GBL620003), to avoid the coverslip and glass side crushing the embryo. Details of the imaging analysis, for each respective transgenic line can be seen in sections 2.9.1 and 2.9.2.

The Zeiss laser scanning confocal microscope (LSM880) was used to image fluorescence across the Z-plane. A 25X lens (LD LCI Plan Apochromat 25x/0.8 1mm Corr DIC M27) set to a water immersion was used. 8X averaging was used for the Tg (Acta1:lifeact-GFP; mCherry(CAAX)) zebrafish line to provide resolution capable of distinguishing ultrastructure and Z-discs/M- bands, allowing for analysis of sarcomere length spacing. Graphics detailing how to calculate these parameters are seen in section 6.2.2. GFP-labelled neutrophils were easily identified, so only 1X averaging was required.

Optimisation of the protocol and parameters for confocal analysis was done alongside Grant Calder; Department of Imaging and Cytometry; Technology Facility; University of York.

2.9.1. Imaging Tg: (Acta1:lifeact-GFP; mCherry(CAAX)) ZAKβ$^{-/-}$ Zebrafish

Much of the analysis was inspired from research by (Ganassi *et al.*, 2018), where fusion of muscle fibres in a myogenin (*Myog*$^{-/-}$) mutant zebrafish was assessed, using the same transgenic line. Wild type and ZAKβ$^{-/-}$ zebrafish embryos at the correct dpf were fixed, and prepared for imaging, as described in section 2.9. The anal vent was used as a reference to ensure that somites 17/18 were always used for analysis.

The number of nuclei across each fibre in the somite was counted to assess any differences in the fusion capabilities of ZAKβ$^{-/-}$ embryos versus wild type.

A cross section of the Z planes, across three separate equally spaced distances across the somite were reconstructed. From this the myotome volume can be calculated. The myotome volume is the average cross-sectional area of the myotome multiplied by the length of the somite. The individual fibre bundle area can also be calculated with in the cross-sectional reconstruction, using the midline of the somite.

The sarcomeric spacing or sarcomere length was calculated by calculating the distance between the troughs of fluorescence in intensity of GFP signal, which correlates to the M band. This is to assess any changes to the ultrastructure of the muscle fibres.

2.9.2. Wound Assay using Tg: (MPX:GFP) ZAKβ$^{-/-}$ Zebrafish

This wounding assay is based on a wounding protocol developed by (Gurevich *et al.*, 2016; Montandon *et al.*, 2021).

4 dpf embryos were anaesthetised (0.0016% v/v MS-222 in E3 medium) and a single puncture wound at a 75^{o} angle was performed to the epaxial muscle, above the cloaca, using a 30-gauge hypodermic needle. The embryos were returned to fresh E3 media and left to recover. Figure 2.1 demonstrates all the stages in the procedure.

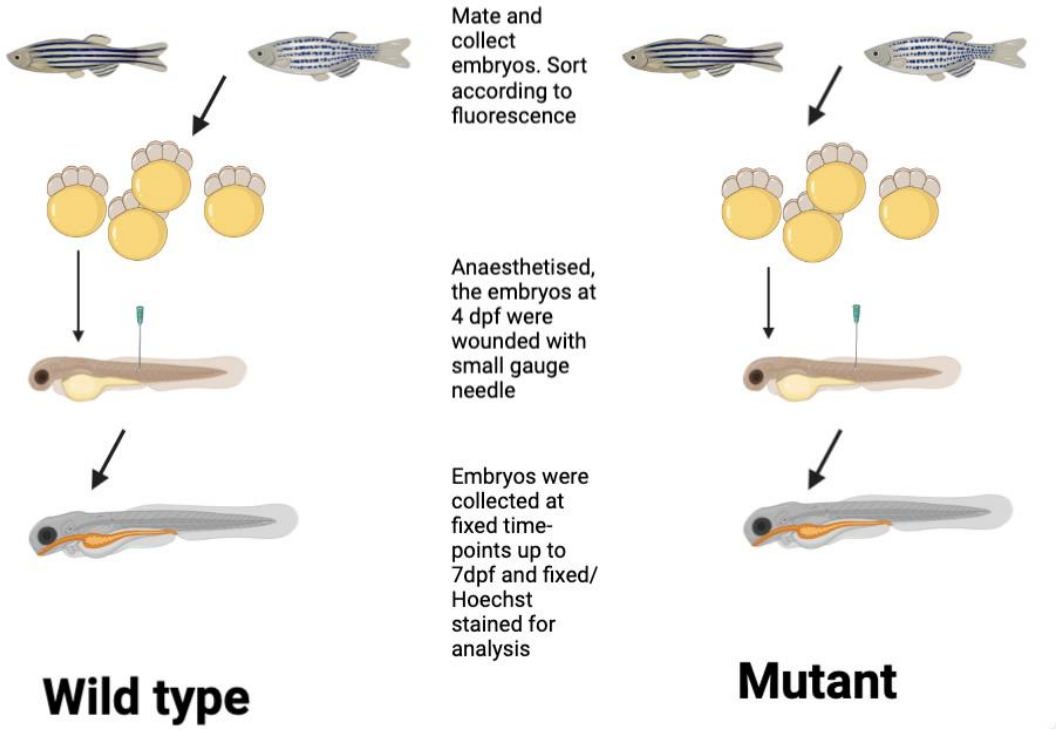

Figure 2.1. Stages of the wounding assay.
Wild type and ZAKβ$^{-/-}$ embryos are raised in E3 media until four days post fertilisation (dpf), at which they are wounded with a single puncture wound with a 30-gauge hypodermic needle. At time-points of 1 hour post injury (hpi), 8 hpi, 24 hpi and 72 hpi, the embryos were collected, fixed and imaged. Figure made using the software Biorender.

Embryos were fixed and imaged, at the following timepoints: 1 hour post injury (hpi), 8 hpi, 24 hpi and 3 days post injury (dpi), using the protocol from earlier in section 2.9. The number of nuclei at the wound site was recorded as well as the number of nuclei on the same somite in un-injured embryos as a control.

The wounding procedure is performed blind to avoid potential bias in the severity of the wounding.

2.9.3. Analysis

All images, from both transgenic lines, were processed using FIJI (Fiji is Just Image J 2 – a modified version of image J with additional plug ins). All graphs and figures, as well as statistical analysis was performed using GraphPad Prism 9.0.

2.10. Measurements of Zebrafish

Sibling zebrafish (ZAK$\beta^{+/-}$ and ZAK$\beta^{-/-}$) were raised in the same tank until 15 weeks post fertilisation. Individual fish were assigned a number for identity and were anaesthetised in MS-222. The mass of each zebrafish was measured by briefly drying the zebrafish before adding to a beaker containing zebrafish system water and measuring on scales. The size of the zebrafish was calculated by taking images of the anaesthetised zebrafish alongside a ruler (mm) for scale. A fin clipping was taken from each zebrafish so that the genotype could be determined. DNA was extracted from the fins prior to PCR amplification and heteroduplex assay, as per section 2.3.4, using the ZAKβ primer pair in table 2.1. The respective mass and length of the zebrafish was matched to the genotype allowing sibling and mutant to be compared.

The height was always measured anterior to the anal fin (HAA) as per (Parichy *et al.*, 2009) and (Jokl *et al.*, 2018b). The zebrafish length was always measured from the tip on the jaw/snout to the base of the tail, anterior to the caudal fin (Parichy *et al.*, 2009). The tail area is calculated by multiplying the length of the tail (the length extending from the HAA line to the base of the tail) by the HAA.

To standardise the weight against the length, Fulton's conditioning factor (K) was used (Fulton, 1904; Froese, 2006). K = mass (g) X length $(cm)^{-3}$ X 100. As reviewed in (Jones *et al.*, 1999), the equation assumes isometric growth for effective normalisation to length. Nevertheless, it remains an important and widely used formula for assessing changes to the weight of fish, independent of length. Body mass index (BMI) was estimated by the following formula: BMI = mass (g) X length $(cm)^{-2}$ (Ganassi *et al.*, 2018; Latha Ramalingam, 2021).

2.11. Tactile Strength Assay

The protocol is modified from (Hirata *et al.*, 2007b; Hirata *et al.*, 2012). An embryo was placed on glass slide, with minimal E3 media. A droplet of 2% LMA in E3 media, melted and cooled to 40^{o}C, was transferred onto the embryo. The embryo was quickly orientated with forceps with the dorsal side facing the camera, ventral side facing the glass slide and the anterior end facing north. LMA surrounding the tail up to the yolk sac was carefully removed and replaced with E3 media, leaving the tail free to move but the head still embedded. Using a micromanipulator for stability, the embryos were gently provided with tactile stimulation from a 30-gauge hypodermic needle. Figure 2.2 is a cartoon demonstrating all steps.

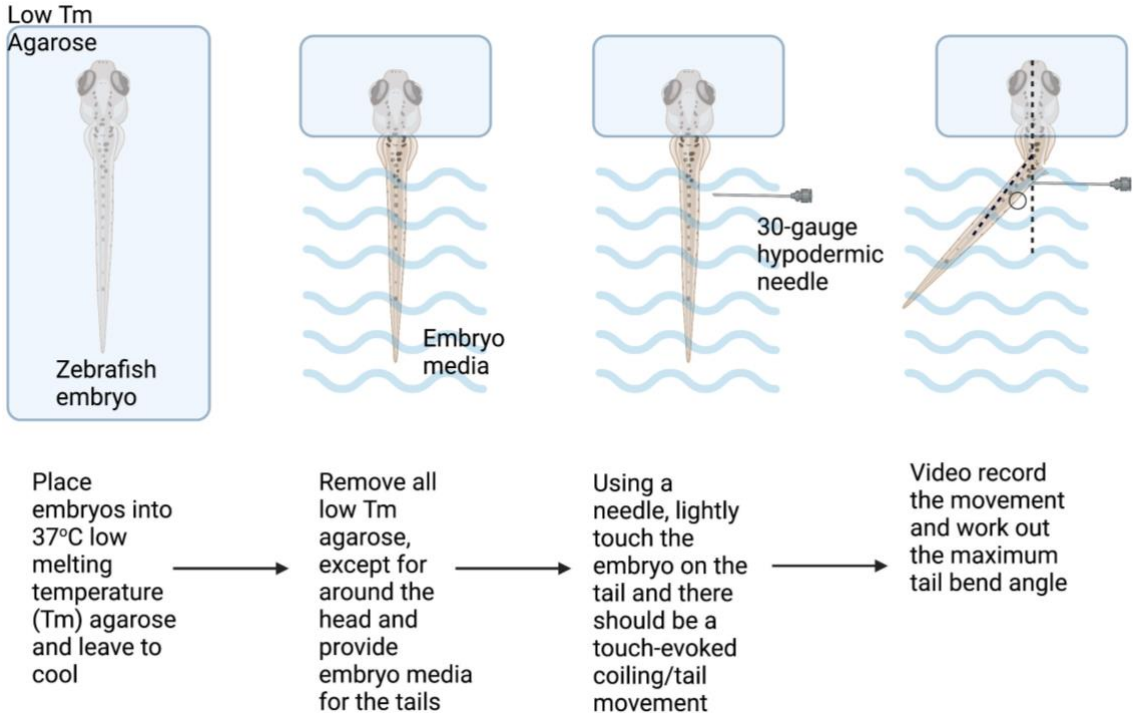

Figure 2.2. Schematic of the steps in the tactile strength assay.
Embryos are embedded in low Tm (melting temperature) agarose. The low Tm agarose is removed from the tail region and replaced with embryo media. The head region remains embedded in low Tm agarose. Using a 30-gauge hypodermic needle, the tails are gently stimulated and will evoke an escape movement. The touch-evoked movement is recorded, and the maximum tail bend angle is determined using FIJI. Image created using Biorender.

A video recording of the movement following tactile stimulation was processed, with individual frames captured using VirtualDub (Available: http://www.virtualdub.org/) and superimposed using FIJI. The maximum angle of the tail bend (caudal trunk angle) was also calculated by using Image J. Bar charts were created using Graphpad Prism 9.0.

2.12. Investigation into Adult Zebrafish Mobility and Locomotion

The protocol was devised and used by Gideon Hughes, 2020, to discern a movement phenotype in adult zebrafish lacking the Parkinson associated gene, DJ-1 (Hughes *et al.*, 2020). Zebrafish are placed in breeding tank, modified with a non-reflective plastic insert covering the base and a hollow cone on top to reduce reflections/shadows on the side of the breeding tank, keep zebrafish in frame and ensure an equal distribution of light. A GoPro Hero 3 Black Edition (GoPro, San Mateo, CA, USA) camera was placed on modified lid, with a hole cut for the lens, enabling the camera to record form above, through the top opening of the hollow cone. The modified breeding tank is kept on a shelf for the duration of filming to prevent disturbances during filming. The tank contains 200 ml of normal fish tank water. Using a net, individual zebrafish are placed into the tank and left to acclimatise for 10 minutes before filming for 5 minutes. A 30 second clip from the initial 2 minutes, 30 seconds and a 30 second clip from the last 2 minutes, 30 seconds was processed. Each fish recording generates 2 different movement data, increasing the amount of data available for comparison. A recording of the tank without a zebrafish present was used as a background for subtraction. Figure 2.3 (a) shows the set-up of the recording tank and figure 2.3 (b) shows the representative birds-eye view recording of the zebrafish.

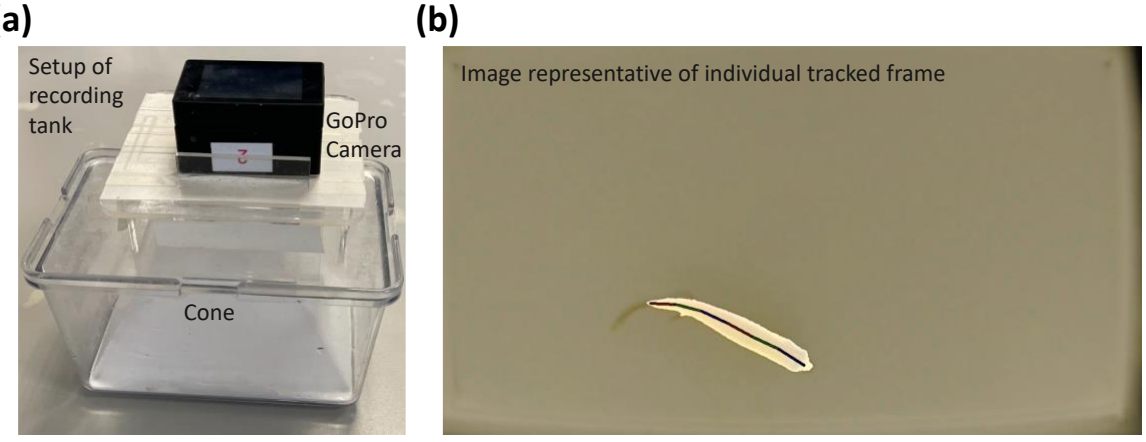

Figure 2.3. Setup of the recording tank for adult zebrafish swimming analysis.
(a) Shows the configuration of the modified recording tank. The GoPro is on a raised platform, where it can record the zebrafish from a birds eye perspective. The zebrafish is contained within the cone, which contains an opening, ensuring equal light displacement and the fish to be in frame at all times. Zebrafish are kept in 200ml zebrafish water. (b) A representative individual tracked frame of the zebrafish recording following the processing of a 30 second clip using shadowfish. Note, the accurate recognition of the zebrafish and the plotting of seven equal X,Y co-ordinates across the spine of the zebrafish.

The movement of the zebrafish is processed by a tracking software, called 'ShadowFish', developed by Matthew Bedder, a former student in the Pownall Lab. The ShadowFish software extracts, at each frame, the X and Y co-ordinates of seven equally spaced points along the spine, from tip of head to base of tail, allowing a bending angle across all points to be determined. Figure 2.3. (b) shows the accurate location of the spine being tracked. The software automatically determines the lateral orientation of zebrafish by the movement direction. It is important to inspect each 30 second recording, to ensure the fish remain in frame and no unexpected shadows are present, that the software could mistake as the co-ordinates of the fish. The extracted raw data output is saved as a comma separated values (CSV) file.

A MATLAB (MathWorks; Natick; MA; USA) code is used to process the tracked data. The code was initially produced by Gideon Hughes, however, I modified it to accommodate the 120 frames per second (fps) of the GoPro, rather than the previous 100 fps. The modified code can be seen in Appendix A. A range of features are studied from the extracted and processed raw data:

- Distance travelled
- Percentage of Time Spent Moving
- Swimming Episode Duration
- Mean Velocity
- Tail Beat Frequency (low, medium and high)
- Tail Bend Amplitude (low, medium and high)

Pythagoras theorem ($a^2 + b^2 = c^2$) was used on the co-ordinates after every 120 frames, to estimate the distance of movement that had taken place within one second. Only movement of greater than 5 mm per second was classified as movement – anything less than 5 mm per second was classed as stationary. The swimming episode duration is the number of seconds that the fish spend moving before a stationary period. The mean velocity was determined from the total distance that the zebrafish made during the 30 second clip by the number of seconds that the fish were actively moving. The total number of tail beats identified per second is the tail beat frequency. The sum of the angles from the seven equally-spaced points, during the peak of the tail bend, was used to determine the tail bend amplitude. Further to the total mean tail beat frequency and amplitude, both tail beat frequency and amplitude of fish swimming at

different speeds were studied: low speed (0.5≤X<2 cm/s), medium speed (2≤X<4 cm/s) or high speed (≥4 cm/s).

All video recordings taken with the GoPro were at 1280 X 720 pixels with 120 frames per second (fps) on the 'narrow' lens option. The 120 fps differs from the 100 fps written on the MATLAB script so I had to modify the script to take this into account. When multiple genotypes were in the same tank, all recordings were done blind. The recordings of the zebrafish moving were done prior to fin clipping and genotyping. Fin clipping prior to recording could result in the fish swimming aberrantly.

2.13. Heart Analysis using Video Analysis

Zebrafish were set up to mate and the embryos were collected, with a maximum of 80 per dish, and were grown in E3, as normal (See section 2.2. Zebrafish Husbandry). Across 1 – 6 dpf, a sample of embryos were placed into a dish containing 0.0016% v/v MS-222 in E3 media. Administration of MS-222 was essential in order to record the larvae for 1 minute, without swimming away or moving. It is important to note that the administration of MS-222 anaesthetic has been shown to reduce heart rate. To mitigate any differences in heart rate across mutant lines being the result of anaesthetic, all zebrafish embryos were given the same concentration (0.0016% v/v) of MS-222. All embryos were immediately recorded for 1 minute following immobilisation and all embryos of differing genotypes were processed in the same anaesthetic dish on the same day, increasing the likelihood that changes in the heart rate across the different lines are the result of the genotype and nothing in the environment. Ensuring the developing heart was clearly in view, the heart rate was measured across the full minute of recording for each zebrafish.

2.14. Transmission Electron Microscopy Sample Preparation and Analysis.

3X aged adult ZAK$\beta^{-/-}$ zebrafish (37 months) and age matched AB wild type (36 months) controls were euthanised in benzocaine. Small muscle dissections were carefully and immediately taken from the adult and added to fixative (2% glutaraldehyde, 2% paraformaldehyde on 0.1 M sodium phosphate buffer (pH 7.4)). The muscle dissections were approximately 1 mm X 2 mm allowing ease of identifying orientation. The samples were fixed for one hour.

Once samples were fixed, the remaining sample preparation, sectioning and imaging was performed by Dr Clare Steele-King, technology facility, Imaging and Cytometry Department, University of York. Following fixing for one hour, the dissected muscle was washed (2X 10 minutes) in 0.1 M sodium phosphate buffer before a secondary fixing for one hour in 1% osmium tetroxide on ice. The dissected muscle was washed (2X 10 minutes) in 0.1 M sodium phosphate buffer before dehydrating in a graded ethanol series before infiltration and embedding on Spurr's resin. The resin was polymerised by heating for 8 hours at 65^{o}C.

70nm ultrathin resin sections (pale gold) were cut using the Leica UC7 Ultramicrotome and then collected on copper grids. The resin sections were then stained with 2% uranyl acetate in ethanol and Reynold's Lead Citrate.

The samples were viewed with a FEI Tecnai 12 BioTWIN G2 TEM operating at 120kV, and a SIS CCD camera. Images were performed by Dr Clare Steele-King, with support and guidance from myself.

2.15. Statistical Software

Graphs were produced using Graphpad Prism 9. Statistical analysis was performed using either SPSS or Graphpad Prism 9. Confocal analysis of embryo length, myotome volume and muscle fibre cross sectional area were performed using FIJI. FIJI was also used to calculate the maximum tail bend angle with the tactile strength assay.

3. Generating a Line of Zebrafish that Lack ZAKα

3.1. Introduction

Model organisms, including zebrafish, can be useful in the study of human disease. Creating a disease model by disrupting a gene orthologous to a known disease-causing gene in humans, has recently been simplified with the advent of CRISPR-Cas9 technology. Using a model organism allows for an investigation into the molecular basis and pathogenicity of the disease. Furthermore, in zebrafish particularly, there is also the downstream application of high throughput drug screening to identify novel targets to treat disease. In the case of ZAK, the two splice isoforms (ZAKα and ZAKβ) in humans, derive from separate genes on different chromosomes in zebrafish, making zebrafish a useful model organism to better understand the role of each isoform individually.

3.1.1. Teleost Whole Genome Duplication Event

In humans, as many as 95% of genes with multiple exons can be alternatively spliced (Pan *et al.*, 2008). A whole genome duplication event (WGD) in the teleost ancestor occurred around 350 million years ago, which consequently means that it is not uncommon to find two non-allelic genes in zebrafish, that have only one copy in terrestrial vertebrates (Amores *et al.*, 1998; Taylor *et al.*, 2003; Hoegg *et al.*, 2004). Although up to 80% of duplicated genes are lost to non-functionalisation (Nadeau and Sankoff, 1997; Postlethwait *et al.*, 2000), many undergo neofunctionalization or sub-functionalisation to increase protein diversity (Force *et al.*, 1999). Sub-functionalisation describes the process through which different gene functions under the control of different DNA regulatory elements become subdivided between the two genes (Force *et al.*, 1999). Neo-functionalisation describes the process whereby mutations in one copy of the gene results in beneficial, additional functions and a novel role, while its paralogue maintains the original function (Force *et al.*, 1999; Sidow, 1996; Soukup, 1974).

3.1.2. *ZAK* Expression in Adult Tissues

In humans and mice, ZAKβ is the predominant isoform with expression levels approximately 10-fold greater than ZAKα (Gross *et al.*, 2002; Nordgaard *et al.*, 2022). ZAKβ is the ZAK isoform exclusively expressed in skeletal muscle (Vasli *et al.*, 2017) and ZAKβ is also expressed in hearts of adult humans (Gross *et al.*, 2002). ZAKα is enriched in the liver of humans and mice (Gross *et al.*, 2002; Nordgaard *et al.*, 2022).

3.1.3. Different Forms of Gene Targeting

Antisense morpholino oligonucleotides have been widely used in zebrafish to investigate gene function by post-transcriptionally disrupting the mRNA transcript by interfering with the translation or splicing (Bassett and Currie, 2003). The modified antisense oligonucleotides are injected into zebrafish embryos at the 1-8 cell stage, where they bind to and knock down the target RNA. (Nasevicius and Ekker, 2000). The use of morpholinos, however, are not heritable, can result in off-target disruption, and only produce transient effects – typically only the first few days of development can be studied (Bill *et al.*, 2009; Bedell *et al.*, 2011). Morpholinos also often fail to completely prevent protein production, with low levels still being detected. This is problematic as the low protein levels might still be able to function efficiently, preventing the full phenotype (Bill *et al.*, 2009; Eisen and Smith, 2008). By using gene editing, *ZAK* genes can be disrupted in a permanent and heritable way. Different forms of gene editing exist, namely zinc finger nucleases (ZFN's), transcription activator-like effector nucleases (TALENS) and cluster regulatory interspaced short palindromic repeats (CRISPR)-Cas9.

ZFNs are enzymes with a Fok1 endonuclease domain, customised to cut DNA at a specific location; the DNA repair mechanism is error prone and insertions/deletions (INDELs) can be identified by genotyping (Ekker, 2008; Porteus and Carroll, 2005). The INDELs can cause frameshift mutations, premature stop codons and absence of the protein through nonsense-mediated decay (Rodgers and McVey, 2016). A pair of ZFN's are required to generate the dsDNA breaks, decreasing the likelihood of off target effects (Cathomen and Keith Joung, 2008). Efficiencies of mutations of up to 33% using ZFNs have been reported (Meng *et al.*, 2008).

TALENs consist of a Fok1 restriction enzyme site (like ZFNs) and a site-specific DNA binding domain, consisting of repeats of 33-35 amino acids, which each recognise a specific nucleotide at the target gene using TAL effector repeat domains from *Xanthomonas* (Moore *et al.*, 2012; Hwang *et al.*, 2014). Like ZFN's, a pair of customised TALENs are required to produce the dsDNA breaks, necessary for the error prone NHEJ and potential INDEL mutations to form (Joung and Sander, 2013). TALENs have been shown to be effective with high efficiencies of creating INDELs in zebrafish of up to 76% (Cade *et al.*, 2012).

CRISPR-Cas9 technology, however, offers a more straightforward and cheaper approach to TALENs and ZFNs (Hwang *et al.*, 2013; Gupta and Musunuru, 2014). Designed RNA (called guide RNA (gRNA)) guides bacterial Cas9 endonuclease to the DNA site, where it can form double stranded DNA breaks; the non-homologous end joining is error prone and can introduce INDELs (Ran *et al.*, 2013). The major limitation of using CRISPR are that it can have high off-target effects by not having two parts (unlike TALENs and ZFNs), and the complementary sequence is typically under 25 base pairs in length, increasing the likelihood of binding to non-specific regions (Gupta and Musunuru, 2014; Liu *et al.*, 2019). The ease of the process, and the ability to outcross CRISPR-generated mutants with wild type zebrafish make this less of an issue and is why I chose CRISPR-Cas9 as my method to produce ZAK null zebrafish. Prior to starting, the *ZAKβ* gene in zebrafish had been targeted using CRISPR-Cas9. The result was a net 33 base insertion containing a premature stop codon. This thesis characterises this line.

3.1.4. Zebrafish NMD Evasion Strategies

Zebrafish also have the ability to detect deleterious mutations and through molecular mechanisms of mRNA processing, evade nonsense-mediated decay. (Anderson *et al.*, 2017) demonstrated in five out of seven mutant lines, various mechanisms of evading nonsense-mediated decay, including: exon skipping; cryptic splice sites; inclusion of pseudo exons, within introns; and intron inclusion for smaller introns. Provided the mRNA processing results in retaining frame, then a slightly altered, but potentially still functional protein may be produced.

3.1.5. Aims

The aims of this chapter are to:

- Characterise the expression profile of both *ZAK* genes in embryos and adults, using *in situ* hybridisation and qRT-PCR respectively.
- Genetically target and disrupt the *ZAK*α gene using CRISPR Cas9.
- Confirm nonsense-mediated decay of the *ZAK*α transcript in the CRISPR-Cas9-targeted zebrafish (also, to confirm nonsense-mediated decay of *ZAK*β transcript in a ZAKβ targeted CRISPR-Cas9 zebrafish line, previously generated).
- Check for nonsense-mediated decay evasion mechanisms, using cDNA sequencing of transcripts for both ZAK CRISPR lines
- Assess genetic compensation of the paralogue isoform in the ZAK$\alpha^{-/-}$ and the ZAK$\beta^{-/-}$ lines.
- Breed a line of zebrafish lacking both ZAKα and ZAKβ.

3.2. Results

3.2.1. Identifying orthologous *ZAK* genes in Zebrafish

The orthologous *ZAK* genes in zebrafish were identified through an NCBI BLAST search using the human sequence of each splice isoform against the zebrafish reference sequence. Two separate genes, one on chromosome six and one on chromosome nine, were identified, suggesting sub-functionalisation following the teleost genome duplication.

The gene for the *ZAK*α orthologue is on chromosome 9 and is comprised of 20 exons, which code for a 789 amino acid protein (ENSDART00000183452.1), with 61.35% amino acid sequence similarity to human *ZAK*α. Most of the conservation is found in the kinase domain, the leucine zipper and the SAM domain. The gene for the *ZAK*β orthologue is on chromosome 6 and comprises 12 exons which code for a 477 amino acid protein (ENSDART00000151393.3) with a 71.43% amino acid sequence similarity. Again, most conservation can be found in the kinase domain and the leucine zipper.

The presence of two genes, rather than a single alternatively spliced gene, has the experimental advantage of making it considerably easier to genetically target each isoform individually in zebrafish. Zebrafish, therefore, provide an excellent model organism for investigating the role of each individual ZAK isoform separately, from a molecular and pathogenic perspective.

3.2.2 Characterising the Expression of Both ZAK Isoforms in Embryo and Adult Zebrafish Tissues

3.2.2.1 Embryonic *ZAK* Expression

In situ hybridisation (ISH) was used to determine the expression pattern of both *ZAK* isoforms in developing zebrafish embryos. The antisense digoxigenin (DIG)-labelled probes will bind to the mRNA of interest allowing an anti-DIG antibody fused with an alkaline phosphatase (AP) tag to bind to the probe, and in the presence of the substrate BM Purple, can produce a colour change. This reveals regions of the zebrafish embryo containing the highest levels of a specific mRNA.

Figure 3.1 shows expression of *ZAK*α to be fairly ubiquitous, with potential regions of greater expression in the developing brain and gut at both 1- and 4-days post fertilisation (dpf). 1 – 4 dpf was chosen to represent both the earlier and later stages of embryonic development for analysis of *ZAK* isoform expression. *ZAK*β expression is greatest in the developing heart and skeletal muscle (somites) at both 1 and 4 dpf.

Figure 3.1. Developmental expression profile of *ZAKα* and *ZAKβ* using *in situ* hybridisation.
At 1 dpf and 4 dpf zebrafish embryos show *ZAKα* to be expressed in the brain and gut. *ZAKβ* expression is in the heart and somites (developing skeletal muscle) at 1 and 4 dpf. *ZAKα* and *ZAKβ* RNA probes antisense to the respective mRNA were designed. These probes contain digoxigenin (DIG) and will bind to anti-DIG antibodies, which are fused with Alkaline phosphatase (AP), allowing for colour changes to be detected in regions of high target mRNA, when substrate BM purple is added. The top left panel shows *ZAKα* expression 1dpf and the top right shows *ZAKα* expression 4dpf. The bottom left panel shows *ZAKβ* expression 1 dpf and the bottom right panel shows *ZAKβ* expression at 4dpf. Tissues with enriched colour change are highlighted with a black arrow.

3.2.2.2. Characterising *ZAK* Expression in Adult Zebrafish Tissues

To investigate the transcription profiles of the two different isoforms in adult zebrafish tissues, RNA was extracted from dissected skeletal muscle, heart, brain, intestines, and liver. This RNA was used to synthesise cDNA for use in qRT-PCR, to investigate transcript levels, relative to the normalisation gene *Ef1α,* and build an expression profile. Figure 3.2 shows the expression profile of *ZAKα* and *ZAKβ* to be non-overlapping, across the tissues investigated. *ZAKα* expression is greatest in the brain and intestines, whereas *ZAKβ* expression is greatest in the muscle and the heart. There was surprisingly no expression of either *ZAKα* or *ZAKβ* in the liver. The mean transcript level of *ZAKβ* is on average 8-fold and 11.3-fold greater than the mean transcript level of *ZAKα* in the skeletal muscle and the heart, respectively. The error bars showing standard error of the mean (SEM) in figure 3.2 demonstrate the variance in the data sets. The mean transcript level of *ZAKα* is on average 3.6-fold and 24.4-fold greater than the mean transcript level of *ZAKβ* in the brain and the intestines, respectively. The expression profile of *ZAKβ* is consistent with humans and mice, making zebrafish a valid candidate to try and understand the role of ZAKβ in skeletal muscle and how it is driving human myopathy.

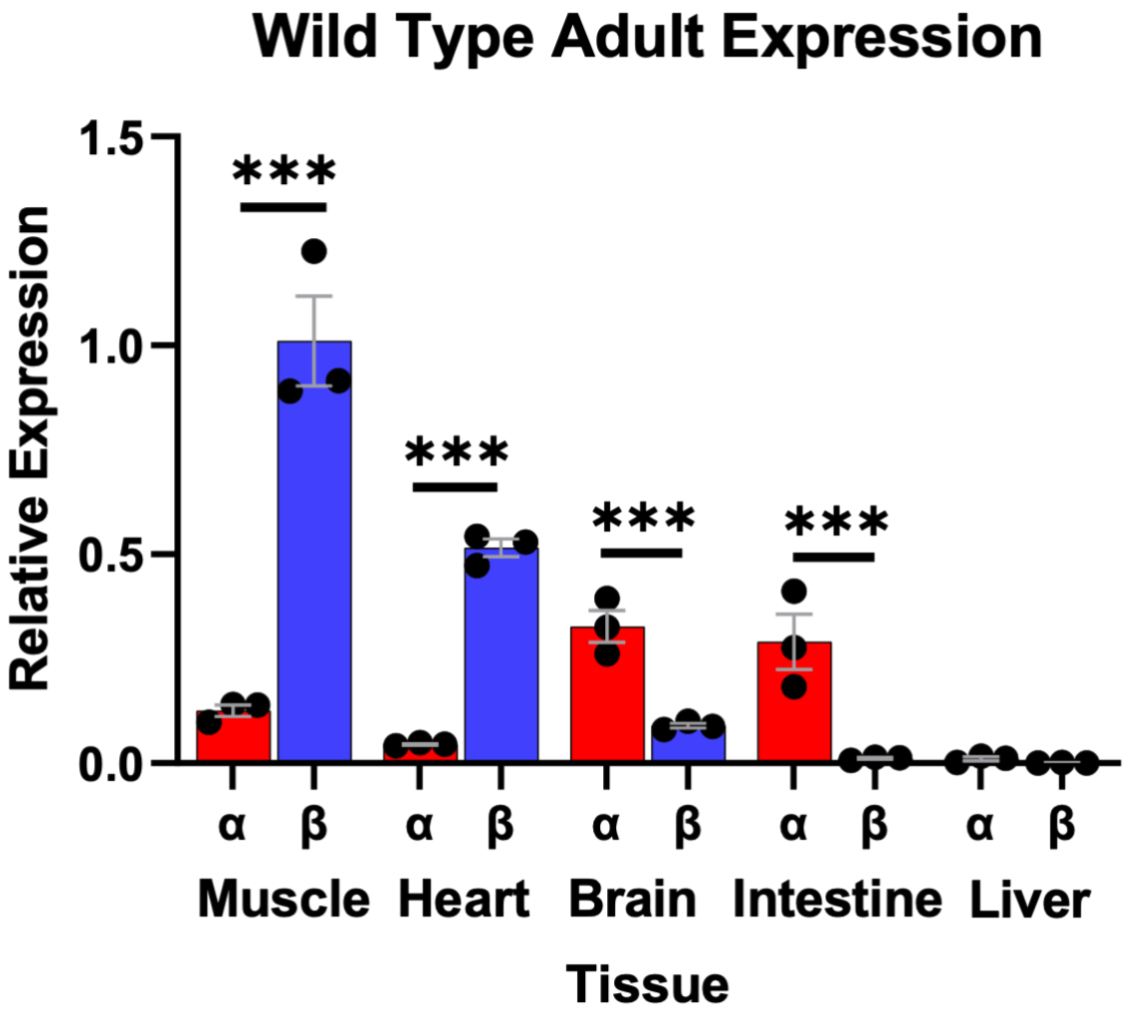

Figure 3.2. *ZAKα* and *ZAKβ* expression in different adult zebrafish tissues.
RNA was extracted the skeletal muscle, heart, brain, intestines, and liver. cDNA was synthesised from the RNA and target genes amplified using qRT-PCR to quantify expression of both isoforms across the various tissues. Mean fold change in expression of both *ZAK* isoforms were normalised to the value of mean *ZAKβ* expression in wild-type muscle as a focal point, as it was the greatest value. *ZAKα* expression is significantly greater in the brain and intestines, whereas *ZAKβ* expression is greater in the heart and skeletal muscle. Neither isoform was expressed in the liver. *** P<0.001. 3 technical repeats were performed on 3 biological repeats (n=3). Two-way ANOVA with Sidak's Post Hoc multiple comparisons performed. The statistical tests were performed on the ΔCT value prior to transforming to fold change (ΔΔCT) to plot the graph. Levene's test of equality of equal variances was used to confirm equal variance prior to statistical analysis. Error bars represent standard error of the mean (SEM).

The larval expression profile is consistent with expression during adulthood, with *ZAKβ* highly expressed in the heart and somites at both 1 and 4 dpf. The expression of *ZAKα* is a bit more ubiquitous, however, it does appear to be expressed in the brain and abdomen between 1 and 4 dpf.

3.2.3. Gene Targeting

3.2.3.1. Use of CRISPR-Cas9 on *ZAK* Isoforms and Validation of 33 Base Pair Insertion for *ZAKβ* Gene

Two guide strand RNA (sgRNA) were designed using the software, CHOPCHOP. Both guide stands are targeting a different region of exon 2 in *ZAKα*. The use of two guide strands to target a gene has been shown to be more effective than a single guide strand (Sunagawa *et al.*, 2016; Hoshijima *et al.*, 2019; Kroll *et al.*, 2021), and can potentially lead to large insertions or deletions (INDELs) of nucleotides (Zhou *et al.*, 2014), which are easier to genotype/identify mutations. Guide strands contain the target sequence, which is upstream of the protospacer adjacent motif (PAM domain – NGG) as well as a T7 promoter region at the 5' end and part of the conserved tracrRNA (for guiding Cas9 to the target sequence) at the 3' end (Gagnon *et al.*, 2014; Santos *et al.*, 2016a). See methodology for further details of the synthesis of sgRNA.

The Pownall Lab generated a genetically-targeted ZAKβ zebrafish line with a net 33 base pair insertion (7 base pair deletion and 40 base pair insertion), containing a premature stop codon in exon 2. The large insertion means that the mutants can easily be identified on a heteroduplex gel (figure 3.3 (a)). Figure 3.3 (b) shows the sequence of the 33 base pair insertion and figure 3.3 (c) illustrates the insertion.

The sgRNA and Cas9 endonuclease are co-injected in embryos at the 1-4 cell stage. Microinjections were performed in embryos from a ZAKβ$^{+/-}$ X ZAKβ$^{-/-}$ mating, aiming for mutations in the ZAKα gene in zebrafish with either ZAKβ$^{+/-}$ or ZAKβ$^{-/-}$ genotype.

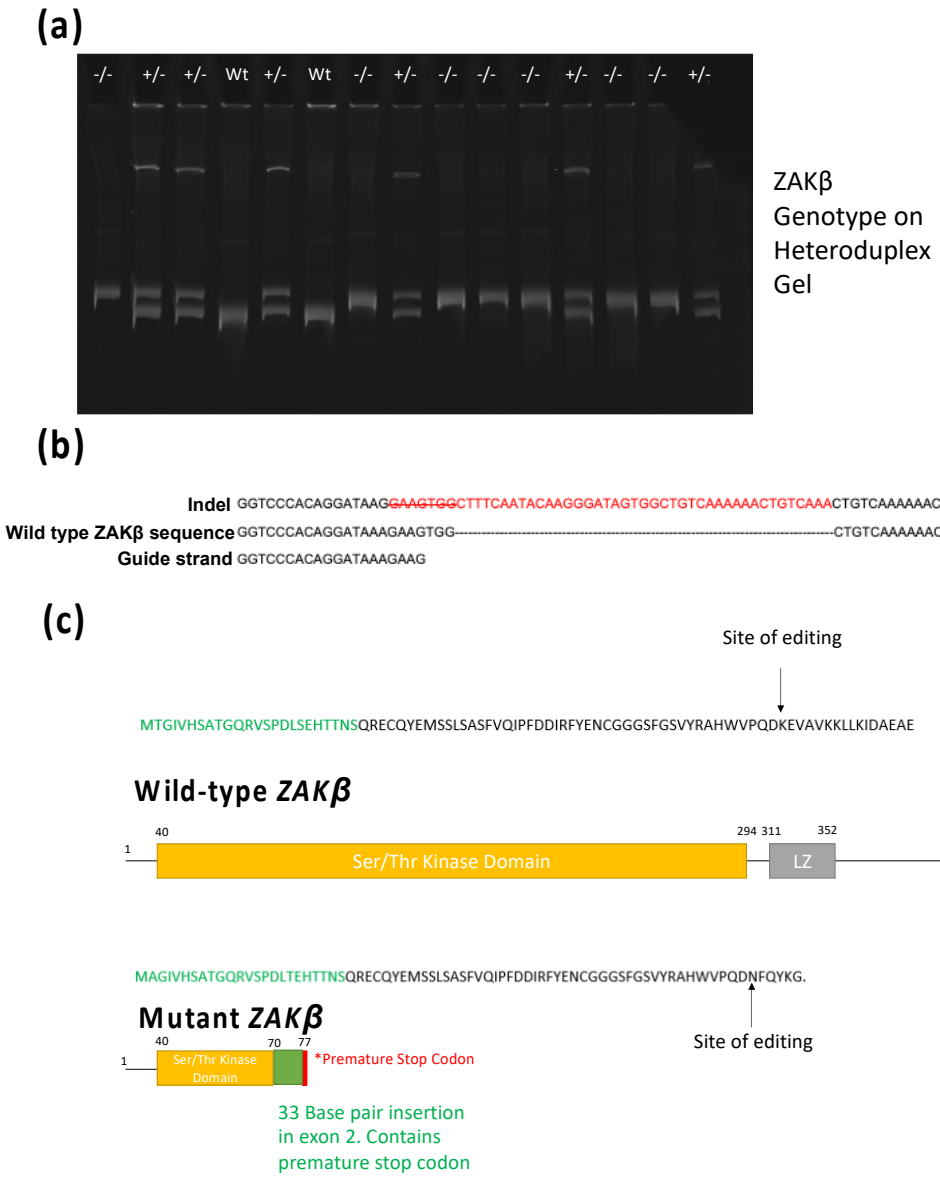

Figure 3.3. Characterising the 33 base pair insertion in *ZAKβ.*
(a) Genotyping a ZAKβ$^{+/-}$ incross. DNA was extracted from 15 embryos and the CRISPR-targeted region of exon 2 was amplified and the PCR product run on a heteroduplex gel. The embryo was labelled with the appropriate genotype based on the band patterning: The 33 base pair insert following in the ZAKβ$^{-/-}$ line runs slower and higher because of the increased amplicon size compared to wild type (wt); The ZAKβ$^{+/-}$ samples have two bands due to the two different sized products.
(b) Sanger sequencing shows the net 33 base pair insertion in the *ZAKβ* gene. The red text with a line running through indicates bases that have been deleted and the red text without the line running through is showing the additional bases.
(c) The 33 base pair insertion in the *ZAKβ* gene contains a premature stop codon with predicted absence of *ZAKβ* through nonsense-mediated decay.

3.2.4. Identifying and Verifying a 71 Base Deletion for *ZAKα*

sgRNA and Cas9 endonuclease-injected embryos are termed founder (F0) embryos. These embryos are genetically mosaic because the Cas9 requires time before it is actively cleaving the target and, meanwhile, cells are dividing so mutations might not be present in every cell. Furthermore, the Cas9 endonuclease remains active and can continue to cleave throughout the early stages of embryonic development, producing mosaic zebrafish with different cells containing different mutations in the target gene (Oliver *et al.*, 2015; Mehravar *et al.*, 2019). Consequently, DNA extracted from founder (F0) embryos is mosaic at the target locus and results in sequencing data that is difficult to interpret; therefore, analysis is done on offspring from F0 zebrafish outcrossed with wildtype zebrafish (F1 generation). Looking for the mutation in F1 zebrafish is much simpler: If successful and present in germ cells, a percentage of F1 embryos will be heterozygote containing both the un-altered allele and the allele with an INDEL. It also demonstrates that the mutation is present in somatic cells and heritable. Five F1 embryos from the same mating and one wild-type control embryo were subject to a DNA extraction, followed by PCR amplification of the targeted ZAKα region and then a heteroduplex assay on the amplicon. PCR products from the five individual embryos are shown in Figure 3.4 (a), where abnormal double banding in lane 1 (embryo 1) indicates a potential INDEL. The presence of 2 bands indicates that the INDEL is likely large, based on the large shift in mobility. The PCR product showing the potential INDEL was cloned into pGEM t-easy vectors and transformed into *E. coli.* Individual colonies are randomly selected to grow overnight before lysis and extraction of the plasmid. The plasmids are then sent for sequencing to identify the sequence of the two different bands. The difference in the size between the two bands was 71 base pairs, which corresponded to a 71 base pair deletion in exon 2 of ZAKα (figure 3.4 (b)). This frameshift mutation results in a predicted premature stop codon in Exon 3 and potential nonsense-mediated decay (figure 3.4 (c)). qRT-PCR will be used to confirm the absence of *ZAK* and, thus, NMD.

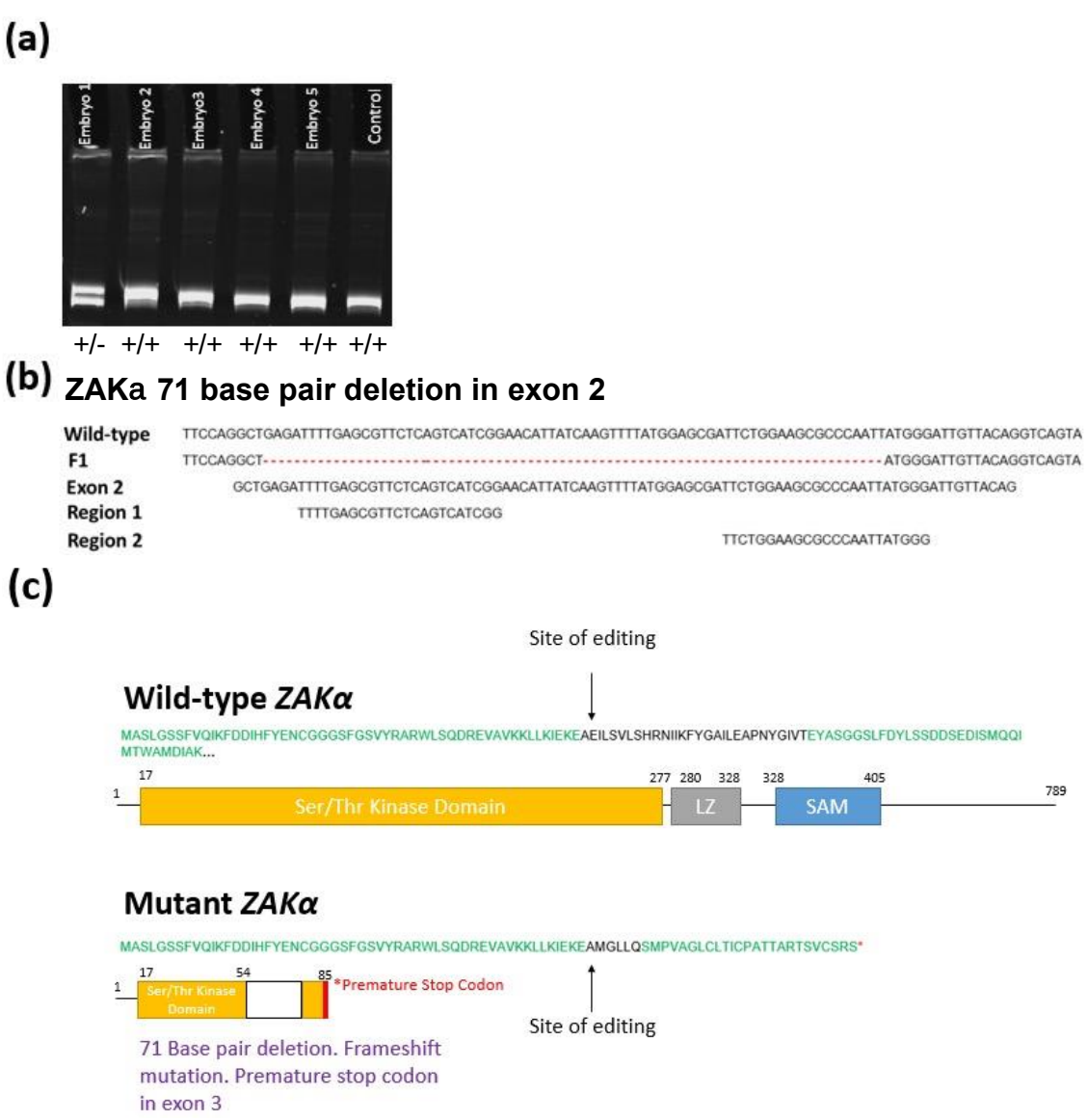

Figure 3.4. Identifying a mutation in *ZAKα* following CRISPR-Cas9 genetic targeting.
(a) A proportion of F1 embryos contain an abnormal DNA sequence due to aberrant band patterning on a heteroduplex assay. DNA was extracted from five F1 embryos and one control (sibling) embryo. The region of DNA encompassing the CRISPR target site (exon 2) was amplified by PCR and analysed by heteroduplex assay to identify sequences with abnormal band patterning, indicative of a mutation. Embryo 1 (lane 1) has a double band patterning, indicating a potential mutation. This embryo was selected for subcloning of individual PCR strands for sequencing. (+/- = heterozygote; +/+ = wildtype)
(b) Sanger sequencing revealed that a proportion of embryos were heterozygous for a 71 base pair deletion in the *ZAKα* gene. The 71 base pair deletion relative to the wild type is also shown in the figure, along with exon 2 and the two guide strand sequences (region 1 and region 2).
(c) The 71 base pair deletion in *ZAKα* causes a frameshift mutation resulting in a premature stop codon in exon 3. This is within the kinase domain (exons 2-9). The leucine zipper is exon 11 and the SAM domain is exons 12-15 Once at homozygosity it is predicted that there will be an absence of *ZAKα* by nonsense-mediated mRNA decay. Exons 1 -3 are represented, and the green and black colour of text represents different exons. The site of editing on the protein sequence is also shown and how that changes the sequence by the frameshift change in DNA. The red asterisk shows the location of the premature stop codon.

3.2.5. Breeding to Homozygosity

Below is a simplified list of the stages involved in generating a homozygous mutant:

1. Inject sgRNA and Cas9 endonuclease into embryos.
2. Raise progeny to sexual maturity (F0 generation).
3. Outcross with un-injected siblings.
4. Extract DNA from a sample of embryos (F1 generation) and assess potential heterozygotes using heteroduplex assay.
5. Sequence DNA with suspected INDELs to assess if mutation is frameshift.
6. Raise F1 embryos with identified frameshift mutation to maturity.
7. Outcross with different un-injected siblings to create a selection pressure against off-target genes, as well as minimising inbreeding.
8. Raise F2 generation to maturity and genotype using heteroduplex assay.
9. Incross heterozygotes.
10. Genotype and separate accordingly. A subset of F3 generation should be homozygous mutant.

Figure 3.5 is a cartoon depicting all of the stages required in the generation of a homozygous *ZAK* mutant.

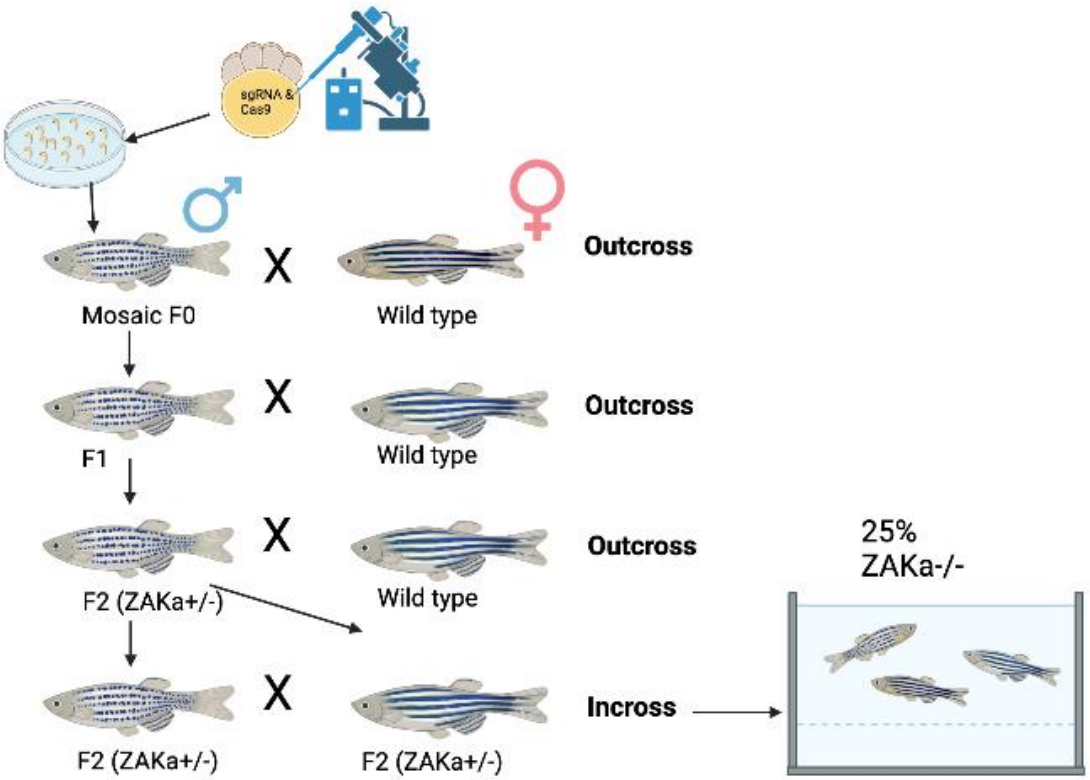

Figure 3.5. The stages of generating homozygous mutants using CRISPR-Cas9. sgRNA and Cas9 endonuclease is injected into embryos at the 1 – 8 cell stage. These F0 founder embryos are grown up to adulthood before outcrossing to produce offspring (F1). F1 are grown to adulthood, genotyped, and the heterozygotes will be selected and outcrossed with another zebrafish line again to form F2 zebrafish. These will be grown up to adulthood. There will then be a further outcross, with a separate zebrafish line, to increase the genetic diversity before incrossing two heterozygotes, whereby 25% of the embryos will be ZAK$\alpha^{-/-}$. Figure was created using BioRender.com

3.2.6. ZAK$\alpha^{-/-}$ ZAK$\beta^{-/-}$ Double Zebrafish Mutants are not Embryonic Lethal

ZAKβ CRISPR-Cas9 genetically-targeted zebrafish were generated by the Pownall Lab prior to my arrival. Figure 3.3 (b) shows the net 33 base pair insertion, containing a premature stop codon in exon 2. Due to the mutation being towards the 5' of the gene, there is predicted absence of ZAKβ through nonsense-mediated decay (NMD) of the truncated mRNA.

A ZAK$\alpha^{+/-}$ ZAK$\beta^{-/-}$ incross resulted in adult zebrafish with a mixture of ZAK$\alpha^{+/+}$, ZAK$\alpha^{+/-}$ and ZAK$\alpha^{-/-}$ genotypes, all in a ZAK$\beta^{-/-}$ genotype (figure 3.6 (a)). The mutation for *ZAKα* is a 71 base pair deletion so the lower band on the heteroduplex gel represents the mutant. The mutation for ***ZAKβ*** is a 33 base pair insertion, so the higher band represents the ZAK$\beta^{-/-}$ mutant. Double mutant zebrafish have been highlighted with a red circle for ease of identification.

Figure 3.6 (b) shows the demonstrates the percentage of each genotype to be very similar to the predicted percentage of each genotype according to Mendelian genetics.

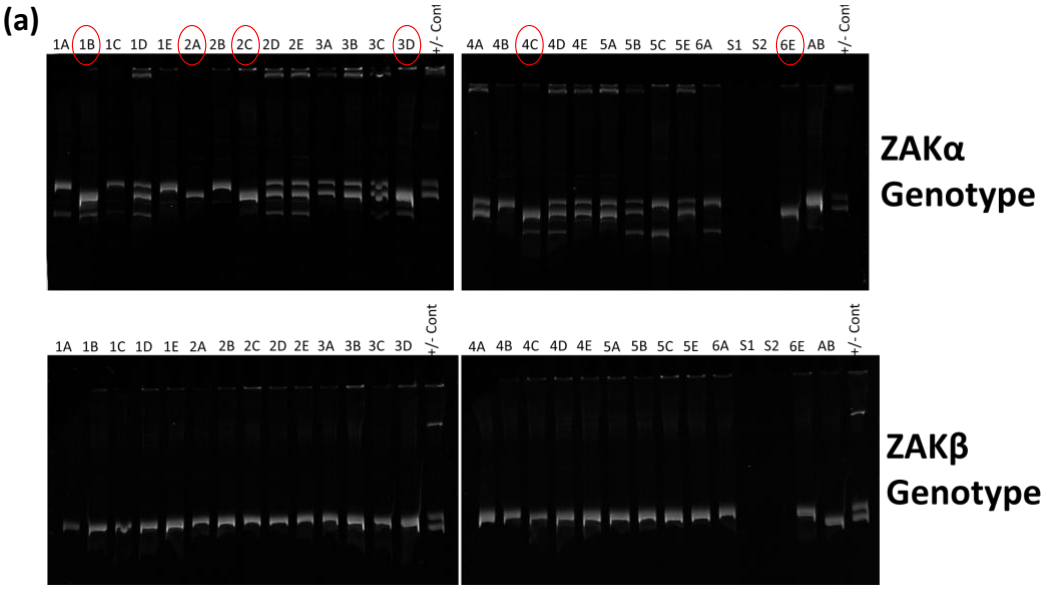

(b)

Genotype	Predicted	Actual
ZAKα+/+ ZAKβ-/-	¼ (25%)	7/25 (28%)
ZAKα+/- ZAKβ-/-	½ (50%)	12/25 (48%)
ZAKα-/- ZAKβ-/-	¼ (25%)	6/25 (24%)

Figure 3.6. Genotyping a ZAK$\alpha^{+/-}$ ZAK$\beta^{-/-}$ incross and assessing Mendelian inheritance of mutations.
(a) Creation of a ZAK$\alpha^{-/-}$ ZAK$\beta^{-/-}$ double mutant. Male and female ZAK$\alpha^{+/-}$ ZAK$\beta^{-/-}$ zebrafish were in-crossed to produce offspring with variable *ZAK*α genotypes in ZAK$\beta^{-/-}$. These embryos were raised to sexual maturity, where the DNA was extracted from individual dissected fins and PCR performed using primers on introns encompassing either side of the CRISPR target region, for each *ZAK* isoform. The amplicon was run on a 12% heteroduplex gel to determine the genotype of each zebrafish. Each number followed by a letter, for example 1A, represents an individual zebrafish. An AB (Wild type) and heterozygous (ZAK$\alpha^{+/-}$ and ZAK$\beta^{+/-}$) fin clip was used as a control. The *ZAK*α mutation is a 71 base pair deletion resulting in the amplicon migrating further due to the smaller size. The *ZAK*β mutation is a net 33 base pair insertion, resulting in the bands migrating slower. ZAK$\alpha^{-/-}$ zebrafish have a red circle around the sample number for easier identification.
(b) Table demonstrating the percentage of the genotypes from the ZAK$\alpha^{+/-}$ ZAK$\beta^{-/-}$ incross to be very similar to the Mendelian predicted inheritance.

3.2.7. Assessing for Nonsense-Mediated Decay

3.2.7.1 Nonsense-Mediated Decay of *ZAKα* in ZAKα$^{-/-}$ Embryos and Adult Zebrafish

The level of *ZAKα* transcripts was assessed in wild type, ZAKα$^{-/-}$, ZAKβ$^{-/-}$ and ZAKα$^{-/-}$ ZAKβ$^{-/-}$ 3 dpf embryos. The reduction of *ZAKα* transcripts in various genotypes, presented by nonsense-mediated decay, is evidenced in figure 3.7 (a). There was a statistically significant reduction ($P \leq 0.0001$) of the mean *ZAKα* transcript levels by 2.6-fold in the ZAKα$^{-/-}$ embryos and 2.4-fold in the ZAKα$^{-/-}$ ZAKβ$^{-/-}$ embryos, relative to the mean wild type *ZAKα* transcript levels. This reduction is likely the result of nonsense-mediated decay. Surprisingly, there is also a significant 1.9-fold decrease ($P \leq 0.001$) in the mean *ZAKα* transcript levels in ZAKβ$^{-/-}$ embryos relative to the mean wild type *ZAKα* transcript levels. This is unexpected, as the *ZAKα* gene is the same as wild type and is the opposite result to that of genetic compensation, discussed later.

Figure 3.7 (b) shows that there was also a statistically significant mean reduction in the level of *ZAKα* transcripts in the brain and liver of adult ZAKα$^{-/-}$ zebrafish compared to wild type. These tissues were selected as they showed the highest *ZAKα* RNA expression of tissues investigated. There was a significant average 2-fold reduction in the brain ($P \leq 0.01$) and an average 6.3-fold reduction of *ZAKα* transcript levels in the liver ($P \leq 0.01$).

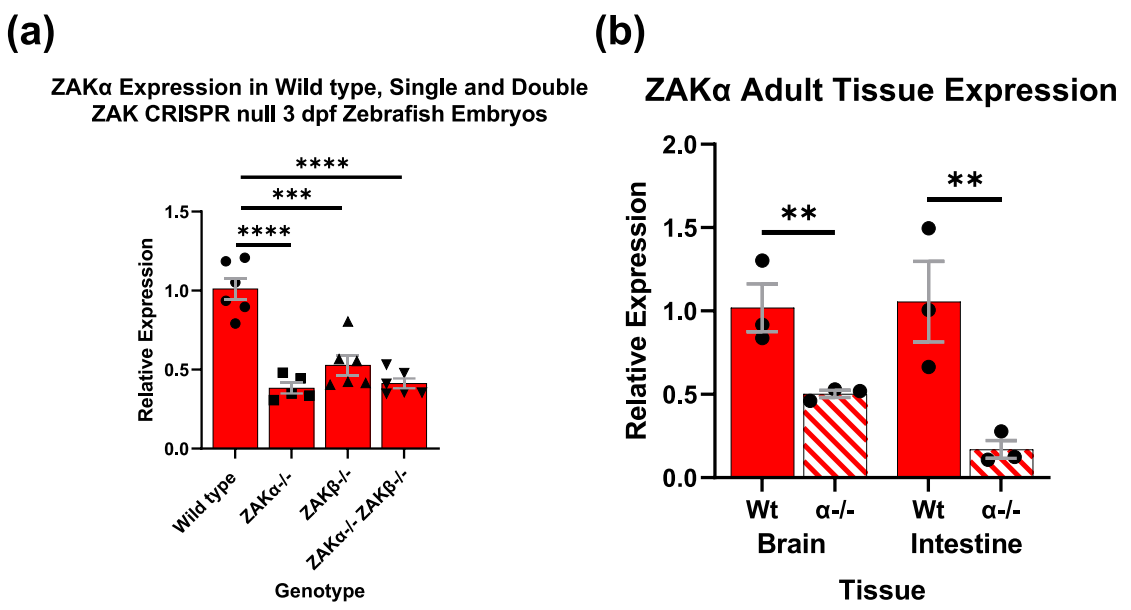

Figure 3.7. Expression of *ZAKα* in *ZAK* mutant embryos and adult zebrafish tissues.
(a) *ZAKα* expression is significantly decreased in ZAKα$^{-/-}$, ZAKβ$^{-/-}$ and double ZAKα$^{-/-}$ ZAKβ$^{-/-}$ zebrafish embryos at 3 dpf. RNA was extracted from five embryos, from one mating, to provide one sample. Six separate mating's were carried out for each genotype to provide a biologic n=6. qRT-PCR was performed to allow for analysis of the relative changes of *ZAKα* transcript levels between wildtype and ZAKα$^{-/-}$, ZAKβ$^{-/-}$ and double ZAKα$^{-/-}$ ZAKβ$^{-/-}$ zebrafish embryos. There is a strong significant reduction in the mean *ZAKα* transcript levels in ZAKα$^{-/-}$ and double ZAKα$^{-/-}$ ZAKβ$^{-/-}$. Unexpectedly, there was a significant reduction of the mean *ZAKα* transcript levels in ZAKβ$^{-/-}$ embryos. *** P ≤ 0.001. **** P ≤ 0.0001 Every sample was performed in triplicate (technical repeats). Fold change in *ZAKα* was normalised to the mean *ZAKα* wild type transcript levels. ** P<0.01. Six separate samples from separate mating's were used (biological repeats). One way ANOVA with Dunnett's post hoc analysis was the statistical test. Bar graphs show mean and error bars represent SEM.
(b) *ZAKα* transcript levels are significantly decreased in the ZAKα$^{-/-}$ zebrafish line. RNA was extracted from the intestine and brain of three wildtype and three ZAKα$^{-/-}$ zebrafish. cDNA was synthesised from the RNA and qRT-PCR was performed to allow for analysis of the relative changes of the mean *ZAKα* transcript levels between wildtype and ZAKα$^{-/-}$ zebrafish line. 3 technical repeats were performed on 3 biological repeats (n=3). Fold change in *ZAKα* was normalised to the mean *ZAKα* transcript levels in the respective wild type tissue. ** P<0.01. An unpaired students t-test (two-tailed) was the statistical test performed. Bar graphs show mean and error bars represent SEM.
ΔΔCT, or Livak method, of calculating fold-change, relative to the wild type *ZAKα* transcript levels was used, following normalisation to the expression of *Ef1α* in the respective sample. All statistics were performed on the ΔCT value prior to transforming to fold change to plot the graph. GraphPad Prism 9.0 was for statistical analysis and graph-making.

3.2.7.2 Nonsense-Mediated Decay of *ZAKβ* in ZAKβ$^{-/-}$ Embryos and Adult Zebrafish

The absence of *ZAKβ* transcripts, presented by nonsense-mediated mRNA decay is evidenced in figure 3.8 (a) and (b). qRT-PCR was used to analyse ZAKβ transcript levels in RNA extracted from either: 3 dpf embryos in ZAKα$^{-/-}$, ZAKβ$^{-/-}$ and ZAKα$^{-/-}$ ZAKβ$^{-/-}$ double mutants, relative to wild type (figure 3.8 (a)); or in adult zebrafish tissue in ZAKβ$^{-/-}$ relative to wild type (figure 3.8 (b)). There was a statistically significant decrease in the mean *ZAKβ* transcript level in ZAKβ$^{-/-}$ and ZAKα$^{-/-}$ ZAKβ$^{-/-}$ 3 dpf embryos relative to the mean wild type *ZAKβ* transcript level (3.2- and 3.1- fold, respectively - $P \leq 0.0001$). There were no significant differences in the mean *ZAKβ* transcript level of ZAKα$^{-/-}$ 3 dpf embryos compared to mean wild type *ZAKβ* transcript level. There was a significant reduction in the mean *ZAKβ* transcript level of ZAKβ$^{-/-}$ zebrafish compared to wild type for skeletal muscle (4-fold - $P \leq 0.01$) and heart (6.3-fold - $P \leq 0.01$). These are the tissues with the greatest levels of *ZAKβ* transcript. The low levels of transcript in the brain are the likely reason for no significant differences in the expression.

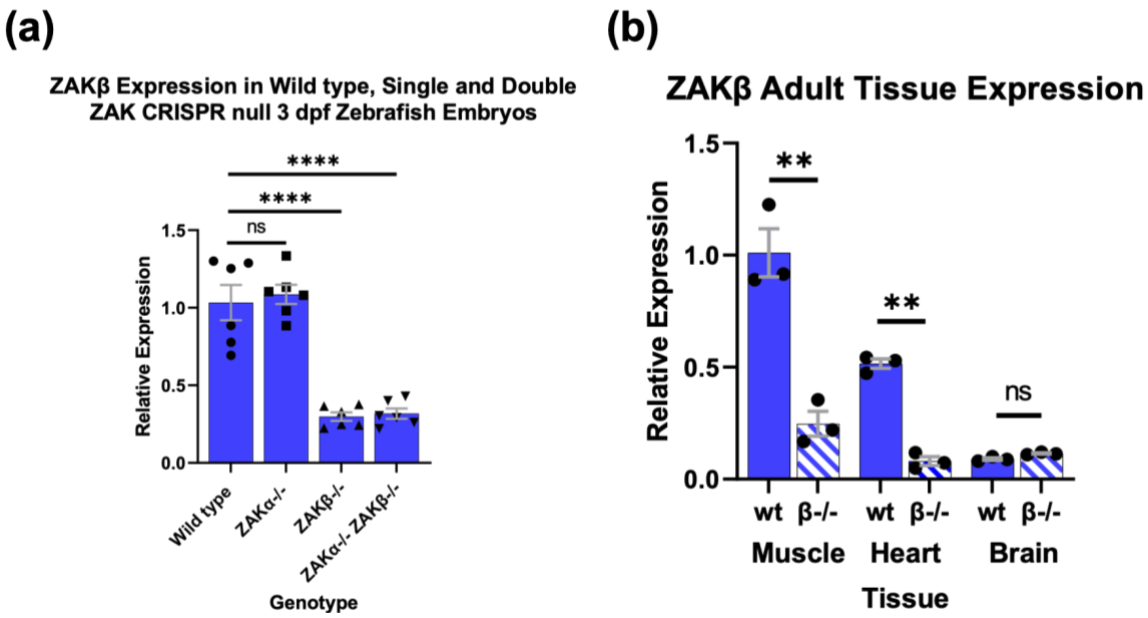

Figure 3.8. Expression of *ZAKβ* in *ZAK* mutant embryos and adult zebrafish tissues.
(a) *ZAKβ* transcript levels are significantly lower in ZAKβ$^{-/-}$ and double ZAK$\alpha^{-/-}$ ZAKβ$^{-/-}$ 3 dpf embryos compared to wild type. RNA was extracted from five embryos, from one mating, to provide one sample. Six separate mating's were carried out for each genotype to provide a biologic n=6. qRT-PCR was performed to allow for analysis of the relative changes to the mean *ZAKβ* transcript levels between wildtype and ZAK$\alpha^{-/-}$, ZAKβ$^{-/-}$ and double ZAK$\alpha^{-/-}$ ZAKβ$^{-/-}$ zebrafish embryos. A strong significant reduction of *ZAKβ* transcripts in the ZAKβ$^{-/-}$ and the ZAK$\alpha^{-/-}$ ZAKβ$^{-/-}$ line. No significant differences in *ZAKβ* transcript levels in ZAK$\alpha^{-/-}$ zebrafish. **** P<0.0001. Every sample was performed in triplicate (technical repeats). Six separate samples from separate matings were used (biological repeats). Fold change in *ZAKβ* was normalised to the mean *ZAKβ* wild type transcript levels. One way ANOVA with Dunnett's post hoc analysis was the statistical test. Bar graphs show mean and error bars represent SEM.
(b) *ZAKβ* transcript levels are significantly reduced in the ZAKβ$^{-/-}$ zebrafish line. RNA was extracted from the brain, heart, and skeletal muscle of 3 wildtype and 3 ZAKβ$^{-/-}$ zebrafish. cDNA was synthesised from the RNA and qRT-PCR was performed to allow for analysis of the relative changes of expression of *ZAKβ* between wildtype and ZAKβ$^{-/-}$ zebrafish line. There was a significant reduction in the mean *ZAKβ* transcript level for ZAKβ$^{-/-}$ skeletal muscle and heart compared to wild type. 3 technical repeats were performed on 3 biological repeats (n=3). Fold change in the *ZAKβ* transcript levels in ZAKβ$^{-/-}$ tissues were normalised to the mean *ZAKβ* transcript levels in the respective wild type tissue. ** P<0.01. Unpaired student's t-test (two-tailed) was the statistical test performed. Bar graphs show mean and error bars represent SEM.
ΔΔCT, or Livak method, of calculating fold-change, relative to the wild type *ZAKβ* transcript levels was used, following normalisation to the expression of *Ef1α* in the respective sample. All statistics were performed on the ΔCT value prior to transforming to fold change to plot the graph. GraphPad Prism 9.0 was for statistical analysis and graph-making.

3.2.8. Assessing Molecular Evasion Strategies in ZAK CRISPR Zebrafish

The need to validate that the mutation does, in fact, result in the absence of the transcript is important as (Anderson *et al.*, 2017) has demonstrated that cryptic splice sites, exon skipping and nonsense-associated alternative splicing can circumvent the penetrance of the mutation. Using different primers in the 1st and 12th exon of both *ZAK*α and *ZAK*β, I amplified cDNA from embryos of either ZAK$\alpha^{-/-}$ and ZAK$\beta^{-/-}$ zebrafish. The amplicon was ligated into pGEM t-easy plasmids individual colonies were selected for sequencing. This is to ensure that the sequence of the mRNA is as expected and that no molecular evasion strategies are being used to evade NMD.

Confirming absence of transcripts as well as the mRNA sequence being correct, provides increased confidence that you have successfully created knockouts of the target gene, in lieu of having antibodies to prove knocking out of the protein.

The *ZAK*α transcript in the ZAK$\alpha^{-/-}$ line, is showing exon skipping (figure 3.9 (a)). The entirety of exon 2 is being skipped (88 base pair deletion), rather than the predicted 71 base pair deletion. This is still a frameshift mutation and there is still a premature stop codon with predicted nonsense-mediated decay (figure 3.9 (c)). There was exon skipping in five out of six embryos sequenced at 3 dpf and six out of six embryos at 6 dpf. The *ZAK*β cDNA sequence is, as expected, based on the genomic DNA, a net 33 base pair insertion (figure 3.9 (b)) in the ZAK$\beta^{-/-}$ line.

Figure 3.9. Sequencing of *ZAK* transcripts to investigate potential NMD-evasion mechanisms.
(a) *ZAK*α cDNA sequencing reveals attempted NMD-evasion techniques used by the zebrafish. RNA was extracted from embryos at 3 and 6 dpf. cDNA was synthesised and amplified using primers in exon 1 and exon 12 for *ZAK*α. The PCR product was ligated into a vector and individual colonies sent for sequencing. The sequencing reveals an 88 base pair deletion in exon 2, rather than the expected 71 base pair deletion in the DNA. The 88 base pair deletion spans the entire exon 2 and demonstrated NMD evasion strategy being used by zebrafish in an attempt to retain frame and functionality of the protein.
(b) *ZAK*β cDNA sequencing is as predicted, with a net increase of 33 base pairs, which contains a premature stop codon. RNA was extracted and cDNA was synthesised and amplified using a forward primer in exon 1 and a reverse primer in exon 12. The amplicon was sequenced in the same way as (a). The black text is normal sequence, the red text indicates additional bases and the red text with a line through indicates deleted bases.
(c) Figure to illustrate that even with the 88 base pair deletion, there is still a frameshift mutation and predicted absence of *ZAK*α, with a premature stop codon in exon 3

3.2.9. Assessing Potential Genetic Compensation in ZAK CRISPR Zebrafish

When a gene is knocked out at the genomic level, the consequence can be a less severe or different phenotype, to one reported when a gene is targeted at the transcript level (e.g. with morpholinos) (Peng, 2019). One potential explanation is genetic compensation from paralogous or genes of similar function (El-Brolosy *et al.*, 2019). The principle of genetic compensation is discussed in greater detail in section 3.3.2. Due to the conservation of the kinase domain across both isoforms in zebrafish it was of interest to investigate if expression of the paralogue isoform in zebrafish would be increased in the absence of either *ZAK*α or ***ZAKβ,*** as a compensatory method.

Rather than an upregulation in *ZAK*α transcript levels, figure 3.7 (a) shows that, surprisingly, when *ZAK*β is absent (ZAK$\beta^{-/-}$), there is a significant decrease in the mean *ZAK*α transcript level to approximately the same value as when *ZAK*α is absent in ZAK$\alpha^{-/-}$ 3 dpf embryos. Figure 3.10 (a) also shows a statistically significant reduction in the mean *ZAK*α transcript level in the brain of adult ZAK$\beta^{-/-}$ zebrafish relative to wild type. This is unexpected and is the complete opposite finding of an increase in *ZAK*α levels, which would indicate compensation.

There are no changes to the average expression of *ZAK*β when *ZAK*α is absent in ZAK$\alpha^{-/-}$ 3 dpf embryos or in the adult brain and liver (figure 3.8 (a) and 3.10 (b)). This indicates that *ZAK*β is not compensating for absence of *ZAK*α.

The findings demonstrates that the absence of ***ZAKβ*** does not trigger compensation through upregulation of the ***ZAKα*** isoform. There is the striking and surprising decrease of *ZAK*α transcripts in ZAK$\beta^{-/-}$ 3 dpf embryos and adult brain.

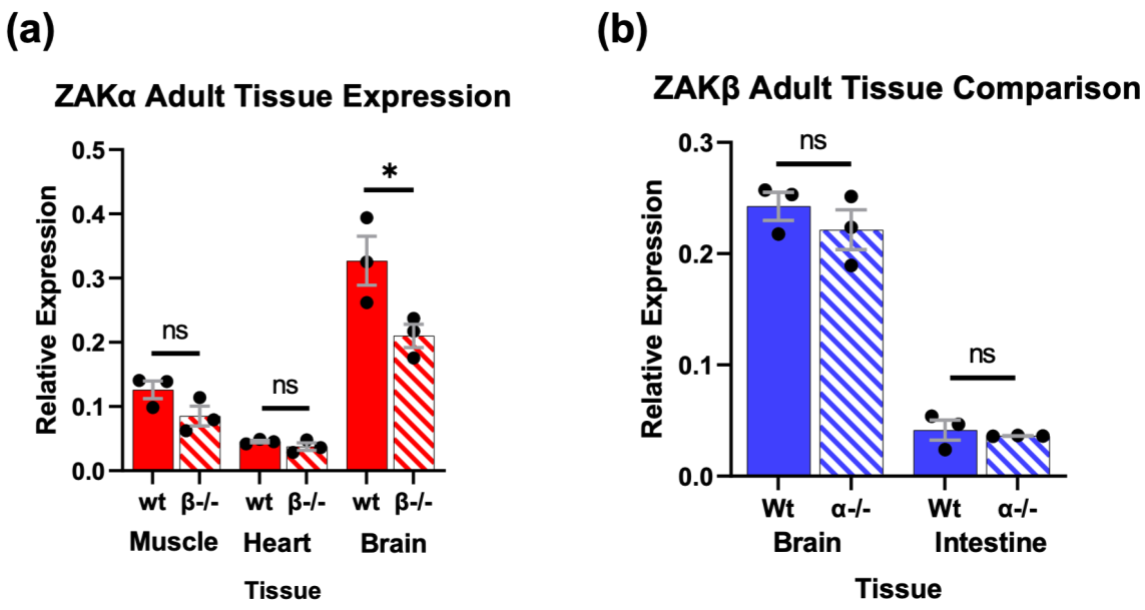

Figure 3.10. Assessing potential genetic compensation with absence of either ZAKα or ZAKβ.
(a) *ZAKα* transcript levels do not increase in response to the absence of *ZAKβ* as part of functional redundancy. Brain, heart and muscle was dissected from 3 adult zebrafish and RNA was then extracted. The fold changes to *ZAKα* levels were then quantified using qRT-PCR. In the absence of *ZAKβ* (ZAKβ$^{-/-}$), *ZAKα* transcript levels do not increase. Surprisingly, there was a significant decrease in the mean transcript level of *ZAKα* in the brain of ZAKβ$^{-/-}$ zebrafish relative to wild type ($P<0.05$). Unpaired student's t-test (two-tailed) was the statistical test. Data was initially normalised to the housekeeping gene *EF1α* before calculating the mean fold change relative to *ZAKβ* in wild type skeletal muscle (the greatest value, with a relative expression value of 1). Expression of both genes in all tissue was normalised to wild type skeletal muscle *ZAKβ* levels. Bar graphs show mean and error bars represent SEM.
(b) *ZAKβ* expression does not increase in response to the absence of *ZAKα* as part of functional redundancy. RNA was extracted from the brain and intestines of adult zebrafish. The fold changes to *ZAKβ* transcript levels were quantified using qRT-PCR. Unpaired student's t-test (two-tailed) was the statistical test. Data was initially normalised to the housekeeping gene *EF1α* before calculating the mean fold change relative to *ZAKα* expression in wild type intestines (the greatest value, with relative expression value of 1). Bar graphs show mean and error bars represent SEM.

3.3. Discussion

3.3.1 ZAK Characterisation in Zebrafish

It appears that in zebrafish, that there has been sub-functionalisation of the two ZAK isoforms on different chromosomes, rather than being the result of alternative splicing. The exon structure of each *ZAK* gene is identical to the respective splice form in humans, and the amino acid length is similar. Splice form sub-functionalisation is not uncommon, with (Lambert *et al.*, 2015) demonstrating with 100 exon divergent zebrafish paralogues, that 25% had an exon structure identical, and code for proteins with a similar amino acid length to co-orthologous splice forms in humans. A negative correlation between gene duplications and the level of alternative splicing has been reported (Kopelman *et al.*, 2005; Su *et al.*, 2006), but is subject to debate, with other studies disagreeing with this correlation (Jin *et al.*, 2008; Roux and Robinson-Rechavi, 2011). Zebrafish have comparatively low levels of alternative splicing and large levels of gene duplication, compared to other teleosts (Lu *et al.*, 2010). In humans, mice and zebrafish, exon divergent paralogues, following a duplication event, generally show lower levels of alternative splicing and a reduced tissue expression than single genes or duplicated genes with the same number of exons (Lambert *et al.*, 2015).

ZAKβ expression in the hearts and skeletal muscle of adult zebrafish is a finding which is supported by other researchers in both humans and mice (Vasli *et al.*, 2017; Gross *et al.*, 2002). This supports the use of zebrafish as a model organism to understand the role of ZAKβ in skeletal muscle, which will be done by using these CRISPR generated knockout zebrafish lines to look for evidence of myopathy. *ZAK*α expression is greatest in the brain and intestine. Surprisingly, there is no *ZAK*α expression in the liver, where it is ordinarily enriched in humans and mice (Nordgaard *et al.*, 2022; Gross *et al.*, 2002). The lack of consistency of *ZAK*α expression between zebrafish and humans/mice does not weaken the use of zebrafish as a model organism, since *ZAK*α is not expressed in the skeletal muscle. ZAKβ is the isoform expressed in muscle and will be the isoform potentially involved in driving the myopathy. In all investigated tissues, there is only one *ZAK* isoform expressed, with low/no levels of the paralogue.

The expression profile is similar in zebrafish embryos to adult tissues, with *ZAKβ* expressed in the somites and heart at 1 and 4 dpf; and *ZAKα* expression being fairly ubiquitous, but especially expressed in the brain and gut at 1 and 4 dpf.

3.3.2 Genetic Compensation in ZAKα CRISPR Lines

I have confirmed nonsense-mediated decay and absence of *ZAKα* in ZAKα$^{-/-}$ 3 dpf embryos as well as adult brain and intestine. I have also confirmed nonsense-mediated decay and absence of *ZAKβ* transcripts in ZAKβ$^{-/-}$ 3 dpf embryos as well as adult hearts and skeletal muscle. There is not an existing ZAK antibody that works in zebrafish, hence, the use of qPCR and mRNA sequencing to confirm the lack of transcript and that the mutation is being transcribed as expected.

The ZAKα$^{-/-}$ ZAKβ$^{-/-}$ zebrafish are able to survive to adulthood and successfully reproduce, showing that absence of ZAK in zebrafish is not fatal or does not create sterile zebrafish. The lack of embryonic lethality supports humans with mutations in ZAK as well as mice models lacking ZAK (Jandhyala *et al.*, 2016; Nordgaard *et al.*, 2022), and contradicts findings of embryonic lethality with absence of ZAK by (Spielmann *et al.*, 2016).

A single nucleotide polymorphism in the SAM domain of ZAK, has been associated with developmental defects in humans, including split hand/split foot malformation and polydactyly (Spielmann *et al.*, 2016). Vind *et al.* recently showed the mutation that causes the developmental defects in question (F368C) to result in constitutive activation of ZAKα (Vind *et al.*, 2020). Using a ZAKα CRISPR knockout cell line, the developmental-disease causing version of ZAKα was introduced and there was constitutive activation of ZAKα, which could not be further increased by ZAKα activator anisomycin (Vind *et al.*, 2020). The researchers propose that the developmental defects are the result of constitutive activation of ZAKα and, thus, the constitutive activation of the ribosomal stress response (Vind *et al.*, 2020).

As previously mentioned in section 3.2.9, using gene editing techniques, such as CRISPR-Cas9, to target a gene at the genomic level can result in a less severe phenotype than if morpholinos were used to knock down a gene at the RNA level (Kok *et al.*, 2015; Peng, 2019). The less severe phenotype could be explained by genetic compensatory mechanisms, with frameshift mutations and premature stop codons leading to genetic compensation, but not gene knockdowns (Rossi *et al.*, 2015). One potential mechanism for this was proposed by (El-Brolosy and Stainier, 2017) and suggested the involvement of degraded mRNA. Following CRISPR-Cas9 gene targeting of several genes in zebrafish, (El-Brolosy *et al.*, 2019) demonstrated a significant upregulation in either the paralogue gene or a family-member gene (termed, adapting gene). Inhibition of the NMD pathway through knockout of *Upf1* resulted in failure of the of these adapting genes to be upregulated. Furthermore, transcriptome analysis of the upregulated genes across multiple different gene knockout cells, revealed that most exhibit a similar sequence to the mutated gene. This indicates that the sequence of the degraded transcript likely plays a role in the genetic upregulation. Additionally, preventing the expression of the transcript by genetically-targeting the promoter region using CRISPR-Cas9 in zebrafish, led to a failure of the adapting gene to be upregulated, highlighting the requirement for mRNA degradation for this process. (El-Brolosy *et al.*, 2019) also demonstrated in multiple gene knock out cells, enrichment of WDR5 and H3K4me3 at the transcriptional start site (TSS) of the adapting genes, as well as the decreased transcription of adapting genes when WDR5 was inhibited by siRNA. This indicates the importance of the role of chromatin remodelling for the upregulation of the adapting gene in genetic compensation. These robust findings demonstrate that it is the degraded mRNA following NMD that is responsible for the genetic compensation, through upregulation of the adapting gene. A mechanism was proposed, whereby following NMD, these decay factors are guided into the nucleus where they can bind to regions of the genome of high sequence similarity, where there is then chromatin remodelling and increased gene expression in an attempt to compensate for loss of the respective transcript (El-Brolosy *et al.*, 2019).

Furthermore, (Schuermann *et al.*, 2015) demonstrated milder phenotypes when there was greater nonsense-mediated decay and less *mt2* transcript in zebrafish.

There was not an increase in *ZAK*α expression in response to *ZAK*β absence in either 3 dpf embryos or adult brains (figures 3.11(a) and (c)), demonstrating absence of *ZAKβ* does not trigger compensation through upregulation of the *ZAKα* isoform. Surprisingly, there was a significant decrease in *ZAK*α transcript levels in ZAK$\beta^{-/-}$ 3 dpf embryos to similar levels to the ZAK$\alpha^{-/-}$ and ZAK$\alpha^{-/-}$ ZAK$\beta^{-/-}$ lines. This is the opposite result to genetic compensation, which would have resulted in an increase in *ZAK*α transcript levels when *ZAK*β was absent. This result could indicate a role for ZAKβ in the expression of *ZAK*α, although further investigation will be required to substantiate this claim. Indeed, overexpression of ZAKβ has been shown to induce ZAKα expression in human osteosarcoma cells (Fu *et al.*, 2018).

There are no transcriptional adaptions and increases in *ZAK*β expression in response to *ZAK*α absence, in either 3 dpf embryos or adult tissues (figure 3.11(b) and (c)). Whilst I can rule out genetic compensation through the paralogue for both ZAKα and ZAKβ, I cannot rule out genetic compensation from another similar protein.

3.3.3. Molecular Evasion Techniques

mRNA sequencing demonstrated the use of a molecular NMD evasion technique in the *ZAK*α CRISPR line, with the entirety of exon 2 being skipped, rather than just the predicted 71 base pair deletion within exon 2. The skipping of exon 2 still results in a frameshift mutation and we have confirmed nonsense-mediated decay in figure 3.8. No other NMD-evasion techniques were detected. The *ZAK*β transcript is as you would expect, based on the genomic DNA, with a 33 base pair insertion and no signs of molecular mechanisms of evading NMD.

3.4. Conclusion

This chapter reports the creation of ZAK$\alpha^{-/-}$ and double ZAK$\alpha^{-/-}$ ZAK$\beta^{-/-}$ mutants that have been raised to adulthood. The absence of *ZAKα* and *ZAKβ* transcripts in their respective CRISPR line, through presumed nonsense-mediated decay, has been confirmed. Zebrafish, mutant for ZAK$\alpha^{-/-}$ were found to activate nonsense-mediated decay evasion mechanisms, in this case exon skipping. Nonetheless, even with skipping exon 2, there is still a frameshift mutation and NMD. No nonsense-mediated decay evasion mechanisms were detected in the ZAK$\beta^{-/-}$ line. Furthermore, neither paralogue appear to compensate for absence of the other isoform. Surprisingly, there was a decrease in *ZAKα* transcript levels in the ZAK$\beta^{-/-}$ line, potentially indicating a role for ZAKβ in the expression of *ZAKα*, however, more research is required to support this theory.

Due to lack of *ZAKα* expression in the muscle of adult zebrafish, even in the absence of *ZAKβ* expression, I will not be investigating this mutant line any further. Embryos from a ZAK$\alpha^{+/-}$ ZAK$\beta^{+/-}$ double heterozygous incross were gifted to our collaborator, Professor Simon Bekker-Jenssen at the University of Copenhagen. The incross will allow wild type, single and double ZAK$\alpha^{-/-}$ ZAK$\beta^{-/-}$ null zebrafish to be used in the investigation of both isoforms in his lab.

4. Investigating the Phenotype of ZAK$\beta^{-/-}$ Zebrafish Part I: Strength of Muscle and Swimming Capabilities

4.1. Introduction

Following successful creation and validation of zebrafish lacking ZAKα, ZAKβ, and both ZAK isoforms, the next step is to investigate the effect that absence of ZAK may have on skeletal muscle. This chapter will focus on the morphology of zebrafish lacking ZAKβ, the strength and swimming activity of ZAKβ$^{-/-}$ embryos and adults, and any impact that absence of both ZAK isoforms has on the activity of the heart.

4.1.1. Assessing Strength and Swimming Capabilities of ZAKβ$^{-/-}$ Zebrafish

A decrease in the strength of certain muscle groups is a common feature of all myopathies. From as early as 17 hours post fertilisation (hpf) zebrafish embryos use their muscles to move, starting with spontaneous coiling, followed by touch-induced alternative coiling at 21 hpf, that transforms into a burst of swimming contractions by 36 hpf (Saint-Amant and Drapeau, 1998). At 24 hpf, the touch-induced alternative coiling is exclusively the result of slow-twitch fibres, whereas, the touch-evoked swimming bursts seen at 48 hpf are predominantly the result of fast-twitch fibres (Moore *et al.*, 2007; Naganawa and Hirata, 2011). Consequently, the early movement represents an opportunity to study the strength of contraction of slow and fast-twitch muscle fibres in ZAKβ$^{-/-}$ zebrafish embryos.

Being able to study zebrafish locomotion is hugely advantageous and has allowed a greater understanding of obesity (Seebacher and James, 2019), ageing (Gilbert *et al.*, 2014), neurology (Kokel *et al.*, 2013; Hughes *et al.*, 2020) and pharmacological interventions (Laggner *et al.*, 2012; Bruni *et al.*, 2016). Zebrafish swimming analysis also provides an opportunity to understand the role of proteins or signalling pathways on skeletal muscle function. Chiefly, it is zebrafish larvae that are used for this swimming analysis, rather than adults (Sztal *et al.*, 2015; Ruparelia *et al.*, 2021; Lambert *et al.*, 2021).

Adult zebrafish trunk muscles drive propulsion, generating body waves through undulations, powering movement in water (McHenry *et al.*, 1995; Gabriel *et al.*, 2008; Berg *et al.*, 2018).

A former student in the Pownall Lab (Matthew Bedder) created software for tracking adult zebrafish swimming called ShadowFish. Another former student (Gideon Hughes) created a protocol and a MATLAB code for automated processing of the (X, Y) dimensions of seven equally spaced points across the spine for each frame (Hughes *et al.*, 2020). A modified version of the code can be seen in (Appendix A). A multitude of different swimming characteristics are automatically processed across a 30 second recording, using the MATLAB code: mean velocity, average time spent moving, distanced travelled and mean swimming duration. Also, the frequency of tailbeats at low, medium and high speeds as well as the amplitude (degree of bending) at low, medium and high speeds, are also assessed. These specific features were included in my analysis, based on swimming assessments from other studies, using either larval or adult zebrafish (Budick and O'Malley, 2000; Ingebretson and Masino, 2013; Keatinge *et al.*, 2015; Godoy *et al.*, 2015). This protocol was used by Gideon Hughes, 2020, to discern a movement phenotype in adult zebrafish lacking the Parkinson associated gene, DJ-1 (Hughes *et al.*, 2020).

Kyphoscoliosis peptidase (KY) is a transglutaminase-like peptidase expressed in skeletal muscle, and like ZAK, KY protein localises to the Z-disc as part of the same protein complex as ZAK and mutations in *KY* have been associated with human congenital myopathy (Beatham *et al.*, 2004; Baker *et al.*, 2010; Ehsani *et al.*, 2022). Consequently, it was of interest to investigate the potential impact that dual absence of KY and ZAKβ had on the strength of slow and fast-twitch skeletal muscle in one and two dpf embryos, as assessed by the tactile strength assay. The role of KY in skeletal muscle is discussed in greater detail in section 5.1.2. Furthermore, with many myopathies following an age-related degeneration in muscle strength, the ability to investigate swimming of adults, as well as larvae, is highly advantageous.

4.1.2. Cardiac Involvement of ZAK

There is evidence to suggest ZAKα forms part of the TGF-β signalling pathway, which stimulates cardiac hypertrophy (Huang *et al.*, 2004b; Nyati *et al.*, 2016). There is a ZAKα-dependent increase in the expression of atrial natriuretic factor (ANF), a marker of hypertrophy, following TGF-β treatment (Huang *et al.*, 2004b). Another marker of hypertrophy, brain natriuretic peptide (BNP), was also increased in the rat myoblast cell line (H9C2) following ZAKα overexpression, as well as increased cell size (Hsieh *et al.*, 2015). Increased nuclear translocation of key hypertrophy transcription factors p-c-JUN and p-GATA-4, are likely causing the upregulation of ANP and BNP (Hsieh *et al.*, 2015). Overexpression of ZAKα in H9C2 cells resulted in increased matrix metalloproteinase (MMP)-2 activity through P38 and JNK signalling, as well as decreased MMP-9 activity through increased tissue inhibitor of metalloproteinases (TIMP)-1/2 expression (Cheng *et al.*, 2009). Overexpression of ZAKα, therefore, also appears to lead to myocardial ECM remodelling and fibrosis, associated with chronic heart diseases (Cheng *et al.*, 2009).

Whilst ZAKβ is the isoform normally expressed in the hearts of humans (GTEx Portal)(Fuller *et al.*, 2015), ZAKα expression has been identified in the human hearts that have had a myocardial infarction (Fu *et al.*, 2016). In the H9C2 cell line, transfection of ZAKβ has been shown to reduce the hypertrophic effects of ZAKα (Fu *et al.*, 2016). Recent research in H9C2 cells has shown upregulated ZAKβ to reduce BNP levels as well as have a protective role against apoptosis and cardiac hypertrophy caused by oxidised low-density lipoproteins (ox-LDLs) (Lin *et al.*, 2022). On the other hand, cardiac-specific ZAKβ over-expression in a transgenic mouse led to myocardial fibrosis, increased cardiac weight as well as a foetal gene expression profile and increased protein synthesis (Christe *et al.*, 2004).

It should be noted, however, that no observable abnormalities in the heart of humans are reported when ZAK is absent, with normal ECG traces and cardiac ultrasound results (Vasli *et al.*, 2017; Ahmad *et al.*, 2022). There is also no observable cardiac phenotype in $ZAK^{-/-}$ mice (Nordgaard *et al.*, 2022).

I have previously demonstrated *ZAKβ* expression in the developing heart, through ISH (figure 3.1), as well as *ZAKβ* expression in adult heart using qRT-PCR (figure

3.2). It is, consequently, of interest to investigate any cardiac abnormalities in zebrafish lacking both ZAK isoforms.

4.1.3. Aims

- Measure the size, mass and tail area of ZAKβ$^{-/-}$ zebrafish, relative to wild type, to determine any morphological phenotype.
- Measure the touch-induced alternative coiling in one and two dpf ZAKβ$^{-/-}$ and KY$^{-/-}$ ZAKβ$^{-/-}$ embryos, to determine if there are any differences in the strength of muscle contractions in the absence of ZAKβ or KY and ZAKβ.
- Assess swimming capability in ZAKβ$^{-/-}$ adult zebrafish, at a range of ages, relative to wild type.
- Investigate a potential role for ZAK heart function by measuring the heart rate embryos lacking ZAKα, ZAKβ and both ZAK isoforms.

4.2. Results

4.2.1. No Morphological Differences were Found in ZAKβ$^{-/-}$ Zebrafish Compared to Siblings

4.2.1.1. Morphology of Three-Month-old ZAKβ$^{-/-}$ Zebrafish

For the analyses reported in this chapter, crosses of ZAKβ$^{+/-}$ X ZAKβ$^{-/-}$ zebrafish were set up to produce tanks of fish where 50% of the progeny are homozygous mutant (ZAKβ$^{-/-}$) and 50% of the progeny are heterozygous siblings that could serve as controls. Both were reared together, with exposure to the same environmental conditions and access to food. This minimises unintended variables, and any investigator bias has been minimised by carrying out the measurements blind, only genotyping after the analyses were completed. The one exception to this method is reported in section 4.2.3.3. where age-matched old wild type controls are compared to ZAKβ$^{-/-}$ zebrafish.

The size and weight were measured at three months of age, prior to fin clipping and genotyping. The height of the zebrafish was always measured immediately anterior to the anal fin (HAA) (Parichy *et al.*, 2009). The length of the zebrafish was measured from the tip of the jaw (snout) to the base of the tail, anterior to the dorsal fin (most posterior region of the caudal peduncle). There were no significant differences in either the height or the length of ZAKβ$^{-/-}$ zebrafish and siblings (figure 4.1 (a) and 4.1 (b)). There was also no difference in the mass (figure 4.1 (c)).

Figure 4.1 (d) demonstrates how the tail area was calculated. This was done by multiplying the height of the zebrafish by the length of the tail. The tail length extends from the HAA line to the base of the tail. There was no difference in the tail area between ZAKβ$^{-/-}$ zebrafish and siblings (figure 4.1 (e))

There is sizeable variation in the length and weight for both genotypes. Fulton's conditioning factor (K) is an equation devised to allow for an accurate comparison in mass between fish, in spite of variations in length (Jones *et al.*, 1999; Froese, 2006). Body mass index (BMI) was also calculated by mass (g) X Length (cm)$^{-2}$ (Ganassi *et al.*, 2018; Latha Ramalingam, 2021). Even when taking the length into consideration, there were still no statistically significant differences in the standardised weight (K) or BMI for ZAKβ$^{-/-}$ zebrafish compared to siblings (figure 4.1 (f) and figure 4.1 (g)).

There were no differences in any of the observable morphological phenotypes between three-month-old ZAKβ$^{-/-}$ zebrafish and siblings.

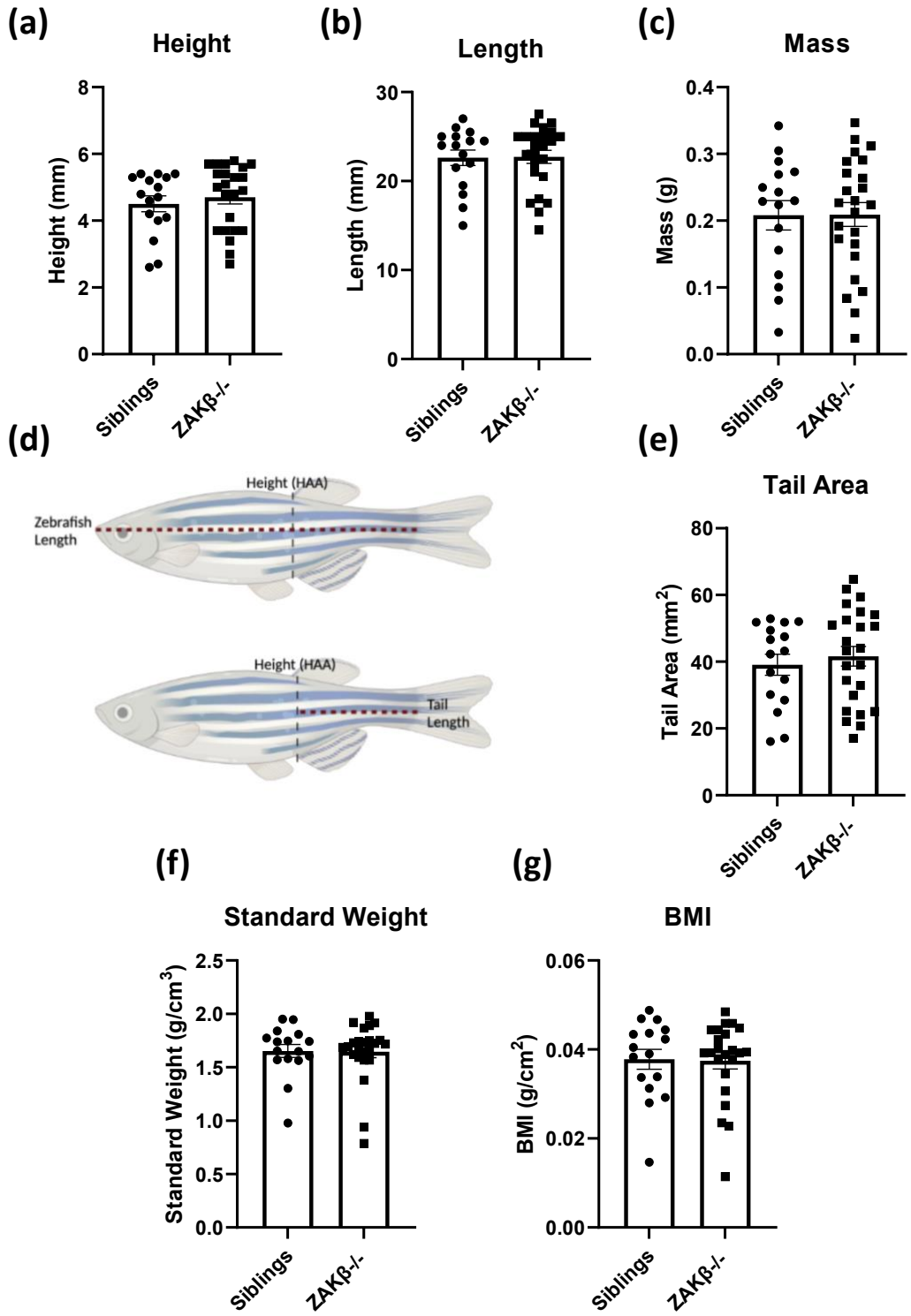

Figure 4.1. Measurements of various morphological differences in three-month-old ZAKβ$^{-/-}$ zebrafish and siblings.
Zebrafish from a ZAKβ$^{+/-}$ X ZAKβ$^{-/-}$ lay were raised before weighing and measuring the length. Zebrafish were fin clipped and genotyped following the measurements. (a) Height (b) Full length. (c) Mass (d) A cartoon detailing how the height at anterior to anal fin (HAA), zebrafish length and tail length were measured. (e) Tail area is calculated by multiplying the HAA by the tail length. (f) Standard weight is calculated by mass(g)/length of fish^3. (g) Body mass index (BMI) is calculated by mass (g)/length^2. Each data point is an individual recording, the bar chart and error bars are mean +/- standard error of the mean. An F-test was used to assess equal variation. An unpaired, two tailed t-test was the statistical test performed. No significant differences between ZAKβ$^{-/-}$ and sibling zebrafish for all body parameters investigated.

4.2.1.2. Morphology of 23-Month-Old ZAKβ$^{-/-}$ Zebrafish

Siblings from a ZAKβ$^{+/-}$ X ZAKβ$^{-/-}$ lay were raised in the same tank until 23-months-old. Measurements were taken and the fish were then fin-clipped and genotyped. The same measurements as in the 3-month-old zebrafish were assessed: the height, length, mass, tail area, standardised weight and BMI were measured, and there were no differences between ZAKβ$^{-/-}$ zebrafish and siblings (figure 4.2 (a-f)).

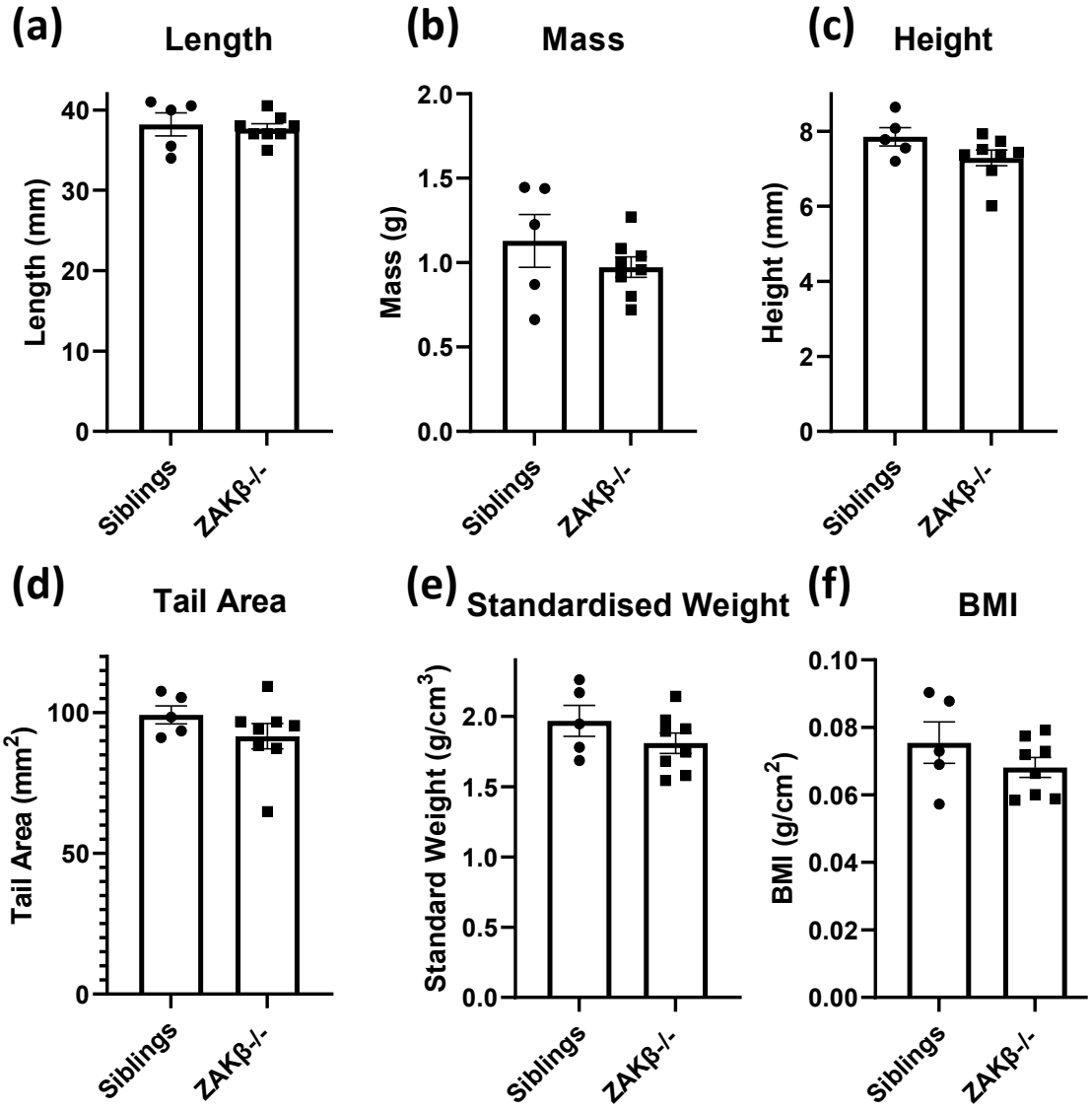

Figure 4.2. Measurements of various morphological differences in 23-month-old ZAKβ$^{-/-}$ zebrafish and siblings.
Zebrafish from a ZAKβ$^{+/-}$ X ZAβ$^{-/-}$ lay were raised before weighing and measuring the length. Zebrafish were fin-clipped and genotyped following the measurements. (a) Full length (b) Mass. (c) Height (d) Tail area is calculated by multiplying the HAA by the tail length. (e) Standard weight is calculated by mass(g)/length of fish^3. (f) Body mass index (BMI) is calculated by mass (g)/length^2. Each data point is an individual recording, the bar chart and error bars are mean +/- standard error of the mean. An F test was used to assess equal variation. An unpaired, two-tailed t-test was the statistical test performed. No significant differences between ZAKβ$^{-/-}$ and sibling zebrafish for all body parameters investigated.

4.2.2. No Differences in the Strength of Contraction in ZAKβ$^{-/-}$ Zebrafish

The heads of 1 and 2 dpf wild type and ZAKβ$^{-/-}$ zebrafish embryos were embedded in low melting temperature agarose, with the tails free to move in E3 media, in order to assess potential abnormalities in locomotion or strength of contraction, occurring with absence of ZAKβ. Further details of the protocol, including a diagram, can be found in section 2.11 (figure 2.2), and are based on research by (Hirata *et al.*, 2012). As an additional variable, zebrafish embryos lacking both KY and ZAKβ were also assessed to see if combined absence of two proteins, where mutations are associated with human congenital myopathy, result in locomotion defects.

Once the heads were embedded, the tails were provided with gentle tactile stimulation and a video recording of the respective movement was recorded. The individual frames across 0.33 second intervals in wild type, ZAKβ$^{-/-}$ and KY$^{-/-}$ ZAKβ$^{-/-}$ zebrafish embryos can be seen in figures 4.3 (a-c). The individual frames were processed and superimposed, with the maximum angle of tail-bend indicating the strength of the muscle contraction (as demonstrated in figure 4.3 (d)).

The average maximum tail-bend angle at 1 dpf was 79^{o} for wild type, 80^{o} for ZAKβ$^{-/-}$ and 75^{o} for KY$^{-/-}$ ZAKβ$^{-/-}$ (figure 4.3 (e)). The average maximum tail-bend angle at 2 dpf was 32^{o} for wild type, 31^{o} for ZAKβ$^{-/-}$ and 29^{o} for KY$^{-/-}$ ZAKβ$^{-/-}$ (figure 4.3 (f)). There were no statistically significant differences in the maximum angle of tail-bend at either 1 dpf or 2 dpf, indicating no differences in the strength of muscle contraction, at least up to 2 dpf, when ZAKβ or KY and ZAKβ are absent.

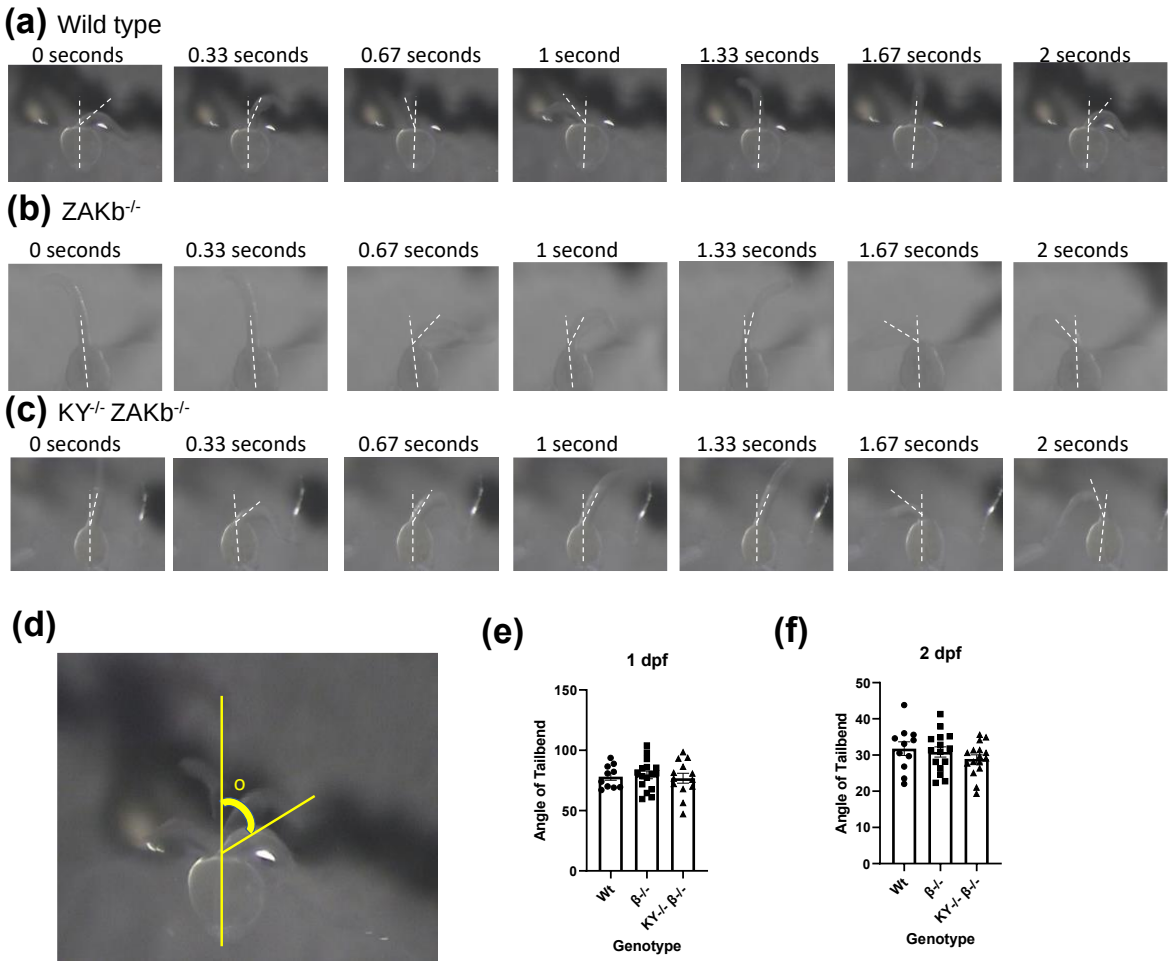

Figure 4.3. Angle of tail bend contraction following tactile stimulation in wild type, ZAKβ$^{-/-}$ and KY$^{-/-}$ ZAKβ$^{-/-}$ embryos.
The heads of embryos were embedded in low melting temperature agarose and the tails free in E3 media. wt = Wild type. β$^{-/-}$ = ZAKβ$^{-/-}$. (a-c) Timelapse of individual frames across multiple time-points for wild type, ZAKβ$^{-/-}$ and KY$^{-/-}$ ZAKβ$^{-/-}$. White dashed lines are to make it easier to identify tails. (d) Superimposed image of the individual frames of a wild type embryo at 1 dpf, demonstrating how the maximum angle of tail bend was calculated (e) No difference in the angle of tail bend at 1 dpf (f) No differences in the angle of tail bend at 2 dpf between wild type, ZAKβ$^{-/-}$ and KY$^{-/-}$ ZAKβ$^{-/-}$ zebrafish. Frames were superimposed and the maximum tail bend angle was determined using Image J. One way ANOVA with Tukey's post hoc analysis was the statistical test. Each data point is an individual recording, the bar chart and error bars are mean +/- standard error of the mean. No asterisk = no significance.

4.2.3. Investigating the Swimming Capabilities of Adult Zebrafish Lacking ZAKβ

Given no differences in the strength of contraction in ZAKβ$^{-/-}$ larvae, it was of interest to investigate differences in the strength/swimming ability of adults. It is arguably more pertinent, given myopathies often follow a progressive degeneration of muscle strength.

Adult zebrafish were transferred to a recording tank and left to acclimatise for 10 minutes, before a five-minute recording of zebrafish swimming is taken. 30 seconds of the first half of the recording, and 30 seconds of the second half of the recording were processed using ShadowFish tracking software, to determine the (X, Y) co-ordinates of seven equal points across the spine of the zebrafish for each frame. The co-ordinates for each frame were processed using MATLAB to investigate a range of parameters: Mean velocity, distanced travelled, average time spent moving, mean swimming duration, the frequency of tailbeats at low, medium and high speeds as well as the amplitude (degree of bending) at low, medium and high speed. See section 2.12 for full details of the procedure, including an image of the setup. Fin clips were taken and zebrafish were genotyped following the recording, allowing the experiment to be performed blind, as well as preventing the dissections from affecting zebrafish swimming behaviour.

Typically laboratory-raised zebrafish have a lifespan of 3-5 years with 'old zebrafish' being described as greater than 25 – 30 months (Gilbert *et al.*, 2014; Dilan *et al.*, 2018). I have raised my lines of Zebrafish to 6 months of age (young), 18 months of age (medium-aged) and 35 months of age (old) for a progressive assessments of swimming capabilities of ZAKβ$^{-/-}$ zebrafish as they age. Young and medium-aged zebrafish are siblings, progeny from a ZAKβ$^{-/-}$ X ZAKβ$^{+/-}$ cross, raised in the same tank, analysed blind and genotyped post-recording. Age-matched wild type and ZAKβ$^{-/-}$ zebrafish are compared for the old-age assessment at 35-months of age.

4.2.3.1 Swimming Parameters in Young (6-months) Adult Zebrafish

Despite a general downward trend in ZAK$\beta^{-/-}$ zebrafish at 6-months of age, there are no significant differences in the average distance travelled, velocity, percentage of time spent moving and swimming episode compared to wild type zebrafish (figures 4.4 (a-d)). In contrast, figures 4.4 (e-l) demonstrate a general trend for increases in the mean tail-beat frequency and amplitude at all speeds for ZAK$\beta^{-/-}$ zebrafish, and a significant increase in the mean low speed tail-bend amplitude. An increase in the tail-bend amplitude for lower speeds, might indicate that the ZAK$\beta^{-/-}$ zebrafish have to work harder by bending the tail more to create the propulsions required to travel, even at slightly lower speeds and distances.

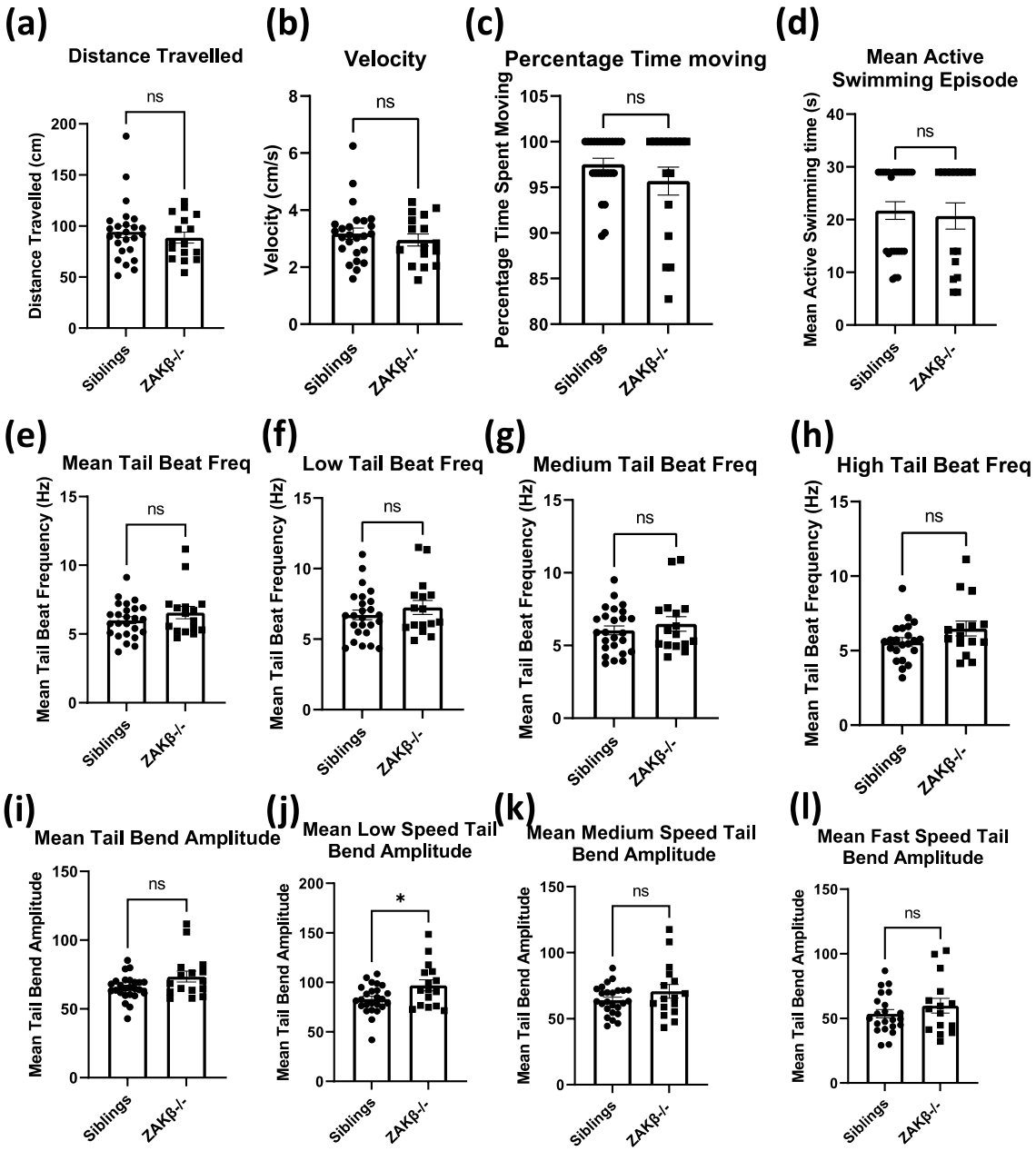

Figure 4.4. Comparison of key swimming attributes between young (6-months-old), adult ZAKβ$^{-/-}$ and siblings.

A ZAKβ$^{+/-}$ X ZAKβ$^{-/-}$ lay were raised in the same tank, together. The zebrafish were transferred to a recording tank, left to acclimatise for 10-minutes, before a 5-minute video recording. A 30-second recording from the first half and a 30-second recording from the second half were processed using ShadowFish and the tracked frames co-ordinates were processed for key swimming attributes using MATLAB: (a) Distance travelled (cm). (b) Velocity (cm/s). (c) Percentage of time moving. (d) Mean length of time for each swimming episode (s). (e) Mean tail beat frequency (hertz). (f-h) Mean tail beat frequency at low, medium and high speeds, respectively. (i) Mean tail bend amplitude. (j-l) The mean tail bend amplitude at low, medium and high speeds, respectively. Each data point is an individual recording, the bar chart and error bars are mean +/- standard error of the mean. An unpaired, two tailed t-test was the statistical test performed. Ns = not significant. * P ≤ 0.05. Twelve Wild type and eight ZAKβ$^{-/-}$zebrafish had recordings taken, providing 24 data points for wild type and 16 data points for ZAKβ$^{-/-}$.

4.2.3.2 Swimming Parameters in Medium-Aged (18-months) Zebrafish

The video capture software, ShadowFish, cannot accurately and consistently track the (X,Y) co-ordinates in older zebrafish. The longer pectoral and tail fins in the older zebrafish can temporarily confuse the tracking software, with the software mistaking a fin for the head. Consequently, the angle of the tail-bend and frequency of the tail-beat are not reliable in fish older than 6 months. The distance travelled, mean velocity, average time spent moving and mean percentage of time spent moving can still be reliably measured.

Measurements of 18-month-old heterozygous sibling zebrafish showed a mean distance travelled per 30 seconds of 100 cm, whereas the mean distance travelled for the ZAKβ$^{-/-}$ zebrafish was 93 cm (figure 4.5 (a)). The mean velocity for siblings was 3.4 cm/s versus 3.1 cm/s for ZAKβ$^{-/-}$ zebrafish (figure 4.5 (b)). All heterozygous sibling zebrafish spent 100% of the time moving, with a mean active swimming episode duration of 30 seconds (figure 4.5 (c-d)), while the mutant ZAKβ$^{-/-}$ zebrafish were moving less, only 95% of the time, with a mean active swimming episode of 22 seconds (figure 4.5 (c-d)).

The trend of decreased distance and velocity in ZAKβ$^{-/-}$ zebrafish compared to siblings is not statistically significant, however, there is a significant decrease in the percentage of time spent moving and the mean duration of swimming episode for ZAKβ$^{-/-}$ zebrafish, compared to heterozygous siblings.

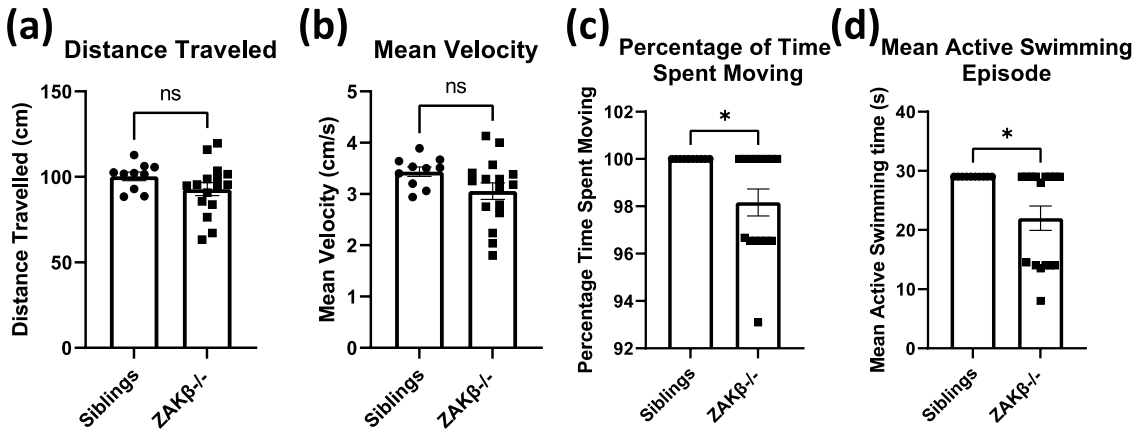

Figure 4.5. Comparison of key swimming attributes between medium-aged (18-months-old), adult ZAK$\beta^{-/-}$ and siblings.

Age-matched ZAK$\beta^{-/-}$ and siblings were placed in recording tank. Following a 10-minute acclimatisation, a 5-minute recording was taken of the fish swimming. A 30-second clip from the first half and a 30-second clip from the second half was processed with ShadowFish tracking software and the co-ordinates automatically processed using MATLAB. Sibling and ZAK$\beta^{-/-}$ zebrafish were compared for a range of swimming categories: (a) The mean distanced travelled. (b) The mean velocity. (c)The percentage of time the zebrafish spends moving. (d) The mean length of time for each swimming episode. Each data point is an individual recording, the bar chart and error bars are mean +/- standard error of the mean. A ROUT test was performed to eliminate anomalies. An unpaired, two-tailed t-test was the statistical test performed. * $P \leq 0.05$. Six Wild type and eight ZAK$\beta^{-/-}$zebrafish recordings were taken, providing twelve data points for wild type and sixteen data points for ZAK$\beta^{-/-}$ zebrafish. ROUT test for anomalies eliminated two data points for wildtype for distance travelled and two data points for mean velocity.

4.2.3.3. Swimming Parameters in Old-Aged (35-month) Zebrafish

Raising a tank of zebrafish to 35 months is challenging as this is very old for laboratory-reared zebrafish (Gilbert *et al.*, 2014; Dilan *et al.*, 2018). Consequently, there is considerable death over time, which can result in an uneven distribution of mutants and control siblings in a mixed-genotype tank. Therefore, for the old-age group, age-matched wild type controls were instead used as a comparison. The age-matched wild type controls were from the same genetic background (AB), but raised in a separate tank from the ZAKβ$^{-/-}$ zebrafish to maximise the number of controls and mutants reared. The distance travelled, mean velocity, average time spent moving and mean percentage of time spent moving were measured and shown in figure 4.6.

Wild type zebrafish had a mean distance travelled per 30 seconds of 80 cm, whereas the mean distance travelled for the ZAKβ$^{-/-}$ zebrafish was 33 cm (figure 4.6 (a)). The speed of swimming was also greatly reduced, with the mean wild type velocity being 2.71 cm/s against the 0.88 cm/s for ZAKβ$^{-/-}$ zebrafish (figure 4.6 (b)). Wild type zebrafish spent 97% of the time moving with a mean active swimming episode duration of 21 seconds. ZAKβ$^{-/-}$ zebrafish, however, spent only 54% of the time moving, with a mean active swimming episode of 7 seconds (figure 4.6 (c-d)). ZAKβ$^{-/-}$ zebrafish are swimming less than aged-matched wild type controls and when they do swim, it is for considerably shorter bursts.

Older zebrafish are slower and spend less time moving than young (6-months; figure 4.4) and medium-aged (18-months; figure 4.5) zebrafish. The mean distance travelled for siblings was 94 cm for young zebrafish, 100 cm for medium-aged zebrafish and 80 cm for old wild type zebrafish, however the mean distance travelled was 33 cm for old ZAKβ$^{-/-}$ zebrafish. The mean velocity of sibling zebrafish was 3.2 cm/s for young, 3.4 cm/s for medium-aged and 2.71 cm/s for old-age wild type zebrafish, however, the mean velocity of old-age ZAKβ$^{-/-}$ zebrafish was 0.88 cm/s. The mean active swimming episode was also reduced in old age wild type zebrafish, compared to young and medium-aged sibling zebrafish, however, this was also greater reduced in ZAKβ$^{-/-}$ zebrafish. These findings could suggest that natural muscle degeneration that occurs during aging is enhanced in the absence of ZAKβ.

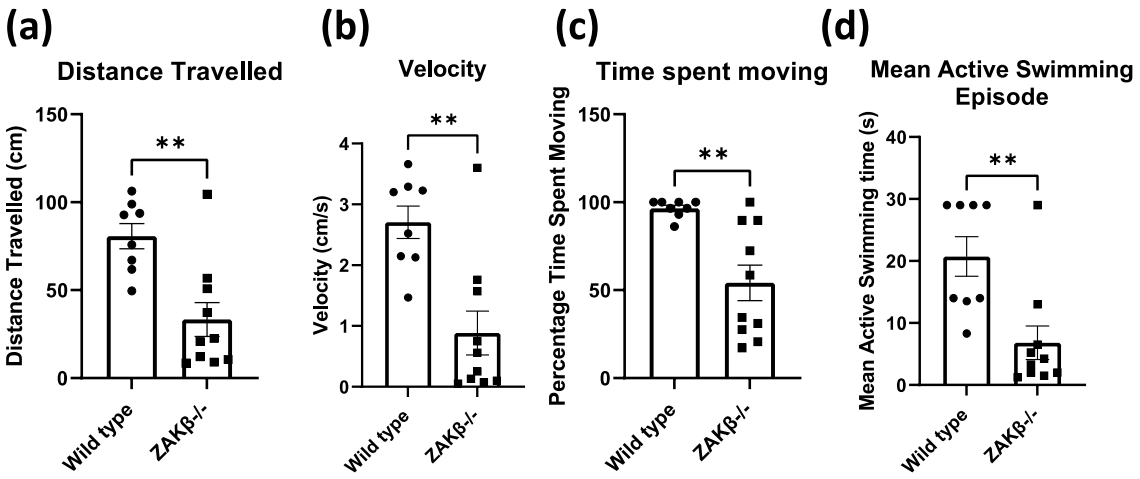

Figure 4.6. Comparison of key swimming attributes between old (35-months-old), adult ZAK$\beta^{-/-}$ and age-matched wild type controls.

Old ZAK$\beta^{-/-}$ zebrafish swim less than age matched wild type control zebrafish. Age-matched ZAK$\beta^{-/-}$ and wild type zebrafish were placed in recording tank. Following a 10-minute acclimatisation, a 5-minute recording was taken of the fish swimming. A 30-second clip from the first half and a 30 second-clip from the second half was processed with ShadowFish tracking software and the co-ordinates automatically processed using MATLAB. Wild type and ZAK$\beta^{-/-}$ were compared for a range of key swimming attributes: (a) The mean distanced travelled. (b) The mean velocity. (c)The percentage of time the zebrafish spends moving. (d) The mean length of time for each swimming episode. Each data point is an individual recording, the bar chart and error bars are mean +/- standard error of the mean. An unpaired, two-tailed t-test was the statistical test performed. ** P ≤ 0.01. Four Wild type and five ZAK$\beta^{-/-}$zebrafish recordings were taken, providing eight data points for wild type and ten data points for ZAK$\beta^{-/-}$ zebrafish.

4.2.4 Alterations to the Heart Rate in Zebrafish Embryos when ZAKα, ZAKβ or Both Isoforms are Absent

There are no reported cardiac abnormalities in humans and mice with mutated *ZAK* (Vasli *et al.*, 2017; Ahmad *et al.*, 2022; Nordgaard *et al.*, 2022). Nevertheless, given the expression of *ZAKβ* in the embryonic and adult hearts of zebrafish, it was still of interest to investigate the possibility of heart abnormalities in the absence of ZAK. Wild type, ZAKβ$^{-/-}$, ZAKα$^{-/-}$ and ZAKα$^{-/-}$ ZAKβ$^{-/-}$ embryos at either 1, 2, 3 or 6 dpf were anaesthetised to prevent movement, and recorded for one-minute to assess any differences in the heart rate. See section 2.13. for further detail on the protocol.

Video analysis of beating hearts in embryos at 1 dpf revealed no differences in the heart rate at 1 dpf between any of the genotypes (figure 4.7 (a)). At 2 dpf, the mean heart rate is 100 bpm for wild type, 89 bpm for ZAKβ$^{-/-}$, 85 bpm for ZAKα$^{-/-}$ and 89 bpm for ZAKα$^{-/-}$ ZAKβ$^{-/-}$ (figure 4.7 (b)). The differences in the mean are not statistically significant, however.

At 3 dpf, embryos, there was a significant reduction in the heart rate when ZAKβ, ZAKα and both isoforms were absent (figure 4.7 (c)). The mean heart rate was 126 bpm for wild type, 103 bpm for ZAKβ$^{-/-}$, 96 bpm for ZAKα$^{-/-}$ and 101 bpm for ZAKα$^{-/-}$ ZAKβ$^{-/-}$.

The same trend of decreases in the heart rate when ZAKα, ZAKβ and both isoforms are absent exists at 6 dpf, however, the reductions are not significant, and appear improved (closer to the wild type heart rate than at 3 dpf) (figure 4.7 (d)). The mean heart rate was 143 bpm for wild type, 124 bpm for ZAKβ$^{-/-}$, 130 bpm for ZAKα$^{-/-}$ and 139 bpm for ZAKα$^{-/-}$ ZAKβ$^{-/-}$.

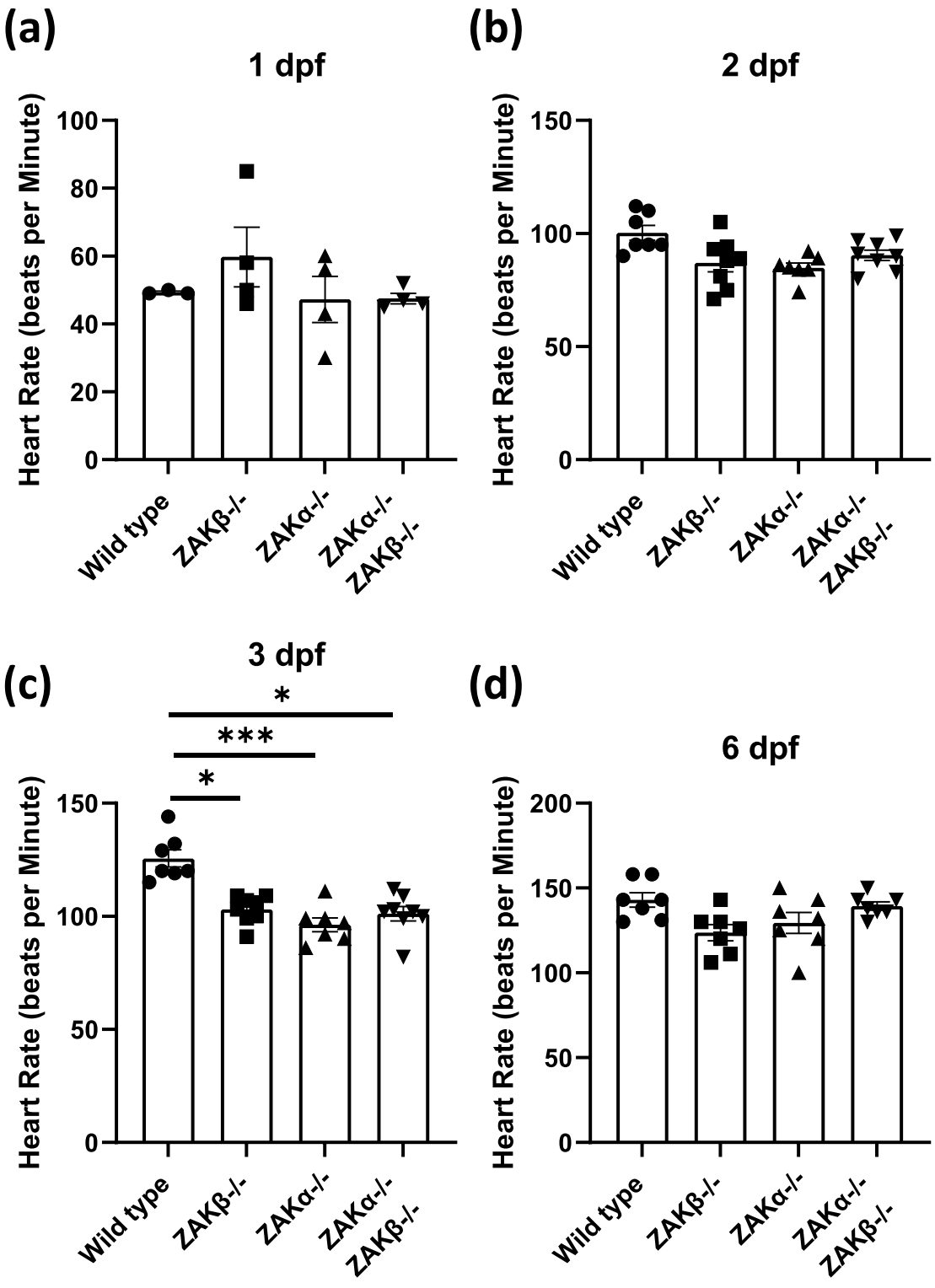

Figure 4.7. The impact of absence of ZAK isoforms on heart rate in zebrafish embryos. There is a significant decrease in the heart rate at 3 dpf when either ZAKα, ZAKβ or both isoforms are absent. Zebrafish were anaesthetised and the heart rate was immediately measured. Wild type, ZAK$\alpha^{-/-}$, ZAK$\beta^{-/-}$ or ZAK$\alpha^{-/-}$ ZAK$\beta^{-/-}$ heart rates were measured at (a) 1 dpf. (b) 2 dpf. (c) 3 dpf. (d) 6 dpf. There was a general trend for decreased heart rates when ZAKα, ZAKβ or both isoforms are absent. The decreased trend was only significant at 3 dpf. Each data point is an individual recording, the bar chart and error bars are mean +/- standard error of the mean. Kruskal Wallace test with Dunn's multiple comparison post hoc analysis was the statistical test for analysis. No asterisk = not significant * $P \leq 0.05$. *** $P \leq 0.001$.

4.3. Discussion

4.3.1. No Morphological Differences in the Absence of ZAKβ

The data presented in this chapter show that there are no overt morphological differences between ZAKβ$^{-/-}$ and siblings in either 3-month-old or 23-month-old zebrafish. The length, height, tail area, mass, standardised mass and BMI were all measured. The lack of differences in the measurements are consistent with the finding that ZAK$^{-/-}$ mice do not have any observable differences in terms of weight compared to their sibling littermates (Nordgaard *et al.*, 2022). The height and weight of humans with a ZAK mutation is not reported and cannot be used for comparison, however, atrophy of thigh muscle was a common phenotype, as were smaller slow-twitch fibres (Vasli *et al.*, 2017; Ahmad *et al.*, 2022).

4.3.2. No changes in the Strength of Muscle Contractions in Zebrafish Larvae in the Absence of ZAKβ or KY and ZAKβ

In zebrafish, slow-twitch fibres are exclusively used for muscle contractions at 24 hpf, with morpholino knockdown of *sMyHC1* and *sMyHC2* resulting in loss of all movement/muscle contraction at 24 hpf but no differences at 48 hpf (Naganawa and Hirata, 2011). Morpholino knockdown in the fast-twitch-specific ryanodine receptor 1 (*ryr1b*) and flightless I homolog (*flii*) did not affect the muscle contractions at 24 hpf, however there was a significant reduction at 48 hpf (Naganawa and Hirata, 2011). This indicates that fast-twitch fibres are required for effective muscle contraction at 48 hpf, but not before. A complete loss of movement at 48 hpf only occurs when *sMyHC1* and *sMyHC2* are both knocked down, suggesting that whilst fast-twitch muscles are primarily responsible for burst swimming at 48 hpf, slow-twitch fibres can still contribute (Hirata *et al.*, 2007b; Naganawa and Hirata, 2011). In the ZAKβ$^{-/-}$ or KY$^{-/-}$ ZAKβ$^{-/-}$ embryos, no differences in the strength of contraction was found at 24 or 48 hpf relative to wild type, indicating that at this early point of development, the absence of ZAKβ, or KY and ZAKβ does not result in any changes to the strength of muscle contractions in either slow-twitch or fast-twitch muscle fibres. In mice, the association of ZAKβ and KY being together as part of a protein complex at the Z-disc (Beatham *et al.*, 2004; Baker *et al.*, 2010), led to the hypothesis that combined absence might result in a more severe phenotype. At this early stage of development, however, combined absence of ZAKβ and KY does not appear

to result in any changes to the strength of muscle contractions in either slow-twitch or fast-twitch muscle fibres. Ideally, single KY$^{-/-}$ zebrafish should be used as an additional variable for the experiment, however, insufficient tank space as well as time to conduct the experiments, prevented the use of KY$^{-/-}$ zebrafish. Thus, single KY mutants should be generated for future work, to facilitate more robust analysis.

4.3.3. Locomotion in ZAKβ$^{-/-}$ Zebrafish at Various Ages

ZAK$^{-/-}$ mice are indistinguishable from their sibling littermates in terms of locomotor activity and exploratory behaviour (Nordgaard *et al.*, 2022). A subset of human patients with mutated ZAK typically shows some delays in motor development, as well as a waddling gait (Vasli *et al.*, 2017). A Pakistani family with a recently identified, novel *ZAK* mutation reported difficulties in movement, with quadrupedal locomotion preferred for this limited movement (Ahmad *et al.*, 2022). This was a much more severe phenotype than reported for any other of the patients, including a separate Pakistani family characterised by (Vasli *et al.*, 2017), and likely due to a confounding genetic background.

The tracking software, ShadowFish, is highly effective and accurate at tracking young adult zebrafish swimming. Fish become larger as they age, as does the fin length. The larger size and fin length appears to cause issues with the tracking software, leading to inaccuracies in locating the spine dimensions, therefore invalidating the accuracy of some of the parameters measured (tail-beat frequency and amplitude). If ShadowFish tracking software is to be used for tracking zebrafish movement parameters, there will need to be further development for processing data in older zebrafish, to avoid the inaccuracies of the tracking co-ordinates.

In young adult zebrafish (6-months old), there was a slight trend for decreased swimming distance, velocity, percentage of time swimming and average duration of swimming burst in young fish lacking ZAKβ, compared to siblings. A small increase in tail-bend amplitude and frequency was also observed in young zebrafish lacking ZAKβ, compared to siblings. None of these measurements showed statistical significance. However, the tail-bend amplitude at low speeds was significantly greater in young zebrafish lacking ZAKβ compared to controls. An increase in the angle of the tail-bend could indicate that ZAKβ$^{-/-}$ zebrafish are

working harder and having to bend their tail more, in order to achieve movement (McHenry and Lauder, 2005; Keatinge *et al.*, 2015).

The same trend for reduced swimming distance, velocity, percentage of time swimming and average duration of swimming episode in fish lacking ZAKβ, was observed in medium-aged zebrafish (18 months). The percentage of time spent moving and the duration of swimming episode were significantly reduced, where ZAKβ$^{-/-}$ zebrafish stop more often, resulting in shorter swimming episodes than their sibling counterparts. This could tie in with the increased tail-bend amplitude in younger ZAKβ$^{-/-}$; with zebrafish lacking ZAKβ, working harder to move and not getting the same coasting momentum that wild type zebrafish achieve, resulting in more frequent stops (similar to a hypothesis by (McHenry and Lauder, 2005)). My hypothesis is that the shorter bursts and greater number of stops require a greater tail-bend amplitude to re-commence movement again, versus general cruising. As this protocol cannot accurately measure the tail-bend amplitude and tail-beat frequency in medium/old-aged zebrafish, it remains unknown as to whether the increased tail-bend identified in young ZAKβ$^{-/-}$ is also seen, or potentially more pronounced, in older zebrafish lacking ZAKβ.

There was a significant reduction in all four swimming parameters assessed in old-age ZAKβ$^{-/-}$ zebrafish (35 months). The aged ZAKβ$^{-/-}$ zebrafish were found to be swimming shorter distances, at slower speeds, with reduced percentage of time spent moving and shorter durations in each burst of swimming-episode. These findings suggest that the myopathic phenotype is progressive and the deterioration in strength and swimming capabilities manifests in older ZAKβ$^{-/-}$ zebrafish. It should be noted that for the old-age condition, the wild type and ZAKβ$^{-/-}$ zebrafish were raised in different tanks and will have had slight differences in the amount of food or fresh system water flow per day and, therefore, the role of a slightly different environment cannot be ruled out. Efforts were made to standardise the environment of the two separate tanks: The two populations are age-matched, with the same population size, same tank size and the same feeding regime. The age-matched wild type zebrafish were of the same genetic background (AB) as the ZAKβ$^{-/-}$ zebrafish, minimising the likelihood of differences in the swimming parameters arising from differences in the swimming capabilities of different strains (Wakamatsu *et al.*, 2019).

This data shows a reduction in swimming speed, distance and time spent moving in old-age zebrafish, compared to young and medium-aged zebrafish. This decline was accelerated when ZAKβ is absent, indicating that absence of ZAKβ may result in an accelerated skeletal muscle ageing process and decline in locomotion. Future studies into the mechanism of ZAK activity should also be investigated using older zebrafish.

4.3.4. There is a Significant Reduction in the Heart Rate of 3 dpf Zebrafish Embryos in the Absence of ZAK

There is a significantly decreased heart rate in embryos lacking ZAKα and ZAKβ that is apparent at 3 dpf, while at other developmental stages, any apparent decreases were not statistically significant. It is difficult to rationalise the changes in heart rate in *ZAK* mutants that are evident at 3 dpf, while not at 6 dpf; perhaps a progressive deterioration in *ZAK* mutant embryos is compensated for by other mechanisms at this later larval stage. Alternatively, the progressive decline could also indicate a delay in the development of the heart, in the absence of either ZAK isoform, that is overcome by 6 dpf. Indeed, lamin A (*lmna*) mutant zebrafish show cardiac abnormalities at 3 dpf that have largely subsided by 7 dpf (Nicolas et al., 2022). The decreases in heart rate when only ZAKα is absent is difficult to interpret, given that the expression analysis (ISH and qRT-PCR, chapter 3) shows *ZAKβ* to be the predominant gene expressed in the embryonic and adult heart, and no compensatory upregulation of *ZAKα* is apparent in the absence of ZAKβ.

Bradycardia (slower-than-normal heart rate) can indicate abnormalities in the heart, including myocarditis (inflammation of the heart) (Sagar *et al.*, 2012), congenital heart defects (Fahed *et al.*, 2014) and cardiomyopathy (Huttner *et al.*, 2013; Sidhu and Marine, 2020). Indeed, there are several cases of neuromuscular diseases resulting in both a skeletal and cardiac muscle myopathy in humans (Finsterer and Stöllberger, 2016; Feingold *et al.*, 2017). Targeting certain genes, such as *BAG3* and *NEB* in zebrafish leads to impaired heart and skeletal muscle function (Norton *et al.*, 2011; Ding *et al.*, 2019; Telfer *et al.*, 2012). All genotypes were raised in the same density, using the same media, thus, ruling out the possibility of bradycardia arising from environmental

differences, such as the composition of the media or stress from the number of embryos.

The expression of *ZAKβ* in the embryonic and adult heart, coupled with the apparent decrease in heart rate when ZAKβ is absent, is encouraging and should lead to further investigation. Homozygous ZAKβ null zebrafish were bred into the Tg (fli1:GFP) transgenic zebrafish line, for image analysis of the vasculature and heart of zebrafish lacking ZAKβ (Lawson and Weinstein, 2002). Unfortunately, due to COVID, there was insufficient time to assess possible abnormalities of ZAKβ-/- embryo hearts in this transgenic line using live-imaging confocal microscopy. A comparison of the general heart morphology, and the percentage fractional shortening, between ZAKβ$^{-/-}$ and wild type controls are examples of analyses that could be performed.

Additionally, investigating the heart rate, as well as structural differences, in adult zebrafish lacking either ZAK and/or KY is a further option to explore for a possible cardiac phenotype. KY has also been shown to be expressed in the heart of mice (Blanco *et al*., 2001), so dual absence may present with a stronger phenotype.

4.4. Conclusion

There were no significant morphological differences in terms of the weight or size of ZAKβ$^{-/-}$ zebrafish, relative to siblings, in young and old adult zebrafish. There were also no significant differences in the strength of muscle contractions in either slow or fast-twitch muscles in embryos lacking ZAKβ or ZAKβ and KY. Video capture and computational analysis of swimming revealed a decrease in swimming features in old-age zebrafish, compared to young and medium-aged zebrafish, that was significantly worse in zebrafish lacking ZAKβ. This is suggestive of a progressive phenotype when ZAKβ is absent in zebrafish, or that the full myopathic phenotype only manifests in older adult zebrafish lacking ZAKβ. The significant decrease in heart rate when ZAKβ, ZAKα and both isoforms are absent at 3 dpf is interesting and potential heart abnormalities, in patients and animal models of ZAK myopathy should be investigated further.

5. Investigating the Phenotype of ZAK$\beta^{-/-}$ Zebrafish. Part II: Molecular Analysis

5.1. Introduction

Following the creation and validation of ZAK$\alpha^{-/-}$, ZAK$\beta^{-/-}$ and ZAK$\alpha^{-/-}$ ZAK$\beta^{-/-}$ genetically-targeted zebrafish, this chapter investigates the molecular phenotype resulting from the lack of ZAK isoforms in skeletal muscle. The analyses of the physical phenotype of muscle strength and swimming capabilities is described in chapter four. This chapter will focus on the effects that ZAKβ might have on downstream signalling pathways and gene expression.

5.1.1. MAP3K (ZAK) Signalling and Downstream Effects

ZAK is a mitogen-activated protein (MAP) triple kinase (MAP3K) and is, thus, a component of the MAP kinase pathway. Whilst ZAK is novel in being the first member of the MAPK signalling pathway to be implicated with human myopathy, a role for the MAPK signalling pathway is well-established in myogenesis and muscle maintenance (Segalés *et al.*, 2016). ZAK has been shown to preferentially activate P38 (P38γ in particular) and JNK pathways through MKK3/MKK6 and MKK4/MKK7 respectively (Liu *et al.*, 2000; Gross *et al.*, 2002). P38 is essential for differentiation of myoblasts through irreversible cell cycle withdrawal (Perdiguero *et al.*, 2007) and P38γ promotes the fusion of myocytes (Ruiz-Bonilla *et al.*, 2008). JNK is a negative regulator of myogenesis, promoting myoblast proliferation (Huang *et al.*, 2007; Xie *et al.*, 2018). ERK1/2 has also been shown to be activated by ZAK (Gotoh *et al.*, 2001) and promotes myoblast proliferation, inhibits differentiation and at least ERK2 appears to be critical for fusion (Jones *et al.*, 2001; Knight and Kothary, 2011; Lathrop *et al.*, 1985). Figure 5.1. shows possible downstream effectors and interactors with ZAK, as well as the possible physiological consequence.

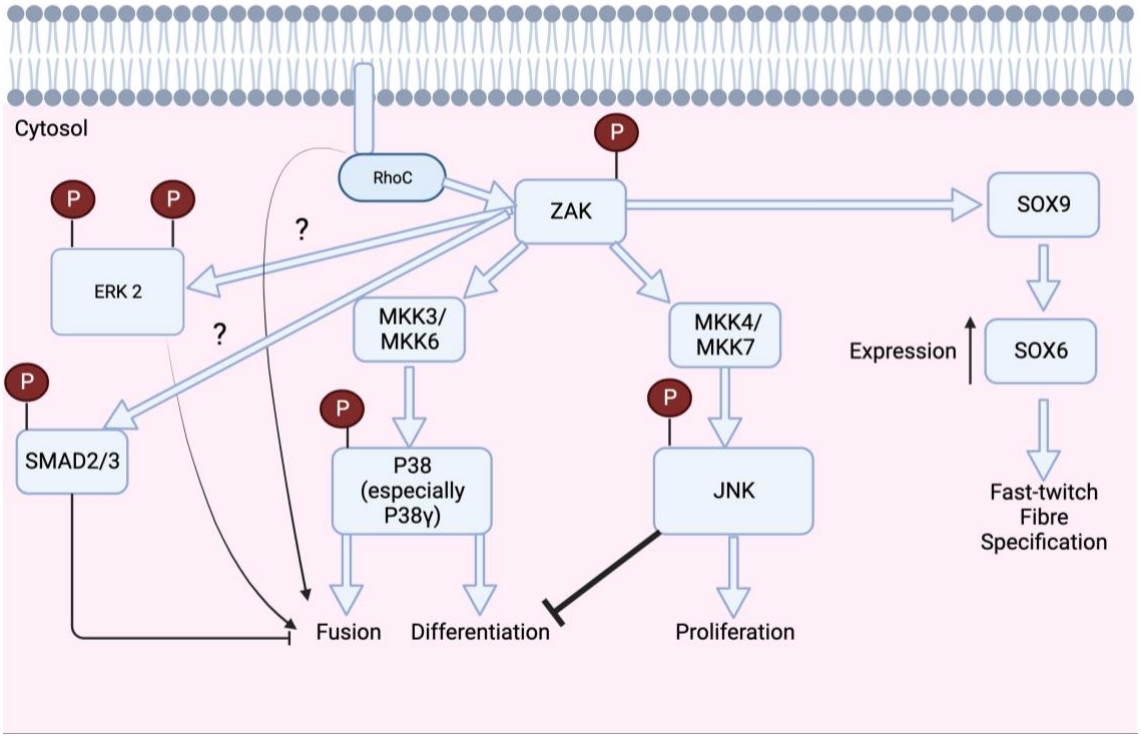

Figure 5.1 Possible ZAK Signalling Pathways in Myogenesis and Muscle Fibre Specification.
Diagram demonstrating possible protein interactors and the potential effects that ZAK signalling could have on myogenesis and muscle fibre specification. ZAK is a known activator of P38 (especially P38γ) and JNK, which have well established roles in myogenesis, promoting differentiation/fusion and proliferation, respectively. ZAK has been shown to activate ERK signalling, with ERK2 also playing a role in myoblast fusion. ZAK has been shown to increase the expression of *SOX6* via SOX9 which is important in the specification of fast-twitch muscle fibres. ZAK has also been shown to be involved in SMAD-dependent canonical TGF-β signalling, which has recently been identified as an important molecular brake in myoblast fusion. '?' indicates further investigation is required to establish if ZAKβ specifically can activate the respective pathway and, thus, the downstream effects. Image created using BioRender (biorender.com).

ZAK has been also been shown to be downstream of the small GTPase family member, RhoC, which plays a role in myoblast fusion, while the related RhoA has been shown to interact with ZAK and is essential for the initiation of myogenesis (Korkina *et al.*, 2013; Bryan *et al.*, 2005; Kong *et al.*, 2019). ZAK has been shown to be required for TGFβ dependent SMAD2/3 phosphorylation (Nyati *et al.*, 2016). This is of note as TGFβ signalling has recently been identified as a molecular brake in muscle fusion, where the process of myoblast fusion results in TGFβR1-TGFβR2 dimerization and activation (Melendez *et al.*, 2021; Girardi *et al.*, 2021). The SMAD dependent signalling results in RAB dependent receptor internalisation and degradation, therefore, no further fusion can occur, temporarily (Girardi *et al.*, 2021; Melendez *et al.*, 2021).

5.1.1.1. Genes Regulated Downstream of ZAK

Interestingly, (Suzuki *et al.*, 2012) showed ZAKβ to induce *SOX6* expression in *Xenopus laevis* (pathway included in figure 5.1). SOX6 belongs to the SOX (SRY-related HMG Box) family of transcription factors. Whole-mount *in situ* hybridisation (ISH) in *Xenopus* revealed *ZAKβ* to be expressed in the paraxial mesoderm and in the somites, with *SOX6* expression is also seen in the somites (Suzuki *et al.*, 2012). ZAKβ inducing *SOX6* expression is interesting, as is the expression in the somites, given the role that SOX6 plays in muscle fibre specification in both zebrafish and mice. Mice deficient in SOX6 display an increase in slow-twitch specific gene expression (Hagiwara *et al.*, 2005; Hagiwara *et al.*, 2007). In zebrafish SOX6 alone is sufficient to inhibit slow-twitch specific gene expression (*tnnc1b* and *smyhc1*) and is restricted to the fast-twitch muscle fibres (Jackson *et al.*, 2015). Any regulation of SOX6 by ZAKβ therefore would be interesting given the predominance of slow-twitch muscle fibres in the novel myopathy associated with absence of ZAK (Vasli *et al.*, 2017; Ahmad *et al.*, 2022).

Further to this, P38γ and MKK3 (part of the ZAK signalling pathway) are expressed at high levels, almost exclusively, in skeletal muscle (Han *et al.*, 1997; Li *et al.*, 1996). P38γ is expressed constitutively in slow-twitch muscle fibres and interestingly mice lacking P38γ have an increase in the number of slow-twitch muscle fibres (Foster *et al.*, 2012). $ZAK^{-/-}$ mice show a predominance of slow-twitch fibres.

RNA-Seq data comparing the transcriptome of soleus and tibialis anterior (TA) muscle dissected from wildtype and $ZAK^{-/-}$ mice was kindly provided to our lab by Dr Simon Bekker-Jensen (also published (Nordgaard *et al.*, 2022)). Two of the differentially expressed genes (DEGs) of interest were *myomaker* and *runt-related transcription factor 1 (RUNX1).* Notably, the upregulation of *myomaker* was one of the greatest in fold change, with a 3.4-fold increase (q=0.002) in the TA of mice lacking ZAK compared to wild type and a 2.25-fold ($q=9.56X10^{-4}$) increase in the soleus of mice lacking ZAK compared to wild type. RUNX1 expression increased by 1.2-fold ($q=8.15X10^{-4}$) in the TA of mice lacking ZAK compared to wild type and increased 2.0-fold ($q=4.33X10^{-27}$) in the soleus of mice lacking ZAK compared to wild type.

Myomaker is a membrane protein essential for fusion in embryonic and adult myoblasts (Millay *et al.*, 2014). This is interesting, given the associations of downstream ZAK effectors with fusion, described above. A critical role for the myogenic regulatory factor (MRF) transcription factor, myogenin, with myocyte fusion has been demonstrated, where myogenin binds to the *myomaker* promotor region and is essential for *myomaker* expression (Ganassi *et al.*, 2018). RUNX1 is a transcription factor, associated with the differentiation of haematopoietic stem cells (Okuda *et al.*, 2001) and is not normally expressed in embryonic muscle progenitors (Simeone *et al.*, 1995; Levanon *et al.*, 2001) or healthy adult skeletal muscle (Zhu *et al.*, 1994). RUNX1, however, is present in damaged skeletal muscle and limits the severity of atrophy by preventing myofibrillar disorganisation as well as promoting proliferation of myoblasts during muscle regeneration (Wang *et al.*, 2005a; Umansky *et al.*, 2015). RUNX1 can also be seen in the muscle of Duchenne muscular dystrophy (DMD) mice (Porter *et al.*, 2003) and humans with congenital myopathies (Bakay *et al.*, 2006).

5.1.2. Role of KY and Association with ZAK

ZAK expression is upregulated in Kyphoscoliosis peptidase $(KY)^{-/-}$ mice extensor digitorum longus (EDL) muscle (Blanco, personal communications). KY is a transglutaminase-like peptidase expressed in skeletal muscle, and like ZAK, KY protein localises to the Z-disc as part of the same protein complex, with immunoglobulin-like fibronectin type III domain containing 1 (IGFN1) and filamin C (FLNC) (Beatham *et al.*, 2004) (Baker *et al.*, 2010; Ehsani *et al.*, 2022). The increase in the expression of ZAK in absence of KY is of note, as mutations in *KY* are the genetic cause of myofibrillar myopathy-7 (Yogev *et al.*, 2017). Myofibrillar myopathies (MFM) are a classification of neuromuscular disease, typically presenting with disintegration of the Z-disc and intracellular accumulation of Z-disc proteins, notably FLNC (Selcen, 2011; Luo *et al.*, 2020). Human patients with deleterious mutations in the *KY* gene present clinically with progressive wasting in both proximal and distal skeletal muscles, atrophy and skeletal deformities, such as scoliosis (Straussberg *et al.*, 2016; Yogev *et al.*, 2017; Ebrahimzadeh-Vesal *et al.*, 2018; Arif *et al.*, 2020). Centralised nuclei (seen in histological sections) and Z-disc streaming (evident in electron microscopy) are histopathological features of KY associated myopathy (Straussberg *et al.*, 2016; Yogev *et al.*, 2017; Ebrahimzadeh-Vesal *et al.*, 2018; Arif *et al.*, 2020).

Another component of this Z-disc protein complex is filamin C (Beatham *et al.*, 2004). The Filamin family is comprised of three Filamin proteins: Filamin A (FLNA), Filamin B (FLNB) and Filamin C (FLNC) (Nakamura *et al.*, 2011). The filamin protein family are actin cross-linking, scaffold proteins (van der Ven *et al.*, 2000). FLNA and FLNB have a fairly ubiquitous expression profile (Gorlin *et al.*, 1990; Takafuta *et al.*, 1998), however, FLNC expression is enriched in striated muscle, localising to Z-discs, sarcolemma, intercalated discs and myotendinous junctions (Thompson *et al.*, 2000). *FLNC* mutations are associated with MFM (Shatunov *et al.*, 2009; Chen *et al.*, 2019) (Verdonschot *et al.*, 2020).

The co-chaperone Bcl-2 associated-athanogene-3 BAG3 has been shown to be important in the turnover of filamin C as part of the tension/muscle contraction-induced chaperone-assisted selected autophagy (CASA) pathway (Arndt *et al.*, 2010). Elevated BAG3 leads to increased release of damaged FLNC from the cytoskeleton to the cytosol, where it can be ubiquitinated by CHIP and degraded. Elevated BAG3 levels also lead to activation of yes-associated protein 1/transcriptional co-activator with a PDZ-binding domain (YAP/TAZ), ultimately resulting in increased transcription of *FLNC* (Ulbricht *et al.*, 2013). Furthermore, mutations in *BAG3* are also associated with MFM (Selcen *et al.*, 2009; Konersman *et al.*, 2015; Scarpini *et al.*, 2021). BAG3, and CASA, therefore, appear to be involved in the turnover of defective FLNC through CASA, and transcription of new *FLNC*, maintaining tissue homeostasis – the disruption of which, can result in muscle disease.

There is a transcriptional upregulation in BAG3 and FLNC in $KY^{-/-}$ zebrafish to levels comparable with methylcellulose-challenged zebrafish embryos (Jokl *et al.*, 2018a). This finding suggests absence of KY results in a transcriptional upregulation of CASA components to the same level as physiologically-stressed muscle fibres (Jokl *et al.*, 2018a).

Given the upregulation of ZAK in absence of KY in mice, coupled with the association of ZAK as part of the Z-disc complex with KY (Baker *et al.*, 2010), it is of interest to see if absence of ZAK is also involved in the transcriptional upregulation of the CASA components. The KY$^{-/-}$ zebrafish line (Jokl *et al.*, 2018a), was successfully crossed with the ZAK$\beta^{-/-}$ zebrafish line, providing a model organism lacking KY and ZAK for analysis. The KY$^{-/-}$ ZAK$\beta^{-/-}$ double mutant zebrafish will be investigated for changes to the expression of the *FLNC* and *BAG3*, using qRT-PCR.

5.1.3 Aims

- Assess changes to the transcriptional profile of slow-twitch and fast-twitch-specific fibres in the absence of ZAKα and ZAKβ
- Investigate a potential role for ZAKβ in the CASA pathway through transcriptional changes to *BAG3* and *FLNC*, using ZAK$\beta^{-/-}$, ZAK$\alpha^{-/-}$ ZAK$\beta^{-/-}$ and KY$^{-/-}$ ZAK$\beta^{-/-}$ methylcellulose stressed embryos, as well as aged ZAK$\beta^{-/-}$ muscle.
- Define any changes to the embryonic spatiotemporal expression profile of *SOX6*, *myogenin* and *myomaker* in the absence of ZAKβ.
- Define any changes in embryos to the transcript levels of fusogenic proteins, *myogenin* and *myomaker*, as well as the transcription factor *RUNX1* in the absence of ZAKβ.
- Assess changes to downstream signalling and protein activation when ZAKβ is absent, using western blot analysis.

5.2. Results

5.2.1. No Significant Differences in the Transcript Levels of Slow or Fast-Twitch Muscle Markers in Either Embryos or in Adult Muscle

ZAKβ has been shown to increase the expression of *SOX6* in *Xenopus laevis (Suzuki et al., 2012)*, SOX6 is a key regulator of fibre type determination in zebrafish, driving fast-twitch differentiation through inhibition of key slow-twitch-specific genes (*smyhc1* and *tnnc1b*) (Jackson *et al.*, 2015). Furthermore, ZAK$^{-/-}$ human and mice exhibit fibre-type disproportion with a predominance of slow-twitch muscle fibres (Vasli *et al.*, 2017; Ahmad *et al.*, 2022; Lin *et al.*, 2022).

The hypothesis that the absence of ZAKβ would lead to decreased expression of *SOX6* and, an associated increase in the expression of slow-twitch genes and/or a decrease in the expression of fast-twitch genes was tested using qRT-PCR analysis by measuring changes to the expression of Alkali-like myosin light chain 1 (*myl1*) or slow myosin heavy chain 1 (*sMyHC1*). myl1 is an early marker for differentiating fast-twitch muscle cells in somites and is exclusively expressed in cells determined to become fast-twitch fibres in zebrafish (Burguière *et al.*, 2011). sMyHC1 is an early marker for slow-twitch muscle fibres, and is the first sMyHC to be expressed in zebrafish embryos (Codina *et al.*, 2010).

RNA was extracted from 3 dpf embryos and cDNA was synthesised. The transcript levels of *myl1* and *sMyHC1* were assessed with absence of ZAKα, ZAKβ or both isoforms using qRT-PCR. Figure 5.2 shows the relative fold change compared to the wild type expression of either *myl1* or *sMyHC1* for each genotype. There were no significant differences in the expression of *myl1* or *sMyHC1* in 3 dpf embryos when ZAKα, ZAKβ or both ZAK isoforms are absent. The mean percentage increase in the expression compared to wild type for *myl1* was 13% for ZAKα$^{-/-}$, 34% for ZAKβ$^{-/-}$ and 52% for ZAKα$^{-/-}$ ZAKβ$^{-/-}$ 3dpf embryos. Whilst there is a trend for an increase in absence of ZAKα or ZAKβ and a greater increase when both are absent, it is not a statistically significant increase.

The mean percentage increase in the expression of *sMyHC1* compared to wild type is: 28% for ZAKα$^{-/-}$, 13% for ZAKβ$^{-/-}$ and 21% for ZAKα$^{-/-}$ ZAKβ$^{-/-}$ 3 dpf embryos.

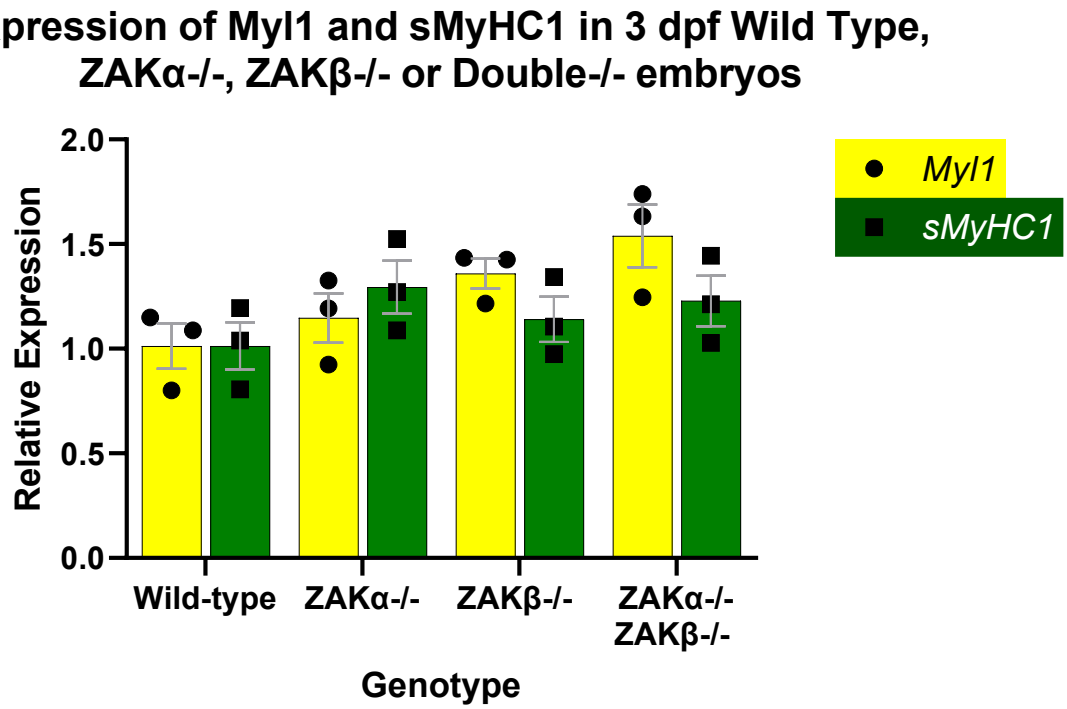

Figure 5.2. Expression of *Myl1* and *sMyHc1* across varying *ZAK* mutant genotypes. There were no significant changes to *myl1* and *sMyHc1* transcript levels in the absence of ZAK isoforms at 3 dpf. For each genotype (wild type, ZAK$\alpha^{-/-}$, ZAK$\beta^{-/-}$ and ZAK$\alpha^{-/-}$ ZAK$\beta^{-/-}$) five embryos were pooled, RNA was extracted and cDNA synthesised. Three separate mating's from different zebrafish provided a biological triplicate. A technical triplicate of each biological repeat was also performed. The transcript levels of the fast-twitch marker myl1 and slow-twitch marker *sMyHC1* were assessed for each genotype using qRT-PCR. A two-way ANOVA with Tukey's multiple comparison post hoc analysis was the statistical test performed. There were no significant differences in the mean transcript levels of either *myl1* or *sMyHc1* levels in 3 dpf embryos with absence of ZAKα, ZAKβ or both.

5.2.2. Absence of ZAKβ Results in Decreased *FLNCA* Expression in 8 dpf ZAKβ$^{-/-}$ Embryos but not in Aged Skeletal Muscle

An orthologue for human *KY* (ENSDARG00000074036) can be found on chromosome 13 in zebrafish, (Jokl *et al.*, 2018a). KY is part of a Z-disc protein complex, along with ZAKβ in skeletal muscle (Beatham *et al.*, 2004; Baker *et al.*, 2010; Ehsani *et al.*, 2022), and mutations in KY are associated with a myopathy in humans and mice (Blanco *et al.*, 2001; Straussberg *et al.*, 2016; Yogev *et al.*, 2017; Ebrahimzadeh-Vesal *et al.*, 2018; Arif *et al.*, 2020). Absence of KY is associated with elevated expression of CASA pathway components *FLNC* and *Bag3* in zebrafish and mice (Jokl *et al.*, 2018a). Given the association of ZAKβ with KY at the Z disc, and increase of ZAK when KY is absent, it was of interest to assess if absence of ZAKβ also affects the CASA pathway. Note, zebrafish appear to have two isoforms for FLNC (denoted FLNCA and FLNCB).

All zebrafish embryos were raised in normal embryo media (E3) until 5 dpf, where 30 embryos of either wild type, ZAKβ$^{-/-}$, ZAKα$^{-/-}$ ZAKβ$^{-/-}$ and KY$^{-/-}$ ZAKβ$^{-/-}$ were placed in 0.6% methylcellulose, used as an inert thickener to challenge swimming. 30 embryos of each genotype also remained in E3 media to act as a non-methylcellulose challenged control. RNA was extracted from E3 media or methylcellulose treated embryos at 8 dpf and cDNA was synthesised. cDNA was also synthesised from RNA extracted from adult skeletal muscle dissected from 36-month age-matched wild type and ZAKβ$^{-/-}$ muscle. qRT-PCR was performed to assess changes to the CASA components: *BAG3*, *FLNCA* and *FLNCB* as well as *KY* transcript levels for all genotypes.

5.2.2.1 CASA Pathway in 8 dpf Embryos with or Without Methylcellulose-Treatment

Firstly, there was a significant reduction of *KY* transcript levels in the KY$^{-/-}$ ZAKβ$^{-/-}$ embryos in all conditions, demonstrating absence of *KY* transcripts in the *KY* mutant line due to nonsense-mediated decay. With the exception of the expression of *KY* in KY$^{-/-}$ ZAKβ$^{-/-}$ embryos, none of the changes in *KY* transcript levels presented in figure 5.3 (a) and (b) are statistically significant, likely due to the considerable variation and low number of biological repeats.

Figure 5.3. (a) demonstrates a statistically significant reduction in the mean transcript level of *FLNCA* for ZAK$\beta^{-/-}$, ZAK$\alpha^{-/-}$ ZAK$\beta^{-/-}$ and KY$^{-/-}$ ZAK$\beta^{-/-}$ 8 dpf unchallenged embryos compared to mean wild type transcript levels. There is a mean 31% reduction when ZAKβ is absent, a mean 30% reduction when ZAKα and ZAKβ are absent and a 34% reduction when KY and ZAKβ are absent. The comparable levels of *FLNCA* reduction in genotypes lacking ZAKβ indicate that it is likely absence of ZAKβ that is driving the reduction. There is a similar trend for decreases in *FLNCA* expression in the 0.6% methylcellulose-challenged 8 dpf embryos (figure 5.3. (b)). There is a mean 25% reduction when ZAKβ is absent, a mean 25% reduction when ZAKα and ZAKβ are absent and a mean 24% reduction when KY and ZAKβ are absent. There was a surprising mean 9% reduction in *FLNCA* levels in wild type methylcellulose-challenged embryos, compared to unchallenged wild type embryos. The *FLNCA* reductions for ZAK$\beta^{-/-}$, ZAK$\alpha^{-/-}$ ZAK$\beta^{-/-}$ and KY$^{-/-}$ ZAK$\beta^{-/-}$ methylcellulose-challenged embryos are not statistically significant, likely due to the considerable variation between biological repeats treated with methylcellulose.

Relative to the wild type *FLNCB* mean transcript levels in 8 dpf unchallenged embryos, there is a mean 24% increase for ZAK$\beta^{-/-}$, a mean 31% increase for ZAK$\alpha^{-/-}$ ZAK$\beta^{-/-}$ and a mean 25% increase for KY$^{-/-}$ ZAK$\beta^{-/-}$ (figure 5.3 (a)). The increase is only significant when ZAKα and ZAKβ are both absent. Figure 5.3 (b) shows for 8 dpf 0.6% methylcellulose-challenged embryos, there is a mean 22% increase in *FLNCB* levels, relative to wild type, for ZAK$\beta^{-/-}$ and a mean 15% increase for ZAK$\alpha^{-/-}$ ZAK$\beta^{-/-}$. There is only a mean 6% increase for KY$^{-/-}$ ZAK$\beta^{-/-}$. However, none of the mean percentage increases for the 0.6% methylcellulose-challenged embryos, relative to wild type, are statistically significant.

There were no significant differences in the *BAG3* transcript levels in ZAK$\beta^{-/-}$, ZAK$\alpha^{-/-}$ ZAK$\beta^{-/-}$ and KY$^{-/-}$ ZAK$\beta^{-/-}$ with or without 0.6% methylcellulose treatment in 8 dpf embryos (figures 5.3. (a) and (b)). For unchallenged embryos, relative to the mean wild type *BAG3* transcript levels, there was a mean 18% increase with ZAK$\beta^{-/-}$, a mean 7% increase with ZAK$\alpha^{-/-}$ ZAK$\beta^{-/-}$ and a mean 4% increase with KY$^{-/-}$ ZAK$\beta^{-/-}$. For 0.6% methylcellulose-challenged embryos, relative to wild type *BAG3* transcript levels, there was no difference in the mean percentage with ZAK$\beta^{-/-}$, a mean 9% increase with ZAK$\alpha^{-/-}$ ZAK$\beta^{-/-}$ and a mean 20% increase with

KY$^{-/-}$ ZAKβ$^{-/-}$. The small percentage changes for *BAG3*, the lack of the overall trend and significance likely means that any differences in percentage are likely just the result of variation of biological repeats.

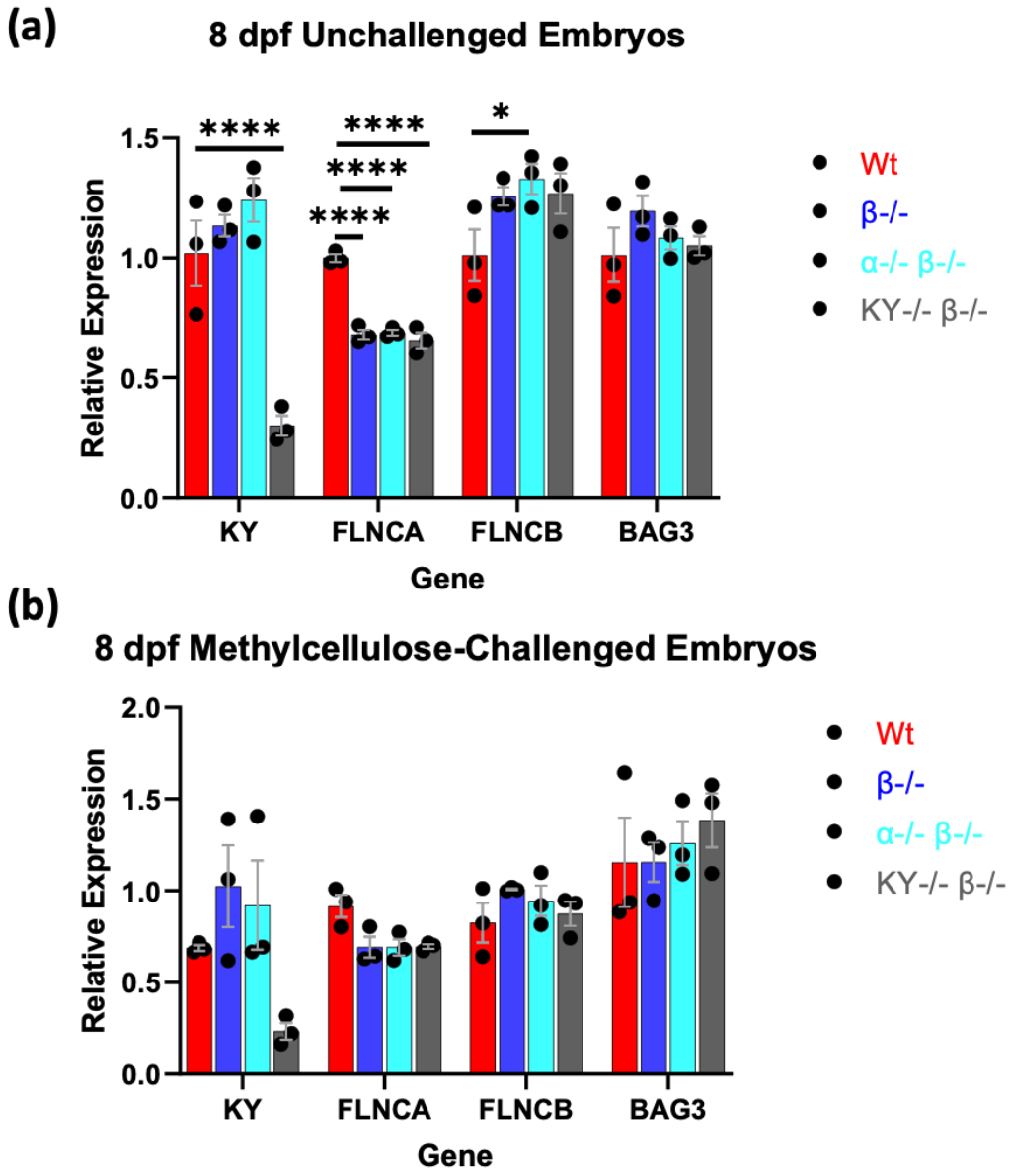

Figure 5.3. *KY*, *FLNC* and *BAG3* expression levels in 8 dpf embryos with varying *ZAK* mutant genotypes.
There is a significant reduction in *FLNCA* transcript levels when ZAKβ is absent. cDNA was synthesised from the RNA of five 8 dpf embryos of either wild type, ZAKβ$^{-/-}$, ZAKα$^{-/-}$ ZAKβ$^{-/-}$ or KY$^{-/-}$ ZAKβ$^{-/-}$ genotype, with or without 0.6% methylcellulose treatment. Three separate matings from different parents provided biological triplicates for each genotype (N=3). All biological triplicates had technical triplicates performed. Wt = wild type (red); β-/- = ZAKβ$^{-/-}$ (blue); α-/- β-/- =, ZAKα$^{-/-}$ ZAKβ$^{-/-}$ (cyan); KY-/- β -/- = KY$^{-/-}$ ZAKβ$^{-/-}$ (grey). (a) Transcript levels of *KY, FLCA, FLNCB* and *BAG3* for the various genotypes with unchallenged embryos. (b) Transcript levels of *KY, FLCA, FLNCB* and *BAG3* for the various genotypes with 0.6% methylcellulose-challenged embryos. Data was normalised to *Ef1α* housekeeping gene transcript levels (ΔCT), prior to further normalisation to the average ΔCT for unchallenged wild type transcript levels, as a reference. Two-way ANOVA with Tukey's multiple comparison post hoc analysis was the statistical test performed on ΔCT values. $2^{-\Delta\Delta CT}$ was used to calculate fold change. No Asterisk = not significant. * P ≤ 0.05. **** P ≤ 0.0001

5.2.2.2. No Changes to CASA Pathway in Old-Age ZAKβ$^{-/-}$ Zebrafish Muscle

There are no significant differences in *KY* or the CASA-component transcript levels in aged ZAKβ$^{-/-}$ zebrafish muscle (figures 5.4 (a-d)). This is likely the result of the large biological variation in transcript levels between different aged zebrafish muscle.

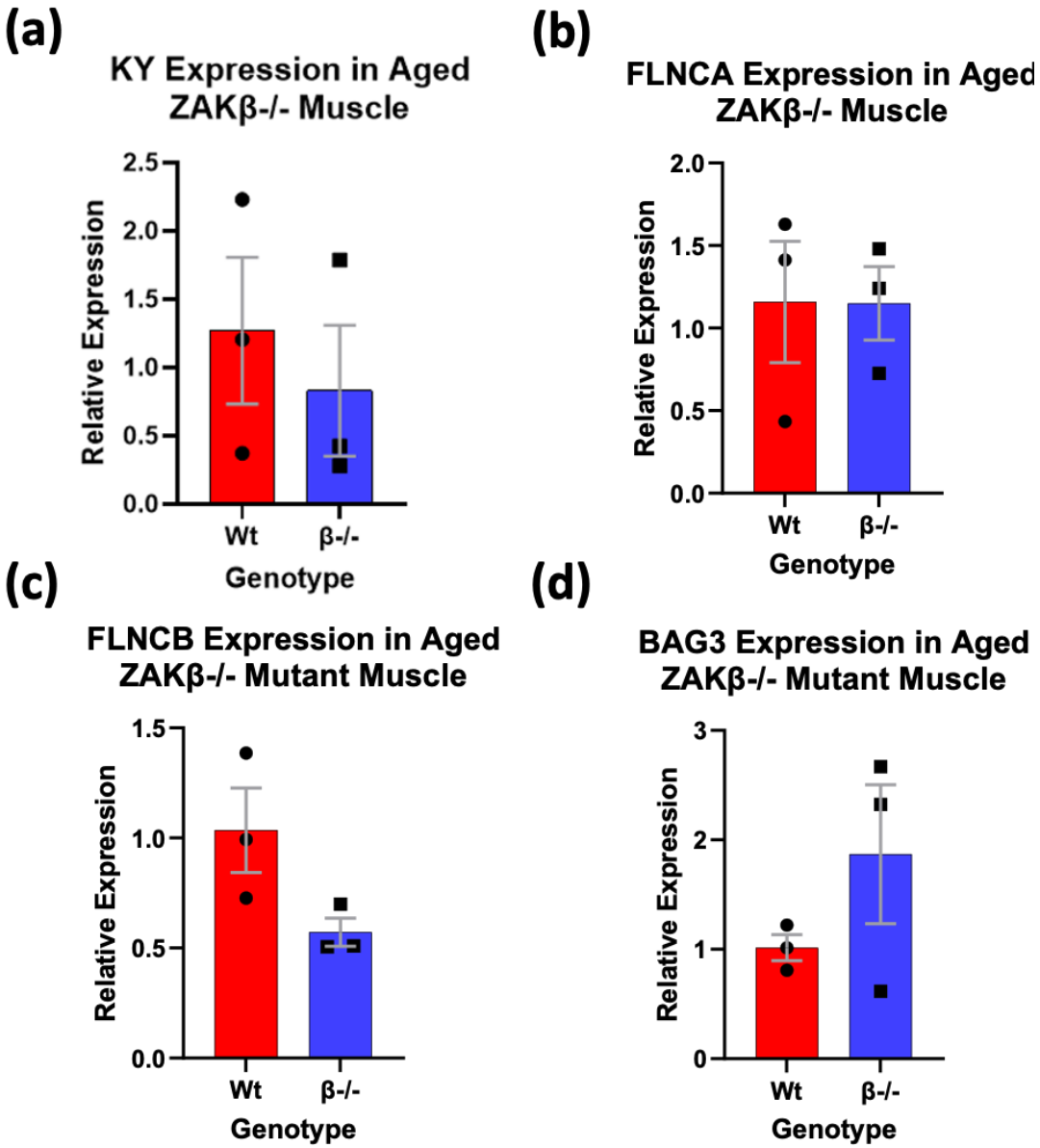

Figure 5.4. *KY, FLNC* and *BAG3* expression levels in aged ZAKβ$^{-/-}$ zebrafish.
There are no statistically significant differences in *KY, FLNCA, FLNCB* and *BAG3* transcript levels in 36-month-old ZAKβ$^{-/-}$ skeletal muscle. cDNA was synthesised from the RNA of 36 month-aged wild type (N=3) or ZAKβ$^{-/-}$ (N=3) muscle. All biological triplicates had a technical triplicate performed too. (a) *KY* transcript levels in old wild type and ZAKβ$^{-/-}$ muscle. (b) *FLNCA* transcript levels in old wild type and ZAKβ$^{-/-}$ muscle. (c) *FLNCB* transcript levels in old wild type and ZAKβ$^{-/-}$ muscle. (d) *BAG3* transcript levels in old wild type and ZAKβ$^{-/-}$ muscle. Data was normalised to housekeeping gene *Ef1α* (ΔCT) $2^{-\Delta\Delta CT}$ was used to calculate fold change. Unpaired, two-tailed student's t-test was performed on transcript levels (ΔCT) of old muscle. No Asterisk = not significant.

5.2.3. Assessing the Transcriptional Profile of Potential Downstream ZAK Effectors in ZAKβ$^{-/-}$ Zebrafish

5.2.3.1. Assessing the Expression of *SOX6*, *Myogenin*, *Myomaker* and *sMyHC1* in Wild type and ZAKβ$^{-/-}$ Embryos using ISH

In situ hybridisation (ISH) was performed on embryos between 1 and 4 dpf, to assess if there were any differences in the spatial or temporal expression profile of *SOX6*, *myomaker*, *myogenin* and *sMyHC1* in ZAKβ$^{-/-}$ embryos.

Figure 5.5 (a) demonstrates *SOX6* expression to be exclusively in the somites, with similar expression intensity levels between 1 dpf wild type and ZAKβ$^{-/-}$ embryos. Whilst *SOX6* expression appears to remain in the somites at 2 dpf for wild type, but not ZAKβ$^{-/-}$ embryos, the ZAKβ$^{-/-}$ embryos appear more developed, as evidenced by the eye definition. At 2 dpf, there is also expression of *SOX6* in the developing pectoral fin muscle and in the head of the embryos. For 3 and 4 dpf, the expression of *SOX6* is largely in the head of the embryos for both wild type and ZAKβ$^{-/-}$ embryos, with no expression in the somites.

The expression profile of *myogenin* is comparable across wild type and ZAKβ$^{-/-}$ embryos in all timepoints investigated (figure 5.5 (b)). At 1 dpf, *myogenin* expression is localised to the caudal somites, in the posterior region of the embryo. Between 2 – 4 dpf, *myogenin* expression is enriched in the dorsal and ventral edges of the somites. There is also expression of *myogenin* in the muscles of the developing pectoral fin and jaw between 2 – 4 dpf.

Figure 5.5 (c) shows the expression of *myomaker* to be localised to the posterior region of the embryo at 1 dpf for wild type and ZAKβ$^{-/-}$embryos. At 2 dpf, the expression of *myomaker* is enriched in the developing pectoral fin muscle and the facial muscle for wild type and ZAKβ$^{-/-}$. The expression intensity is comparable between wild type and ZAKβ$^{-/-}$ embryos at 1 and 2 dpf.

sMyHC1 expression is localised to the somites and the facial muscle for both wild type and ZAKβ$^{-/-}$ (figure 5.5 (d)). The expression of *sMyHC1* appears reduced in ZAKβ$^{-/-}$ embryos for all timepoints investigated. qRT-PCR in figure 5.2 shows no significant differences in the expression of *sMyHC1*, demonstrating that whilst ISH is an appropriate procedure for qualitatively assessing the spatiotemporal

mRNA expression profile, the assay is limited in the reliability of quantifying intensity.

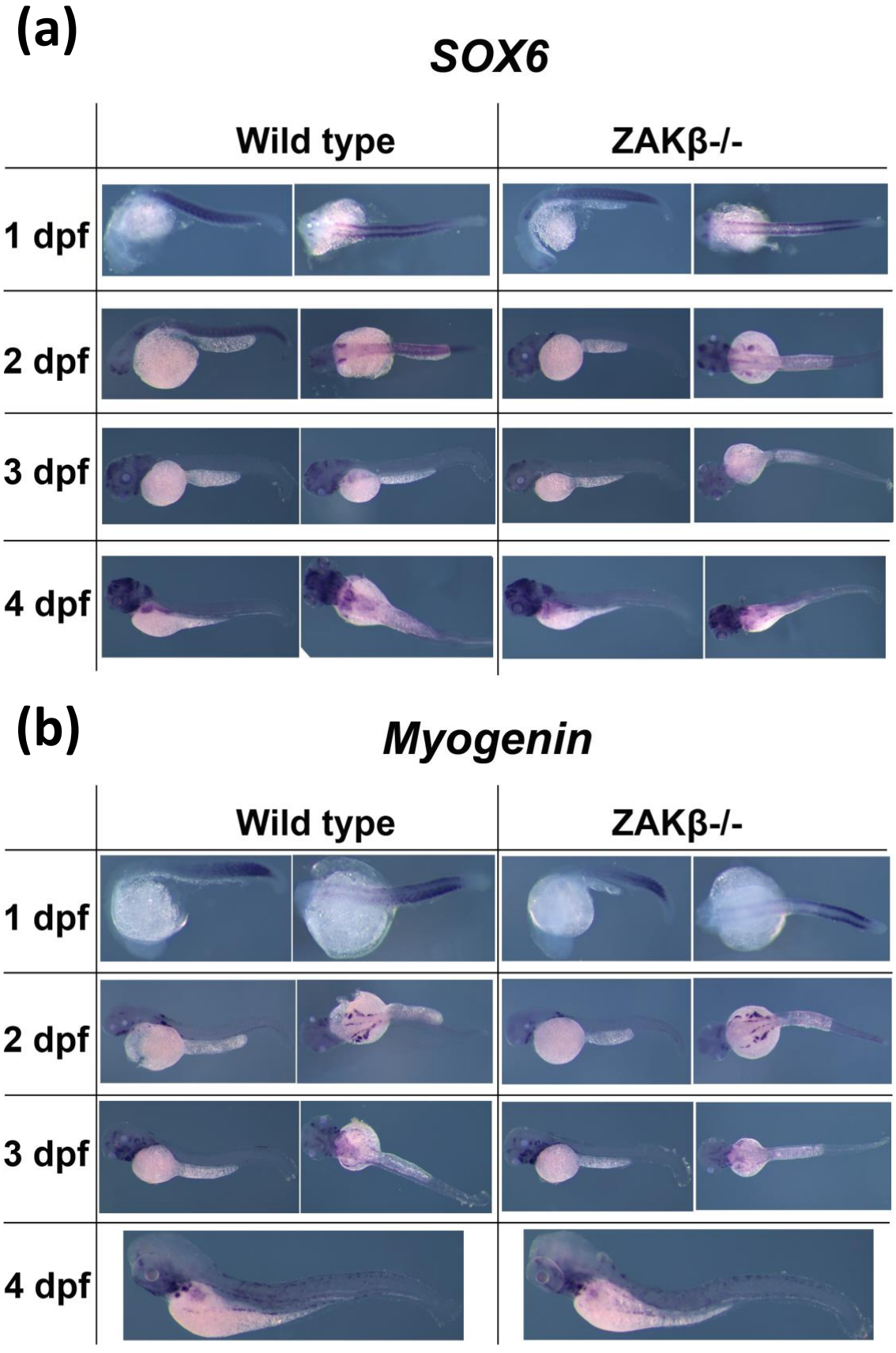

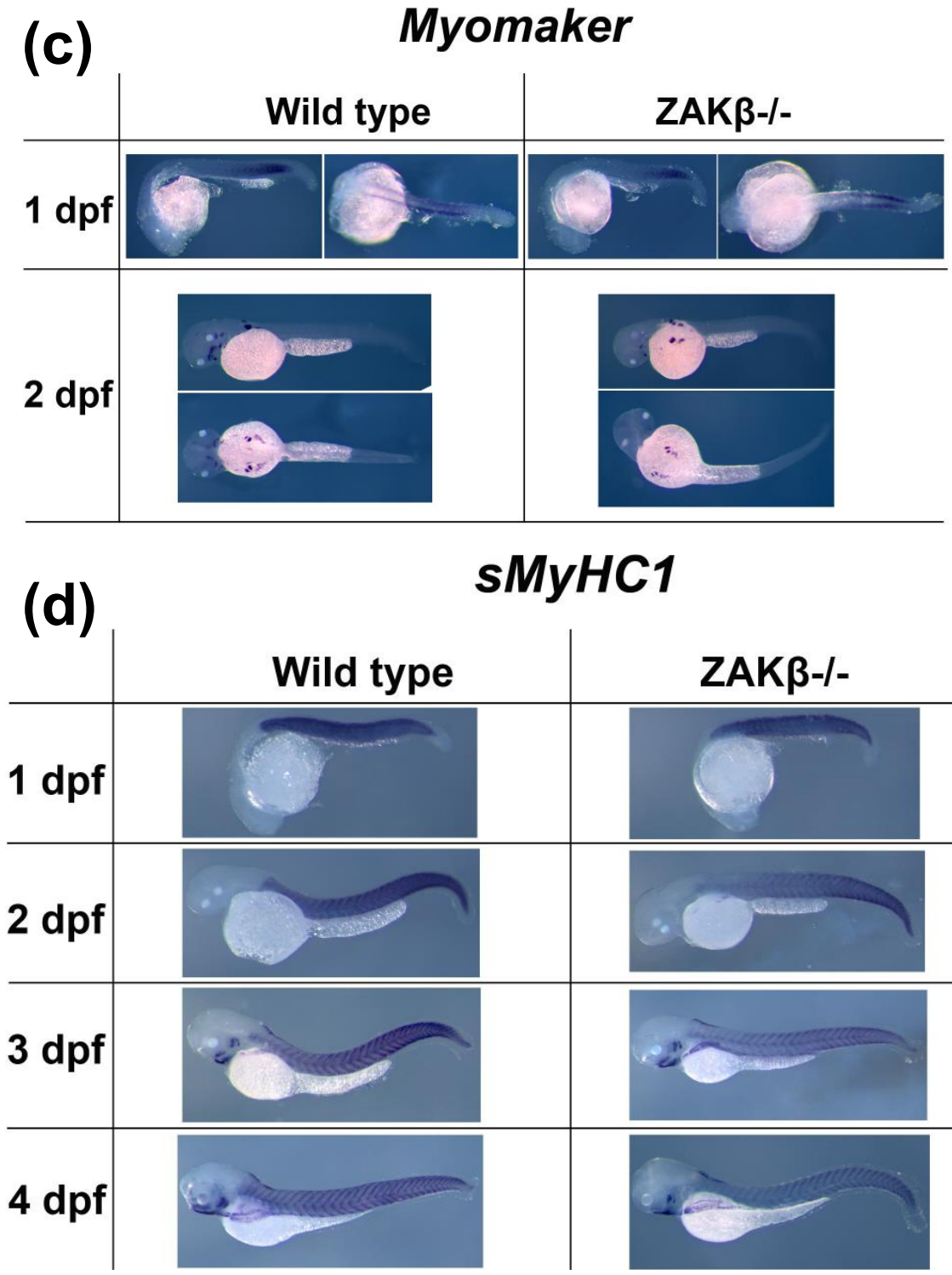

Figure 5.5. The expression profile of *SOX6*, *Myogenin*, *Myomaker* and *sMyHC* in zebrafish embryos lacking ZAKβ.

RNA probes antisense to the respective mRNA were designed, which contain digoxigenin (DIG) and bind to anti dig antibodies, fused with the enzyme AP, allowing for detection of colour change in regions of high mRNA expression. (a) Expression of *SOX6* is in the somites at 1 dpf and in small amounts at 2 dpf in wild type. After 2 dpf, the expression is greatest in the developing neurula and head. There is no difference in the expression of *SOX6* in ZAK$\beta^{-/-}$ embryos. (b) Expression of *myogenin* is in the caudal somites (posterior) at 1 dpf and from 2 dpf is at the edges of the somites. There is no difference in the expression of *myogenin* in the ZAK$\beta^{-/-}$ mutant line (c) Expression of *myomaker* is in the somites at 1 dpf and then just the pectoral fins/facial muscle at 2 dpf. There are no differences in the expression in ZAK$\beta^{-/-}$ embryos. (d) *sMyHC1* expression is in the somites and facial muscle, and appears reduced in ZAK$\beta^{-/-}$ embryos.

5.2.3.2. There is a Significant Upregulation of *Myogenin* and *Myomaker* in 8 dpf ZAKβ$^{-/-}$ Embryos, Independent of Methylcellulose-Challenging

qRT-PCR was used to assess if there are any statistically significant changes to the expression of *myomaker* and *RUNX1*, as seen in RNA-seq data on ZAK$^{-/-}$ mice. *Myogenin* expression was also investigated, as it is required for the expression of *myomaker* (Luo *et al.*, 2015; Ganassi *et al.*, 2018). All embryos were raised in zebrafish E3 growth media until 5 dpf, where 30 wild type and ZAKβ$^{-/-}$ embryos were placed in 0.6% methylcellulose in E3 (normal zebrafish) media. 30 embryos of each genotype also remained in E3 media as an unchallenged control. Skeletal muscle was dissected from 36-month-old wild type and ZAKβ$^{-/-}$ zebrafish. cDNA was synthesised from RNA extracted from embryos with or without methylcellulose treatment at 8 dpf and from the old skeletal muscle. The expression levels of *myogenin, myomaker* and *RUNX1* were assessed using qRT-PCR.

Figure 5.6 (a) shows there was a significant increase in the mean *myogenin* expression in 8 dpf ZAKβ$^{-/-}$ embryos, as detected by qRT-PCR (143%, compared to wild type). Methylcellulose treatment did not affect wild type expression levels of *myogenin* and led to a comparable increase in ZAKβ$^{-/-}$ embryos (141%), suggesting this upregulation of *myogenin* expression in ZAKβ mutants is refractory to any additional stress to muscle. There was a significant 105% increase in the mean *myomaker* transcript level in non-methylcellulose challenged ZAKβ$^{-/-}$ embryos at 8 dpf, compared to wild type (figure 5.6 (b)). Like with *myogenin*, the increase of *myomaker* was not enhanced in methylcellulose-challenged embryos. There were no significant differences in the expression of *RUNX1* in 8 dpf embryos with/without methylcellulose treatment (figure 5.6 (c)).

There are no significant differences in the expression of *myogenin*, *myomaker* or *RUNX1* in old adult ZAKβ$^{-/-}$ muscle (figure 5.6 (d-f)). The high variability in the expression of *myogenin* and *myomaker* was the same for wild type and ZAKβ$^{-/-}$ aged-muscle.

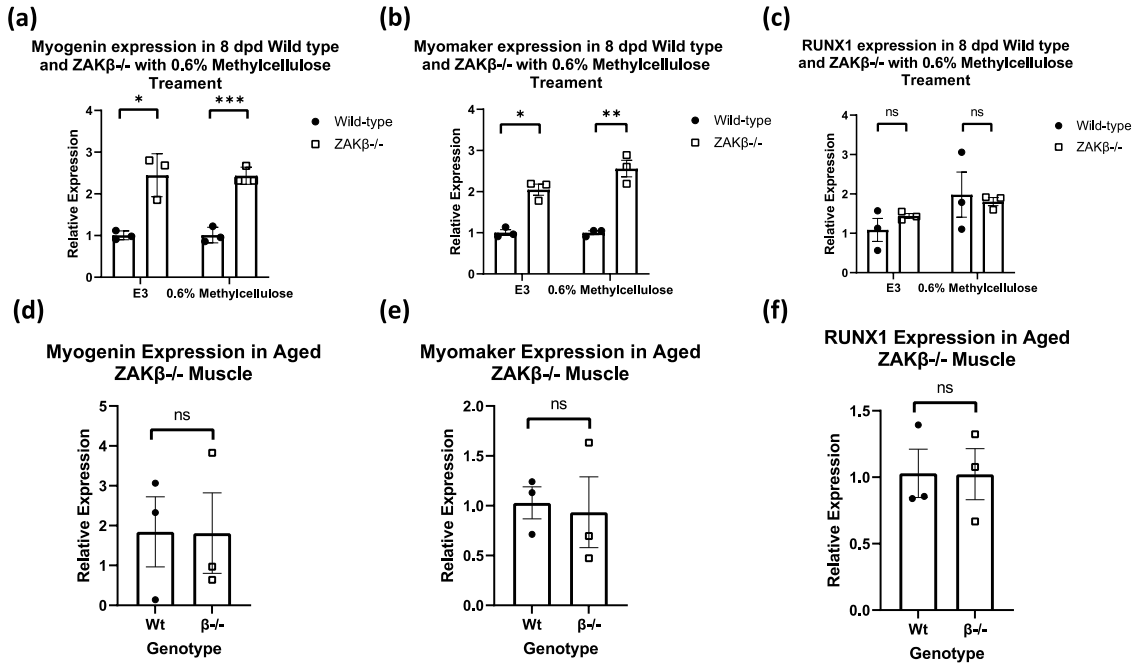

Figure 5.6. *Myogenin, myomaker* and *RUNX1* expression levels in ZAKβ$^{-/-}$ embryos and aged zebrafish.

There is a significant upregulation of *myogenin* and *myomaker* expression in 8 dpf embryos. cDNA was synthesised from RNA extracted from 8 dpf embryos with/without methylcellulose treatment. cDNA was also synthesised from RNA extracted from old adult muscle. qRT-PCR was used to quantify expression of wild type and ZAKβ$^{-/-}$ (a) *myogenin* in 8 dpf embryos with/without 0.6% methylcellulose (b) *myomaker* in 8 dpf embryos with/without 0.6% methylcellulose. (c) *RUNX1* in 8 dpf embryos with/without methylcellulose. (d) *Myogenin* in old adult muscle. (e) *Myomaker* old adult muscle. (f) *RUNX1* in old adult muscle. cDNA was synthesised from RNA extracted from five embryos, from three separate wild type and ZAKβ$^{-/-}$ matings (n=3). Three wild type and three ZAKβ$^{-/-}$ old-age adult skeletal muscle samples were dissected. Three technical repeats were performed on the three biological repeats. Fold change was calculated by initially normalising the expression to *Ef1a* (ΔCT) before then calculating the fold change to average wild type CT. 2-ΔΔCT was the method of analysis. Unpaired two-tailed students T-test was the statistical test. Ns = No significance. *<0.05; ***<0.001.

5.2.4. Investigating Protein Activation in the Absence of ZAK Signalling

To look more directly at the signalling pathways regulated by ZAK, western blots were used to assess any changes to the activation of components of the MAPK pathway in the absence of ZAKβ or ZAKα and ZAKβ. This was done using embryos cultured in normal media and those where the swimming/skeletal muscle force was challenged by culturing embryos in either 0.6% or 1% methylcellulose, where we expected any effects from the lack of ZAK would be enhanced (see section 2.7). Protein was also extracted from dissected age-matched (9 months) wild type, ZAKβ$^{-/-}$ and ZAKα$^{-/-}$ ZAKβ$^{-/-}$ muscle, for the western blot results in figure 5.7 (c) (See section 2.6 for full details of the western blot protocol). Commercially available antibodies that recognise the phosphorylated forms of P38, AKT and ERK were used to investigate the activation in the absence of ZAK proteins. Western blots shown are preliminary findings and representative of a single biological sample, due to complications with the protein extraction protocol and limited number of fish, which prevented the generation of biological repeats.

An apparent increase in the levels of phosphorylated-P38 (p-P38) is detected in the absence of ZAKβ and both ZAK isoforms, in 8 dpf embryos (figure 5.7 (a)). This effect is no longer detected when embryos are stressed in either 0.6% or 1% methylcellulose. Total ERK levels were used as a normalisation/loading control and were comparable across all samples, although with slight decreases seen with ZAKα$^{-/-}$ ZAKβ$^{-/-}$ embryos.

Figure 5.7 (b) shows a comparable increase in the phosphorylation of P38 in the absence of either ZAKβ or both ZAKα and ZAKβ, relative to wild type. Phosphorylation of AKT, on the other hand, appears to decrease in the absence of ZAKβ and further decreases to virtually no p-AKT in the absence of both ZAK isoforms, in 8 dpf embryos. The levels of ERK activation look comparable in wild type, ZAKβ$^{-/-}$ and ZAKα$^{-/-}$ ZAKβ$^{-/-}$ 8 dpf embryos.

Figure 5.7 (c) demonstrates in adult muscle, no apparent changes in the phosphorylation of P38 or AKT is evident in the absence of either ZAKβ or ZAKα and ZAKβ. There potentially might be a slight decrease in p-P38 levels in ZAKβ$^{-/-}$ muscle but not ZAKα$^{-/-}$ ZAKβ$^{-/-}$ skeletal muscle. ERK activation in skeletal

muscle appears to be marginally increased when ZAKβ is absent and further increased when both ZAKα and ZAKβ are absent.

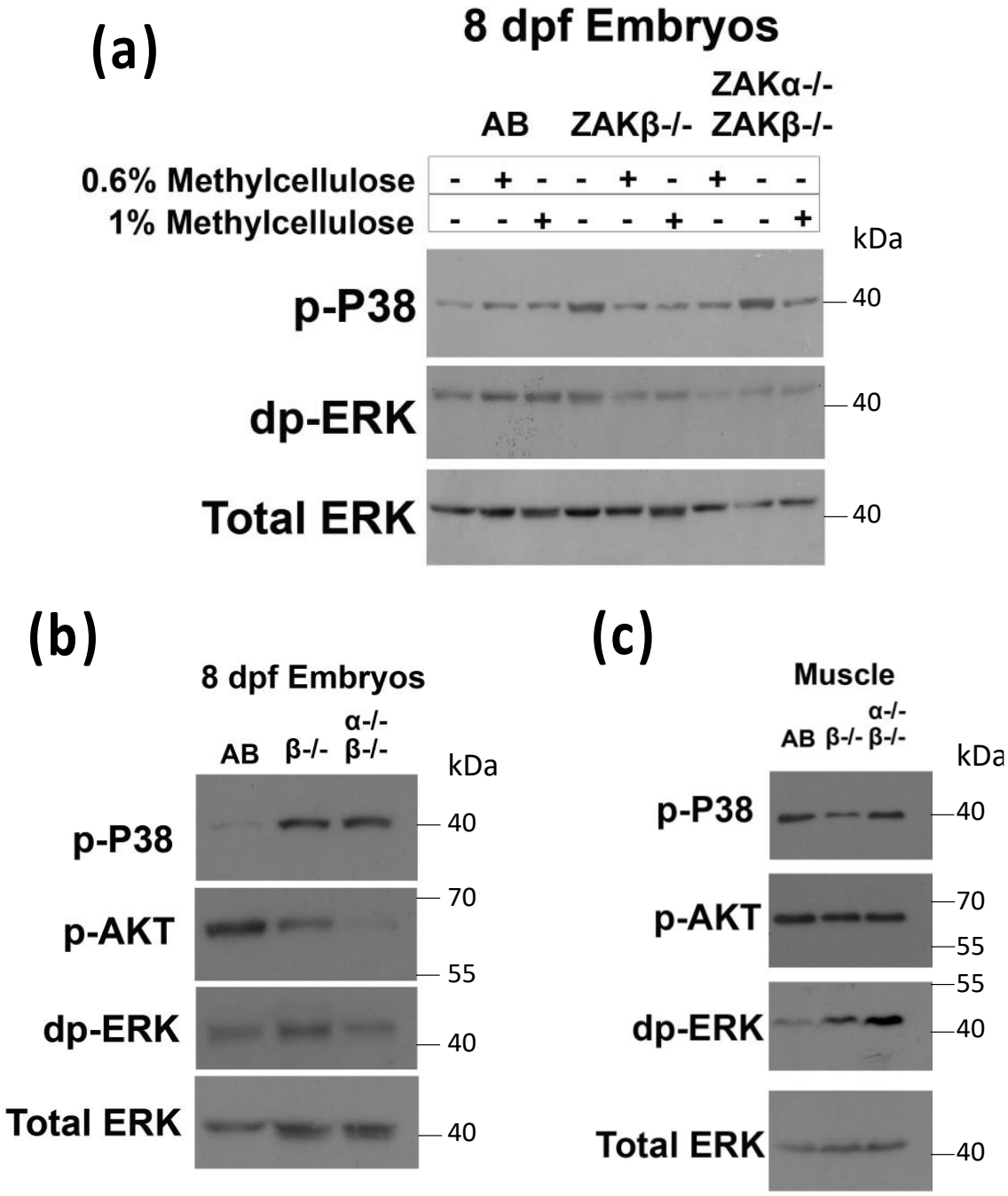

Figure 5.7. Analysis of protein activation in the absence of ZAK isoforms using western blot.
(a) The levels of p-P38 and dp-ERK compared to total ERK when embryos were stressed in 0.6% or 1% methylcellulose-enriched E3 media, in the absence of ZAKβ or ZAKα and ZAKβ. (b) Activation of P38, AKT and ERK in the absence of either ZAKβ or ZAKα and ZAKβ in 8 dpf embryos. Total ERK is the loading control. (c) Activation of P38, AKT or ERK in 9-month-old adult skeletal muscle lacking ZAKβ or ZAKα and ZAKβ. Western blot figures are preliminary and representative of n=1. Molecular weight (kilodalton (kDa)) was determined using PageRuler Plus protein ladder and shown for all figures. Total ERK is the loading control.

5.3. Discussion

5.3.1. Fast and Slow-Twitch-Specific Gene Expression in 3 dpf Zebrafish Embryos

There are no significant differences for the *myl1* and *sMyHC1* transcript levels when ZAKα, ZAKβ or both isoforms are absent in 3 dpf zebrafish embryos. There is, however, a general trend for increased *myl1* when ZAKα or ZAKβ are absent, with the greatest change being a 52% increase in the mean expression when both isoforms are absent. As discussed, this trend, however, is not significant, either representing natural variation from a low number of biological repeats, or just a marginal increase. It should be noted, that ectopic expression of *SOX6* in zebrafish only resulted in approximately a 20% decrease in *sMyHC1* levels, so the relative fold change is comparable (Jackson *et al.*, 2015). Furthermore, absence of SOX6 in zebrafish leads to aberrant expression of *tnnc1b* in fast-twitch fibres, but not *sMyHC1,* demonstrating the role of multiple factors in fast-twitch fibre-type determination (Jackson *et al.*, 2015). This means that any effect on fibre type from ZAK is likely to only be a part of fibre-type determination and may not produce substantial changes.

An increase in *myl1* when ZAKβ is absent is surprising, given the association of ZAKβ increasing *SOX6* expression (Suzuki *et al.*, 2012), which in turn reduces the expression of slow-twitch specific genes, such as *sMyHC1* (Jackson *et al.*, 2015). An increase in *myl1* and no change to the expression of *sMyHC1* is, consequently, difficult to rationalise. There are no known associations of ZAK with proteins involved in specifying slow-twitch fate and repression of fast-twitch gene expression, such as BLIMP1 (also known as prdm1) (Liew *et al.*, 2008; Burguière *et al.*, 2011).

Due to the non-significant nature of the result, this experiment will require repeats to assess if the trend is meaningful and not just natural variation, arising from a low number of biological repeats. Any significant changes to transcript levels would also need validating with Immunostaining of slow-twitch and fast-twitch markers in adult muscle before any final conclusions on the effects of ZAK on the fibre-type proportion in zebrafish could be made.

5.3.2. There is a Significant Reduction of *FLNCA* in the Absence of ZAKβ in Zebrafish Embryos

There was a significant decrease in the levels of *FLNCA* when ZAKβ; ZAKα and ZAKβ, and KY and ZAKβ were absent in 8 dpf unchallenged embryos, suggesting a role for ZAKβ activity in the expression of *FLNCA*. There was also a significant increase in *FLNCB* levels when both ZAKα and ZAKβ are absent in 8 dpf unchallenged embryos, which could either be a compensatory mechanism for lack of ZAKβ, or a potential role for ZAKβ activity for the downregulation of *FLNCB* expression. I also validated the $KY^{-/-}$ zebrafish line, demonstrating a statistically significant reduction of KY transcript, presumably through nonsense-mediated decay.

(Jokl *et al.*, 2018a) showed a statistically significant upregulation in the expression of *FLNCA*, *FLNCB* and *BAG3* in wild type methylcellulose-challenged embryos, compared to unchallenged embryos. For wild type 8 dpf methylcellulose-challenged embryos, there was a 9% reduction in the mean *FLNCA* levels and an 18% reduction in the mean *FLNCB* levels, compared to unchallenged wild type mean expression; albeit the changes were not statistically significant. There was also a 32% reduction in *KY* in wild type 8 dpf embryos, following methylcellulose treatment. A greater number of biological repeats would better assess if these changes are meaningful or just a result of variation between different fish.

(Jokl *et al.*, 2018a) found significant upregulation of *BAG3*, *FLNCA* and *FLNCB* in $KY^{-/-}$ 7 dpf embryos and adult zebrafish, proposing that absence of KY results in a compensatory upregulation of CASA-component transcripts. Whilst I see a 25% increase in the mean *FLNCB* levels in 8 dpf E3-treated $KY^{-/-}$ $ZAK\beta^{-/-}$ and a 20% increase in the mean *BAG3* levels in 8 dpf methylcellulose-challenged $KY^{-/-}$ $ZAK\beta^{-/-}$ embryos, these increases are not significant and should be treated with caution. Furthermore, there is a statistically significant decrease in the mean *FLNCA* levels in unchallenged $KY^{-/-}$ $ZAK\beta^{-/-}$ 8 dpf embryos. This demonstrates that even with absence of KY, shown to increase *FLNC* levels, there is still significant downregulation of *FLNCA* caused by absence of ZAKβ. One explanation for this finding is that ZAKβ signalling results in increased *FLNCA* expression, in absence of *KY*, as a compensatory mechanism in an attempt to

minimise pathology. This theory could also explain the increase of ZAKβ in the soleus of $KY^{-/-}$ mice.

Notably for old-age muscle, there was not the reduction in *FLNCA* transcript levels seen in embryos when ZAKβ was absent; however there was a mean, albeit not statistically significant, percentage reduction in *FLNCB* levels. This could imply that ZAKβ induced *FLNCB* transcription is important in adult or old-aged muscle, whereas ZAKβ induced *FLNCA* transcription is important for maintaining embryonic/juvenile muscle integrity. Understanding the importance of these proteins for aging of muscle can be important with regards to sarcopenia (age-related muscle loss). *FLNC* and *BAG3* levels have been shown to be increased in old-age mouse muscle (Lin *et al.*, 2018).

The decrease in *FLNCA* seen in zebrafish is intriguing. Indeed, transcriptome analysis on one of the $ZAK^{-/-}$ myopathy patients, compared to two control patients, revealed a decrease in sarcomeric components of the cytoskeleton and Z-disc, which included *FLNC* (Vasli *et al.*, 2017). This suggests a possible role for ZAKβ signalling to increase *FLNC* expression for maintenance of muscle integrity, that is conserved between humans and zebrafish. The importance of FLNC for muscle integrity can be demonstrated by mutations in the gene resulting in human myopathies (Shatunov *et al.*, 2009; Chen *et al.*, 2019; Verdonschot *et al.*, 2020).

The 84% increase in mean *BAG3* transcript levels in adult $ZAK\beta^{-/-}$ muscle is surprising, given it is not accompanied with an increase in *FLNCA/B*. The increase, therefore, might allude to a greater demand for BAG3-mediated protein turnover in old muscle when ZAKβ is absent, but not for increased CASA-component transcription. As the increase is not significant, it could just be variation between different $ZAK\beta^{-/-}$ zebrafish, with further repeats required.

Despite the limitations of a low number of biological repeats and the lack of a single $KY^{-/-}$ control, the results are promising and do hint at a potential role for ZAKβ in the CASA pathway in zebrafish and/or the Hippo pathway, leading to increased expression of *FLNC* to maintain muscle integrity. Further experimentation using single $KY^{-/-}$ zebrafish is required before any conclusions can be made.

5.3.3. Transcription of *sMyHC1*, *SOX6*, *Myogenin*, *Myomaker* and *RUNX1* in ZAKβ$^{-/-}$ Zebrafish Embryos

There are no statistically significant differences in the expression of the slow-twitch specific gene *sMyHC1* and the fast-twitch specific gene *Myl1* in ZAKβ$^{-/-}$ 3 dpf embryos. This finding disputes the apparent weaker colourimetric intensity, found using ISH probes against *sMyHC1* on ZAKβ$^{-/-}$ embryos, across all timepoints. The discrepancy demonstrates how ISH is more of a qualitative assay, aimed at assessing the spatiotemporal expression profile rather than quantification.

The expression profile for *SOX6* is comparable between wild type and ZAKβ$^{-/-}$ embryos. The presence of *SOX6* expression in the somites of 2 dpf wild type, but not ZAKβ$^{-/-}$ embryos, is likely just the result of the embryos being slightly less developed and is probably not meaningful. *SOX6* is exclusively expressed in the somites at 1 dpf, where it will be likely involved in specifying fast-twitch fibres through inhibition of slow-twitch fibres (Jackson *et al.*, 2015). In subsequent dpf, the somite expression is lost and *SOX6* is expressed in the heads of zebrafish embryos, where it will likely be involved in the craniofacial cartilage differentiation (Suzuki *et al.*, 2012) and neurogenesis (Lee *et al.*, 2014; Li *et al.*, 2022).

The expression of *myogenin* initially is in the posterior somites of 1 dpf embryos. Between 2 – 4 dpf, the expression becomes more localised to the dorsal and ventral edges of the myotome, across the full tail. There is also an enrichment of *myogenin* expression in the face muscles and the muscles of the developing pectoral fin. There were no obvious differences in the expression of *myogenin* between wild type and ZAKβ$^{-/-}$ embryos. There were also no differences in the expression profile of *myomaker* at 1 and 2 dpf, between wild type ZAKβ$^{-/-}$ embryos. The expression of *myomaker* is in the posterior region of the trunk, in the caudal somites. In 2 dpf embryos, the expression is enriched in the developing pectoral fin muscle and the facial muscle. For future work, it would be of interest to assess *myomaker* expression in embryos younger than 1 dpf, to assess potential transient expression changes during the different stages of somitogenesis.

qRT-PCR revealed a significant increase in the expression of *myogenin* and *myomaker* in 8 dpf ZAKβ$^{-/-}$ embryos, independent to stress of muscle through 0.6% methylcellulose treatment. The increase in *myogenin* and *myomaker* in 8 dpf ZAKβ$^{-/-}$ embryos might be compensating for absence of ZAKβ. There is also the possibility that ZAKβ signalling plays an inhibitory role for *myogenin* and *myomaker* expression, which would be surprising as there has not been an association between P38 or JNK signalling and *myogenin* or *myomaker* levels. The fusion capabilities of ZAKβ$^{-/-}$ mutant zebrafish embryos will be assessed using transgenic zebrafish and confocal microscopy in chapter 6. The upregulation of *myomaker* and *myogenin* is not seen in old adult ZAKβ$^{-/-}$ muscle, indicating the importance of ZAKβ in fusion to be more pertinent when zebrafish larvae are developing.

5.3.4. Changes to Protein Activation in Zebrafish Lacking ZAKβ

All antibodies used were developed using human or mouse epitopes. As I am interested in zebrafish protein levels, only antibodies that produced a single, discrete band at the correct molecular weight were used. Sadly, antibodies for p-JNK and p-SMAD2/3 produced multiple non-specific bands, at the wrong molecular weight, so were not included for analysis. Moreover, ideally, total P38 and AKT antibodies would have been used to normalise the activation of these proteins to their respective total levels. In the absence of these antibodies, the activation was normalised to the total ERK levels. A further limitation of the analysis of protein activation using western blot, is the lack of biological repeats performed. The need for optimisation of the protein extraction protocol using zebrafish tissue, as well as insufficient biological samples and time, meant it was not possible to perform biological repeats. The results are therefore subject to replication, which would subsequently facilitate more robust densitometry analysis of bands to quantify and validate the findings.

The preliminary results obtained from the western blots are difficult to decipher, due to the lack of consistency. Stressing embryos through swimming in methylcellulose did not alter the activation of either P38 or ERK. Sadly, there was a lack of zebrafish-specific antibody for JNK, which has been shown to be activated by ZAK. JNK activity increases upon mechanical load, where it regulates proliferation, hypertrophy, and apoptosis (Olsen *et al.*, 2019; Lessard *et al.*, 2018; Tan *et al.*, 2009), making it an ideal candidate for assessing

activation following methylcellulose stress. ZAK has been shown to phosphorylate and activate P38 (Liu *et al.*, 2000; Gross *et al.*, 2002). An increase in P38 activation was seen in non-methylcellulose stressed embryos lacking ZAKβ or ZAKα and ZAKβ. The increase in P38 phosphorylation could indicate compensation from other pathways in the absence of ZAK. Surprisingly, when ZAKβ$^{-/-}$ or ZAKα$^{-/-}$ ZAKβ$^{-/-}$ embryos were stressed with methylcellulose, P38 phosphorylation was reduced to levels comparable with wild type, which is difficult to rationalise. The increase in p-P38 levels in the absence of ZAKβ or ZAKα and ZAKβ, is not present in adult muscle. On the contrary, p-P38 levels appear slightly reduced in ZAKβ$^{-/-}$ skeletal muscle. One explanation for the lack of consistency in P38 phosphorylation levels between embryos and adults is that ZAK preferentially activates P38γ whereas, the antibody in question detects three of the four activated isoforms of P38 (α, β and γ). Changes to the levels of activation of an individual P38 isoform might be masked by the other isoforms. Additionally, protein was extracted from whole embryos, therefore, any changes to protein activation are not muscle-specific. ZAKβ is enriched in the developing heart and skeletal muscle, therefore, it is likely that the protein activation changes are present in these tissues.

Multiple studies have shown the potential for ZAK to phosphorylate AKT (Fu *et al.*, 2016; Wang *et al.*, 2021). The AKT/mTOR pathway is important for hypertrophy and preventing atrophy in skeletal muscle (Rommel *et al.*, 2001; Bodine *et al.*, 2001). In 8 dpf embryos, there was a decrease in the level of AKT activation when ZAKβ was absent and an even greater decrease when both ZAKα and ZAKβ were absent. There was no difference in the levels of phosphorylated AKT in adult skeletal muscle, therefore, the role of ZAK in activating AKT could be more important during development, rather than in adult muscle maintenance or hypertrophy. Interestingly, cross talk between the Hippo pathway and AKT/mTOR activity has been reported (Fischer *et al.*, 2016). YAP-induced reduction in PTEN (inhibitor of AKT) leads to increased AKT activity (Tumaneng *et al.*, 2012). The decreased AKT levels when ZAKβ is absent in 8 dpf embryos, coupled with the significantly reduced *FLNCA* transcription in ZAKβ$^{-/-}$ 8 dpf embryos, again alludes to potential involvement of ZAKβ signalling in the hippo signalling pathway in zebrafish. ZAKα has been shown to activate YAP through the tyrosine kinase, SRC (Fu *et al.*, 2019; Silva *et al.*, 2022), however,

an association for ZAKβ to the Hippo pathway has not yet been identified, to my knowledge.

The opposite trend for activation of ERK can be seen, with no differences in the activation of ERK in 8 dpf embryos, but an apparent increase when ZAKβ or ZAKα and ZAKβ were absent in adult skeletal muscle. The increased ERK activation could be a compensatory mechanism to maintain muscle mass and prevent atrophy (Shi *et al.*, 2009). Constitutive activation in ERK resulted in a fast-to-slow fibre-type switching that minimised severity of disease progression in a mouse model for limb girdle muscular dystrophy (Boyer *et al.*, 2019).

Whilst the changes to protein activation are not validated, they could hint at potential changes to larval zebrafish and adult skeletal muscle when either just ZAKβ or both isoforms are absent. Potential repeats of the experiment with more specific antibodies could validate these preliminary findings. Further to this, phosphoproteomics would provide a non-biased approach to investigate alterations in protein phosphorylation in absence of ZAKβ and should be considered for future work.

5.4. Conclusion

Many changes to the levels of transcript expression in the absence of ZAKβ are small and not significant. The significant reduction of *FLNCA* in 8 dpf embryos lacking ZAKβ might hint at a role for ZAKβ signalling to increase transcription of *FLNC* in stressed muscle fibres. A role for ZAKβ in the CASA pathway and/or hippo pathway should be investigated further. The significant upregulation of *myogenin* and *myomaker* in 8 dpf ZAKβ$^{-/-}$ could indicate abnormal fusion is occurring and will be investigated further in chapter 6.

6. Imaging Skeletal Muscle in Zebrafish Lacking ZAKβ

6.1. Introduction

In this chapter, the structure and ultrastructure of skeletal muscle is investigated in embryos and adult zebrafish lacking ZAKβ and age-matched controls. To do this, ZAKβ$^{-/-}$ zebrafish were crossed into two different transgenic zebrafish lines: Tg (mpx:GFP)^{i114} to assess the neutrophil infiltration following skeletal muscle wounding (Renshaw *et al.*, 2006); and Tg (Acta1:lifeact-GFP;mCherry((CAAX)) in order to assess the development of skeletal muscle (Berger *et al.*, 2014). Transmission electron microscopy (TEM) of skeletal muscle dissected from old-age ZAKβ$^{-/-}$ zebrafish and age-matched wild type controls (36-months), is used to analyse the ultrastructure of mutant and wild type myofibres.

6.1.1. Role of Inflammation in Skeletal Muscle Repair and Regeneration Following Injury

Inflammation is important to initiate the repair response of skeletal muscle following injury or damage (Ziemkiewicz *et al.*, 2021). Polymorphonuclear granulocytes, called neutrophils, are the first immune cells to appear at damaged skeletal muscle, arriving as soon as one hour following insult (Fielding *et al.*, 1993). The maximum levels of neutrophils are seen between 6 – 12 hours post injury (Malm *et al.*, 2000). Following injury or fibre necrosis in skeletal muscle, damage associated molecular patterns (DAMPs) are released, which include DNA, high mobility group box 1 protein (HMGB1) and ATP (Bours *et al.*, 2006; Venereau *et al.*, 2012; Wang, 2018). These DAMPs can activate surrounding cells in the tissue, such as mast cells and endothelial cells to produce and secrete proinflammatory cytokines and chemokines, for example, interleukin (IL)-1β, tumour necrosis factor α (TNF-α) and IL-8, which can recruit and activate neutrophils (Kaplanski *et al.*, 1994; Radley and Grounds, 2006; Howard *et al.*, 2020). Neutrophils release reactive oxide species (ROS) and enzymes, such as elastase and myeloperoxidase, and phagocytose debris in the skeletal muscle (Wang, 2018). Furthermore, neutrophils release pro inflammatory cytokines and chemokines, such as IL-1, IL-8 and CCL2, which can aid the recruitment and activation of circulating monocytes into proinflammatory (M1) macrophages in the damaged skeletal muscle (Yoshimura and Takahashi, 2007; Selders *et al.*, 2017; Howard *et al.*, 2020). Neutrophils are usually cleared and no longer detected by around one week after injury (Marsolais *et al.*, 2001). Despite phagocytosing

debris and increasing vascularisation following insult (Dalli *et al.*, 2013), there has been contradictory results in how essential neutrophils are for skeletal muscle regeneration in mice (Teixeira *et al.*, 2003; Dumont *et al.*, 2008).

Tissue-resident or circulating monocyte-derived phagocytes, named macrophages, arrive at the wound site after neutrophils (Wang *et al.*, 2014; Brigitte *et al.*, 2010). Albeit an overly-simplistic representation, macrophages can be thought of as having two phenotypes: Pro-inflammatory (M1) macrophages, which reach peak levels between 1-2 days post injury (dpi) and anti-inflammatory macrophages (M2), which replace M1 macrophages as the prevalent macrophage from 3 dpi, reaching a peak and plateauing at 7 dpi (Arnold *et al.*, 2007). M1 macrophages are important for phagocytosis, clearing cell debris as well as the production of pro-inflammatory cytokines, such as TNF-α, IL-1 and IL-6 (Mills *et al.*, 2000; Mantovani *et al.*, 2004). Conversely, M2 Macrophages are important for healing and the resolution of inflammation, producing anti-inflammatory cytokines, such as TGF-β and IL-10 (Mills *et al.*, 2000; Mantovani *et al.*, 2004; Arnold *et al.*, 2007). Interestingly, phagocytosing necrotic debris as well as apoptotic neutrophils can result in the conversion of M1 macrophages to M2 macrophages (Huynh *et al.*, 2002; Xu *et al.*, 2006; Arnold *et al.*, 2007). The importance of macrophages is emphasised by reduced skeletal muscle regeneration following wounding, when monocyte/macrophage migration via ccr2 was absent (Lu *et al.*, 2011). Moreover, the switch from M1 to M2 macrophages is also critical for effective skeletal muscle regeneration (Mounier *et al.*, 2013).

Other white blood cells, such as T and B-cells contribute to the pro-inflammatory response, through the production of cytokines as well as the regenerative the anti-inflammatory response, directly acting on satellite cells as well as aiding the conversion of M1 macrophages into an M2 phenotype (Fu *et al.*, 2015; Ziemkiewicz *et al.*, 2021). Experiments using confocal imaging have revealed an interaction between macrophages and satellite cells in wounded zebrafish embryos and demonstrated a role for ‘dwelling’ macrophages in stimulating satellite cell proliferation (Ratnayake *et al.*, 2021). With neutrophils also playing an important role in the innate immune response, this chapter will use confocal imaging to analyse neutrophil behaviour in wounded muscle in the presence or absence of ZAKβ.

Activated satellite cells will undergo myogenesis by proliferating, before differentiating and fusing either to existing myofibres or to each other, forming new fibres (Fu *et al.*, 2015). Typically, pro-inflammatory cytokines, produced by neutrophils, M1 macrophages and effector T cells will result in the activation and proliferation of satellite cells, as well as inhibition of terminal differentiation (Li, 2003; Broussard *et al.*, 2004). On the other hand, anti-inflammatory cytokines and growth factors produced by M2 macrophages and regulatory T (Treg) cells are more pertinent for promoting differentiation and fusion of satellite cells (Arnold *et al.*, 2007; Burzyn *et al.*, 2013). See section 1.2 for further details on satellite cells and regeneration.

Dysregulation of the inflammatory response can result in pathology, as evidenced by the sustained presence/recruitment of neutrophils in skeletal muscle of mice and canine models of Duchenne muscular dystrophy (Arecco *et al.*, 2016; Terrill *et al.*, 2016). The continuous inflammation and chronic neutrophil accumulation causes tissue damage, through reactive oxide species and persistent toxic antimicrobial enzyme production, which can inhibit the differentiation of myoblasts and, thus, skeletal muscle regeneration (Haycock *et al.*, 1996; Terrill *et al.*, 2016; Arecco *et al.*, 2016). Sustained attempts of degeneration and regeneration will also lead to the replacement of fibres with fat and connective tissue, resulting in fibrosis (Mastaglia *et al.*, 1970; Juban *et al.*, 2018). Inhibition of inflammation or neutrophil activity in mice has shown positive effects of attenuating pathology and improving muscle function (Hodgetts *et al.*, 2006; Henriques-Pons *et al.*, 2014).

ZAK signalling, through P38 and JNK, has been shown to increase the production of pro-inflammatory cytokines, with ZAK-deficient or chemically-inhibited mice producing macrophages with significant reductions in secreted IL-1β, IL-6 and CXCL1 (neutrophil chemokine) (Wong *et al.*, 2013). ZAKα, along with activated P38, phosphorylates and activates the linker region of the inflammasome protein NLRP1, which can then activate caspase-1, leading to pyroptosis and release of the pro-inflammatory cytokine IL-1β (Hu *et al.*, 2010; Robinson *et al.*, 2022). Given the critical role of maintaining homeostasis of inflammation in skeletal muscle, to avoid pathology, and the association of ZAK with regards to inflammation, it was of interest to investigate potential defects in zebrafish lacking ZAKβ following wounding.

6.1.2. Skeletal Muscle Fusion

The upregulation of *myomaker* in RNA-seq data of ZAK$^{-/-}$ mice, coupled with the upregulation of *myogenin* and *myomaker* in 8 dpf ZAK$\beta^{-/-}$ zebrafish embryos made investigating skeletal muscle fusion an interesting prospect. Section 1.2 describes the full process of myogenesis, from an embryonic and regenerative process, in greater detail. The specific role that myogenin and myomaker play in myoblast fusion are discussed below.

Absence of myogenin in mice results in death shortly after birth, as a result of severe muscle disruption (Hasty *et al.*, 1993). Zebrafish lacking myogenin are viable, however, there is almost complete absence of fusion; and muscle progenitor cells (MPC) isolated from these *Myog*$^{-/-}$ zebrafish are also fusion incompetent but capable of terminal differentiation (Ganassi *et al.*, 2018). Myogenin increases the expression of fusogenic proteins, such as myomaker and myomerger (also known as myomixer) (Ganassi *et al.*, 2018). Myomaker and myomerger are membrane proteins and are both essential for fusion (Millay *et al.*, 2013; Bi *et al.*, 2017). Myomaker is required for hemifusion, whereas myomerger is required for the pore formation and drives completion of myoblast fusion (Leikina *et al.*, 2018). Inhibition of actin polymerisation resulted in failure of cells to fuse, despite the presence of myomaker and myomerger in the cell membrane (Millay *et al.*, 2013; Zhang *et al.*, 2017). Actin cytoskeletal remodelling has been proposed as producing invasive membrane protrusions that are essential in myoblast fusion (Shilagardi *et al.*, 2013). Myomaker and myomerger have been proposed as regulating the actin cytoskeletal reorganisation, however, the extracellular location of the c-terminus of myomerger weakens this theory (Leikina *et al.*, 2018).

6.1.3. Aims

- Image and measure the presence of neutrophils in ZAKβ$^{-/-}$ Tg (mpx:GFP) zebrafish embryos following injury
- Investigate the fusion capabilities of 2 and 5 dpf ZAKβ$^{-/-}$ zebrafish embryos, relative to wild type.
- Analyse the ultrastructure of old (37-month) ZAKβ$^{-/-}$ zebrafish skeletal muscle compared to age-matched wild type using TEM.

6.2. Results

6.2.1. ZAKβ$^{-/-}$ Zebrafish Embryos Display Comparable Neutrophil Activity to Wild Type

To assess abnormalities in the repair and regeneration of skeletal muscle, ZAKβ$^{-/-}$ zebrafish were crossed into a transgenic line Tg (mpx:GFP)^{i114} (Renshaw *et al.*, 2006). This transgenic line expresses GFP under the myeloperoxidase (*mpx or mpo)* promoter and has been validated for response to injury (Renshaw *et al.*, 2006). The *mpx* gene is exclusively expressed in neutrophils and neutrophil-progenitors in embryonic/larval zebrafish (Lieschke *et al.*, 2001).

Wild type and ZAKβ$^{-/-}$ zebrafish were raised as normal until four days post fertilisation (dpf), when, following anaesthetic, a single puncture wound was performed to the epaxial skeletal muscle in somites 17/18. The embryos were left to recover in fresh zebrafish embryo media before fixing and imaging at set timepoints following injury.

Neutrophils are not present in unwounded skeletal muscle, with or without the presence of ZAKβ, as demonstrated in figure 6.1 (a). The speed of recruitment of neutrophils was not altered when ZAKβ was absent, as comparable numbers of neutrophils were present at one hour post injury (hpi) (figure 6.1 (b)). There are no significant differences between wild type and ZAKβ$^{-/-}$ zebrafish in the numbers of neutrophils recruited at any timepoint (figure 6.1 (b-e)), suggesting the recruitment or strength of response to be unaffected by absence of ZAKβ. Lack of ZAKβ does not affect the resolution of neutrophils, as by 72 hpi, the majority of neutrophils have been cleared from the wound site (figure 6.1 (e)).

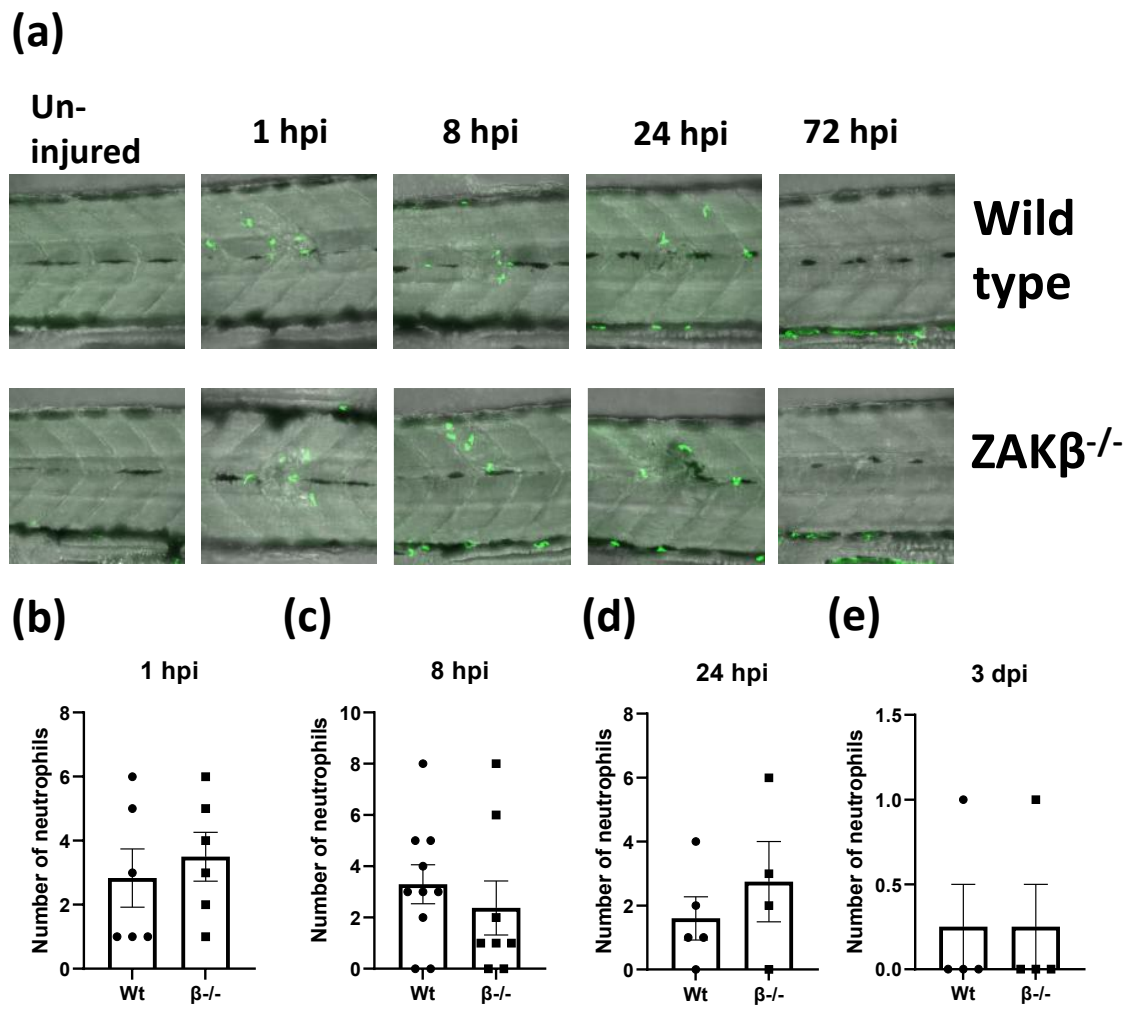

Figure 6.1. Assessing Neutrophil behaviour following skeletal muscle wounding in ZAKβ$^{-/-}$ zebrafish embryos.
(a) Representative image of the GFP-labelled neutrophils (Tg: MPX-GFP) in either a wild type or ZAKβ$^{-/-}$ genetic background, at various timepoint following injury. Embryos were raised to 4 days post fertilization (dpf), before the epaxial muscle above the cloaca (somites 17/18) are wounded with a single puncture, using a 30-gauge hypodermic needle. A subset of embryos were not wounded as an un-injured control. The wounding and analysis were performed blind to prevent bias in the severity of wounding. There were no significant differences in the number of neutrophils at the wound site between wild type and ZAKβ$^{-/-}$ zebrafish at any of timepoints following wounding: (b) 1 hpi. (c) 8 hpi. (d) 24 hpi. (e) 72 hpi. Each data point is an individual count of the number of nuclei. Error bars represent SEM. The statistical test was an unpaired student's t-test (two-tailed). A 25X lens (LD LCI Plan Apochromat 25x/0.8 1mm Corr DIC M27) set to a water immersion was used to take the images.

6.2.2. Assessing Fusion Capabilities and Morphology of Skeletal Muscle in Tg (Acta1:lifeact-GFP; mCherry (CAAX)) embryos lacking ZAKβ

Tg (Acta1:lifeact-GFP; mCherry (CAAX)) were created and validated by (Berger *et al.*, 2014) and kindly gifted by Peter Currie. The ZAKβ$^{-/-}$ zebrafish line was crossed into this transgenic line and bred to homozygosity. Wild type and ZAKβ$^{-/-}$ zebrafish embryos were collected at either 2 or 5 dpf and fixed in 4% PFA with Hoechst DNA stain and visualised for a variety of parameters. Analysis of myocyte fusion using the Tg (Acta1:lifeact-GFP; mCherry(CAAX)) was carried out as in (Ganassi *et al.*, 2018), where a *myogenin* mutation in zebrafish embryos resulted in almost complete loss of myocyte fusion. Somites 17/18 were used for all analyses, providing a precise positional reference by proximity to the anal vent, as represented by figure 6.2 (a).

6.2.2.1. No fusion defects with ZAKβ$^{-/-}$ Zebrafish, but reduced Myofibre Area at 2 dpf

The ability of the muscle cell lineage to fuse and form multinuclear myofibres (in part mediated by the transcription factor myogenin and the membrane protein myomaker), was measured by counting the number of nuclei present in a single myofibre; this is possible as the membrane in this transgenic line is labelled with mCherry. Despite the increases in *myogenin* and *myomaker* transcript levels in ZAKβ$^{-/-}$ embryos, there were no changes in the average number of nuclei per myofiber in ZAKβ$^{-/-}$ zebrafish compared to controls. Figure 6.2 (b) and (c) demonstrates that the proportions of fibres with a particular number of nuclei is comparable between wild type and ZAKβ$^{-/-}$ embryos at 2 dpf, indicating comparable levels of fusion.

The myotome volume was calculated by multiplying the somite length by the average cross-sectional area of the myotome (see figure 6.2 (a)). The area of the myotome was measured at three equal distances across the somite length and an average was used in determining the myotome volume. There were no differences in the myotome volume between wild type and ZAK$\beta^{-/-}$ embryos (figure 6.2 (e)). The embryo length of ZAK$\beta^{-/-}$ embryos was also comparable to wild type embryos at 2 dpf (figure 6.2 (d)).

Note, attempts were made to assess the average distance between M-bands (sarcomere length or sarcomeric spacing) to assess if the skeletal muscle was forming normally from an ultrastructural perspective. However, due to the size of the yolk sac at 2 dpf, the tail of the embryos was a considerable distance from the coverslip, limiting the resolution of the sarcomeres.

A cross sectional view of the mCherry-fluoresence was taken at the mid-point of the somite. The area of every muscle fibre at this region was calculated and later pooled to produce a mean muscle fibre area for wild type and ZAK$\beta^{-/-}$ embryos. Figure 6.2 (f) demonstrates how the area of each muscle fibre was calculated. There is a significant reduction in the mean myofiber area, with a mean area of 85 μm^2 for wild type and 77 μm^2 for ZAK$\beta^{-/-}$ (figure 6.2 (g)). ZAK$\beta^{-/-}$ embryos have myofibres with a marginally reduced area compared to their wild type counterparts at 2 dpf.

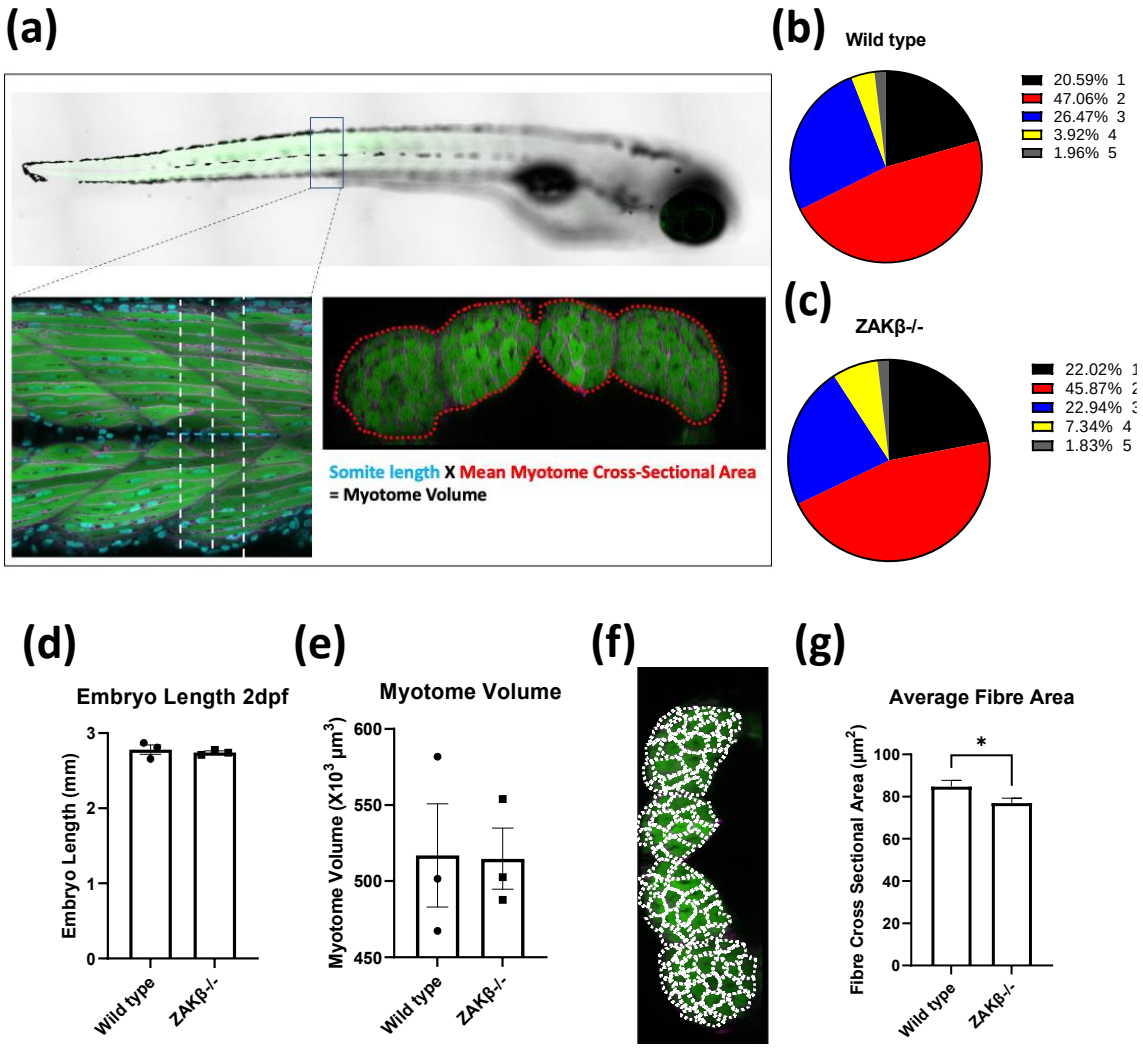

Figure 6.2. Investigations of fusion and myotome morphology in 2 dpf ZAKβ$^{-/-}$ embryos using Tg (acta1:lifeact-GFP; mCherry (CAAX)) zebrafish.
(a) Schematic showing how to calculate the myotome volume. Somites 17/18 are highlighted in the black box and a representative 24X image is shown below. The cyan blue dashed line represents the somite length, and the white dashed lines show the three equally spaced distances across the somite length, through which the cross-sectional area was calculated. The red dashed line represents the cross-sectional area of the myotome. Myotome volume = somite length x Mean myotome cross sectional area. (b) Percentage of fibres with a particular number of nuclei in wild type embryos. (c) Percentage of fibres with a particular number of nuclei in ZAKβ$^{-/-}$ embryos. (d) No difference in the embryo length between wild type and ZAKβ$^{-/-}$ 2 dpf embryos. (e) No difference in the myotome volume between wild type and ZAKβ$^{-/-}$ 2 dpf embryos. (f) White dotted lines represent the area of each muscle fibre measured within the myotome. (g) There was a significant reduction in the mean myofiber area when ZAKβ is absent. A total of 98 myofibres were measured across three separate wild type embryos and 108 myofibers across three separate ZAKβ$^{-/-}$ embryos. All error bars are SEM. For statistical tests, Chi squared was used to assess the proportions of nuclei. An unpaired student's T-test (two-tailed) was used to assess all other data sets. No asterisk = not significant. * = $P \leq 0.05$

6.2.2.2. No fusion Defects with ZAKβ$^{-/-}$ Zebrafish, but Reduced Myofibre Area at 5 dpf

Figure 6.3 (a) and (b) demonstrate that the proportions of fibres with a particular number of nuclei were not different between wild type and ZAKβ$^{-/-}$ embryos at 5 dpf, indicating comparable levels of fusion.

The reduced yolk sac size at five days of development allowed the tail to be closer to the coverslip and sarcomeric spacing to be assessed. The M-bands, contained within the H-zone of the sarcomere, do not contain any actin and, therefore, appear darker. The distance between the M-bands was used to determine the 'sarcomeric spacing' or sarcomere length (see figure 6.3 (c)). The formation of sarcomeres is a tightly regulated event and highly accurate, with consistent distances (sarcomere length) between the M-bands in both wild type and ZAKβ$^{-/-}$ zebrafish (figure 6.3(d)). The ultrastructure and formation of the sarcomere appears to be unaffected at 5 dpf in the absence of ZAKβ$^{-/-}$.

With regards to the morphology, there is no difference between the mean embryo length in wild type and ZAKβ$^{-/-}$ embryos (figure 6.3(e)). There is also no difference in the myotome volume between wild type and ZAKβ$^{-/-}$ zebrafish embryos at 5 dpf (figure 6.3 (f)). There is, however, a significant reduction in the mean myofiber area, with the average wild type area being 102 μm^2, and ZAKβ$^{-/-}$ being 90 μm^2 (figure 6.3 (g)). This reduction in muscle fibre area is apparent at both 2 dpf and 5 dpf, and is not due to a defect in fusion in ZAKβ$^{-/-}$ embryos.

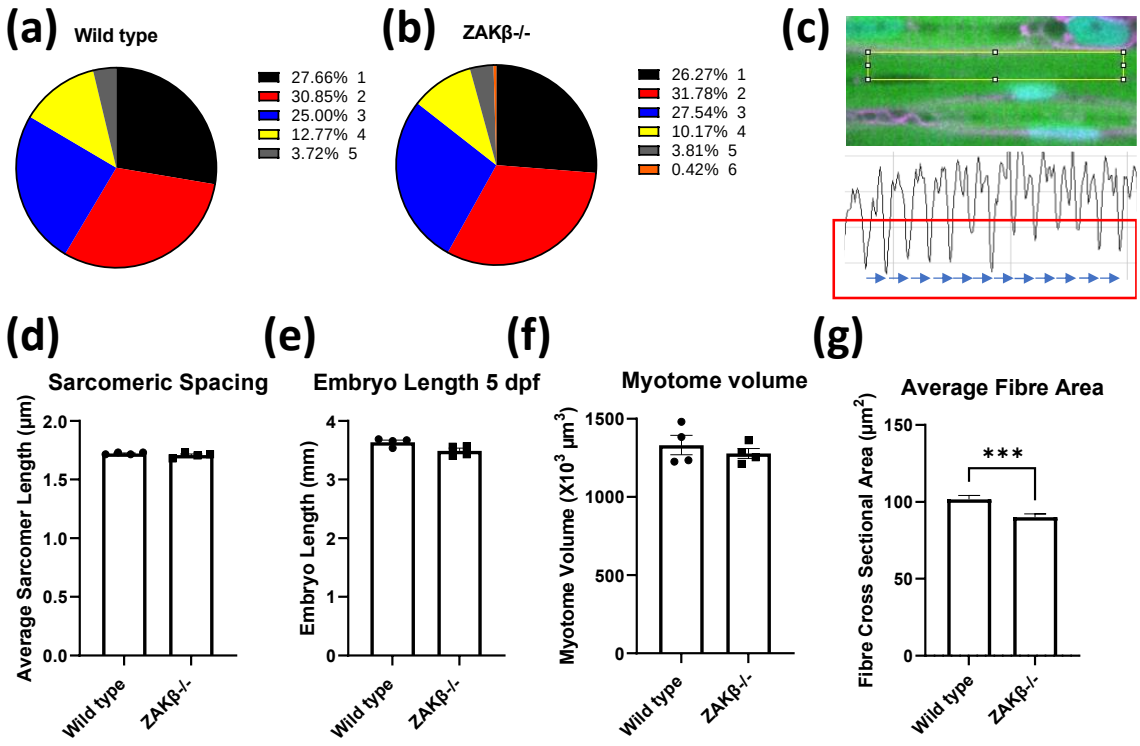

Figure 6.3. Investigations of fusion and myotome morphology in 5 dpf ZAK$\beta^{-/-}$ embryos using Tg (acta1:lifeact-GFP; mCherry (CAAX)) zebrafish.
(a) Percentage of fibres with a particular number of nuclei in wild type embryos. (b) Percentage of fibres with a particular number of nuclei in ZAK$\beta^{-/-}$ embryos. (c) Schematic demonstrating how sarcomere length is calculated. A plot profile of the fluorescent intensity is calculated and the distance between the lowest actin GFP-intensity (middle of the M-band), represented by the blue arrows, is used to determine the sarcomeric spacing. (d) No difference in the size of the sarcomeres between wild type and ZAK$\beta^{-/-}$ zebrafish embryos. (e) Comparable embryo length in wild type and ZAK$\beta^{-/-}$ embryos. (f) No differences in the myotome volume when ZAKβ is absent. (g) There was a significant reduction in the mean myofiber area when ZAKβ is absent. A total of 452 myofibres were measured across four separate wild type embryos and 477 myofibers across four separate ZAK$\beta^{-/-}$ embryos. All error bars are SEM. For statistical tests, Chi squared was used to assess the proportions of nuclei. An unpaired student's T-test (two-tailed) was used to assess all other data sets. No asterisk = not significant. *** = P ≤ 0.001

6.2.3. Ultrastructure of Old Age ZAKβ$^{-/-}$ Zebrafish and Age-Matched Wild Type Controls

In order to determine any possible skeletal muscle phenotype in the ZAKβ mutant zebrafish, it is essential to investigate the ultrastructure of the functional unit of skeletal muscle: the sarcomere. This analysis was carried out using transmission electron microscopy (TEM) of skeletal muscle dissected from old-age zebrafish (37-months-old) lacking ZAKβ, compared to skeletal muscle from age-matched controls. Skeletal muscle was dissected from the same region of the tail from three 37-month aged ZAKβ$^{-/-}$ and three 36-month-old wild type zebrafish. 36/37-months of age is very old for laboratory-reared zebrafish (Gilbert *et al.*, 2014; Dilan *et al.*, 2018). Skeletal muscle was dissected from the same region of three ZAKβ$^{-/-}$ zebrafish and three age-matched wild type controls. Sections were prepared, as detailed in section 2.14, before visualising and taking images using TEM.

6.2.3.1. No Changes in the Appearance of Mitochondria and Nucleus in the Absence of ZAKβ

There were many technical difficulties with the TEM analyses: the sectioning and staining of the samples was error-ridden, with knife marks visible in many of the sections (can be seen in figure 6.4(a)). There was also the unusual appearance of electron light regions, presumably the sarcoplasm and the sarcoplasmic reticulum (SR), which appear to be occurring at a cross-section, rather than the expected longitudinal orientation in the sarcomere (can be seen in figure 6.4(c)). Artifacts such as random accumulations of dark patches as well as small black dots were present in both wild type and ZAKβ$^{-/-}$ sections and did not appear physiological. Despite these problems, some samples were sectioned and stained well, as evidenced by a 'typical' sarcomere appearance, for example in figure 6.4(b), showing distinct Z-discs, I-bands and M-bands, with minimal knife marks or artifacts. Despite the technical problems – which were common across both genotypes – the ultrastructure is still visible, and some analysis can still be made.

There were no observable abnormalities in the nuclei of ZAKβ$^{-/-}$ or wild type zebrafish as demonstrated by figure 6.4(a) and 6.4(c). The chromatin was located peripherally and although difficult to identify, there appears be a round nucleolus in the centre of the nuclei for both genotypes.

The mitochondria have well-defined tubular cristae demonstrating the integrity of the sections (figures 6.4 (b) and (d)). The mitochondria were similar in zebrafish skeletal muscle, with or without ZAKβ, often forming clusters and accumulating together, which has been noted in zebrafish (Kayman Kürekçi *et al.*, 2021). Figures 6.4 (b) and (d) demonstrate the appearance of the mitochondria was as expected and there were no signs of swollen mitochondria or inclusions, which can be indicative of pathology (Tagliavini *et al.*, 2013). Images selected are representative of the mitochondria seen across several different samples, from different fish, with similar observations made from muscle taken from both wild type and ZAKβ$^{-/-}$.

Note the strange phenotype of a cracked or ‘zigzag’ pattern of the sarcomere in the ZAKβ$^{-/-}$ sample shown in figure 6.4 (d), running along the M-band, which may be an artifact. More sections will be required to determine if this is a rare phenotypic abnormality that arises when ZAKβ is absent.

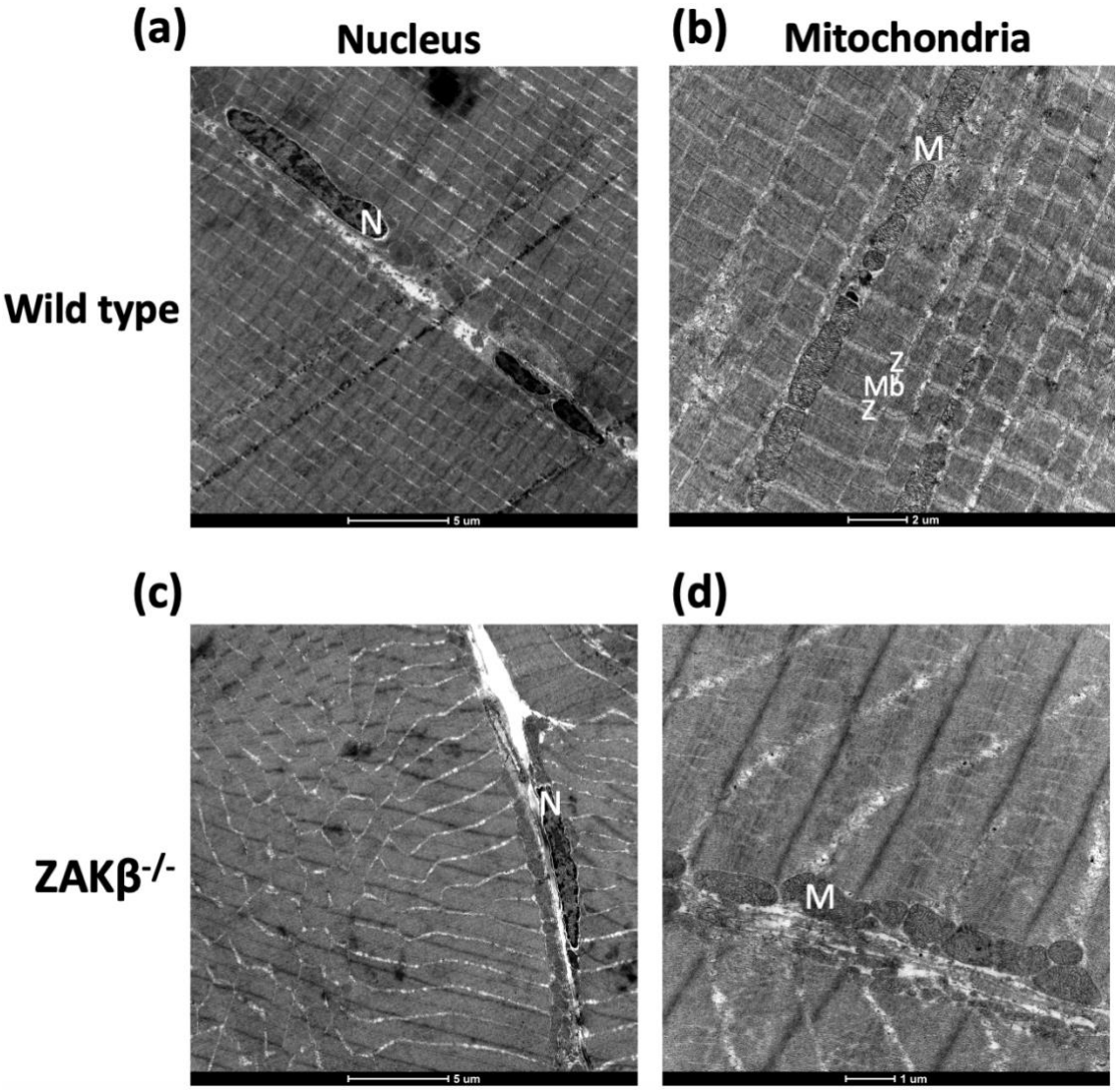

Figure 6.4. TEM Images showcasing ultrastructure, nuclei and mitochondria in old age wild type and ZAKβ$^{-/-}$ zebrafish skeletal muscle.
(a) and (c) are representative images of nuclei belonging to wild type or ZAKβ$^{-/-}$ skeletal muscle, respectively. Note the well-defined peripheral chromatin and nucleolus. N = nucleus (b) Wild type mitochondria contains well defined tubular cristae. The mitochondria are labelled by the letter 'M'. The ultrastructure is clearly visible with Z-discs (Z) and the M-band (Mb) labelled. The I-band (not labelled) is the electron light region surrounding the electron dense Z-disc. (d) ZAKβ$^{-/-}$ mitochondria also are well-defined and similar in morphology to wild type. Note the presence of a rare zigzag structure running the length of all M-bands. Unclear as to whether this is pathology or an artifact. (c) and (d) both show unusual location of electron light regions, presumably the sarcoplasm and the SR. There were examples of this for both wild type and ZAKβ$^{-/-}$ sections. Images selected are representative of three repeats for wild type and ZAKβ$^{-/-}$. Following dissection of skeletal muscle, all further steps of sample preparation, sectioning, staining and imaging were performed by the University of York Imaging and Cytometry department of the Technology Facility.

6.2.3.2. Possible Loss of Sarcomere integrity in ZAKβ-/- Muscle

An interesting observation using TEM on aged ZAKβ$^{-/-}$ zebrafish was the frequent disintegration or dissolution in the organization of the myofibril (figure 6.5(b i - iv)). The complete loss of sarcomere structure was a common feature of all ZAKβ$^{-/-}$ zebrafish and was not observed in any of the age-matched wild type controls. Myofibrils often appeared well formed, with structured and defined sarcomeres, that would later completely disintegrate into a complete lack of identifiable structure. The complete loss of organization appears to extend to the triad with seemingly random arrangements of triads, which are usually centred around Z-discs. Panoramic examples of age-matched wild type zebrafish skeletal muscle with well-defined and organized sarcomeres can be seen in figure 6.5 (a (i-ii)). There were considerably fewer extended regions of high sarcomere and myofibrillar organization in ZAKβ$^{-/-}$ skeletal muscle, compared to wild type sections.

The identifiable presence of some ultrastructure in figures 6.5 (b (i-iv)) that later becomes a region devoid of any sarcomere organisation strengthens the argument for the lack of structure to be a phenotype and not an artifact from the preparation of the samples. Furthermore, the loss of sarcomere organisation was present on all three of the ZAKβ$^{-/-}$ skeletal muscle and none of the wild type skeletal muscle samples, which were prepared identically.

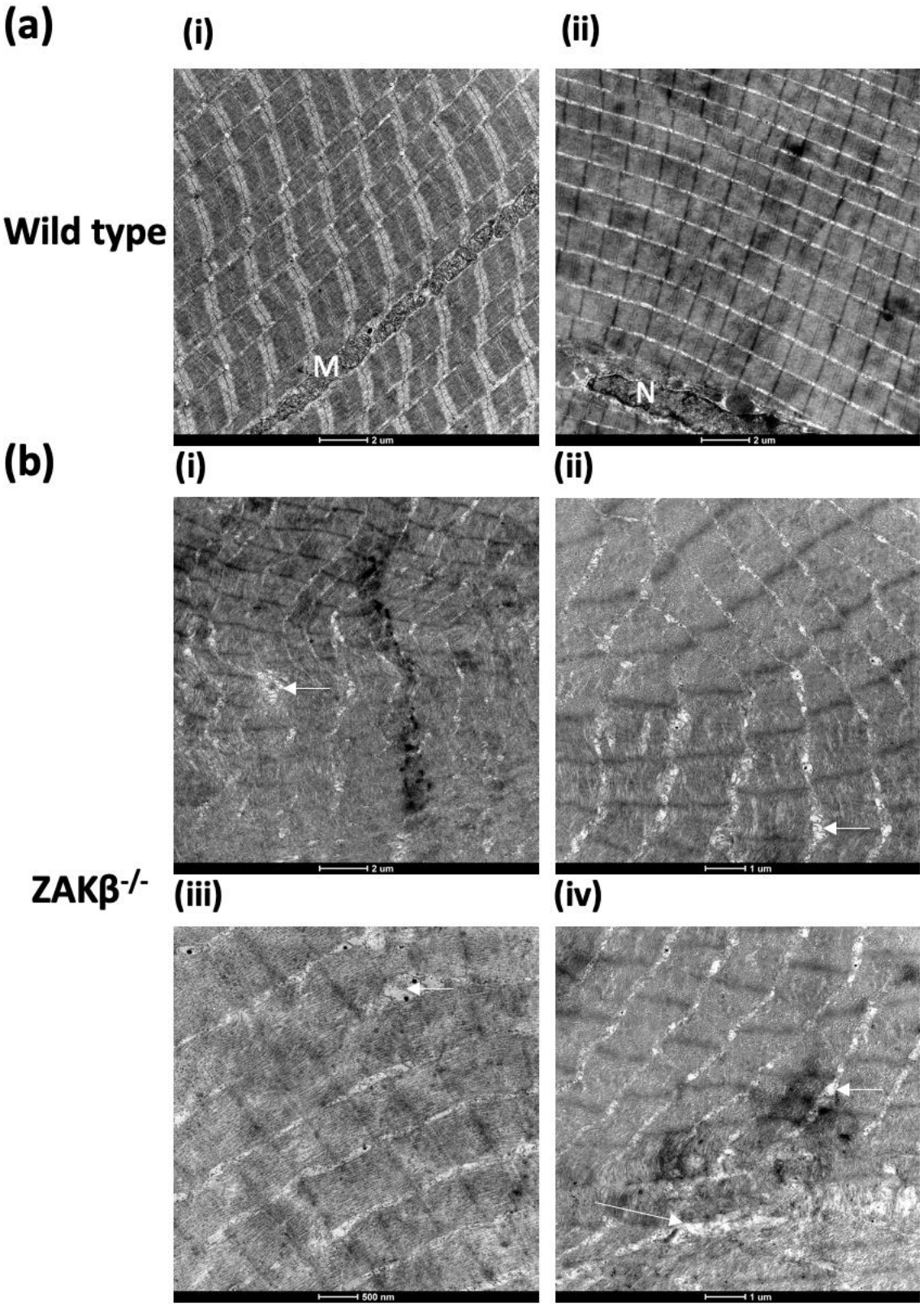
(a)
(i)
(ii)
Wild type
M
N
2 um
2 um
(b)
(i)
(ii)
2 um
1 um
ZAKβ-/-
(iii)
(iv)
500 nm
1 um

Figure 6.5. TEM images of dissolution of sarcomere and myofibrillar organisation in old-age ZAK$\beta^{-/-}$ skeletal muscle.
(a) (i-ii) Panoramic images of wild type skeletal muscle to demonstrate the organisation and structure of skeletal muscle. (b) (i-iv) Demonstrate the large areas of skeletal muscle devoid of structure and sarcomere organisation. Often there is ultrastructure that can disintegrate into no organisation. All three ZAK$\beta^{-/-}$ zebrafish are represented in these images. (iii) Example of a mild loss of sarcomere structure that may dissolve into loss of myofibrillar structure in the future. (iv) Example of the most severe dissolution of myofibrillar organisation. White arrows represent possible disorganised triad. Following dissection of skeletal muscle, all further steps of sample preparation, sectioning, staining and imaging were performed by the University of York Imaging and Cytometry department of the Technology Facility.

6.2.3.3. Highly irregular Arrangement of myofibrils in the Absence of ZAKβ

An unusual occurrence in ZAKβ$^{-/-}$ skeletal muscle was the abrupt switch from myofibrils in a longitudinal orientation to a transverse orientation (figures 6.6 (a-c)). Whilst sections of wild type skeletal muscle were sometimes sliced at a cross section by mistake, there were no examples of longitudinal sections abruptly being replaced by myofibrils in an orthogonal arrangement in any of the wild type sections processed.

It is unclear whether it is the existing myofibril that is changing orientation, causing the shift from longitudinal to transverse, or another myofibril is displacing the original longitudinal myofibril. Either way, myofibrils appear to be not as highly organised in ZAKβ$^{-/-}$ zebrafish compared to wild type.

Whilst the change in orientation could be the result of artifacts/errors when processing the sample, the unique presence of this phenotype in only the three ZAKβ$^{-/-}$ zebrafish weakens this hypothesis.

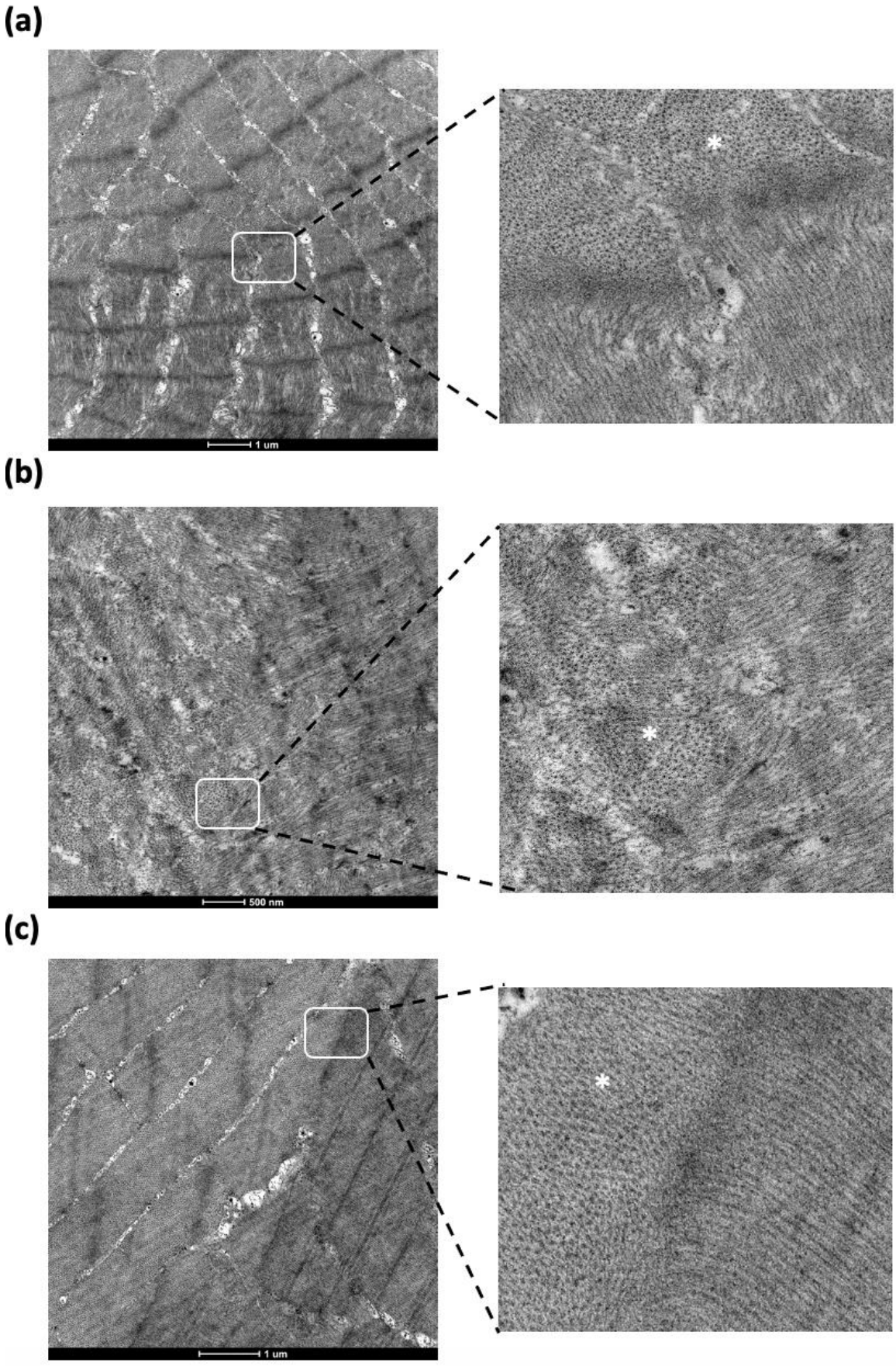
(a)
1 um
(b)
500 nm
(c)
1 um

Figure 6.6. TEM of unusual arrangement of myofibrils unique to *ZAKβ* mutant zebrafish. (A-C) show longitudinal sarcomeres with visible filaments that abruptly terminate and are replaced with myofibrils at a cross sectional orientation (highlighted with white asterisk). Left image is panoramic and the right image is zoomed to see the transverse sections of myofibrils. Orthogonal arrangement was seen in all three ZAK$\beta^{-/-}$ zebrafish, with each image an example of a different ZAK$\beta^{-/-}$ zebrafish. Whilst there were examples of a cross sectional appearance for wild type, these were more likely the result of mistakes in sectioning, as they were never accompanied with the characteristic longitudinal myofibrillar arrangement. Following dissection of skeletal muscle, all further steps of sample preparation, sectioning, staining and imaging were performed by the University of York Imaging and Cytometry department of the Technology Facility.

6.3. Discussion

The availability of zebrafish lines carrying transgenes that allow visualisation of specific cell types, and even distinct regions of the cell, is a key advantage of using this model organism to understand cell behaviour and differentiation. When combined with efficient protocols for gene targeting in zebrafish, this allows the molecular analysis of gene function in cell processes. Generating a ZAK$\beta^{-/-}$ line of zebrafish where the skeletal muscle has actin filaments tagged with a GFP-labelled actin binding protein (lifeact) as well as membranes labelled with mCherry, has allowed the investigation of this mutant at a cellular level.

6.3.1. Absence of ZAKβ Does not Alter the Behaviour of Neutrophils

In the absence of any injury, there are no neutrophils present in embryonic skeletal muscle, regardless of the presence or absence of ZAKβ. In contrast, *sapje* zebrafish model for Duchenne muscular dystrophy provides an example of abnormal neutrophil behaviour, with persistent neutrophil presence in the skeletal muscle of larval zebrafish (Berger *et al.*, 2010).

ZAK$^{-/-}$ mice show decreased production of the neutrophil chemokine, IL-8 (also called CXCL-8) by macrophages (Jandhyala *et al.*, 2016). Combined with P38 and JNK inflammatory signalling, it was, therefore, of interest to see if there were any abnormalities on the behaviour of neutrophils in zebrafish lacking ZAKβ. Following injury, the speed of recruitment of neutrophils, as well as the number of neutrophils were comparable between wild type and ZAK$\beta^{-/-}$ zebrafish embryos. The rate of clearance of neutrophils following wounding was also comparable between wild type and ZAK$\beta^{-/-}$ embryos. Absence of ZAKβ does not appear to affect the activity or resolution of neutrophils in larval skeletal muscle following injury. This reduces the likelihood of any pathology in the absence of ZAK arising from sustained inflammation and fibrosis, caused by neutrophils.

The variability in the number of neutrophils present at every timepoint, for both genotypes, is likely the result of marginal differences in the wounding of each embryo. Attempts were made to standardise the wounding procedure, such as the same needle was used throughout, and the needle was attached to a micromanipulator to ensure the single puncture was at the same angle for each embryo. Furthermore, all wounding and imaging was performed blind to prevent potential bias in the severity of the wound inflicted. Nevertheless, there will be unavoidable slight differences in the precise location and the degree of wounding between each embryo.

Neutrophils only represent the initial phase of the immune response in muscle following injury. Macrophages arrive later, becoming the most prevalent white blood cell at 3 dpi and on top of contributing to the pro-inflammatory environment for phagocytosis, macrophages also mediate the switch from a pro-inflammatory environment to an anti-inflammatory environment, which is critical for repair (Brigitte *et al.*, 2010; Arnold *et al.*, 2007). Attempts were made to cross the ZAK$\beta^{-/-}$ line into a Tg (mpeg1:mCherry(CAAX)), where the membranes of macrophages are fluorescently labelled with mCherry, allowing the macrophage response to be assessed in the absence of ZAKβ (Bojarczuk *et al.*, 2016). However, the intensity of the fluorescence was too low to detect when sorting embryos from the mating, based on the presence or absence of fluorescence at 3 dpf (when the fluorescence should be easily visible). Tg (mpeg1:mCherry(CAAX)) were created and gifted by (Bojarczuk *et al.*, 2016). For future work, acquiring potentially brighter Tg (mpeg1:mCherry(CAAX)) zebrafish to cross with ZAK$\beta^{-/-}$ zebrafish would be useful in allowing the later stages of inflammation, and a more comprehensive assessment of wound repair response to be studied.

6.3.2. Absence of ZAKβ results in a Reduction in the Muscle Fibre Area

Transgenic zebrafish (Tg Acta1:lifeact-GFP; mCherry(CAAX)) were used to investigate if the upregulation of *myogenin* and *myomaker* in ZAKβ$^{-/-}$ zebrafish embryos resulted in a fusion defect. The fusion capability was assessed by measuring the proportions of fibres with a particular number of nuclei; this was found to be almost identical between wild type and ZAKβ$^{-/-}$ embryos at both 2 and 5 dpf, suggesting comparable fusion was taking place. The observed increases in *myogenin* and *myomaker* expression could be the result of compensation for the absence of ZAKβ, ensuring that skeletal muscle fusion remains unaffected. Interestingly, despite no change in fusion as measured by the number of nuclei per myofiber, the mutant embryo show a reduced myofiber diameter, indicating a potential growth phenotype.

From an ultrastructural perspective, the average sarcomere length was tightly regulated with no differences between wild type and ZAKβ$^{-/-}$ at 5 dpf. Note, analysis of the sarcomere length was unable to be performed at 2 dpf due to the protruding yolk sac increasing the distance between the tail and the coverslip, reducing the resolution of the image obtained. The yolk sac would need removing prior to embedding in low Tm agarose, to allow closer proximity of the tail to the coverslip, for investigation of the sarcomere length in 2 dpf embryos.

The embryo morphology was also comparable between wild type and embryos lacking ZAKβ, with no differences observed in either the embryo length or the myotome volume at either 2 or 5 dpf.

There was a significant decrease in the average muscle fibre area at both 2 and 5 dpf in ZAKβ$^{-/-}$ embryos, that could be attributed to hypotrophy or atrophy. Muscle fibres fail to fully grow to the same size, or may progressively waste, in the absence of ZAKβ, which might result in a myopathic phenotype. Humans with myopathy arising from mutations in *ZAK* show fibre size variation with atrophic fibres interspersed amongst normal and hypertrophic fibres (Vasli *et al.*, 2017). Sections taken from the soleus of ZAK$^{-/-}$ mice show a significant reduction in the cross-sectional area of both type I and type II fibres, that is attributed to atrophy (Nordgaard *et al.*, 2022).

6.3.3. Signs of defects at the Ultrastructural level in old-age ZAKβ$^{-/-}$ zebrafish

The quality of some of the staining and sectioning was less than optimal and made analysis complex and more difficult to decipher. For future work, further sections should be taken from the dissected skeletal muscle and optimisation work should be performed on the staining protocol, so that the ultrastructure can be more easily assessed. Nevertheless, many of the sections were still useable and allowed analysis of many aspects of the ultrastructure of skeletal muscle in old-age zebrafish.

The mitochondria and nuclei of old-age ZAKβ$^{-/-}$ zebrafish appeared normal and comparable to age-matched wild type zebrafish. There were some unusual features of the skeletal muscle seen in old-age ZAKβ$^{-/-}$ that were not/rarely observed in age-matched controls:

Firstly, there appeared to be the dissolution of myofibrillar organisation and sarcomere structure, whereby the structure of organised myofibrils would abruptly become completely disorganised, with a complete loss of discernible structure. The presence of ultrastructure prior to the disintegration of myofibrillar organisation indicates that there was likely once ultrastructure and functioning skeletal muscle, however, this was unstable and prone to degenerate. The visible presence of some ultrastructure in the section also reduces the likelihood of this phenomena being the result of artifacts in the preparation of the sample. Furthermore, the loss of sarcomere organisation was present in all three of the ZAKβ$^{-/-}$ zebrafish and none of the age-matched wild type samples, which were prepared at the same time, in an identical manner.

Secondly, there is the unusual phenotype of fibres at a cross-section intercepting the normal, longitudinal arrangement of the myofibrils. The unusual arrangement of myofibrils occurred in sections belonging to all three of the ZAKβ$^{-/-}$ zebrafish and none of the sections belonging to wild type zebrafish. This is a rare phenotype. There is evidence of myofibrils with different orientations in the skeletal muscle of zebrafish treated with *ambra1b* morpholino (Skobo *et al.*, 2014), however, there appeared to be more separation between the longitudinal and transversely orientated myofibrils, compared to that seen in ZAKβ$^{-/-}$ skeletal muscle. Unfortunately, with sections on the skeletal muscle occurring on a 2D plane, it is difficult to know whether the fibres are at an orthogonal or

perpendicular arrangement as a result of bends or kinks in the myofibrils, or whether myofibrils are protruding through or displacing the myofibrils and interfering with the ultrastructure. Either way, both theories demonstrate potential loss of myofibrillar organisation.

These results hint at possible changes to the skeletal muscle ultrastructure that could explain why old-age ZAKβ$^{-/-}$ zebrafish appear to swim less than their age-matched wild type counterparts (section 4.2.3.3.). Further repeats are required using an optimised protocol for staining dissected skeletal muscle sections. This will validate that the findings are indeed a phenotype, indicating pathology, and not the result of artifacts or errors from sample preparation. Further sections, spanning a greater range of the dissected muscle, could also allow the identification of rarer pathological differences in old-age ZAKβ$^{-/-}$ zebrafish. Furthermore, sections without abnormalities in the location of the SR will allow assessment of the triad formation and any possible abnormalities in the triad/SR appearance in ZAKβ$^{-/-}$ zebrafish. Lastly, imaging dissected muscle from aged zebrafish using light microscopy would allow for greater perspective on the degree of disorganisation, over a larger area, in *ZAKβ* mutant zebrafish.

6.4. Conclusion

The absence of ZAKβ does not appear to affect the initial phase of acute inflammation through neutrophils, following wounding to skeletal muscle. Absence of ZAK does not appear to affect the fusion of skeletal muscle fibres, with comparable proportions of nuclei between wild type and ZAKβ$^{-/-}$ mutant, suggesting the observed upregulation of *myogenin* and *myomaker* might be to compensate for absence of ZAKβ. Interestingly, there was a reduction in the mean area for individual muscle fibres, suggesting potential hypotrophy or atrophy of muscle fibres in absence of ZAKβ, which concurs with humans and mice lacking ZAK. TEM revealed abnormalities with regards to dissolution of myofibrillar organisation, which may hint at pathology occurring in old (36/37-month) zebrafish. There was also the surprising occurrence of myofibrils orientated orthogonally to one-another, which might also be another pathological consequence of absence of ZAKβ.

7. Discussion

7.1. Overview

In this chapter I will summarise the main findings from my research, from the use of CRISPR-Cas9 to produce single and double ZAK mutant zebrafish, to investigation into the impact that absence of ZAK isoforms has on zebrafish, ranging from embryonic development, up to old-age zebrafish. I will discuss how results may tie-in with each other and provide rationale for future experiments that I believe should be employed to understand the role of ZAK isoforms, and ZAKβ specifically, in skeletal muscle in greater detail.

7.2. Use of Zebrafish as a Model Organism and Characterisation of ZAK Isoforms in Zebrafish

Mice remain the most frequently used model organism to understand the pathology of muscle diseases, with the vast majority of human neuromuscular diseases having a genetic mouse model (Sztretye *et al.*, 2020). Zebrafish remain a useful model organism to supplement or further investigate the genetic and molecular pathogenesis of disease. I discuss the advantages of using zebrafish as a model organism in detail in section 1.8.1. Many of the features that make zebrafish useful model organisms have been utilised, throughout my investigation into the impact of ZAKβ absence on skeletal muscle.

The transparency of the externally developing embryos enables whole-mount *in situ* hybridisation to be performed, allowing tissue-specific mRNA enrichment during embryonic development to be assessed. There are validated transgenic zebrafish lines that produce fluorescent proteins in particular tissues under the influence of specific promoters. ZAKβ$^{-/-}$ zebrafish have been crossed into several of these lines, allowing investigation into immune cell migration during skeletal muscle repair, as well as skeletal muscle architecture during embryo development. The relatively short life span of zebrafish compared to humans has allowed me to investigate the effects of absence of ZAKβ in old-age zebrafish, where it appears there may be greater pathology compared to younger ZAKβ$^{-/-}$ zebrafish. The advantages of producing and validating zebrafish disease models are emphasised by the high throughput drug development work that can be done. In fact, certain drugs show a more comparable response to human administration, when given to zebrafish rather than mice. An example of this is the action of

thalidomide with regards to teratogenicity, typically with limb development, that occurs with humans and zebrafish but not mice (Ito *et al.*, 2010). Drug screening originating in zebrafish has been translated into human clinical trials (Patton *et al.*, 2021). An example of this is Clemizole, which is a compound initially identified as a potential therapeutic against genetic epilepsy in zebrafish and is now in phase 2 clinical trials for assessing the effectiveness in humans (identifier: NCT04462770) (Baraban *et al.*, 2013).

When considering skeletal muscle diseases specifically, as of 2016, as many as 1000 therapeutics/treatments have been utilised for potential therapeutics using the *sapje* model for DMD (Kawahara *et al.*, 2011; Widrick *et al.*, 2016). Additionally, the use of exon-skipping morpholinos in the zebrafish model for DMD resulted in restoration of a truncated form of dystrophin, rather than the expected absence; as well as improvements in the skeletal muscle architecture as assessed by birefringence (Berger *et al.*, 2011). The basis of this is centred around the milder phenotype of Becker muscular dystrophy, where mutations can result in a truncated but partially functional dystrophin protein (Mercuri *et al.*, 2019). Exon skipping using antisense oligonucleotides is currently in development in human clinical trials. The antisense oligonucleotide used depends on the location of the mutation in the *DMD* gene (Eser and Topaloğlu, 2022). Several of these antisense oligonucleotides are in phase 3 clinical trials at the moment, with results from earlier phases reporting increases in dystrophin production and decreased rate of decline in walking capabilities (Eser and Topaloğlu, 2022).

The expression patterns of *ZAKβ* in zebrafish are similar to that of humans and mice, with enriched expression in the heart and skeletal muscle (Gross *et al.*, 2002; Vasli *et al.*, 2017; Nordgaard *et al.*, 2022). This expression pattern was present from as early as 1 dpf and remained into adulthood. *ZAKβ* is the predominant isoform, which is consistent with humans and mice, where there is approximately 10-fold greater expression of ZAKβ than ZAKα (Gross *et al.*, 2002; Nordgaard *et al.*, 2022). These findings support the use of zebrafish to model the impact that absence of ZAKβ has on skeletal muscle. Although, whilst the greatest levels of ZAKα are seen in the liver of humans and mice (Gross *et al.*, 2002; Nordgaard *et al.*, 2022), there is low/no expression of *ZAKα* in the liver of zebrafish. Instead, the greatest expression of *ZAKα*, in tissues investigated, was

in the intestines. However, the lack of consistency of *ZAK*α expression between zebrafish and humans/mice does not weaken the use of zebrafish as a model organism when considering the role *ZAK* could play in myopathies, since *ZAK*α is not expressed in the skeletal muscle.

Absence of both isoforms resulted in a mild phenotype with no overt signs of pathology, as well as a normal life expectancy and fertility. The lack of embryonic lethality supports other mice models lacking ZAK (Jandhyala *et al.*, 2016; Nordgaard *et al.*, 2022), and contradicts findings of embryonic lethality with absence of ZAK by (Spielmann *et al.*, 2016). The mild phenotype is unsurprising as humans and mice with mutations in ZAK generally present with a mild pathology (Vasli *et al.*, 2017; Nordgaard *et al.*, 2022). The zebrafish phenotype does appear to be milder than the mouse phenotype, with one potential theory being that water provides protection from gravitational forces and stress on skeletal muscle. Any research performed in zebrafish should be validated and performed alongside research using $ZAK^{-/-}$ mice. If indeed further investigations validate additional similarities to ZAK-associated mouse/human myopathy, the zebrafish model will be further justified as a reliable model, which could open the door to prospective screening for potential therapeutics in the future.

I have detailed many advantages of using zebrafish as a model organism, several of which have been utilised as part of my research, however, there are also several limitations that should be considered. Firstly, zebrafish are considerably more evolutionarily distant from humans compared to other commonly used model organisms, such as mice, as their genomes diverged ~450 million years ago rather than ~100 million years ago (Kumar and Hedges, 1998; Woods *et al.*, 2000). Secondly, zebrafish are not mammals and, consequently, have a differing physiology and anatomy from humans. Some examples of differences include: zebrafish are ectothermic (cold-blooded) aquatic organisms (Le Goc *et al.*, 2021), with an optimal physiological temperature of 28^{o}C, versus the 37^{o}C for humans (Avdesh *et al.*, 2012); the zebrafish respiratory system utilises gills rather than lungs (Santoriello and Zon, 2012; Messerli *et al.*, 2020); and zebrafish have an ex-utero reproductive system (van Rooijen *et al.*, 2017), where there is also an environmental influence on sex determination (Uchida *et al.*, 2004; Shang *et al.*, 2006). When considering skeletal muscle, whilst the separation of slow and fast-twitch fibres in zebrafish allows for the different fibre types to be studied more

easily, this potentially limits the relevance of any findings to humans, where fast and slow-twitch fibres exist together within the same muscle (Jackson and Ingham, 2013; Keenan and Currie, 2019). Lastly, as discussed in the previous paragraph, zebrafish are protected from the stress of gravity and constitutive mechanical loading on skeletal muscle, due to the buoyant support provided by water (Turko *et al.*, 2017; Dietrich *et al.*, 2021). Contrastingly, land mammals use postural/tonic muscles to hold their body upright against the force of gravity, resulting in the constitutive strain/tension of these muscles (Shenkman, 2016; Carini *et al.*, 2017). These limitations, especially the lack of constitutive tension of skeletal muscle, could explain the milder phenotype exhibited by zebrafish lacking ZAK, compared to humans and mice (Vasli *et al.*, 2017; Ahmad *et al.*, 2022; Nordgaard *et al.*, 2022). As previously mentioned, the drawbacks of using zebrafish demonstrate the requirement for use of other model organisms, such as mice, to validate whether any potential findings could be relevant to humans.

7.3. Creation and Validation of ZAK$^{-/-}$ Zebrafish

CRISPR-Cas9 was used to generate mutations in both *ZAK* isoforms in zebrafish. Both mutations resulted in a premature stop codon and absence of the respective transcript through presumed nonsense-mediated decay (NMD), which was confirmed using qRT-PCR. The mRNA transcripts for *ZAK*α and *ZAK*β were sequenced to investigate potential molecular mechanisms for NMD-evasion, see (Anderson *et al.*, 2017). No NMD-evasion mechanisms were detected for *ZAK*β transcripts. However, the *ZAK*α transcript sequence revealed attempts to skip exon 2 (88 bases), rather than the expected 71 base pair deletion. Skipping exon 2 still resulted in a frameshift mutation and a predicted premature stop codon in exon 3. No other molecular evasion mechanisms were detected. In lieu of a commercial ZAK antibody that recognises the zebrafish ZAK isoforms, the significant reduction in transcript seen with qRT-PCR and the confirmation of a frameshift mutation, through transcript sequencing, provides evidence of the successful creation of ZAK$\alpha^{-/-}$ and ZAK$\beta^{-/-}$ zebrafish. A zebrafish-specific ZAK antibody should be developed to confirm that the significant reduction in transcript levels for both isoforms equates to complete absence of the respective ZAK isoform at the protein level, for complete validation.

The use of more sophisticated gene editing techniques, such as CRISPR, revealed that the phenotype was usually less severe or different to that seen with morpholino targeting (Kok *et al.*, 2015; El-Brolosy *et al.*, 2019). Genetic compensation describes the upregulation of a paralogous gene or family member with a similar sequence following NMD of the transcript with the premature stop codon (El-Brolosy and Stainier, 2017; El-Brolosy *et al.*, 2019). Any genetic compensation was not via the paralogous gene, however, with qRT-PCR confirming neither gene was upregulated in the absence of the other isoform in embryos or adult tissue. Strikingly, there was a significant reduction in *ZAK*α transcript levels in ZAK$\beta^{-/-}$ embryos and adult brains. This finding hints at a potential role for ZAKβ in the expression of *ZAK*α, however, this is hard to justify given the general exclusivity of isoform expression in specific tissues. In osteosarcoma cells, ZAKβ overexpression results in increased expression of ZAKα (Fu *et al.*, 2018). Whilst genetic compensation through the paralogue gene can be ruled out, upregulation of a similar protein in absence of ZAK, for compensation, cannot.

To supplement findings achieved through the CRISPR-generated *ZAK* mutant zebrafish, it would be of interest to potentially investigate the effects of absence of ZAK without NMD and, thus, genetic compensation. Morpholinos could be used, and have been widely used on zebrafish in the past to understand congenital myopathies/muscular dystrophies in greater detail (Bassett and Currie, 2003). On the other hand, the potential for non-specific effects, coupled with only the transient effects of morpholino injection and the potential for failure to completely deplete protein levels weaken the validity for use (Bill *et al.*, 2009; Bedell *et al.*, 2011). Other forms of CRISPR could be utilised, such as targeting the promoter region (El-Brolosy *et al.*, 2019), as well as CRISPR interference (CRISPRi), whereby enzyme-dead, or deactivated (d)Cas9 is guided to the gene or transcription start site (TSS) and blocks transcription from occurring (Larson *et al.*, 2013; Savage *et al.*, 2019). Both techniques would reduce the levels of expression of the transcript without activating genetic compensation through NMD. Assessing the impact of absence of ZAKβ without genetic compensation could provide a more severe phenotype and potentially greater insight into the role that ZAKβ is playing in skeletal muscle.

7.4. Further Investigation Required into the Effects of Absence of ZAKβ on the Heart

Due to COVID, there was insufficient time to research the heart of zebrafish lacking ZAKβ as much as I would have liked. The expression of *ZAKβ* in the heart from as early as 1 dpf and remaining until adulthood, coupled with the significant reduction in the heart rate at 3 dpf when ZAKβ was absent was noteworthy. There is not enough data to make a statement about the importance of ZAKβ in the heart, however, I do believe there is enough justification to warrant greater research into the role that ZAKβ may play. Furthermore, despite a lack of observable cardiac phenotype in humans lacking ZAK, ZAKα is upregulated in the hearts of myocardial infarction patients, and ZAKβ has been shown to have a protective role at preventing apoptosis and cardiac hypertrophy (Fu *et al.*, 2016; Lin *et al.*, 2022).

Real-time investigation of the heart using transgenic zebrafish (Tg (*fli1*:GFP)) (Lawson and Weinstein, 2002), which express GFP under the *fli1* promoter, would allow better visualisation of the vasculature and an investigation into atrial and ventricular fractional area change (FAC) in absence of ZAK (Huttner *et al.*, 2018). Histopathology in adults lacking ZAK can be assessed through sectioning adult hearts and staining with Haemotoxylin and Eosin (H&E), for gross morphology differences. The ultrastructure of cardiac muscle could also be assessed in zebrafish hearts lacking ZAK using TEM.

7.5. Absence of ZAKβ Does Not Affect Neutrophil Response for Skeletal Muscle Repair

There were no differences in the rate at which neutrophils were recruited to the wound site, the numbers of neutrophils recruited or the resolution and clearance of neutrophils following injury. Whilst neutrophils appear to be largely unaffected by absence of ZAKβ, the rest of the immune response remains uninvestigated. For example, macrophages arrive later and play an enormous role both in inflammation and removing debris, as well as mediating the transition from a pro-inflammatory environment to an anti-inflammatory environment (Arnold *et al.*, 2007; Mounier *et al.*, 2013). Attempts were made to cross the ZAKβ$^{-/-}$ line into a Tg (mpeg1:mCherry(CAAX)) with mCherry fluorescently labelled macrophage membranes, so that the effects of absence of ZAKβ on macrophages could be investigated (Bojarczuk *et al.*, 2016). Unfortunately, the embryos from these zebrafish were not bright enough to facilitate selection, so consequently, could not be used to supplement the analysis of neutrophil behaviour without ZAKβ. Obtaining Tg (mpeg1:mCherry(CAAX)) that produce brighter mCherry-macrophages and crossing with ZAKβ$^{-/-}$ zebrafish to homozygosity would allow the macrophage response following wounding to be studied in absence of ZAKβ.

I also touched upon the issues with standardising the wounding procedure in section 6.3.1. An emerging way of standardising the wound repair procedure and muscle regeneration in zebrafish is through transgenic zebrafish that produce a bacterial enzyme nitroreductase (ntr) under a muscle specific promoter, such as *mylpfa* or *acta1* (Pourghadamyari *et al.*, 2019). Ntr catalyses the conversion of the prodrug metronidazole (MTZ) into a toxic substrate that will specifically damage skeletal muscle (Curado *et al.*, 2007). Breeding the ZAKβ$^{-/-}$ line into this transgenic line and exposing wild type and ZAKβ$^{-/-}$ zebrafish to a set dose of MTZ, would make the wounding procedure more standardised and reproducible. This could work in tandem with the ZAKβ$^{-/-}$ Tg (mpeg1:mCherry(CAAX)), providing a more comprehensive understanding of wound repair and muscle regenerative capabilities of zebrafish lacking ZAKβ.

7.6. Absence of ZAKβ Results in Reduced Skeletal Muscle Fibre Cross Sectional Area

The upregulation of *myogenin* and *myomaker* in ZAKβ$^{-/-}$ zebrafish embryos did not seem to alter the levels of fusion, suggesting these increases may be the result of compensatory mechanisms for absence of ZAKβ. The gross morphology in terms of embryo length and myotome volume remained unaffected by ZAKβ absence. The average muscle fibre area was reduced in ZAKβ$^{-/-}$ embryos at both 2 and 5 dpf, however, suggesting potential hypotrophy or atrophy. This correlates well with humans and mice with mutated ZAK, where reduced muscle fibre area, attributed to atrophy has also been reported (Vasli *et al.*, 2017; Nordgaard *et al.*, 2022).

Interestingly p-AKT levels appeared to be reduced on western blots performed on 8 dpf embryos. This finding is in line with the observation of AKT activation following transfecting cells with ZAKβ (Fu *et al.*, 2016), and following activation of ZAK in human and mice primary CD4^{+} T cells (Wang *et al.*, 2021). The AKT/mTOR pathway is important for hypertrophy and preventing atrophy in skeletal muscle (Rommel *et al.*, 2001; Bodine *et al.*, 2001). Activation of AKT phosphorylates and inhibits tuberous sclerosis (TSC1/2) proteins, preventing TSC1/2 from inhibiting Ras homology enriched in brain (Rheb), which can then bind to mTOR and phosphorylate it, allowing mTOR to increase protein synthesis and for hypertrophy to occur (Inoki *et al.*, 2002; Garami *et al.*, 2003). Activated AKT can further increase protein production through phosphorylation and inhibition of glycogen synthase kinase (GSK)-3β, which in turn prevents the inhibition of transcription factor eIF2B (Rommel *et al.*, 2001; Bodine *et al.*, 2001). p-AKT can also inhibit forkhead box O (FOXO) preventing protein degradation and protecting against atrophy (Sandri *et al.*, 2004). Activating mTOR allows for a net increase in protein synthesis and growth of a muscle fibre independent of hyperplasia (formation of new muscle fibres) (Yoon, 2017). Decreased activation of AKT signalling results in decreased protein synthesis/increased protein degradation and lack of protection against atrophy, all of which might explain the average decrease in muscle fibre cross sectional area when ZAKβ is absent.

Since the reductions in fibre cross sectional area when ZAKβ is absent were only marginal (approximately 10% smaller on average), this could explain the relative lack of differences in general swimming capabilities between siblings and ZAKβ$^{-/-}$ zebrafish when young (6-months) and middle-aged (18-months). Whilst average muscle fibre area has been assessed in 2 and 5 dpf embryos, it has yet to be assessed in adult zebrafish lacking ZAKβ. Performing sections on adult skeletal muscle, of varying ages, would allow an understanding if this hypotrophy/atrophy continues into adulthood, and whether it worsens with time. H&E staining on sectioned muscle would also allow for an assessment for the presence of centralised nuclei on in aged ZAKβ$^{-/-}$ skeletal muscle, as is seen in humans and mice with myopathy associated with ZAK mutations (Vasli *et al.*, 2017; Nordgaard *et al.*, 2022).

7.7. ZAKβ as a candidate gene for sarcopenia.

The ageing process in vertebrates can be thought of as the decline in physiological function and is characterised by nine hallmarks, including cellular senescence and genomic instability following lifelong accumulation of damage and decreases in DNA repair mechanisms (Li *et al.*, 2021). Sarcopenia specifically relates to the age-related decline in skeletal muscle mass, function and strength; with genetic, epigenetic, physiological and lifestyle factors all contributing to the development of sarcopenia (Walston, 2012; Cruz-Jentoft and Sayer, 2019). In the United Kingdom, as of 2018, the estimated cost of sarcopenia to the healthcare system is £2.5 billion (Pinedo-Villanueva *et al.*, 2019).

The pathology that may arise with absence of ZAKβ appears to worsen with age. This is unsurprising as many neuromuscular diseases, including myopathy associated with mutated ZAK, present with a slowly progressive muscle weakness (Vasli *et al.*, 2017; Ahmad *et al.*, 2022). The swimming capabilities in absence of ZAKβ$^{-/-}$ zebrafish appeared to decline at a faster rate than wild type counterparts, where the aged ZAKβ$^{-/-}$ zebrafish swam reduced distances, at a slower rate and had more frequent stops compared to the age-matched wild type counterparts. Whilst there is a decline in swimming parameters in old wild type, compared to younger wild type zebrafish, it is not as substantial as the decline seen with absence of ZAKβ. Furthermore, skeletal muscle dissected from old

zebrafish showed signs of pathology that age-matched wild type counterparts did not. There appeared to be dissolution of sarcomere structure as well as unusually orientated myofibrils, indicating a lack of myofibrillar organisation in absence of ZAKβ. These findings hint at potential promise of ZAKβ and the respective signalling pathway as possible candidates for skeletal muscle aging and sarcopenia treatment.

Zebrafish have a substantially shorter lifespan than humans, making them useful model organisms for studying aging (Gilbert *et al.*, 2014). On the other hand, the lifespan of zebrafish is typically comparable to the length of time for a PhD project (Gilbert *et al.*, 2014). The 'old' zebrafish used were at least 35 months of age, thus, there is insufficient time to fully investigate the full phenotypic spectrum of aged ZAKβ$^{-/-}$ zebrafish.

There is growing interest in using alternative fish with lower life expectancies to better understand the effects of ageing on skeletal muscle and sarcopenia, for example, the African turquoise Killifish (*Nothobranchius furzeri*) (Kim *et al.*, 2016). Killifish belong to the Teleostei infraclass like zebrafish, however, the average captive lifespan of Killifish is between approximately 4-6 months and the time taken to reach sexual maturity is 3-4 weeks, rather than the 3-4 months for zebrafish (Valenzano *et al.*, 2015). The genome has been sequenced, with the GRZ (a highly-inbred strain) used to generate a reference genome (Valenzano *et al.*, 2015), allowing CRISPR-Cas9 to be successfully performed to target specific genes (Harel *et al.*, 2015; Oginuma *et al.*, 2022). *Tol2* transgenesis as well as CRISPR-mediated GFP knock in have been successfully performed in Killifish (Hartmann and Englert, 2012; Allard *et al.*, 2013; Oginuma *et al.*, 2022). 'old' killifish can be defined as older than three months and typically swim less and slower than younger counterparts, suggesting the skeletal muscle of these fish are susceptible to the effects of accelerated aging (Valenzano *et al.*, 2006). The use of Killifish as a model organism has the potential for a substantially more time-efficient way of exploring candidate genes involved in sarcopenia, as well as other age-related conditions.

7.8. Future Work

Further to the future work that I have discussed in the individual sections within this chapter, there are some future experiments that I believe should be performed to greater understand the role of ZAKβ in zebrafish.

Firstly, research should be aligned with the recent work by (Nordgaard *et al.*, 2022), where it was proposed that Z-disc-localised-ZAKβ recognises muscle contraction and converts the stimuli into discernible P38 signalling. ZAK$^{-/-}$ mice were seen to have a predominance of slow-twitch muscle fibres. Whilst I investigated the expression of slow and fast-twitch specific genes during development, there should also be an investigation into the slow and fast-twitch specific genes in adults as well for completion. Immunostaining sections of zebrafish would allow understanding of the proportions of slow and fast-twitch fibres, as well the relative muscle fibre areas for each fibre-type. ZAKβ localisation in skeletal muscle of zebrafish should be explored, with transgenesis or fluorescently-tagged ZAKβ mRNA injections assessed using confocal microscopy. Such analysis would validate if ZAKβ localises to the Z-disc in zebrafish, as it does with mice. Embryos from a ZAKα$^{+/-}$ ZAKβ$^{+/-}$ incross have been gifted to the Bekker-Jenssen lab so that zebrafish lacking ZAK isoforms can be used to supplement analysis performed using mice.

Investigation into downstream signalling in ZAKβ$^{-/-}$ zebrafish have largely been informed by RNA-seq data performed on humans and mice lacking ZAK. For example, *FLNC* was downregulated in humans with mutated ZAK (Vasli *et al.*, 2017), and *myomaker* was upregulated in mice with mutated ZAK (Nordgaard *et al.*, 2022). To truly understand the role that ZAKβ is playing in skeletal muscle, and potentially the heart of zebrafish, RNA-seq should be performed using ZAKβ$^{-/-}$ zebrafish. RNA should be extracted from embryos as well as adult skeletal muscle and hearts. Through this, I would obtain a non-biased list of differentially expressed genes (DEGs) that specifically occur with absence of ZAKβ in zebrafish, in different tissues/at different stages. Comparisons between zebrafish specific DEGs to those of mice/humans would allow a greater understanding of the specific role that ZAKβ is performing in the skeletal muscle of zebrafish.

In a similar vein to RNA-sequencing data providing a non-biased list of DEGs in absence of ZAKβ, phosphoproteomic analysis could be performed using liquid chromatography tandem mass spectrometry (LC-MS), as in (Wang *et al.*, 2020). This procedure would allow an assessment of alterations in phosphorylated proteins when ZAKβ is absent. Furthermore, kinase dead, wild type and constitutively active forms of ZAKβ could be injected into embryos, and changes in phosphorylation of proteins could be assessed.

Given the association of KY and ZAK at the Z-disc of skeletal muscle in mice (Baker *et al.*, 2010), I believe that repetition of analysis performed on ZAK lines, as well as those discussed in potential future plans, should also be performed on a double $KY^{-/-}$ $ZAK\beta^{-/-}$ line. The single $KY^{-/-}$ zebrafish line did not show a strong phenotype (considerably weaker than mice models), however, the absence of both KY and ZAKβ could produce a stronger phenotype (if the proteins are involved in similar processes or interact) (Jokl *et al.*, 2018b).

Performing the analyses discussed above, in old-age $ZAK\beta^{-/-}$ zebrafish and age-matched wild type zebrafish controls will provide further validation if, indeed, there is an enhanced or more prominent deterioration of skeletal muscle in aged zebrafish lacking ZAKβ, compared to wild type zebrafish.

7.9. Summary and Final Remarks

In this report, I validate the expression of *ZAKα* and *ZAKβ* in zebrafish as comparable to humans and mice. I have demonstrated the successful creation of single and double $ZAK\alpha^{-/-}$ $ZAK\beta^{-/-}$ zebrafish. Absence of ZAK resulted in a mild phenotype, normal life expectancy and fertility/survival of offspring. This was unsurprising given the mild phenotype is also typically seen with humans and mice. Investigation of ZAKβ absence in old zebrafish show decreased swimming capabilities and skeletal muscle abnormalities at an ultrastructural level, hinting at an accelerated ageing process that could make ZAKβ a novel candidate for sarcopenia research. There is still the requirement for further research to investigate the validity of using zebrafish to model human congenital myopathy associated with ZAK, as well as the potential role for ZAKβ signalling as a candidate for sarcopenia.

Appendices

Appendix A. Modified MATLAB code for extracting zebrafish movement at 120 fps

```
clear all;

filestoprocess = dir('Mut2_F_2.csv'); % stores details on all .csv files in the current folder

for f = 1 : length(filestoprocess) % loops for each .csv file in the folder

    clearvars -except filestoprocess f distTravelArray velocityArray timeMovingArray
fileNames activeTimeArray actTailbeatFreqArray lowTailbeatFreq medTailbeatFreq
highTailbeatFreq avgTBangleArray lowPeakArray medPeakArray highPeakArray

    fileID = fopen(filestoprocess(f).name); % opens current file as fileID

    disp(filestoprocess(f).name) % displays the name of the file being processed

    C = textscan(fileID,'%d %d %f %f %f %f %f %d %d %d %d %d %d %d %d %d %d %d %d
%d %d','Delimiter',','); % stores values from current file in cell array

    % stores spine angles in an array and converts to degrees
    spine(1,:)=C{3};
    spine(2,:)=C{4};
    spine(3,:)=C{5};
    spine(4,:)=C{6};
    spine(5,:)=C{7};
    spine = double(spine)*(180/pi);

    % stores X coordinates in an array and converts to cm
    nodeXCoord(1,:)=C{8};
    nodeXCoord(2,:)=C{10};
    nodeXCoord(3,:)=C{12};
    nodeXCoord(4,:)=C{14};
    nodeXCoord(5,:)=C{16};
    nodeXCoord(6,:)=C{18};
    nodeXCoord(7,:)=C{20};
    nodeXCoord = double(nodeXCoord)/1280*13.4;

    % stores Y coordinates in an array and converts to cm
    nodeYCoord(1,:)=C{9};
    nodeYCoord(2,:)=C{11};
    nodeYCoord(3,:)=C{13};
    nodeYCoord(4,:)=C{15};
    nodeYCoord(5,:)=C{17};
    nodeYCoord(6,:)=C{19};
    nodeYCoord(7,:)=C{21};
    nodeYCoord = double(nodeYCoord)/720*7.2;
    nodeYCoord = 7.2 - nodeYCoord; % corrects direction of y axis

    %% Calculates the distance travelled per second in cm using node 4

    n = 1;
       for i = 121:120:length(nodeXCoord)
          distSec(n) = sqrt(double((nodeXCoord(4,i)-nodeXCoord(4,i-
120))^2+(nodeYCoord(4,i)-nodeYCoord(4,i-120))^2));
          n = n + 1;
       end

    distTravel = sum(distSec);
    velocity = distTravel/(length(distSec));
```

```
 %% Sums together angles for each frame

for i = 1:length(spine)
   headtoTail(i) = 0;
   for j = 1:5
   if abs(spine(j,i)) > 5
      headtoTail(i) = headtoTail(i) + abs(spine(j,i));
   else
   end
   end
end

%% Plots the sum of angles over time

smoothedTail = smooth(headtoTail,5); % running average over 5 frames

figure;
axisTime = [0.0083333333333333:0.008333333333333:(length(spine)/120)];

[pos_pks,pos_locs] = findpeaks(smoothedTail,'MinPeakDistance',5,'MinPeakProminence',5);
% finds the peaks

noSpeed = 0;
lowSpeed = 0;
medSpeed = 0;
highSpeed = 0;

   for i = 1:length(distSec) % loops for each second

   j= i*120+1; % j is the counter for the final frame in a second
   k =j-120; % k is the counter for the first frame in a second

      if distSec(i) < 0.5 % counts less than 5mm in 1 second as no movement

         movement(i) = 0; % array for which seconds have movement and which don't

         noSpeed = noSpeed + 1; % counter for how many seconds the fish is stationary
         statPeaks = find(pos_locs>k & pos_locs<j); % finds the peaks in this second

         pos_pks(statPeaks)=NaN; % replaces the peaks with NaN in the main peak array
         pos_locs(statPeaks)=NaN;

   elseif distSec(i) < 2 % counts less than 2cm in 1 second as low speed
         movement(i) = 1;
         lowSpeed = lowSpeed + 1; %low speed for this second

         lowPeaks = find(pos_locs>k & pos_locs<j);
         lowPeakAng = pos_pks(lowPeaks);

         if lowSpeed == 1
            lowCount = vertcat(lowPeaks);
            lowPeakAngles = vertcat(lowPeakAng);
         else
            lowCount = vertcat(lowCount,lowPeaks);
            lowPeakAngles = vertcat(lowPeakAngles,lowPeakAng);
         end

   elseif distSec(i) <= 4
         movement(i) = 1;
         medSpeed = medSpeed + 1; % medium speed

         medPeaks = find(pos_locs>k & pos_locs<j);
         medPeakAng = pos_pks(medPeaks);
```

```
        if medSpeed == 1
            medCount = vertcat(medPeaks);
            medPeakAngles = vertcat(medPeakAng);
        else
           medCount = vertcat(medCount,medPeaks);
           medPeakAngles = vertcat(medPeakAngles, medPeakAng);
        end

    else
        movement(i) = 1;
        highSpeed = highSpeed + 1; % high speed

        highPeaks = find(pos_locs>k & pos_locs<j);
        highPeakAng = pos_pks(highPeaks);

         if highSpeed == 1
           highCount = vertcat(highPeaks);
           highPeakAngles = vertcat(highPeakAng);
        else
           highCount = vertcat(highCount,highPeaks);
           highPeakAngles = vertcat(highPeakAngles, highPeakAng);
        end
    end
    end

    if lowSpeed == 0
       avgLowPeak = NaN;
    else
       avgLowPeak = mean(lowPeakAngles);
    end

    if medSpeed == 0
       avgMedPeak = NaN;
    else
       avgMedPeak = mean(medPeakAngles);
    end

    if highSpeed == 0
       avgHighPeak = NaN;
    else
       avgHighPeak = mean(highPeakAngles);
    end

    if lowSpeed>0
    lowTBfreq = length(lowCount)/lowSpeed;
    else
       lowTBfreq = NaN;
    end

    if medSpeed > 0
    medTBfreq = length(medCount)/medSpeed;
    else
    medTBfreq = NaN;
    end

    if highSpeed>0
    highTBfreq = length(highCount)/highSpeed;
    else
    highTBfreq = NaN;
    end

    % creates new array for peaks removing NaN from stationary seconds
```

```
        n = 1;
        for i=1:length(pos_locs)
            if isnan(pos_locs(i))
            else
                nanPos_locs(n) = pos_locs(i);
                nanPos_pks(n)= pos_pks(i);
                n = n+1;
            end
        end

        avgTailBendAngle = mean(nanPos_pks); %calculates avg TB angle only when the fish is
moving

    plot(axisTime, smoothedTail,'-k');
    hold on
    plot(axisTime(nanPos_locs), nanPos_pks, 'or');
    hold off
    xlabel('Time (s)');
    ylabel('Tail bend amplitude');

    tailbeatFreq = length(nanPos_locs)/((length(spine)/120));

    timeMoving = ((sum(movement(:) == 1))/length(movement))*100;
    actTailbeatFreq = tailbeatFreq*(100/timeMoving);
    velocity = velocity * (timeMoving/100); % calculates velocity for when fish is actively moving

    activeTime = zeros(1,1000);

    m = 1;
    n = 1;
    for i = 1:length(movement)
        if movement(i) == 0
            if i == length(movement)
            elseif movement(i+1) == 1
                m = m + 1; % if there is movement in the next 1s period we update the restTime
counter
            else
            end
        elseif movement(i) == 1
            activeTime(n) = activeTime(n)+1; % with movement 1s is added to the active time
duration
            if i == length(movement)
            elseif movement(i+1) == 0
                n = n + 1;  % if there is no movement in the next 1s period we update the activeTime
counter
            else
            end
        end
    end

    if activeTime(n) == 0
        n = n-1;
    else
    end

    activeTimeAvg = sum(activeTime)/n;

    %% Storing calculated values in arrays

    fileNames(f,1) = string(filestoprocess(f).name);
    distTravelArray(f,1) = distTravel;
    velocityArray(f,1) =  velocity;
    timeMovingArray(f,1) = timeMoving;
```

```
    activeTimeArray(f,1) = activeTimeAvg;
    actTailbeatFreqArray(f,1) = actTailbeatFreq;
    lowTailbeatFreq(f,1) = lowTBfreq;
    medTailbeatFreq(f,1) = medTBfreq;
    highTailbeatFreq(f,1) = highTBfreq;
    avgTBangleArray(f,1) = avgTailBendAngle;
    lowPeakArray(f,1) = avgLowPeak;
    medPeakArray(f,1) = avgMedPeak;
    highPeakArray(f,1) = avgHighPeak;

end

LowTBfreq = lowTailbeatFreq(~isnan(lowTailbeatFreq));
MedTBfreq = medTailbeatFreq(~isnan(medTailbeatFreq));
HighTBfreq = highTailbeatFreq(~isnan(highTailbeatFreq));
highSpeedPeak = highPeakArray(~isnan(highPeakArray));
medSpeedPeak = medPeakArray(~isnan(medPeakArray));
lowSpeedPeak = lowPeakArray(~isnan(lowPeakArray));

%% Outputting data in a .csv file with averages

file = 'FishAnalyserData.csv'; % creates .csv file to save all FishAnalyser data
outputHeaders = ["File", "Distance Travelled(cm)", "Mean active velocity(cm s^-1)", "Mean
active tail beat frequency" "Time spent moving(%)", "Mean active time duration(s)", "Low speed
tail beat frequency", "Medium speed tail beat frequency", "High speed tail beat frequency",
"Mean tail bend amplitude", "Mean low speed tail bend amplitude", "Mean medium speed tail
bend amplitude", "Mean high speed tail bend amplitude"];
outputData = cell(length(filestoprocess),13);
outputData = [fileNames, distTravelArray, velocityArray, actTailbeatFreqArray,
timeMovingArray, activeTimeArray, lowTailbeatFreq, medTailbeatFreq, highTailbeatFreq,
avgTBangleArray, lowPeakArray, medPeakArray, highPeakArray];
averages = ["Mean", mean(distTravelArray), mean(velocityArray), mean(actTailbeatFreqArray),
mean(timeMovingArray), mean(activeTimeArray), mean(LowTBfreq), mean(MedTBfreq),
mean(HighTBfreq), mean(avgTBangleArray), mean(lowSpeedPeak), mean(medSpeedPeak),
mean(highSpeedPeak)];
standardDeviations = ["Standard Deviation", std(distTravelArray), std(velocityArray),
std(actTailbeatFreqArray), std(timeMovingArray), std(activeTimeArray), std(LowTBfreq),
std(MedTBfreq), std(HighTBfreq), std(avgTBangleArray), std(lowSpeedPeak),
std(medSpeedPeak), std(highSpeedPeak)];

fID = fopen('FishAnalyserData.csv','wt');
fprintf(fID,'%s, %s, %s, %s, %s, %s, %s, %s, %s, %s, %s, %s, %s\n',outputHeaders(:));
for i = 1:(length(filestoprocess))
    fprintf(fID,'%s, %0.2f, %0.2f, %0.2f, %0.2f, %0.2f, %0.2f, %0.2f, %0.2f, %0.2f, %0.2f,
%0.2f\n',outputData(i,1:13));
end
fprintf(fID,'\n%s, %0.2f, %0.2f, %0.2f, %0.2f, %0.2f, %0.2f, %0.2f, %0.2f, %0.2f, %0.2f,
%0.2f\n', averages(:));
fprintf(fID,'\n%s, %0.2f, %0.2f, %0.2f, %0.2f, %0.2f, %0.2f, %0.2f, %0.2f, %0.2f, %0.2f,
%0.2f', standardDeviations(:));
fclose(fID);

fclose(fileID);
```

Abbreviations

ACTA1	skeletal alpha actin 1 gene
ANOVA	analysis of variance
ANS	autonomic nervous system
AP	alkaline phosphatase
APS	ammonium persulphate
ATP	adenosine triphosphate
Bcl-xL	B cell lymphoma-extra-large
bHLH	basic helix loop helix
BIN1	amphiphysin 2 gene
BLAST	basic local alignment search tool
BMI	body mass index
BNP	B-type natriuretic peptide or brain natriuretic peptide
CASA	chaperone-assisted selected autophagy
CCD	central core disease
cDNA	Complementary DNA
CFTD	congenital fibre type disproportion
CK	creatine kinase
CRISPR	clustered regularly interspaced short palindromic repeats
crRNA	crispr RNA
CT	cycle threshold
CTP	cytidine triphosphate
DAMPs	damage associated molecular patterns
DEGs	differentially expressed genes
DGC	dystrophin-glycoprotein complex
DHPR	dihydropyridine receptor
DIG	Digoxigenin
DMD	dystrophin gene
DMD	Duchenne muscular dystrophy
DNA	Deoxyribonucleic acid
DNM2	dynamin 2 gene
dNTP	deoxyribonucleotide triphosphate
dpf	days post fertilisation
dpi	days post injury
dsDNA	double stranded DNA
DTT	dithiothreitol
DuCD	dusty core disease
e-c	excitation-contraction
E3	normal embryo media
ECM	extra-cellular matrix
EDL	extensor digitorum longus muscle
EDTA	ethylenediaminetetraacetic acid
EM	electron microscopy
ENU	N-ethyl-N-nitrosourea
F0	founder embryos
F1	F0 offspring
FAC	fractional area change
FLNA/B/C	filamin A/B/C
FPS	Frames per second
GCN2	general control nonderepressible 2
GFP	green fluorescent protein

GTP	guanosine triphosphate
H&E	haematoxylin and eosin
HAA	height anterior to the anal fin
HMGB1	high mobility group box 1 protein
hpf	hours post fertilisation
hpi	hours post injury
IGFN1	immunoglobulin-like fibronectin type III domain containing 1
INDELs	insertions/deletions
ISH	in situ hybridisation
JNK	c-Jun N-terminal kinase
K	Fulton's conditioning factor
kDa	kilodalton
KY	kyphoscoliosis peptidase
LB	lysogeny broth
LMA	low melting temperature agarose
M1	pro-inflammatory macrophages
M2	anti-inflammatory macrophages
MABT	maleic acid buffer with tween-20
MAPK	mitogen-activated protein kinase
MFF	medial fast fibres
MFM	myofibrillar myopathies
MmD	multi-minicore disease
MPC	muscle progenitor cells
MRF	myogenic regulatory factors
Mrf4	myogenic regulatory factor 4
MRI	magnetic resonance imaging
mRNA	messenger RNA
MTM1	myotubularin gene
MTZ	metronidazole
Myf5	myogenic factor 5
MyHC	slow/β-cardiac myosin heavy chain
myl1	Myosin light chain 1 gene
myl2	myosin light chain 2 gene
MyoD	myogenic differentiation factor
nAChRs	nicotinic acetylcholine receptors
NADH-TR	nicotinamide adenine dinucleotide tetrazolium reductase
NLRP1	NOD-like receptor family pyrin domain-containing 1
NMD	nonsense mediated decay
ntr	nitroreductase enzyme
oxLDL	oxidised low-density lipoproteins
PAGE	polyacrylamide gel electrophoresis
PAM	protospacer adjacent motif
PAX3/7	paired box 3/7
PBS	phosphate buffered saline
PCR	polymerase chain reaction
PFA	paraformaldehyde
PI3K	phosphatidyl isolsitol-3 kinase
qRT-PCR	quantitative reverse transcriptase polymerase chain reaction
RNA	Ribonucleic acid
ROS	reactive oxygen species
RQC	ribosome-associated quality control
rRNA	ribosomal RNA

RSR	ribosomal stress response
RT	reverse transcriptase
RTK	receptor tyrosine kinase
RUNX1	runt-related transcription factor 1 gene
RYR1	ryanodine receptor 1 gene
S1	subfragment 1
SAM	sterile alpha motif
SDS	Sodium dodecyl sulphate
SEM	Standard error of the mean
SEPN1	selenoprotein N gene
SFBD	stress fibre binding domain
sgRNA	single guide RNA
shh	sonic hedgehog
sMyHC1	Slow myosin heavy chain 1 gene
SOD2	super oxide dismutase-2
SOX	SRY-related HMG box
SR	sarcoplasmic reticulum
SSC	saline sodium citrate buffer
SSF	superficial slow fibres
t-tubules	transverse tubules
TA	tibialis anterior
TALEN	transcriptional activator-like effector nucleases
TAE	Tris-Acetate-EDTA Buffer
TBE	Tris-Borate-EDTA Buffer
TEM	transmission electron microscopy
TEMED	tetramethylethylenediamine
TGF	transforming growth factor
TNF-α	tumour necrosis factor alpha
TPM3	tropomyosin 3 gene
tracrRNA	transactivating RNA
TSS	transcriptional start site
TTN	titin gene
UTP	uridine triphosphate
XMTM	X-linked myotubular myopathy
YAP/TAZ	yes-associated protein 1/transcriptional co-activator with a PDZ-binding domain
ZFN	zinc finger nucleases

References

Abath Neto, O., Moreno, C. a. M., Malfatti, E., Donkervoort, S., Böhm, J., Guimarães, J. B., Foley, A. R., Mohassel, P., Dastgir, J., Bharucha-Goebel, D. X., Monges, S., Lubieniecki, F., Collins, J., Medne, L., Santi, M., Yum, S., Banwell, B., Salort-Campana, E., Rendu, J., Fauré, J., Yis, U., Eymard, B., Cheraud, C., Schneider, R., Thompson, J., Lornage, X., Mesrob, L., Lechner, D., Boland, A., Deleuze, J. F., Reed, U. C., Oliveira, A. S. B., Biancalana, V., Romero, N. B., Bönnemann, C. G., Laporte, J. & Zanoteli, E. 2017. Common and variable clinical, histological, and imaging findings of recessive RYR1-related centronuclear myopathy patients. *Neuromuscul Disord,* 27**,** 975-985.

Adamson, K. I., Sheridan, E. & Grierson, A. J. 2018. Use of zebrafish models to investigate rare human disease. *Journal of Medical Genetics,* 55**,** 641.

Agarkova, I., Ehler, E., Lange, S., Schoenauer, R. & Perriard, J.-C. 2003. M-band: a safeguard for sarcomere stability? *Journal of Muscle Research & Cell Motility,* 24**,** 191-203.

Agrawal, P. B., Pierson, C. R., Joshi, M., Liu, X., Ravenscroft, G., Moghadaszadeh, B., Talabere, T., Viola, M., Swanson, L. C., Haliloğlu, G., Talim, B., Yau, K. S., Allcock, R. J., Laing, N. G., Perrella, M. A. & Beggs, A. H. 2014. SPEG interacts with myotubularin, and its deficiency causes centronuclear myopathy with dilated cardiomyopathy. *Am J Hum Genet,* 95**,** 218-26.

Ahmad, I., Khan, A., Noor Ul Ayan, H., Budde, B., Altmüller, J., Korejo, A. A., Nürnberg, G., Thiele, H., Tariq, M., Nürnberg, P. & Erdmann, J. 2022. A novel MAP3K20 mutation causing centronuclear myopathy-6 with fiber-type disproportion in a Pakistani family. *Journal of Human Genetics*.

Aigner, B., Renner, S., Kessler, B., Klymiuk, N., Kurome, M., Wünsch, A. & Wolf, E. 2010. Transgenic pigs as models for translational biomedical research. *Journal of Molecular Medicine,* 88**,** 653-664.

Al-Qusairi, L. & Laporte, J. 2011. T-tubule biogenesis and triad formation in skeletal muscle and implication in human diseases. *Skeletal Muscle,* 1**,** 26.

Allard, J. B., Kamei, H. & Duan, C. 2013. Inducible transgenic expression in the short-lived fish Nothobranchius furzeri. *Journal of Fish Biology,* 82**,** 1733-1738.

Amburgey, K., Tsuchiya, E., De Chastonay, S., Glueck, M., Alverez, R., Nguyen, C.-T., Rutkowski, A., Hornyak, J., Beggs, A. H. & Dowling, J. J. 2017. A natural history study of X-linked myotubular myopathy. *Neurology,* 89**,** 1355-1364.

Amores, A., Force, A., Yan, Y. L., Joly, L., Amemiya, C., Fritz, A., Ho, R. K., Langeland, J., Prince, V., Wang, Y. L., Westerfield, M., Ekker, M. & Postlethwait, J. H. 1998. Zebrafish hox clusters and vertebrate genome evolution. *Science,* 282**,** 1711-4.

Andersen, P. 1975. Capillary Density in Skeletal Muscle of Man. *Acta Physiologica Scandinavica,* 95**,** 203-205.

Anderson, J. L., Mulligan, T. S., Shen, M.-C., Wang, H., Scahill, C. M., Tan, F. J., Du, S. J., Busch-Nentwich, E. M. & Farber, S. A. 2017. mRNA processing in mutant zebrafish lines generated by chemical and CRISPR-mediated mutagenesis produces unexpected transcripts that escape nonsense-mediated decay. *PLOS Genetics,* 13**,** e1007105.

Andresen, B., De Marees, M., Schiffer, T., Bloch, W. & Suhr, F. 2022. Skeletal muscle fiber type-specific expressions of mechanosensors integrin-linked kinase, talin, and vinculin and their modulation by loading and environmental conditions in humans. *The FASEB Journal,* 36**,** e22458.

Anthony Lai, F., Erickson, H. P., Rousseau, E., Liu, Q.-Y. & Meissner, G. 1988. Purification and reconstitution of the calcium release channel from skeletal muscle. *Nature,* 331**,** 315-319.

Arecco, N., Clarke, C. J., Jones, F. K., Simpson, D. M., Mason, D., Beynon, R. J. & Pisconti, A. 2016. Elastase levels and activity are increased in dystrophic muscle and impair myoblast cell survival, proliferation and differentiation. *Scientific Reports,* 6**,** 24708.

Arif, B., Rasheed, A., Kumar, K. R., Fatima, A., Abbas, G., Wohler, E., Sobriera, N., Lohmann, K. & Naz, S. 2020. A novel homozygous KY variant causing a complex neurological disorder. *Eur J Med Genet,* 63**,** 104031.

Arndt, V., Dick, N., Tawo, R., Dreiseidler, M., Wenzel, D., Hesse, M., Fürst, D. O., Saftig, P., Saint, R., Fleischmann, B. K., Hoch, M. & Höhfeld, J. 2010. Chaperone-assisted selective autophagy is essential for muscle maintenance. *Curr Biol,* 20**,** 143-8.

Arnold , L., Henry , A., Poron , F. O., Baba-Amer , Y., Van Rooijen , N., Plonquet , A., Gherardi , R. K. & Chazaud , B. N. D. 2007. Inflammatory monocytes recruited after skeletal muscle injury switch into antiinflammatory macrophages to support myogenesis. *Journal of Experimental Medicine,* 204**,** 1057-1069.

Asfour, H. A., Allouh, M. Z. & Said, R. S. 2018. Myogenic regulatory factors: The orchestrators of myogenesis after 30 years of discovery. *Exp Biol Med (Maywood),* 243**,** 118-128.

Attali, R., Aharoni, S., Treves, S., Rokach, O., Becker Cohen, M., Fellig, Y., Straussberg, R., Dor, T., Daana, M., Mitrani-Rosenbaum, S. & Nevo, Y. 2013. Variable myopathic presentation in a single family with novel skeletal RYR1 mutation. *PLoS One,* 8**,** e69296.

Attarian, S. & Azulay, J. P. 2001. [Infectious myopathies]. *Rev Prat,* 51**,** 284-8.

Avdesh, A., Chen, M., Martin-Iverson, M. T., Mondal, A., Ong, D., Rainey-Smith, S., Taddei, K., Lardelli, M., Groth, D. M., Verdile, G. & Martins, R. N. 2012. Regular care and maintenance of a zebrafish (Danio rerio) laboratory: an introduction. *J Vis Exp***,** e4196.

Bakay, M., Wang, Z., Melcon, G., Schiltz, L., Xuan, J., Zhao, P., Sartorelli, V., Seo, J., Pegoraro, E., Angelini, C., Shneiderman, B., Escolar, D., Chen, Y.-W., Winokur, S. T., Pachman, L. M., Fan, C., Mandler, R., Nevo, Y., Gordon, E., Zhu, Y., Dong, Y., Wang, Y. & Hoffman, E. P. 2006. Nuclear envelope dystrophies show a transcriptional fingerprint suggesting disruption of Rb–MyoD pathways in muscle regeneration. *Brain,* 129**,** 996-1013.

Baker, J., Riley, G., Romero, M. R., Haynes, A. R., Hilton, H., Simon, M., Hancock, J., Tateossian, H., Ripoll, V. M. & Blanco, G. 2010. Identification of a Z-band associated protein complex involving KY, FLNC and IGFN1. *Experimental Cell Research,* 316**,** 1856-1870.

Baraban, S. C., Dinday, M. T. & Hortopan, G. A. 2013. Drug screening in Scn1a zebrafish mutant identifies clemizole as a potential Dravet syndrome treatment. *Nat Commun,* 4**,** 2410.

Barohn, R. J., Brumback, R. A. & Mendell, J. R. 1994. Hyaline body myopathy. *Neuromuscul Disord,* 4**,** 257-62.

Barth, P. G. & Dubowitz, V. 1998. X-linked myotubular myopathy--a long-term follow-up study. *Eur J Paediatr Neurol,* 2**,** 49-56.

Barthélémy, I., Hitte, C. & Tiret, L. 2019. The Dog Model in the Spotlight: Legacy of a Trustful Cooperation. *J Neuromuscul Dis,* 6**,** 421-451.

Bassett, D. I., Bryson-Richardson, R. J., Daggett, D. F., Gautier, P., Keenan, D. G. & Currie, P. D. 2003. Dystrophin is required for the formation of stable muscle attachments in the zebrafish embryo. *Development,* 130**,** 5851-5860.

Bassett, D. I. & Currie, P. D. 2003. The zebrafish as a model for muscular dystrophy and congenital myopathy. *Human Molecular Genetics,* 12**,** R265-R270.

Baxendale, S., Davison, C., Muxworthy, C., Wolff, C., Ingham, P. W. & Roy, S. 2004. The B-cell maturation factor Blimp-1 specifies vertebrate slow-twitch muscle fiber identity in response to Hedgehog signaling. *Nature Genetics,* 36**,** 88-93.

Beatham, J., Romero, R., Townsend, S. K. M., Hacker, T., Van Der Ven, P. F. M. & Blanco, G. 2004. Filamin C interacts with the muscular dystrophy KY protein and is abnormally distributed in mouse KY deficient muscle fibres. *Human Molecular Genetics,* 13**,** 2863-2874.

Bedell, V. M., Westcot, S. E. & Ekker, S. C. 2011. Lessons from morpholino-based screening in zebrafish. *Briefings in functional genomics,* 10**,** 181-188.

Beecroft, S. J., Van De Locht, M., De Winter, J. M., Ottenheijm, C. A., Sewry, C. A., Mohammed, S., Ryan, M. M., Woodcock, I. R., Sanders, L., Gooding, R., Davis, M. R., Oates, E. C., Laing, N. G., Ravenscroft, G., Mclean, C. A. & Jungbluth, H. 2019. Recessive MYH7-related myopathy in two families. *Neuromuscular Disorders,* 29**,** 456-467.

Bennett, C. M., Kanki, J. P., Rhodes, J., Liu, T. X., Paw, B. H., Kieran, M. W., Langenau, D. M., Delahaye-Brown, A., Zon, L. I., Fleming, M. D. & Look, A. T. 2001. Myelopoiesis in the zebrafish, Danio rerio. *Blood,* 98**,** 643-651.

Bennett, P., Rees, M. & Gautel, M. 2020. The Axial Alignment of Titin on the Muscle Thick Filament Supports Its Role as a Molecular Ruler. *Journal of Molecular Biology,* 432**,** 4815-4829.

Berg, E. M., Björnfors, E. R., Pallucchi, I., Picton, L. D. & El Manira, A. 2018. Principles Governing Locomotion in Vertebrates: Lessons From Zebrafish. *Frontiers in Neural Circuits,* 12.

Bergen, B. J., Carry, M. P., Wilson, W. B., Barden, M. T. & Ringel, S. P. 1980. Centronuclear myopathy: extraocular- and limb-muscle findings in an adult. *Muscle Nerve,* 3**,** 165-71.

Berger, J., Berger, S., Hall, T. E., Hall, T. E., Lieschke, G. J. & Currie, P. D. 2010. Dystrophin-deficient zebrafish feature aspects of the Duchenne muscular dystrophy pathology. *Neuromuscular Disorders,* 20**,** 826-832.

Berger, J., Berger, S., Jacoby, A. S., Wilton, S. D. & Currie, P. D. 2011. Evaluation of exon-skipping strategies for Duchenne muscular dystrophy utilizing dystrophin-deficient zebrafish. *J Cell Mol Med,* 15**,** 2643-51.

Berger, J., Berger, S., Li, M. & Currie, P. D. 2017. Myo18b is essential for sarcomere assembly in fast skeletal muscle. *Human Molecular Genetics,* 26**,** 1146-1156.

Berger, J., Tarakci, H., Berger, S., Li, M., Hall, T. E., Arner, A. & Currie, P. D. 2014. Loss of Tropomodulin4 in the zebrafish mutant träge causes cytoplasmic rod formation and muscle weakness reminiscent of nemaline myopathy. *Dis Model Mech,* 7**,** 1407-15.

Bi, P., Ramirez-Martinez, A., Li, H., Cannavino, J., Mcanally, J. R., Shelton, J. M., Sánchez-Ortiz, E., Bassel-Duby, R. & Olson, E. N. 2017. Control of muscle formation by the fusogenic micropeptide myomixer. *Science,* 356**,** 323-327.

Bill, B. R., Petzold, A. M., Clark, K. J., Schimmenti, L. A. & Ekker, S. C. 2009. A primer for morpholino use in zebrafish. *Zebrafish,* 6**,** 69-77.

Blagden, C. S., Currie, P. D., Ingham, P. W. & Hughes, S. M. 1997. Notochord induction of zebrafish slow muscle mediated by Sonic hedgehog. *Genes Dev,* 11**,** 2163-75.

Blanco, G., Coulton, G. R., Biggin, A., Grainge, C., Moss, J., Barrett, M., Berquin, A., Maréchal, G., Skynner, M., Van Mier, P., Nikitopoulou, A., Kraus, M., Ponting, C. P., Mason, R. M. & Brown, S. D. 2001. The kyphoscoliosis (ky) mouse is deficient in hypertrophic responses and is caused by a mutation in a novel muscle-specific protein. *Hum Mol Genet,* 10**,** 9-16.

Bloem, L. J., Pickard, T. R., Acton, S., Donoghue, M., Beavis, R. C., Knierman, M. D. & Wang, X. 2001. Tissue distribution and functional expression of a

cDNA encoding a novel mixed lineage kinase. *J Mol Cell Cardiol,* 33**,** 1739-50.

Bodine, S. C., Stitt, T. N., Gonzalez, M., Kline, W. O., Stover, G. L., Bauerlein, R., Zlotchenko, E., Scrimgeour, A., Lawrence, J. C., Glass, D. J. & Yancopoulos, G. D. 2001. Akt/mTOR pathway is a crucial regulator of skeletal muscle hypertrophy and can prevent muscle atrophy in vivo. *Nature Cell Biology,* 3**,** 1014-1019.

Bohlega, S., Abu-Amero, S. N., Wakil, S. M., Carroll, P., Al-Amr, R., Lach, B., Al-Sayed, Y., Cupler, E. J. & Meyer, B. F. 2004. Mutation of the slow myosin heavy chain rod domain underlies hyaline body myopathy. *Neurology,* 62**,** 1518.

Böhm, J., Biancalana, V., Dechene, E. T., Bitoun, M., Pierson, C. R., Schaefer, E., Karasoy, H., Dempsey, M. A., Klein, F., Dondaine, N., Kretz, C., Haumesser, N., Poirson, C., Toussaint, A., Greenleaf, R. S., Barger, M. A., Mahoney, L. J., Kang, P. B., Zanoteli, E., Vissing, J., Witting, N., Echaniz-Laguna, A., Wallgren-Pettersson, C., Dowling, J., Merlini, L., Oldfors, A., Bomme Ousager, L., Melki, J., Krause, A., Jern, C., Oliveira, A. S., Petit, F., Jacquette, A., Chaussenot, A., Mowat, D., Leheup, B., Cristofano, M., Poza Aldea, J. J., Michel, F., Furby, A., Llona, J. E., Van Coster, R., Bertini, E., Urtizberea, J. A., Drouin-Garraud, V., Béroud, C., Prudhon, B., Bedford, M., Mathews, K., Erby, L. A., Smith, S. A., Roggenbuck, J., Crowe, C. A., Brennan Spitale, A., Johal, S. C., Amato, A. A., Demmer, L. A., Jonas, J., Darras, B. T., Bird, T. D., Laurino, M., Welt, S. I., Trotter, C., Guicheney, P., Das, S., Mandel, J. L., Beggs, A. H. & Laporte, J. 2012. Mutation spectrum in the large GTPase dynamin 2, and genotype-phenotype correlation in autosomal dominant centronuclear myopathy. *Hum Mutat,* 33**,** 949-59.

Bojarczuk, A., Miller, K. A., Hotham, R., Lewis, A., Ogryzko, N. V., Kamuyango, A. A., Frost, H., Gibson, R. H., Stillman, E., May, R. C., Renshaw, S. A. & Johnston, S. A. 2016. Cryptococcus neoformans Intracellular Proliferation and Capsule Size Determines Early Macrophage Control of Infection. *Sci Rep,* 6**,** 21489.

Bours, M. J., Swennen, E. L., Di Virgilio, F., Cronstein, B. N. & Dagnelie, P. C. 2006. Adenosine 5'-triphosphate and adenosine as endogenous signaling molecules in immunity and inflammation. *Pharmacol Ther,* 112**,** 358-404.

Boyer, J. G., Prasad, V., Song, T., Lee, D., Fu, X., Grimes, K. M., Sargent, M. A., Sadayappan, S. & Molkentin, J. D. 2019. ERK1/2 signaling induces skeletal muscle slow fiber-type switching and reduces muscular dystrophy disease severity. *JCI Insight,* 5.

Brandman, O. & Hegde, R. S. 2016. Ribosome-associated protein quality control. *Nature Structural & Molecular Biology,* 23**,** 7-15.

Braun, T., Bober, E., Rudnicki, M. A., Jaenisch, R. & Arnold, H. H. 1994. MyoD expression marks the onset of skeletal myogenesis in Myf-5 mutant mice. *Development,* 120**,** 3083-3092.

Braun, T., Buschhausen-Denker, G., Bober, E., Tannich, E. & Arnold, H. H. 1989. A novel human muscle factor related to but distinct from MyoD1 induces myogenic conversion in 10T1/2 fibroblasts. *Embo j,* 8**,** 701-9.

Brigitte, M., Schilte, C., Plonquet, A., Baba-Amer, Y., Henri, A., Charlier, C., Tajbakhsh, S., Albert, M., Gherardi, R. K. & Chrétien, F. 2010. Muscle resident macrophages control the immune cell reaction in a mouse model of notexin-induced myoinjury. *Arthritis Rheum,* 62**,** 268-79.

Brooke, M. H. & Engel, W. K. 1969. The histographic analysis of human muscle biopsies with regard to fiber types. *Neurology,* 19**,** 221.

Broussard, S. R., Mccusker, R. H., Novakofski, J. E., Strle, K., Shen, W. H., Johnson, R. W., Dantzer, R. & Kelley, K. W. 2004. IL-1beta impairs insulin-like growth factor i-induced differentiation and downstream activation signals of the insulin-like growth factor i receptor in myoblasts. *J Immunol,* 172**,** 7713-20.

Bruni, G., Rennekamp, A. J., Velenich, A., Mccarroll, M., Gendelev, L., Fertsch, E., Taylor, J., Lakhani, P., Lensen, D., Evron, T., Lorello, P. J., Huang, X.-P., Kolczewski, S., Carey, G., Caldarone, B. J., Prinssen, E., Roth, B. L., Keiser, M. J., Peterson, R. T. & Kokel, D. 2016. Zebrafish behavioral profiling identifies multitarget antipsychotic-like compounds. *Nature Chemical Biology,* 12**,** 559-566.

Bryan, B. A., Li, D., Wu, X. & Liu, M. 2005. The Rho family of small GTPases: crucial regulators of skeletal myogenesis. *Cell Mol Life Sci,* 62**,** 1547-55.

Budick, S. A. & O'malley, D. M. 2000. Locomotor repertoire of the larval zebrafish: swimming, turning and prey capture. *J Exp Biol,* 203**,** 2565-79.

Bugiardini, E., Morrow, J. M., Shah, S., Wood, C. L., Lynch, D. S., Pitmann, A. M., Reilly, M. M., Houlden, H., Matthews, E., Parton, M., Hanna, M. G., Straub, V. & Yousry, T. A. 2018. The Diagnostic Value of MRI Pattern Recognition in Distal Myopathies. *Frontiers in Neurology,* 9.

Bulfield, G., Siller, W. G., Wight, P. A. & Moore, K. J. 1984. X chromosome-linked muscular dystrophy (mdx) in the mouse. *Proceedings of the National Academy of Sciences,* 81**,** 1189-1192.

Buono, S., Ross, J. A., Tasfaout, H., Levy, Y., Kretz, C., Tayefeh, L., Matson, J., Guo, S., Kessler, P., Monia, B. P., Bitoun, M., Ochala, J., Laporte, J. & Cowling, B. S. 2018. Reducing dynamin 2 (DNM2) rescues DNM2-related dominant centronuclear myopathy. *Proc Natl Acad Sci U S A,* 115**,** 11066-11071.

Burguière, A. C., Nord, H. & Von Hofsten, J. 2011. Alkali-like myosin light chain-1 (myl1) is an early marker for differentiating fast muscle cells in zebrafish. *Developmental Dynamics,* 240**,** 1856-1863.

Burzyn, D., Kuswanto, W., Kolodin, D., Shadrach, Jennifer l., Cerletti, M., Jang, Y., Sefik, E., Tan, Tze g., Wagers, Amy j., Benoist, C. & Mathis, D. 2013. A Special Population of Regulatory T Cells Potentiates Muscle Repair. *Cell,* 155**,** 1282-1295.

Cade, L., Reyon, D., Hwang, W. Y., Tsai, S. Q., Patel, S., Khayter, C., Joung, J. K., Sander, J. D., Peterson, R. T. & Yeh, J. R. 2012. Highly efficient generation of heritable zebrafish gene mutations using homo- and heterodimeric TALENs. *Nucleic Acids Res,* 40**,** 8001-10.

Cancilla, P. A., Kalyanaraman, K., Verity, M. A., Munsat, T. & Pearson, C. M. 1971. Familial myopathy with probable lysis of myofibrils in type I fibers. *Neurology,* 21**,** 579.

Cardamone, M., Darras, B. T. & Ryan, M. M. 2008. Inherited myopathies and muscular dystrophies. *Semin Neurol,* 28**,** 250-9.

Cargnello, M. & Roux, P. P. 2011. Activation and function of the MAPKs and their substrates, the MAPK-activated protein kinases. *Microbiology and molecular biology reviews : MMBR,* 75**,** 50-83.

Carini, F., Mazzola, M., Fici, C., Palmeri, S., Messina, M., Damiani, P. & Tomasello, G. 2017. Posture and posturology, anatomical and physiological profiles: overview and current state of art. *Acta Biomed,* 88**,** 11-16.

Cathomen, T. & Keith Joung, J. 2008. Zinc-finger Nucleases: The Next Generation Emerges. *Molecular Therapy,* 16**,** 1200-1207.

Catteruccia, M., Fattori, F., Codemo, V., Ruggiero, L., Maggi, L., Tasca, G., Fiorillo, C., Pane, M., Berardinelli, A., Verardo, M., Bragato, C., Mora, M., Morandi, L., Bruno, C., Santoro, L., Pegoraro, E., Mercuri, E., Bertini, E. & D'amico, A. 2013. Centronuclear myopathy related to dynamin 2 mutations: clinical, morphological, muscle imaging and genetic features of an Italian cohort. *Neuromuscul Disord,* 23**,** 229-38.

Ceyhan-Birsoy, O., Agrawal, P. B., Hidalgo, C., Schmitz-Abe, K., Dechene, E. T., Swanson, L. C., Soemedi, R., Vasli, N., Iannaccone, S. T., Shieh, P. B., Shur, N., Dennison, J. M., Lawlor, M. W., Laporte, J., Markianos, K., Fairbrother, W. G., Granzier, H. & Beggs, A. H. 2013. Recessive truncating titin gene, TTN, mutations presenting as centronuclear myopathy. *Neurology,* 81**,** 1205-14.

Chagovetz, A. A., Klatt Shaw, D., Ritchie, E., Ritchie, E., Hoshijima, K. & Grunwald, D. J. 2019. Interactions among ryanodine receptor isotypes contribute to muscle fiber type development and function. *Dis Model Mech,* 13.

Chandrasekhar, A. 2004. Turning heads: development of vertebrate branchiomotor neurons. *Dev Dyn,* 229**,** 143-61.

Charge, S. B. & Rudnicki, M. A. 2004. Cellular and Molecular Regulation of Muscle Regeneration. *Physiological Reviews,* 84**,** 209-238.

Chen, J., Wu, J., Han, C., Li, Y., Guo, Y. & Tong, X. 2019. A mutation in the filamin c gene causes myofibrillar myopathy with lower motor neuron syndrome: a case report. *BMC Neurology,* 19**,** 198.

Cheng, Y.-C., Kuo, W.-W., Wu, H.-C., Lai, T.-Y., Wu, C.-H., Hwang, J.-M., Wang, W.-H., Tsai, F.-J., Yang, J.-J., Huang, C.-Y. & Chu, C.-H. 2009. ZAK induces MMP-2 activity via JNK/p38 signals and reduces MMP-9 activity by increasing TIMP-1/2 expression in H9c2 cardiomyoblast cells. *Molecular and Cellular Biochemistry,* 325**,** 69-77.

Childers, M. K., Joubert, R., Poulard, K., Moal, C., Grange, R. W., Doering, J. A., Lawlor, M. W., Rider, B. E., Jamet, T., Danièle, N., Martin, S., Rivière, C., Soker, T., Hammer, C., Van Wittenberghe, L., Lockard, M., Guan, X., Goddard, M., Mitchell, E., Barber, J., Williams, J. K., Mack, D. L., Furth, M. E., Vignaud, A., Masurier, C., Mavilio, F., Moullier, P., Beggs, A. H. & Buj-Bello, A. 2014. Gene Therapy Prolongs Survival and Restores Function in Murine and Canine Models of Myotubular Myopathy. *Science Translational Medicine,* 6**,** 220ra10-220ra10.

Christ, B. & Ordahl, C. P. 1995. Early stages of chick somite development. *Anat Embryol (Berl),* 191**,** 381-96.

Christe, M., Jin, N., Wang, X., Gould, K. E., Iversen, P. W., Yu, X., Lorenz, J. N., Kadambi, V., Zuckerman, S. H. & Bloem, L. J. 2004. Transgenic mice with cardiac-specific over-expression of MLK7 have increased mortality when exposed to chronic b-adrenergic stimulation. *Journal of Molecular and Cellular Cardiology,* 37**,** 705-715.

Claeys, K. G. 2020. Congenital myopathies: an update. *Developmental Medicine & Child Neurology,* 62**,** 297-302.

Clarke, N. F. 2011. Congenital Fiber-Type Disproportion. *Seminars in Pediatric Neurology,* 18**,** 264-271.

Clarke, N. F., Kidson, W., Quijano-Roy, S., Estournet, B., Ferreiro, A., Guicheney, P., Manson, J. I., Kornberg, A. J., Shield, L. K. & North, K. N. 2006. SEPN1: associated with congenital fiber-type disproportion and insulin resistance. *Ann Neurol,* 59**,** 546-52.

Clarke, N. F., Kolski, H., Dye, D. E., Lim, E., Smith, R. L. L., Patel, R., Fahey, M. C., Bellance, R., Romero, N. B., Johnson, E. S., Labarre-Vila, A., Monnier, N., Laing, N. G. & North, K. N. 2008. Mutations in TPM3 are a common cause of congenital fiber type disproportion. *Annals of Neurology,* 63**,** 329-337.

Clarke, N. F. & North, K. N. 2003. Congenital fiber type disproportion--30 years on. *J Neuropathol Exp Neurol,* 62**,** 977-89.

Clarke, N. F., Smith, R. L. L., Bahlo, M. & North, K. N. 2005. A novel X-linked form of congenital fiber-type disproportion. *Annals of Neurology,* 58**,** 767-772.

Clarke, N. F., Waddell, L. B., Cooper, S. T., Perry, M., Smith, R. L. L., Kornberg, A. J., Muntoni, F., Lillis, S., Straub, V., Bushby, K., Guglieri, M., King, M. D., Farrell, M. A., Marty, I., Lunardi, J., Monnier, N. & North, K. N. 2010. Recessive mutations in RYR1 are a common cause of congenital fiber type disproportion. *Human Mutation,* 31**,** E1544-E1550.

Codina, M., Li, J., Gutiérrez, J., Kao, J. P. Y. & Du, S. J. 2010. Loss of Smyhc1 or Hsp90α1 Function Results in Different Effects on Myofibril Organization in Skeletal Muscles of Zebrafish Embryos. *PLOS ONE,* 5**,** e8416.

Cohen, B. H. 2019. Mitochondrial and Metabolic Myopathies. *CONTINUUM: Lifelong Learning in Neurology,* 25**,** 1732-1766.

Colegrave, M. & Peckham, M. 2014. Structural Implications of β-Cardiac Myosin Heavy Chain Mutations in Human Disease. *The Anatomical Record,* 297**,** 1670-1680.

Collins, C. A. & Morgan, J. E. 2003. Duchenne's muscular dystrophy: animal models used to investigate pathogenesis and develop therapeutic strategies. *Int J Exp Pathol,* 84**,** 165-72.

Collins, C. A., Olsen, I., Zammit, P. S., Heslop, L., Petrie, A., Partridge, T. A. & Morgan, J. E. 2005. Stem Cell Function, Self-Renewal, and Behavioral Heterogeneity of Cells from the Adult Muscle Satellite Cell Niche. *Cell,* 122**,** 289-301.

Cornelio, F. & Dones, I. 1984. Muscle fiber degeneration and necrosis in muscular dystrophy and other muscle diseases: Cytochemical and immunocytochemical data. *Annals of Neurology,* 16**,** 694-701.

Cruz-Jentoft, A. J. & Sayer, A. A. 2019. Sarcopenia. *The Lancet,* 393**,** 2636-2646.

Cullup, T., Lamont, P. J., Cirak, S., Damian, M. S., Wallefeld, W., Gooding, R., Tan, S. V., Sheehan, J., Muntoni, F., Abbs, S., Sewry, C. A., Dubowitz, V., Laing, N. G. & Jungbluth, H. 2012. Mutations in MYH7 cause Multi-minicore Disease (MmD) with variable cardiac involvement. *Neuromuscular Disorders,* 22**,** 1096-1104.

Curado, S., Anderson, R. M., Jungblut, B., Mumm, J., Schroeter, E. & Stainier, D. Y. R. 2007. Conditional targeted cell ablation in zebrafish: A new tool for regeneration studies. *Developmental Dynamics,* 236**,** 1025-1035.

Dalakas, M. C. 2009. Toxic and drug-induced myopathies. *Journal of Neurology, Neurosurgery & Psychiatry,* 80**,** 832.

Dalli, J., Montero-Melendez, T., Norling, L. V., Yin, X., Hinds, C., Haskard, D., Mayr, M. & Perretti, M. 2013. Heterogeneity in neutrophil microparticles reveals distinct proteome and functional properties. *Mol Cell Proteomics,* 12**,** 2205-19.

Davis, M. R., Haan, E., Jungbluth, H., Sewry, C., North, K., Muntoni, F., Kuntzer, T., Lamont, P., Bankier, A., Tomlinson, P., Sánchez, A., Walsh, P., Nagarajan, L., Oley, C., Colley, A., Gedeon, A., Quinlivan, R., Dixon, J., James, D., Müller, C. R. & Laing, N. G. 2003. Principal mutation hotspot for central core disease and related myopathies in the C-terminal transmembrane region of the RYR1 gene. *Neuromuscular Disorders,* 13**,** 151-157.

Davis, R. L., Weintraub, H. & Lassar, A. B. 1987. Expression of a single transfected cDNA converts fibroblasts to myoblasts. *Cell,* 51**,** 987-1000.

Daya, A., Donaka, R. & Karasik, D. 2020. Zebrafish models of sarcopenia. *Dis Model Mech,* 13.

Dayal, A., Schrötter, K., Pan, Y., Föhr, K., Melzer, W. & Grabner, M. 2017. The Ca2+ influx through the mammalian skeletal muscle dihydropyridine receptor is irrelevant for muscle performance. *Nature Communications,* 8**,** 475.

De Angelis, M. S., Palmucci, L., Leone, M. & Doriguzzi, C. 1991. Centronuclear myopathy: clinical, morphological and genetic characters a review of 288 cases. *Journal of the Neurological Sciences,* 103**,** 2-9.

Dehkharghani, F., Sarnat, H. B., Brewster, M. A. & Roth, S. I. 1981. Congenital muscle fiber-type disproportion in Krabbe's leukodystrophy. *Arch Neurol,* 38**,** 585-7.

Di Gioia, S. A., Connors, S., Matsunami, N., Cannavino, J., Rose, M. F., Gilette, N. M., Artoni, P., De Macena Sobreira, N. L., Chan, W.-M., Webb, B. D., Robson, C. D., Cheng, L., Van Ryzin, C., Ramirez-Martinez, A., Mohassel, P., Leppert, M., Scholand, M. B., Grunseich, C., Ferreira, C. R., Hartman, T., Hayes, I. M., Morgan, T., Markie, D. M., Fagiolini, M., Swift, A., Chines, P. S., Speck-Martins, C. E., Collins, F. S., Jabs, E. W., Bönnemann, C. G., Olson, E. N., Andrews, C. V., Barry, B. J., Hunter, D. G., Mackinnon, S. E., Shaaban, S., Erazo, M., Frempong, T., Hao, K., Naidich, T. P., Rucker, J. C., Zhang, Z., Biesecker, B. B., Bonnycastle, L. L., Brewer, C. C., Brooks, B. P., Butman, J. A., Chien, W. W., Farrell, K., Fitzgibbon, E. J., Gropman, A. L., Hutchinson, E. B., Jain, M. S., King, K. A., Lehky, T. J., Lee, J., Liberton, D. K., Narisu, N., Paul, S. M., Sadeghi, N., Snow, J., Solomon, B., Summers, A., Toro, C., Thurm, A., Zalewski, C. K., Carey, J. C., Robertson, S. P., Manoli, I., Engle, E. C. & Moebius Syndrome Research, C. 2017. A defect in myoblast fusion underlies Carey-Fineman-Ziter syndrome. *Nature Communications,* 8**,** 16077.

Dietrich, K., Fiedler, I. A., Kurzyukova, A., López-Delgado, A. C., Mcgowan, L. M., Geurtzen, K., Hammond, C. L., Busse, B. & Knopf, F. 2021. Skeletal Biology and Disease Modeling in Zebrafish. *Journal of Bone and Mineral Research,* 36**,** 436-458.

Dilan, C.-B., Begun, E., Ahmet Tugrul, O., Hulusi, K. & Michelle, A. 2018. Zebrafish Aging Models and Possible Interventions. *In:* YUSUF, B. (ed.) *Recent Advances in Zebrafish Researches.* Rijeka: IntechOpen.

Dimario, J. X., Uzman, A. & Strohman, R. C. 1991. Fiber regeneration is not persistent in dystrophic (MDX) mouse skeletal muscle. *Dev Biol,* 148**,** 314-21.

Ding, Y., Dvornikov, A. V., Ma, X., Zhang, H., Wang, Y., Lowerison, M., Packard, R. R., Wang, L., Chen, J., Zhang, Y., Hsiai, T., Lin, X. & Xu, X. 2019. Haploinsufficiency of mechanistic target of rapamycin ameliorates bag3 cardiomyopathy in adult zebrafish. *Disease Models & Mechanisms,* 12.

Diofano, F., Weinmann, K., Schneider, I., Thiessen, K. D., Rottbauer, W. & Just, S. 2020. Genetic compensation prevents myopathy and heart failure in an in vivo model of Bag3 deficiency. *PLoS Genet,* 16**,** e1009088.

Dowling, J. J., Arbogast, S., Hur, J., Nelson, D. D., Mcevoy, A., Waugh, T., Marty, I., Lunardi, J., Brooks, S. V., Kuwada, J. Y. & Ferreiro, A. 2012. Oxidative stress and successful antioxidant treatment in models of RYR1-related myopathy. *Brain,* 135**,** 1115-27.

Duan, D., Goemans, N., Takeda, S. I., Mercuri, E. & Aartsma-Rus, A. 2021. Duchenne muscular dystrophy. *Nature Reviews Disease Primers,* 7**,** 13.

Dubowitz, V. & Pearse, A. G. 1960. Oxidative enzymes and phosphorylase in central-core disease of muscle. *Lancet,* 2**,** 23-4.

Dumont, N., Bouchard, P. & Frenette, J. 2008. Neutrophil-induced skeletal muscle damage: a calculated and controlled response following hindlimb unloading and reloading. *Am J Physiol Regul Integr Comp Physiol,* 295**,** R1831-8.

Ebrahimzadeh-Vesal, R., Teymoori, A., Dourandish, A. M. & Azimi-Nezhad, M. 2018. Identification of a novel nonsense mutation in kyphoscoliosis peptidase gene in an Iranian patient with myofibrillar myopathy. *Genes & Diseases,* 5**,** 331-334.

Ehsani, E., Khamirani, H. J., Abbasi, Z., Gohari, M., Zoghi, S., Mohammadi, S., Dianatpour, M., Tabei, S. M. B., Mohamadjani, O. & Dastgheib, S. A. 2022. Genotypic and phenotypic spectrum of Myofibrillar Myopathy 7 as a result of Kyphoscoliosis Peptidase deficiency: The first description of a missense mutation in KY and literature review. *European Journal of Medical Genetics,* 65**,** 104552.

Eisen, J. S. & Smith, J. C. 2008. Controlling morpholino experiments: don't stop making antisense. *Development,* 135**,** 1735-43.

Ekker, S. C. 2008. Zinc finger-based knockout punches for zebrafish genes. *Zebrafish,* 5**,** 121-3.

El-Brolosy, M. A., Kontarakis, Z., Rossi, A., Kuenne, C., Günther, S., Fukuda, N., Kikhi, K., Boezio, G. L. M., Takacs, C. M., Lai, S.-L., Fukuda, R., Gerri, C., Giraldez, A. J. & Stainier, D. Y. R. 2019. Genetic compensation triggered by mutant mRNA degradation. *Nature,* 568**,** 193-197.

El-Brolosy, M. A. & Stainier, D. Y. R. 2017. Genetic compensation: A phenomenon in search of mechanisms. *PLoS genetics,* 13**,** e1006780-e1006780.

Engel, A. G., Gomez, M. R. & Groover, R. V. 1971. Multicore disease. A recently recognized congenital myopathy associated with multifocal degeneration of muscle fibers. *Mayo Clin Proc,* 46**,** 666-81.

Englund, D. A., Murach, K. A., Dungan, C. M., Figueiredo, V. C., Vechetti, I. J., Jr., Dupont-Versteegden, E. E., Mccarthy, J. J. & Peterson, C. A. 2020. Depletion of resident muscle stem cells negatively impacts running

volume, physical function, and muscle fiber hypertrophy in response to lifelong physical activity. *Am J Physiol Cell Physiol,* 318**,** C1178-c1188.

Ennion, S., Sant'ana Pereira, J., Sargeant, A. J., Young, A. & Goldspink, G. 1995. Characterization of human skeletal muscle fibres according to the myosin heavy chains they express. *J Muscle Res Cell Motil,* 16**,** 35-43.

Eser, G. & Topaloğlu, H. 2022. Current Outline of Exon Skipping Trials in Duchenne Muscular Dystrophy. *Genes (Basel),* 13.

Espinosa, K. G., Geissah, S., Groom, L., Volpatti, J., Scott, I. C., Dirksen, R. T., Zhao, M. & Dowling, J. J. 2022. Characterization of a novel zebrafish model of SPEG-related centronuclear myopathy. *Dis Model Mech,* 15.

Fahed, A. C., Roberts, A. E., Mital, S. & Lakdawala, N. K. 2014. Heart failure in congenital heart disease: a confluence of acquired and congenital. *Heart Fail Clin,* 10**,** 219-27.

Feingold, B., Mahle, W. T., Auerbach, S., Clemens, P., Domenighetti, A. A., Jefferies, J. L., Judge, D. P., Lal, A. K., Markham, L. W., Parks, W. J., Tsuda, T., Wang, P. J. & Yoo, S.-J. 2017. Management of Cardiac Involvement Associated With Neuromuscular Diseases: A Scientific Statement From the American Heart Association. *Circulation,* 136**,** e200-e231.

Ferreiro, A., Estournet, B., Chateau, D., Romero, N. B., Laroche, C., Odent, S., Toutain, A., Cabello, A., Fontan, D., Dos Santos, H. G., Haenggeli, C. A., Bertini, E., Urtizberea, J. A., Guicheney, P. & Fardeau, M. 2000. Multi-minicore disease--searching for boundaries: phenotype analysis of 38 cases. *Ann Neurol,* 48**,** 745-57.

Ferreiro, A., Monnier, N., Romero, N. B., Leroy, J.-P., Bönnemann, C., Haenggeli, C.-A., Straub, V., Voss, W. D., Nivoche, Y., Jungbluth, H., Lemainque, A., Voit, T., Lunardi, J., Fardeau, M. & Guicheney, P. 2002a. A recessive form of central core disease, transiently presenting as multi-minicore disease, is associated with a homozygous mutation in the ryanodine receptor type 1 gene. *Annals of Neurology,* 51**,** 750-759.

Ferreiro, A., Quijano-Roy, S., Pichereau, C., Moghadaszadeh, B., Goemans, N., Bönnemann, C., Jungbluth, H., Straub, V., Villanova, M., Leroy, J.-P., Romero, N. B., Martin, J.-J., Muntoni, F., Voit, T., Estournet, B., Richard, P., Fardeau, M. & Guicheney, P. 2002b. Mutations of the Selenoprotein N Gene, Which Is Implicated in Rigid Spine Muscular Dystrophy, Cause the Classical Phenotype of Multiminicore Disease: Reassessing the Nosology of Early-Onset Myopathies. *The American Journal of Human Genetics,* 71**,** 739-749.

Fielding, R. A., Manfredi, T. J., Ding, W., Fiatarone, M. A., Evans, W. J. & Cannon, J. G. 1993. Acute phase response in exercise. III. Neutrophil and IL-1 beta accumulation in skeletal muscle. *Am J Physiol,* 265**,** R166-72.

Finsterer, J. & Stöllberger, C. 2016. Heart Disease in Disorders of Muscle, Neuromuscular Transmission, and the Nerves. *Korean Circ J,* 46**,** 117-34.

Fiorillo, C., Astrea, G., Savarese, M., Cassandrini, D., Brisca, G., Trucco, F., Pedemonte, M., Trovato, R., Ruggiero, L., Vercelli, L., D'amico, A., Tasca, G., Pane, M., Fanin, M., Bello, L., Broda, P., Musumeci, O., Rodolico, C., Messina, S., Vita, G. L., Sframeli, M., Gibertini, S., Morandi, L., Mora, M., Maggi, L., Petrucci, A., Massa, R., Grandis, M., Toscano, A., Pegoraro, E., Mercuri, E., Bertini, E., Mongini, T., Santoro, L., Nigro, V., Minetti, C., Santorelli, F. M., Bruno, C. & On Behalf of the Italian Network on Congenital, M. 2016. MYH7-related myopathies: clinical, histopathological and imaging findings in a cohort of Italian patients. *Orphanet Journal of Rare Diseases,* 11**,** 91.

Fischer, M., Rikeit, P., Knaus, P. & Coirault, C. 2016. YAP-Mediated Mechanotransduction in Skeletal Muscle. *Front Physiol,* 7**,** 41.

Flück, M. & Hoppeler, H. 2003. Molecular basis of skeletal muscle plasticity--from gene to form and function. *Rev Physiol Biochem Pharmacol,* 146**,** 159-216.

Force, A., Lynch, M., Pickett, F. B., Amores, A., Yan, Y. L. & Postlethwait, J. 1999. Preservation of duplicate genes by complementary, degenerative mutations. *Genetics,* 151**,** 1531-1545.

Foster, W. H., Tidball, J. G. & Wang, Y. 2012. p38γ activity is required for maintenance of slow skeletal muscle size. *Muscle & nerve,* 45**,** 266-273.

Frank, D., Kuhn, C., Katus, H. A. & Frey, N. 2006. The sarcomeric Z-disc: a nodal point in signalling and disease. *Journal of Molecular Medicine,* 84**,** 446-468.

Froese, R. 2006. Cube law, condition factor and weight–length relationships: history, meta-analysis and recommendations. *Journal of Applied Ichthyology,* 22**,** 241-253.

Fu, C.-Y., Chen, M.-C., Tseng, Y.-S., Chen, M.-C., Zhou, Z., Yang, J.-J., Lin, Y.-M., Viswanadha, V. P., Wang, G. & Huang, C.-Y. 2019. Fisetin activates Hippo pathway and JNK/ERK/AP-1 signaling to inhibit proliferation and induce apoptosis of human osteosarcoma cells via ZAK overexpression. *Environmental Toxicology,* 34**,** 902-911.

Fu, C.-Y., Kuo, W.-W., Ho, T.-J., Wen, S.-Y., Lin, L.-C., Tseng, Y.-S., Hung, H.-C., Viswanadha, V. P., Yang, J.-J. & Huang, C.-Y. 2016. ZAKβ antagonizes and ameliorates the cardiac hypertrophic and apoptotic effects induced by ZAKα. *Cell Biochemistry and Function,* 34**,** 606-612.

Fu, C. Y., Tseng, Y. S., Chen, M. C., Hsu, H. H., Yang, J. J., Tu, C. C., Lin, Y. M., Viswanadha, V. P., Ding, K., Kuo, W. W. & Huang, C. Y. 2018. Overexpression of ZAKβ in human osteosarcoma cells enhances ZAKα expression, resulting in a synergistic apoptotic effect. *Cell Biochem Funct,* 36**,** 176-182.

Fu, X., Xiao, J., Wei, Y., Li, S., Liu, Y., Yin, J., Sun, K., Sun, H., Wang, H., Zhang, Z., Zhang, B. T., Sheng, C., Wang, H. & Hu, P. 2015. Combination of inflammation-related cytokines promotes long-term muscle stem cell expansion. *Cell Res,* 25**,** 655-73.

Fuller, S. J., Osborne, S. A., Leonard, S. J., Hardyman, M. A., Vaniotis, G., Allen, B. G., Sugden, P. H. & Clerk, A. 2015. Cardiac protein kinases: the cardiomyocyte kinome and differential kinase expression in human failing hearts. *Cardiovascular Research,* 108**,** 87-98.

Fulton, T. W. 1904. The rate of growth of fishes. *Twenty-second Annual Report,* 0**,** 141-241.

Fürst, D. O., Osborn, M., Nave, R. & Weber, K. 1988. The organization of titin filaments in the half-sarcomere revealed by monoclonal antibodies in immunoelectron microscopy: a map of ten nonrepetitive epitopes starting at the Z line extends close to the M line. *J Cell Biol,* 106**,** 1563-72.

Gabriel, J. P., Mahmood, R., Walter, A. M., Kyriakatos, A., Hauptmann, G., Calabrese, R. L. & Manira, A. E. 2008. Locomotor Pattern in the Adult Zebrafish Spinal Cord In Vitro. *Journal of Neurophysiology,* 99**,** 37-48.

Gagnon, J. A., Valen, E., Thyme, S. B., Huang, P., Akhmetova, L., Pauli, A., Montague, T. G., Zimmerman, S., Richter, C. & Schier, A. F. 2014. Efficient mutagenesis by Cas9 protein-mediated oligonucleotide insertion and large-scale assessment of single-guide RNAs. *PloS one,* 9**,** e98186-e98186.

Ganassi, M., Badodi, S., Ortuste Quiroga, H. P., Zammit, P. S., Hinits, Y. & Hughes, S. M. 2018. Myogenin promotes myocyte fusion to balance fibre number and size. *Nature Communications,* 9**,** 4232.

Ganassi, M., Badodi, S., Wanders, K., Zammit, P. S. & Hughes, S. M. 2020. Myogenin is an essential regulator of adult myofibre growth and muscle stem cell homeostasis. *eLife,* 9**,** e60445.

Ganassi, M., Muntoni, F. & Zammit, P. S. 2022. Defining and identifying satellite cell-opathies within muscular dystrophies and myopathies. *Exp Cell Res,* 411**,** 112906.

Garami, A., Zwartkruis, F. J. T., Nobukuni, T., Joaquin, M., Roccio, M., Stocker, H., Kozma, S. C., Hafen, E., Bos, J. L. & Thomas, G. 2003. Insulin Activation of Rheb, a Mediator of mTOR/S6K/4E-BP Signaling, Is Inhibited by TSC1 and 2. *Molecular Cell,* 11**,** 1457-1466.

Garibaldi, M., Fattori, F., Bortolotti, C. A., Brochier, G., Labasse, C., Verardo, M., Servian-Morilla, E., Gibellini, L., Pinti, M., Di Rocco, G., Raffa, S., Pennisi, E. M., Bertini, E. S., Paradas, C., Romero, N. B. & Antonini, G. 2018. Core-rod myopathy due to a novel mutation in BTB/POZ domain of KBTBD13 manifesting as late onset LGMD. *Acta Neuropathologica Communications,* 6**,** 94.

Garibaldi, M., Rendu, J., Brocard, J., Lacene, E., Fauré, J., Brochier, G., Beuvin, M., Labasse, C., Madelaine, A., Malfatti, E., Bevilacqua, J. A., Lubieniecki, F., Monges, S., Taratuto, A. L., Laporte, J., Marty, I., Antonini, G. & Romero, N. B. 2019. 'Dusty core disease' (DuCD): expanding morphological spectrum of RYR1 recessive myopathies. *Acta Neuropathol Commun,* 7**,** 3.

Ge, L., Fu, X., Zhang, W., Wang, D., Wang, Z., Yuan, Y., Nonaka, I. & Xiong, H. 2019. Recessive mutations in proximal I-band of TTN gene cause severe congenital multi-minicore disease without cardiac involvement. *Neuromuscul Disord,* 29**,** 350-357.

Geach, T. J., Hirst, E. M. & Zimmerman, L. B. 2015. Contractile activity is required for Z-disc sarcomere maturation in vivo. *Genesis,* 53**,** 299-307.

Gilbert, M. J. H., Zerulla, T. C. & Tierney, K. B. 2014. Zebrafish (Danio rerio) as a model for the study of aging and exercise: Physical ability and trainability decrease with age. *Experimental Gerontology,* 50**,** 106-113.

Gineste, C. & Laporte, J. 2023. Therapeutic approaches in different congenital myopathies. *Current Opinion in Pharmacology,* 68**,** 102328.

Girardi, F., Taleb, A., Ebrahimi, M., Datye, A., Gamage, D. G., Peccate, C., Giordani, L., Millay, D. P., Gilbert, P. M., Cadot, B. & Le Grand, F. 2021. TGFβ signaling curbs cell fusion and muscle regeneration. *Nature Communications,* 12**,** 750.

Godoy, R., Noble, S., Yoon, K., Anisman, H. & Ekker, M. 2015. Chemogenetic ablation of dopaminergic neurons leads to transient locomotor impairments in zebrafish larvae. *Journal of Neurochemistry,* 135**,** 249-260.

Gorlin, J. B., Yamin, R., Egan, S., Stewart, M., Stossel, T. P., Kwiatkowski, D. J. & Hartwig, J. H. 1990. Human endothelial actin-binding protein (ABP-280, nonmuscle filamin): a molecular leaf spring. *J Cell Biol,* 111**,** 1089-105.

Gotoh, I., Adachi, M. & Nishida, E. 2001. Identification and Characterization of a Novel MAP Kinase Kinase Kinase, MLTK. *Journal of Biological Chemistry,* 276**,** 4276-4286.

Granzow, B. & Kristan, W. B. 1986. Inhibitory connections between motor neurons modify a centrally generated motor pattern in the leech nervous system. *Brain Research,* 369**,** 321-325.

Greenfield, J. G., Cornman, T. & Shy, G. M. 1958. The prognostic value of the muscle biopsy in the floppy infant. *Brain,* 81**,** 461-84.

Gross, E. A., Callow, M. G., Waldbaum, L., Thomas, S. & Ruggieri, R. 2002. MRK, a mixed lineage kinase-related molecule that plays a role in gamma-radiation-induced cell cycle arrest. *J Biol Chem,* 277**,** 13873-82.

Grove, B. K., Kurer, V., Lehner, C., Doetschman, T. C., Perriard, J. C. & Eppenberger, H. M. 1984. A new 185,000-dalton skeletal muscle protein detected by monoclonal antibodies. *J Cell Biol,* 98**,** 518-24.

Groves, J. A., Hammond, C. L. & Hughes, S. M. 2005. Fgf8 drives myogenic progression of a novel lateral fast muscle fibre population in zebrafish. *Development,* 132**,** 4211-22.

Gupta, R. M. & Musunuru, K. 2014. Expanding the genetic editing tool kit: ZFNs, TALENs, and CRISPR-Cas9. *The Journal of Clinical Investigation,* 124**,** 4154-4161.

Gupta, V., Kawahara, G., Gundry, S. R., Chen, A. T., Lencer, W. I., Zhou, Y., Zon, L. I., Kunkel, L. M. & Beggs, A. H. 2011. The zebrafish dag1 mutant: a novel genetic model for dystroglycanopathies. *Hum Mol Genet,* 20**,** 1712-25.

Gupta, V. A., Kawahara, G., Myers, J. A., Chen, A. T., Hall, T. E., Manzini, M. C., Currie, P. D., Zhou, Y., Zon, L. I., Kunkel, L. M. & Beggs, A. H. 2012. A Splice Site Mutation in Laminin-α2 Results in a Severe Muscular Dystrophy and Growth Abnormalities in Zebrafish. *PLOS ONE,* 7**,** e43794.

Gurevich, D. B., Nguyen, P. D., Siegel, A. L., Ehrlich, O. V., Sonntag, C., Phan, J. M., Berger, S., Ratnayake, D., Hersey, L., Berger, J., Verkade, H., Hall, T. E. & Currie, P. D. 2016. Asymmetric division of clonal muscle stem cells coordinates muscle regeneration in vivo. *Science,* 353**,** aad9969.

Gurung, R., Ono, Y., Baxendale, S., Lee, S. L., Moore, S., Calvert, M. & Ingham, P. W. 2017. A Zebrafish Model for a Human Myopathy Associated with Mutation of the Unconventional Myosin MYO18B. *Genetics,* 205**,** 725-735.

Guyon, J. R., Goswami, J., Jun, S. J., Thorne, M., Howell, M., Pusack, T., Kawahara, G., Steffen, L. S., Galdzicki, M. & Kunkel, L. M. 2009. Genetic isolation and characterization of a splicing mutant of zebrafish dystrophin. *Hum Mol Genet,* 18**,** 202-11.

Hackman, P., Marchand, S., Sarparanta, J., Vihola, A., Pénisson-Besnier, I., Eymard, B., Pardal-Fernández, J. M., Hammouda, E.-H., Richard, I., Illa, I. & Udd, B. 2008. Truncating mutations in C-terminal titin may cause more severe tibial muscular dystrophy (TMD). *Neuromuscular Disorders,* 18**,** 922-928.

Hagiwara, N., Ma, B. & Ly, A. 2005. Slow and fast fiber isoform gene expression is systematically altered in skeletal muscle of the Sox6 mutant, p100H. *Dev Dyn,* 234**,** 301-11.

Hagiwara, N., Yeh, M. & Liu, A. 2007. Sox6 is required for normal fiber type differentiation of fetal skeletal muscle in mice. *Dev Dyn,* 236**,** 2062-76.

Hall, T. E., Bryson-Richardson, R. J., Berger, S., Jacoby, A. S., Cole, N. J., Hollway, G. E., Berger, J. & Currie, P. D. 2007a. The zebrafish candyfloss mutant implicates extracellular matrix adhesion failure in laminin alpha2-deficient congenital muscular dystrophy. *Proc Natl Acad Sci U S A,* 104**,** 7092-7.

Hall, T. E., Bryson-Richardson, R. J., Berger, S., Jacoby, A. S., Cole, N. J., Hollway, G. E., Berger, J. & Currie, P. D. 2007b. The zebrafish candyfloss mutant implicates extracellular matrix adhesion failure in laminin-deficient congenital muscular dystrophy. *Proceedings of the National Academy of Sciences,* 104**,** 7092-7097.

Hamade, A., Deries, M., Begemann, G., Bally-Cuif, L., Genêt, C., Sabatier, F., Bonnieu, A. & Cousin, X. 2006. Retinoic acid activates myogenesis in vivo through Fgf8 signalling. *Developmental Biology,* 289**,** 127-140.

Han, J., Wang, X., Jiang, Y., Ulevitch, R. J. & Lin, S. 1997. Identification and characterization of a predominant isoform of human MKK3. *FEBS Lett,* 403**,** 19-22.

Harel, I., Benayoun, B. A., Machado, B., Singh, P. P., Hu, C. K., Pech, M. F., Valenzano, D. R., Zhang, E., Sharp, S. C., Artandi, S. E. & Brunet, A. 2015. A platform for rapid exploration of aging and diseases in a naturally short-lived vertebrate. *Cell,* 160**,** 1013-1026.

Hartmann, N. & Englert, C. 2012. A microinjection protocol for the generation of transgenic killifish (Species: Nothobranchius furzeri). *Developmental Dynamics,* 241**,** 1133-1141.

Hasty, P., Bradley, A., Morris, J. H., Edmondson, D. G., Venuti, J. M., Olson, E. N. & Klein, W. H. 1993. Muscle deficiency and neonatal death in mice with a targeted mutation in the myogenin gene. *Nature,* 364**,** 501-506.

Haycock, J. W., Macneil, S., Jones, P., Harris, J. B. & Mantle, D. 1996. Oxidative damage to muscle protein in Duchenne muscular dystrophy. *Neuroreport,* 8**,** 357-61.

Henriques-Pons, A., Yu, Q., Rayavarapu, S., Cohen, T. V., Ampong, B., Cha, H. J., Jahnke, V., Van Der Meulen, J., Wang, D., Jiang, W., Kandimalla, E. R., Agrawal, S., Spurney, C. F. & Nagaraju, K. 2014. Role of Toll-like receptors in the pathogenesis of dystrophin-deficient skeletal and heart muscle. *Hum Mol Genet,* 23**,** 2604-17.

Hernández-Hernández, J. M., García-González, E. G., Brun, C. E. & Rudnicki, M. A. 2017. The myogenic regulatory factors, determinants of muscle development, cell identity and regeneration. *Seminars in Cell & Developmental Biology,* 72**,** 10-18.

Hinman, M. N., Richardson, J. I., Sockol, R. A., Aronson, E. D., Stednitz, S. J., Murray, K. N., Berglund, J. A. & Guillemin, K. 2021. Zebrafish mbnl mutants model physical and molecular phenotypes of myotonic dystrophy. *Disease Models & Mechanisms,* 14.

Hinterberger, T. J., Sassoon, D. A., Rhodes, S. J. & Konieczny, S. F. 1991. Expression of the muscle regulatory factor MRF4 during somite and skeletal myofiber development. *Developmental Biology,* 147**,** 144-156.

Hirata, H., Watanabe, T., Hatakeyama, J., Sprague, S. M., Saint-Amant, L., Nagashima, A., Cui, W. W., Zhou, W. & Kuwada, J. Y. 2007a. Zebrafish relatively relaxed mutants have a ryanodine receptor defect, show slow swimming and provide a model of multi-minicore disease. *Development,* 134**,** 2771-2781.

Hirata, H., Watanabe, T., Hatakeyama, J., Sprague, S. M., Saint-Amant, L., Nagashima, A., Cui, W. W., Zhou, W. & Kuwada, J. Y. 2007b. Zebrafish relatively relaxed mutants have a ryanodine receptor defect, show slow swimming and provide a model of multi-minicore disease. *Development,* 134**,** 2771-81.

Hirata, H., Wen, H., Kawakami, Y., Naganawa, Y., Ogino, K., Yamada, K., Saint-Amant, L., Low, S. E., Cui, W. W., Zhou, W., Sprague, S. M., Asakawa, K., Muto, A., Kawakami, K. & Kuwada, J. Y. 2012. Connexin 39.9 protein is necessary for coordinated activation of slow-twitch muscle and normal behavior in zebrafish. *J Biol Chem,* 287**,** 1080-9.

Hodgetts, S., Radley, H., Davies, M. & Grounds, M. D. 2006. Reduced necrosis of dystrophic muscle by depletion of host neutrophils, or blocking TNFalpha function with Etanercept in mdx mice. *Neuromuscul Disord,* 16**,** 591-602.

Hoegg, S., Brinkmann, H., Taylor, J. S. & Meyer, A. 2004. Phylogenetic timing of the fish-specific genome duplication correlates with the diversification of teleost fish. *J Mol Evol,* 59**,** 190-203.

Hoshijima, K., Jurynec, M. J., Klatt Shaw, D., Jacobi, A. M., Behlke, M. A. & Grunwald, D. J. 2019. Highly Efficient CRISPR-Cas9-Based Methods for Generating Deletion Mutations and F0 Embryos that Lack Gene Function in Zebrafish. *Developmental cell,* 51**,** 645-657.e4.

Howard, E. E., Pasiakos, S. M., Blesso, C. N., Fussell, M. A. & Rodriguez, N. R. 2020. Divergent Roles of Inflammation in Skeletal Muscle Recovery From Injury. *Frontiers in Physiology,* 11.

Howe, K., Clark, M. D., Torroja, C. F., Torrance, J., Berthelot, C., Muffato, M., Collins, J. E., Humphray, S., Mclaren, K., Matthews, L., Mclaren, S., Sealy, I., Caccamo, M., Churcher, C., Scott, C., Barrett, J. C., Koch, R., Rauch, G. J., White, S., Chow, W., Kilian, B., Quintais, L. T., Guerra-Assunção, J. A., Zhou, Y., Gu, Y., Yen, J., Vogel, J. H., Eyre, T., Redmond, S., Banerjee, R., Chi, J., Fu, B., Langley, E., Maguire, S. F., Laird, G. K., Lloyd, D., Kenyon, E., Donaldson, S., Sehra, H., Almeida-King, J., Loveland, J., Trevanion, S., Jones, M., Quail, M., Willey, D., Hunt, A., Burton, J., Sims, S., Mclay, K., Plumb, B., Davis, J., Clee, C., Oliver, K., Clark, R., Riddle, C., Elliot, D., Threadgold, G., Harden, G., Ware, D., Begum, S., Mortimore, B., Kerry, G., Heath, P., Phillimore, B., Tracey, A., Corby, N., Dunn, M., Johnson, C., Wood, J., Clark, S., Pelan, S., Griffiths, G., Smith, M., Glithero, R., Howden, P., Barker, N., Lloyd, C., Stevens, C., Harley, J., Holt, K., Panagiotidis, G., Lovell, J., Beasley, H., Henderson, C., Gordon, D., Auger, K., Wright, D., Collins, J., Raisen, C., Dyer, L., Leung, K., Robertson, L., Ambridge, K., Leongamornlert, D., Mcguire, S., Gilderthorp, R., Griffiths, C., Manthravadi, D., Nichol, S., Barker, G.*, et al.* 2013. The zebrafish reference genome sequence and its relationship to the human genome. *Nature,* 496**,** 498-503.

Hsieh, Y.-L., Tsai, Y.-L., Shibu, M. A., Su, C.-C., Chung, L.-C., Pai, P., Kuo, C.-H., Yeh, Y.-L., Viswanadha, V. P. & Huang, C.-Y. 2015. ZAK induces cardiomyocyte hypertrophy and brain natriuretic peptide expression via p38/JNK signaling and GATA4/c-Jun transcriptional factor activation. *Molecular and Cellular Biochemistry,* 405**,** 1-9.

Hu, Y., Liang, D., Li, X., Liu, H.-H., Zhang, X., Zheng, M., Dill, D., Shi, X., Qiao, Y., Yeomans, D., Carvalho, B., Angst, M. S., Clark, J. D. & Peltz, G. 2010.

The Role of Interleukin-1 in Wound Biology. Part II: In Vivo and Human Translational Studies. *Anesthesia & Analgesia,* 111.

Huang, C.-Y., Ju Chueh, P., Tseng, C.-T., Liu, K.-Y., Tsai, H.-Y., Kuo, W.-W., Chou, M.-Y. & Yang, J.-J. 2004a. ZAK re-programs atrial natriuretic factor expression and induces hypertrophic growth in H9c2 cardiomyoblast cells. *Biochemical and Biophysical Research Communications,* 324**,** 973-980.

Huang, C. Y., Kuo, W. W., Chueh, P. J., Tseng, C. T., Chou, M. Y. & Yang, J. J. 2004b. Transforming growth factor-beta induces the expression of ANF and hypertrophic growth in cultured cardiomyoblast cells through ZAK. *Biochem Biophys Res Commun,* 324**,** 424-31.

Huang, K., Bi, F.-F. & Yang, H. 2021. A Systematic Review and Meta-Analysis of the Prevalence of Congenital Myopathy. *Frontiers in Neurology,* 12.

Huang, Z., Chen, D., Zhang, K., Yu, B., Chen, X. & Meng, J. 2007. Regulation of myostatin signaling by c-Jun N-terminal kinase in C2C12 cells. *Cell Signal,* 19**,** 2286-95.

Hughes, G. L., Lones, M. A., Bedder, M., Currie, P. D., Smith, S. L. & Pownall, M. E. 2020. Machine learning discriminates a movement disorder in a zebrafish model of Parkinson's disease. *Dis Model Mech,* 13.

Huttner, I. G., Trivedi, G., Jacoby, A., Mann, S. A., Vandenberg, J. I. & Fatkin, D. 2013. A transgenic zebrafish model of a human cardiac sodium channel mutation exhibits bradycardia, conduction-system abnormalities and early death. *J Mol Cell Cardiol,* 61**,** 123-32.

Huttner, I. G., Wang, L. W., Santiago, C. F., Horvat, C., Johnson, R., Cheng, D., Frieling-Salewsky, M. V., Hillcoat, K., Bemand, T. J., Trivedi, G., Braet, F., Hesselson, D., Alford, K., Hayward, C. S., Seidman, J. G., Seidman, C. E., Feneley, M. P., Linke, W. A. & Fatkin, D. 2018. A-Band Titin Truncation in Zebrafish Causes Dilated Cardiomyopathy and Hemodynamic Stress Intolerance. *Circulation: Genomic and Precision Medicine,* 11**,** e002135.

Huxley, A. F. & Niedergerke, R. 1954. Structural changes in muscle during contraction; interference microscopy of living muscle fibres. *Nature,* 173**,** 971-3.

Huxley, H. & Hanson, J. 1954. Changes in the Cross-Striations of Muscle during Contraction and Stretch and their Structural Interpretation. *Nature,* 173**,** 973-976.

Huynh, M. L., Fadok, V. A. & Henson, P. M. 2002. Phosphatidylserine-dependent ingestion of apoptotic cells promotes TGF-beta1 secretion and the resolution of inflammation. *J Clin Invest,* 109**,** 41-50.

Hwang, W. Y., Fu, Y., Reyon, D., Maeder, M. L., Kaini, P., Sander, J. D., Joung, J. K., Peterson, R. T. & Yeh, J.-R. J. 2013. Heritable and Precise Zebrafish Genome Editing Using a CRISPR-Cas System. *PLOS ONE,* 8**,** e68708.

Hwang, W. Y., Peterson, R. T. & Yeh, J.-R. J. 2014. Methods for targeted mutagenesis in zebrafish using TALENs. *Methods (San Diego, Calif.),* 69**,** 76-84.

Hynes, T. R., Block, S. M., White, B. T. & Spudich, J. A. 1987. Movement of myosin fragments in vitro: Domains involved in force production. *Cell,* 48**,** 953-963.

Iannaccone, S. T., Bove, K. E., Vogler, C. A. & Buchino, J. J. 1987. Type 1 fiber size disproportion: morphometric data from 37 children with myopathic, neuropathic, or idiopathic hypotonia. *Pediatr Pathol,* 7**,** 395-419.

Ibata, N. & Terentjev, E. M. 2021. Why exercise builds muscles: titin mechanosensing controls skeletal muscle growth under load. *Biophysical Journal,* 120**,** 3649-3663.

Ingebretson, J. J. & Masino, M. A. 2013. Quantification of locomotor activity in larval zebrafish: considerations for the design of high-throughput behavioral studies. *Front Neural Circuits,* 7**,** 109.

Inoki, K., Li, Y., Zhu, T., Wu, J. & Guan, K.-L. 2002. TSC2 is phosphorylated and inhibited by Akt and suppresses mTOR signalling. *Nature Cell Biology,* 4**,** 648-657.

Iordanov, M. S., Pribnow, D., Magun, J. L., Dinh, T. H., Pearson, J. A., Chen, S. L. & Magun, B. E. 1997. Ribotoxic stress response: activation of the stress-activated protein kinase JNK1 by inhibitors of the peptidyl transferase reaction and by sequence-specific RNA damage to the alpha-sarcin/ricin loop in the 28S rRNA. *Molecular and Cellular Biology,* 17**,** 3373-3381.

Isaacs, H., Heffron, J. J. & Badenhorst, M. 1975. Central core disease. A correlated genetic, histochemical, ultramicroscopic, and biochemical study. *Journal of neurology, neurosurgery, and psychiatry,* 38**,** 1177-1186.

Ito, T., Ando, H., Suzuki, T., Ogura, T., Hotta, K., Imamura, Y., Yamaguchi, Y. & Handa, H. 2010. Identification of a primary target of thalidomide teratogenicity. *Science,* 327**,** 1345-50.

Jackson, H. E. & Ingham, P. W. 2013. Control of muscle fibre-type diversity during embryonic development: The zebrafish paradigm. *Mechanisms of Development,* 130**,** 447-457.

Jackson, H. E., Ono, Y., Wang, X., Elworthy, S., Cunliffe, V. T. & Ingham, P. W. 2015. The role of Sox6 in zebrafish muscle fiber type specification. *Skeletal Muscle,* 5**,** 2.

Jacoby, A. S., Busch-Nentwich, E., Bryson-Richardson, R. J., Hall, T. E., Berger, J., Berger, S., Sonntag, C., Sachs, C., Geisler, R., Stemple, D. L. & Currie, P. D. 2009. The zebrafish dystrophic mutant softy maintains muscle fibre viability despite basement membrane rupture and muscle detachment. *Development,* 136**,** 3367-76.

Jaka, O., Casas-Fraile, L., López De Munain, A. & Sáenz, A. 2015. Costamere proteins and their involvement in myopathic processes. *Expert Reviews in Molecular Medicine,* 17**,** e12.

James, D. M., Davidson, E. A., Yanes, J., Moshiree, B. & Dallman, J. E. 2021. The Gut-Brain-Microbiome Axis and Its Link to Autism: Emerging Insights and the Potential of Zebrafish Models. *Frontiers in Cell and Developmental Biology,* 9.

Jandhyala, D. M., Wong, J., Mantis, N. J., Magun, B. E., Leong, J. M. & Thorpe, C. M. 2016. A Novel Zak Knockout Mouse with a Defective Ribotoxic Stress Response. *Toxins,* 8**,** 259.

Jin, L., Kryukov, K., Clemente, J. C., Komiyama, T., Suzuki, Y., Imanishi, T., Ikeo, K. & Gojobori, T. 2008. The evolutionary relationship between gene duplication and alternative splicing. *Gene,* 427**,** 19-31.

Jokl, E. J., Hughes, G. L., Cracknell, T., Pownall, M. E. & Blanco, G. 2018a. Transcriptional upregulation of Bag3, a chaperone-assisted selective autophagy factor, in animal models of KY-deficient hereditary myopathy. *Dis Model Mech,* 11.

Jokl, E. J., Hughes, G. L., Cracknell, T., Pownall, M. E. & Blanco, G. 2018b. Transcriptional upregulation of Bag3, a chaperone-assisted selective autophagy factor, in animal models of KY-deficient hereditary myopathy. *Dis Model Mech,* 11**,** 033225.

Jones, N. C., Fedorov, Y. V., Rosenthal, R. S. & Olwin, B. B. 2001. ERK1/2 is required for myoblast proliferation but is dispensable for muscle gene expression and cell fusion. *J Cell Physiol,* 186**,** 104-15.

Jones, R. E., Petrell, R. J. & Pauly, D. 1999. Using modified length–weight relationships to assess the condition of fish. *Aquacultural Engineering,* 20**,** 261-276.

Joseph, M., Pai, G. S., Holden, K. R. & Herman, G. 1995. X-linked myotubular myopathy: clinical observations in ten additional cases. *Am J Med Genet,* 59**,** 168-73.

Joung, J. K. & Sander, J. D. 2013. TALENs: a widely applicable technology for targeted genome editing. *Nature reviews. Molecular cell biology,* 14**,** 49-55.

Juban, G., Saclier, M., Yacoub-Youssef, H., Kernou, A., Arnold, L., Boisson, C., Ben Larbi, S., Magnan, M., Cuvellier, S., Théret, M., Petrof, B. J., Desguerre, I., Gondin, J., Mounier, R. & Chazaud, B. 2018. AMPK Activation Regulates LTBP4-Dependent TGF-β1 Secretion by Pro-inflammatory Macrophages and Controls Fibrosis in Duchenne Muscular Dystrophy. *Cell Rep,* 25**,** 2163-2176.e6.

Jungbluth, H., Sewry, C., Brown, S. C., Manzur, A. Y., Mercuri, E., Bushby, K., Rowe, P., Johnson, M. A., Hughes, I., Kelsey, A., Dubowitz, V. & Muntoni, F. 2000. Minicore myopathy in children: a clinical and histopathological study of 19 cases. *Neuromuscular Disorders,* 10**,** 264-273.

Jungbluth, H., Sewry, C. A. & Muntoni, F. 2011. Core Myopathies. *Seminars in Pediatric Neurology,* 18**,** 239-249.

Jungbluth, H., Wallgren-Pettersson, C. & Laporte, J. 2008. Centronuclear (myotubular) myopathy. *Orphanet Journal of Rare Diseases,* 3**,** 26.

Jungbluth, H., Zhou, H., Hartley, L., Halliger-Keller, B., Messina, S., Longman, C., Brockington, M., Robb, S. A., Straub, V., Voit, T., Swash, M., Ferreiro, A., Bydder, G., Sewry, C. A., Müller, C. & Muntoni, F. 2005. Minicore myopathy with ophthalmoplegia caused by mutations in the ryanodine receptor type 1 gene. *Neurology,* 65**,** 1930.

Kahane, N., Cinnamon, Y. & Kalcheim, C. 1998. The cellular mechanism by which the dermomyotome contributes to the second wave of myotome development. *Development,* 125**,** 4259-4271.

Kaindl, A. M., Rüschendorf, F., Krause, S., Goebel, H. H., Koehler, K., Becker, C., Pongratz, D., Müller-Höcker, J., Nürnberg, P., Stoltenburg-Didinger, G., Lochmüller, H. & Huebner, A. 2004. Missense mutations of ACTA1; cause dominant congenital myopathy with cores. *Journal of Medical Genetics,* 41**,** 842.

Kaplanski, G., Farnarier, C., Kaplanski, S., Porat, R., Shapiro, L., Bongrand, P. & Dinarello, C. A. 1994. Interleukin-1 induces interleukin-8 secretion from endothelial cells by a juxtacrine mechanism. *Blood,* 84**,** 4242-8.

Karagounis, L. G. & Hawley, J. A. 2010. Skeletal muscle: Increasing the size of the locomotor cell. *The International Journal of Biochemistry & Cell Biology,* 42**,** 1376-1379.

Karlsson, J., Von Hofsten, J. & Olsson, P.-E. 2001. Generating Transparent Zebrafish: A Refined Method to Improve Detection of Gene Expression During Embryonic Development. *Marine Biotechnology,* 3**,** 522-527.

Kassar-Duchossoy, L., Gayraud-Morel, B., Gomès, D., Rocancourt, D., Buckingham, M., Shinin, V. & Tajbakhsh, S. 2004. Mrf4 determines skeletal muscle identity in Myf5:Myod double-mutant mice. *Nature,* 431**,** 466-471.

Katz, M., Amit, I. & Yarden, Y. 2007. Regulation of MAPKs by growth factors and receptor tyrosine kinases. *Biochim Biophys Acta,* 1773**,** 1161-76.

Kaufmann, U., Kirsch, J., Irintchev, A., Wernig, A. & Starzinski-Powitz, A. 1999. The M-cadherin catenin complex interacts with microtubules in skeletal muscle cells: implications for the fusion of myoblasts. *J Cell Sci,* 112 (Pt 1)**,** 55-68.

Kaveh, A., Bruton, F. A., Buckley, C., Oremek, M. E. M., Tucker, C. S., Mullins, J. J., Taylor, J. M., Rossi, A. G. & Denvir, M. A. 2020. Live Imaging of Heart Injury in Larval Zebrafish Reveals a Multi-Stage Model of Neutrophil and Macrophage Migration. *Frontiers in Cell and Developmental Biology,* 8.

Kawahara, G., Karpf, J. A., Myers, J. A., Alexander, M. S., Guyon, J. R. & Kunkel, L. M. 2011. Drug screening in a zebrafish model of Duchenne muscular dystrophy. *Proc Natl Acad Sci U S A,* 108**,** 5331-6.

Kayman Kürekçi, G., Kural Mangit, E., Koyunlar, C., Unsal, S., Saglam, B., Ergin, B., Gizer, M., Uyanik, I., Boustanabadimaralan Düz, N., Korkusuz, P., Talim, B., Purali, N., Hughes, S. M. & Dincer, P. R. 2021. Knockout of zebrafish desmin genes does not cause skeletal muscle degeneration but alters calcium flux. *Scientific Reports,* 11**,** 7505.

Keatinge, M., Bui, H., Menke, A., Chen, Y. C., Sokol, A. M., Bai, Q., Ellett, F., Da Costa, M., Burke, D., Gegg, M., Trollope, L., Payne, T., Mctighe, A., Mortiboys, H., De Jager, S., Nuthall, H., Kuo, M. S., Fleming, A., Schapira, A. H., Renshaw, S. A., Highley, J. R., Chacinska, A., Panula, P., Burton, E. A., O'neill, M. J. & Bandmann, O. 2015. Glucocerebrosidase 1 deficient Danio rerio mirror key pathological aspects of human Gaucher disease and provide evidence of early microglial activation preceding alpha-synuclein-independent neuronal cell death. *Hum Mol Genet,* 24**,** 6640-52.

Keenan, S. R. & Currie, P. D. 2019. The Developmental Phases of Zebrafish Myogenesis. *J Dev Biol,* 7.

Kellermayer, M. S. Z., Smith, S. B., Granzier, H. L. & Bustamante, C. 1997. Folding-Unfolding Transitions in Single Titin Molecules Characterized with Laser Tweezers. *Science,* 276**,** 1112-1116.

Kim, D.-E., Lee, J.-H., Ji, K.-B., Park, K.-S., Kil, T.-Y., Koo, O. & Kim, M.-K. 2022. Generation of genome-edited dogs by somatic cell nuclear transfer. *BMC Biotechnology,* 22**,** 19.

Kim, E. K. & Choi, E. J. 2010. Pathological roles of MAPK signaling pathways in human diseases. *Biochim Biophys Acta,* 1802**,** 396-405.

Kim, Y., Nam, H. G. & Valenzano, D. R. 2016. The short-lived African turquoise killifish: an emerging experimental model for ageing. *Dis Model Mech,* 9**,** 115-29.

Klein, A., Jungbluth, H., Clement, E., Lillis, S., Abbs, S., Munot, P., Pane, M., Wraige, E., Schara, U., Straub, V., Mercuri, E. & Muntoni, F. 2011. Muscle Magnetic Resonance Imaging in Congenital Myopathies Due to Ryanodine Receptor Type 1 Gene Mutations. *Archives of Neurology,* 68**,** 1171-1179.

Klymiuk, N., Blutke, A., Graf, A., Krause, S., Burkhardt, K., Wuensch, A., Krebs, S., Kessler, B., Zakhartchenko, V., Kurome, M., Kemter, E., Nagashima, H., Schoser, B., Herbach, N., Blum, H., Wanke, R., Aartsma-Rus, A., Thirion, C., Lochmüller, H., Walter, M. C. & Wolf, E. 2013. Dystrophin-deficient pigs provide new insights into the hierarchy of physiological derangements of dystrophic muscle. *Human Molecular Genetics,* 22**,** 4368-4382.

Knight, J. D. & Kothary, R. 2011. The myogenic kinome: protein kinases critical to mammalian skeletal myogenesis. *Skeletal muscle,* 1**,** 29-29.

Knöll, R., Buyandelger, B. & Lab, M. 2011. The Sarcomeric Z-Disc and Z-Discopathies. *Journal of Biomedicine and Biotechnology,* 2011**,** 569628.

Kok, F. O., Shin, M., Ni, C. W., Gupta, A., Grosse, A. S., Van Impel, A., Kirchmaier, B. C., Peterson-Maduro, J., Kourkoulis, G., Male, I., Desantis, D. F., Sheppard-Tindell, S., Ebarasi, L., Betsholtz, C., Schulte-Merker, S., Wolfe, S. A. & Lawson, N. D. 2015. Reverse genetic screening reveals poor correlation between morpholino-induced and mutant phenotypes in zebrafish. *Developmental cell,* 32**,** 97-108.

Kokel, D., Cheung, C. Y. J., Mills, R., Coutinho-Budd, J., Huang, L., Setola, V., Sprague, J., Jin, S., Jin, Y. N., Huang, X.-P., Bruni, G., Woolf, C. J., Roth, B. L., Hamblin, M. R., Zylka, M. J., Milan, D. J. & Peterson, R. T. 2013. Photochemical activation of TRPA1 channels in neurons and animals. *Nature Chemical Biology,* 9**,** 257-263.

Konersman, C. G., Bordini, B. J., Scharer, G., Lawlor, M. W., Zangwill, S., Southern, J. F., Amos, L., Geddes, G. C., Kliegman, R. & Collins, M. P. 2015. BAG3 myofibrillar myopathy presenting with cardiomyopathy. *Neuromuscul Disord,* 25**,** 418-22.

Kong, D., He, M., Yang, L., Zhou, R., Yan, Y.-Q., Liang, Y. & Teng, C.-B. 2019. MiR-17 and miR-19 cooperatively promote skeletal muscle cell differentiation. *Cellular and Molecular Life Sciences,* 76**,** 5041-5054.

Kopelman, N. M., Lancet, D. & Yanai, I. 2005. Alternative splicing and gene duplication are inversely correlated evolutionary mechanisms. *Nature Genetics,* 37**,** 588-589.

Korkina, O., Dong, Z., Marullo, A., Warshaw, G., Symons, M. & Ruggieri, R. 2013. The MLK-related kinase (MRK) is a novel RhoC effector that mediates lysophosphatidic acid (LPA)-stimulated tumor cell invasion. *The Journal of biological chemistry,* 288**,** 5364-5373.

Kornegay, J. N. 2017. The golden retriever model of Duchenne muscular dystrophy. *Skeletal Muscle,* 7**,** 9.

Kravchenko, I. V., Furalyov, V. A., Chatziefthimiou, S., Wilmanns, M. & Popov, V. O. 2015. Induction of insulin-like growth factor 1 splice forms by subfragments of myofibrillar proteins. *Molecular and Cellular Endocrinology,* 399**,** 69-77.

Kroll, F., Powell, G. T., Ghosh, M., Gestri, G., Antinucci, P., Hearn, T. J., Tunbak, H., Lim, S., Dennis, H. W., Fernandez, J. M., Whitmore, D., Dreosti, E., Wilson, S. W., Hoffman, E. J. & Rihel, J. 2021. A simple and effective F0 knockout method for rapid screening of behaviour and other complex phenotypes. *eLife,* 10**,** e59683.

Kuang, S., Chargé, S. B., Seale, P., Huh, M. & Rudnicki, M. A. 2006. Distinct roles for Pax7 and Pax3 in adult regenerative myogenesis. *J Cell Biol,* 172**,** 103-13.

Kudo, H., Amizuka, N., Araki, K., Inohaya, K. & Kudo, A. 2004. Zebrafish periostin is required for the adhesion of muscle fiber bundles to the myoseptum and

for the differentiation of muscle fibers. *Developmental Biology,* 267**,** 473-487.

Kumar, S. & Hedges, S. B. 1998. A molecular timescale for vertebrate evolution. *Nature,* 392**,** 917-920.

Labeit, S., Gautel, M., Lakey, A. & Trinick, J. 1992. Towards a molecular understanding of titin. *Embo j,* 11**,** 1711-6.

Laggner, C., Kokel, D., Setola, V., Tolia, A., Lin, H., Irwin, J. J., Keiser, M. J., Cheung, C. Y. J., Minor, D. L., Roth, B. L., Peterson, R. T. & Shoichet, B. K. 2012. Chemical informatics and target identification in a zebrafish phenotypic screen. *Nature Chemical Biology,* 8**,** 144-146.

Laing, N. G., Clarke, N. F., Dye, D. E., Liyanage, K., Walker, K. R., Kobayashi, Y., Shimakawa, S., Hagiwara, T., Ouvrier, R., Sparrow, J. C., Nishino, I., North, K. N. & Nonaka, I. 2004. Actin mutations are one cause of congenital fibre type disproportion. *Ann Neurol,* 56**,** 689-94.

Laitila, J. & Wallgren-Pettersson, C. 2021. Recent advances in nemaline myopathy. *Neuromuscular Disorders,* 31**,** 955-967.

Laitila, J. M., Mcnamara, E. L., Wingate, C. D., Goullee, H., Ross, J. A., Taylor, R. L., Van Der Pijl, R., Griffiths, L. M., Harries, R., Ravenscroft, G., Clayton, J. S., Sewry, C., Lawlor, M. W., Ottenheijm, C. a. C., Bakker, A. J., Ochala, J., Laing, N. G., Wallgren-Pettersson, C., Pelin, K. & Nowak, K. J. 2020. Nebulin nemaline myopathy recapitulated in a compound heterozygous mouse model with both a missense and a nonsense mutation in Neb. *Acta Neuropathologica Communications,* 8**,** 18.

Lambert, M. J., Cochran, W. O., Wilde, B. M., Olsen, K. G. & Cooper, C. D. 2015. Evidence for widespread subfunctionalization of splice forms in vertebrate genomes. *Genome Res,* 25**,** 624-32.

Lambert, M. R., Spinazzola, J. M., Widrick, J. J., Pakula, A., Conner, J. R., Chin, J. E., Owens, J. M. & Kunkel, L. M. 2021. PDE10A Inhibition Reduces the Manifestation of Pathology in DMD Zebrafish and Represses the Genetic Modifier PITPNA. *Molecular Therapy,* 29**,** 1086-1101.

Lange, S., Himmel, M., Auerbach, D., Agarkova, I., Hayess, K., Fürst, D. O., Perriard, J.-C. & Ehler, E. 2005. Dimerisation of Myomesin: Implications for the Structure of the Sarcomeric M-band. *Journal of Molecular Biology,* 345**,** 289-298.

Laporte, J., Hu, L. J., Kretz, C., Mandel, J. L., Kioschis, P., Coy, J. F., Klauck, S. M., Poustka, A. & Dahl, N. 1996. A gene mutated in X-linked myotubular myopathy defines a new putative tyrosine phosphatase family conserved in yeast. *Nat Genet,* 13**,** 175-82.

Larson, M. H., Gilbert, L. A., Wang, X., Lim, W. A., Weissman, J. S. & Qi, L. S. 2013. CRISPR interference (CRISPRi) for sequence-specific control of gene expression. *Nature Protocols,* 8**,** 2180-2196.

Larsson, L., Edstrom, L., Lindegren, B., Gorza, L. & Schiaffino, S. 1991. MHC composition and enzyme-histochemical and physiological properties of a novel fast-twitch motor unit type. *American Journal of Physiology-Cell Physiology,* 261**,** C93-C101.

Larsson, L. & Moss, R. L. 1993. Maximum velocity of shortening in relation to myosin isoform composition in single fibres from human skeletal muscles. *J Physiol,* 472**,** 595-614.

Latha Ramalingam, C. M., Glad Mohesh 2021. Creating a simple obesity working model of zebrafish. *National Journal of Physiology, Pharmacy and Pharmacology* 11**,** 1136-1140.

Lathrop, B., Thomas, K. & Glaser, L. 1985. Control of myogenic differentiation by fibroblast growth factor is mediated by position in the G1 phase of the cell cycle. *J Cell Biol,* 101**,** 2194-8.

Lawal, T. A., Todd, J. J. & Meilleur, K. G. 2018. Ryanodine Receptor 1-Related Myopathies: Diagnostic and Therapeutic Approaches. *Neurotherapeutics,* 15**,** 885-899.

Lawlor, M. W., Beggs, A. H., Buj-Bello, A., Childers, M. K., Dowling, J. J., James, E. S., Meng, H., Moore, S. A., Prasad, S., Schoser, B. & Sewry, C. A. 2016. Skeletal Muscle Pathology in X-Linked Myotubular Myopathy: Review With Cross-Species Comparisons. *J Neuropathol Exp Neurol,* 75**,** 102-10.

Lawlor, M. W., Dechene, E. T., Roumm, E., Geggel, A. S., Moghadaszadeh, B. & Beggs, A. H. 2010. Mutations of tropomyosin 3 (TPM3) are common and associated with type 1 myofiber hypotrophy in congenital fiber type disproportion. *Hum Mutat,* 31**,** 176-83.

Lawson, N. D. & Weinstein, B. M. 2002. In Vivo Imaging of Embryonic Vascular Development Using Transgenic Zebrafish. *Developmental Biology,* 248**,** 307-318.

Lazure, F., Blackburn, D. M., Corchado, A. H., Sahinyan, K., Karam, N., Sharanek, A., Nguyen, D., Lepper, C., Najafabadi, H. S., Perkins, T. J., Jahani-Asl, A. & Soleimani, V. D. 2020. Myf6/MRF4 is a myogenic niche regulator required for the maintenance of the muscle stem cell pool. *EMBO reports,* 21**,** e49499.

Le Goc, G., Lafaye, J., Karpenko, S., Bormuth, V., Candelier, R. & Debrégeas, G. 2021. Thermal modulation of Zebrafish exploratory statistics reveals constraints on individual behavioral variability. *BMC Biology,* 19**,** 208.

Lee, K. E., Seo, J., Shin, J., Ji, E. H., Roh, J., Kim, J. Y., Sun, W., Muhr, J., Lee, S. & Kim, J. 2014. Positive feedback loop between Sox2 and Sox6 inhibits neuronal differentiation in the developing central nervous system. *Proc Natl Acad Sci U S A,* 111**,** 2794-9.

Lehman, W., Craig, R. & Vibert, P. 1994. Ca2+-induced tropomyosin movement in Limulus thin filaments revealed by three-dimensional reconstruction. *Nature,* 368**,** 65-67.

Leikina, E., Gamage, D. G., Prasad, V., Goykhberg, J., Crowe, M., Diao, J., Kozlov, M. M., Chernomordik, L. V. & Millay, D. P. 2018. Myomaker and Myomerger Work Independently to Control Distinct Steps of Membrane Remodeling during Myoblast Fusion. *Dev Cell,* 46**,** 767-780.e7.

Lessard, S. J., Macdonald, T. L., Pathak, P., Han, M. S., Coffey, V. G., Edge, J., Rivas, D. A., Hirshman, M. F., Davis, R. J. & Goodyear, L. J. 2018. JNK regulates muscle remodeling via myostatin/SMAD inhibition. *Nature Communications,* 9**,** 3030.

Levanon, D., Brenner, O., Negreanu, V., Bettoun, D., Woolf, E., Eilam, R., Lotem, J., Gat, U., Otto, F., Speck, N. & Groner, Y. 2001. Spatial and temporal expression pattern of Runx3 (Aml2) and Runx1 (Aml1) indicates non-redundant functions during mouse embryogenesis. *Mechanisms of Development,* 109**,** 413-417.

Levraud, J.-P., Rawls, J. F. & Clatworthy, A. E. 2022. Using zebrafish to understand reciprocal interactions between the nervous and immune systems and the microbial world. *Journal of Neuroinflammation,* 19**,** 170.

Li, L., Medina-Menéndez, C., García-Corzo, L., Córdoba-Beldad, C. M., Quiroga, A. C., Calleja Barca, E., Zinchuk, V., Muñoz-López, S., Rodríguez-Martín, P., Ciorraga, M., Colmena, I., Fernández, S., Vicario, C., Nicolis, S. K., Lefebvre, V., Mira, H. & Morales, A. V. 2022. SoxD genes are required for adult neural stem cell activation. *Cell Rep,* 38**,** 110313.

Li, Y. P. 2003. TNF-alpha is a mitogen in skeletal muscle. *Am J Physiol Cell Physiol,* 285**,** C370-6.

Li, Z., Jiang, Y., Ulevitch, R. J. & Han, J. 1996. The Primary Structure of p38γ: A New Member of p38 Group of MAP Kinases. *Biochemical and Biophysical Research Communications,* 228**,** 334-340.

Li, Z., Zhang, Z., Ren, Y., Wang, Y., Fang, J., Yue, H., Ma, S. & Guan, F. 2021. Aging and age-related diseases: from mechanisms to therapeutic strategies. *Biogerontology,* 22**,** 165-187.

Liao, C. & Beisel, C. L. 2021. The tracrRNA in CRISPR Biology and Technologies. *Annual Review of Genetics,* 55**,** 161-181.

Lieschke, G. J. & Currie, P. D. 2007. Animal models of human disease: zebrafish swim into view. *Nature Reviews Genetics,* 8**,** 353-367.

Lieschke, G. J., Oates, A. C., Crowhurst, M. O., Ward, A. C. & Layton, J. E. 2001. Morphologic and functional characterization of granulocytes and macrophages in embryonic and adult zebrafish. *Blood,* 98**,** 3087-3096.

Liew, H. P., Choksi, S. P., Wong, K. N. & Roy, S. 2008. Specification of vertebrate slow-twitch muscle fiber fate by the transcriptional regulator Blimp1. *Developmental Biology,* 324**,** 226-235.

Liewluck, T., Sorenson, E. J., Walkiewicz, M. A., Rumilla, K. M. & Milone, M. 2017. Autosomal dominant distal myopathy due to a novel ACTA1 mutation. *Neuromuscular Disorders,* 27**,** 742-746.

Lin, I. H., Chang, J.-L., Hua, K., Huang, W.-C., Hsu, M.-T. & Chen, Y.-F. 2018. Skeletal muscle in aged mice reveals extensive transformation of muscle gene expression. *BMC Genetics,* 19**,** 55.

Lin, Y.-M., Situmorang, J. H., Guan, J.-Z., Hsieh, D. J.-Y., Yang, J.-J., Chen, M. Y.-C., Loh, C.-H., Kuo, C.-H., Lu, S.-Y., Liou, Y.-M. & Huang, C.-Y. 2022. ZAKβ Alleviates Oxidized Low-density Lipoprotein (ox-LDL)-Induced Apoptosis and B-type Natriuretic Peptide (BNP) Upregulation in Cardiomyoblast. *Cell Biochemistry and Biophysics,* 80**,** 547-554.

Liu, K., Petree, C., Requena, T., Varshney, P. & Varshney, G. K. 2019. Expanding the CRISPR Toolbox in Zebrafish for Studying Development and Disease. *Frontiers in Cell and Developmental Biology,* 7.

Liu, T. C., Huang, C. J., Chu, Y. C., Wei, C. C., Chou, C. C., Chou, M. Y., Chou, C. K. & Yang, J. J. 2000. Cloning and expression of ZAK, a mixed lineage kinase-like protein containing a leucine-zipper and a sterile-alpha motif. *Biochem Biophys Res Commun,* 274**,** 811-6.

Livak, K. J. & Schmittgen, T. D. 2001. Analysis of relative gene expression data using real-time quantitative PCR and the 2(-Delta Delta C(T)) Method. *Methods,* 25**,** 402-8.

Livne, H., Avital, T., Ruppo, S., Harazi, A., Mitrani-Rosenbaum, S. & Daya, A. 2022. Generation and characterization of a novel gne Knockout Model in Zebrafish. *Frontiers in Cell and Developmental Biology,* 10.

Lu, H., Huang, D., Saederup, N., Charo, I. F., Ransohoff, R. M. & Zhou, L. 2011. Macrophages recruited via CCR2 produce insulin-like growth factor-1 to repair acute skeletal muscle injury. *The FASEB Journal,* 25**,** 358-369.

Lu, J., Peatman, E., Wang, W., Yang, Q., Abernathy, J., Wang, S., Kucuktas, H. & Liu, Z. 2010. Alternative splicing in teleost fish genomes: same-species and cross-species analysis and comparisons. *Molecular Genetics and Genomics,* 283**,** 531-539.

Luo, W., Li, E., Nie, Q. & Zhang, X. 2015. Myomaker, Regulated by MYOD, MYOG and miR-140-3p, Promotes Chicken Myoblast Fusion. *International Journal of Molecular Sciences,* 16**,** 26186-26201.

Luo, Y.-B., Peng, Y., Lu, Y., Li, Q., Duan, H., Bi, F. & Yang, H. 2020. Expanding the Clinico-Genetic Spectrum of Myofibrillar Myopathy: Experience From a Chinese Neuromuscular Center. *Frontiers in Neurology,* 11.

Luther, P. K. 2009. The vertebrate muscle Z-disc: sarcomere anchor for structure and signalling. *Journal of Muscle Research and Cell Motility,* 30**,** 171-185.

Luther, P. K., Barry, J. S. & Squire, J. M. 2002. The three-dimensional structure of a vertebrate wide (slow muscle) Z-band: lessons on Z-band assembly11Edited by J. Karn. *Journal of Molecular Biology,* 315**,** 9-20.

Magee, K. R. & Shy, G. M. 1956. A new congenital non-progressive myopathy. *Brain,* 79**,** 610-21.

Malm, C., Nyberg, P., Engstrom, M., Sjodin, B., Lenkei, R., Ekblom, B. & Lundberg, I. 2000. Immunological changes in human skeletal muscle and blood after eccentric exercise and multiple biopsies. *J Physiol,* 529 Pt 1**,** 243-62.

Mantovani, A., Sica, A., Sozzani, S., Allavena, P., Vecchi, A. & Locati, M. 2004. The chemokine system in diverse forms of macrophage activation and polarization. *Trends Immunol,* 25**,** 677-86.

Manzur, A. Y., Sewry, C. A., Ziprin, J., Dubowitz, V. & Muntoni, F. 1998. A severe clinical and pathological variant of central core disease with possible autosomal recessive inheritance. *Neuromuscular Disorders,* 8**,** 467-473.

Marsolais, D., Cŏté, C. H. & Frenette, J. 2001. Neutrophils and macrophages accumulate sequentially following Achilles tendon injury. *Journal of Orthopaedic Research,* 19**,** 1203-1209.

Marttila, M., Win, W., Al-Ghamdi, F., Abdel-Hamid, H. Z., Lacomis, D. & Beggs, A. H. 2019. MYL2-associated congenital fiber-type disproportion and cardiomyopathy with variants in additional neuromuscular disease genes; the dilemma of panel testing. *Cold Spring Harb Mol Case Stud,* 5.

Mary Elizabeth Pownall, Marcus K. Gustafsson & Charles P. Emerson, J. 2002. Myogenic Regulatory Factors and the Specification of Muscle Progenitors in Vertebrate Embryos. *Annual Review of Cell and Developmental Biology,* 18**,** 747-783.

Mastaglia, F. L., Papadimitriou, J. M. & Kakulas, B. A. 1970. Regeneration of muscle in Duchenne muscular dystrophy: an electron microscope study. *J Neurol Sci,* 11**,** 425-44.

Masuzugawa, S., Kuzuhara, S., Narita, Y., Naito, Y., Taniguchi, A. & Ibi, T. 1997. Autosomal Dominant Hyaline Body Myopathy Presenting As Scapuloperoneal Syndrome. *Neurology,* 48**,** 253.

Mathes, S., Vanmunster, M., Bloch, W. & Suhr, F. 2019. Evidence for skeletal muscle fiber type-specific expressions of mechanosensors. *Cellular and Molecular Life Sciences,* 76**,** 2987-3004.

Matsakas, A., Otto, A., Elashry, M. I., Brown, S. C. & Patel, K. 2010. Altered primary and secondary myogenesis in the myostatin-null mouse. *Rejuvenation Res,* 13**,** 717-27.

Mauro, A. 1961. Satellite cell of skeletal muscle fibers. *J Biophys Biochem Cytol,* 9**,** 493-5.

Mccarthy, J. J., Mula, J., Miyazaki, M., Erfani, R., Garrison, K., Farooqui, A. B., Srikuea, R., Lawson, B. A., Grimes, B., Keller, C., Van Zant, G., Campbell, K. S., Esser, K. A., Dupont-Versteegden, E. E. & Peterson, C. A. 2011. Effective fiber hypertrophy in satellite cell-depleted skeletal muscle. *Development,* 138**,** 3657-3666.

Mcentagart, M., Parsons, G., Buj-Bello, A., Biancalana, V., Fenton, I., Little, M., Krawczak, M., Thomas, N., Herman, G., Clarke, A. & Wallgren-Pettersson,

C. 2002. Genotype–phenotype correlations in X-linked myotubular myopathy. *Neuromuscular Disorders,* 12**,** 939-946.

Mcgrath, E. R., Doughty, C. T. & Amato, A. A. 2018. Autoimmune Myopathies: Updates on Evaluation and Treatment. *Neurotherapeutics,* 15**,** 976-994.

Mchenry, M. J. & Lauder, G. V. 2005. The mechanical scaling of coasting in zebrafish (Danio rerio). *J Exp Biol,* 208**,** 2289-301.

Mchenry, M. J., Pell, C. A. & Long, J. H., Jr 1995. Mechanical control of swimming speed: stiffness and axial wave form in undulating fish models. *Journal of Experimental Biology,* 198**,** 2293-2305.

Mehravar, M., Shirazi, A., Nazari, M. & Banan, M. 2019. Mosaicism in CRISPR/Cas9-mediated genome editing. *Developmental Biology,* 445**,** 156-162.

Melendez, J., Sieiro, D., Salgado, D., Morin, V., Dejardin, M.-J., Zhou, C., Mullen, A. C. & Marcelle, C. 2021. TGFβ signalling acts as a molecular brake of myoblast fusion. *Nature Communications,* 12**,** 749.

Meng, X., Noyes, M. B., Zhu, L. J., Lawson, N. D. & Wolfe, S. A. 2008. Targeted gene inactivation in zebrafish using engineered zinc-finger nucleases. *Nature Biotechnology,* 26**,** 695-701.

Mercuri, E., Bönnemann, C. G. & Muntoni, F. 2019. Muscular dystrophies. *The Lancet,* 394**,** 2025-2038.

Meredith, C., Herrmann, R., Parry, C., Liyanage, K., Dye, D. E., Durling, H. J., Duff, R. M., Beckman, K., De Visser, M., Van Der Graaff, M. M., Hedera, P., Fink, J. K., Petty, E. M., Lamont, P., Fabian, V., Bridges, L., Voit, T., Mastaglia, F. L. & Laing, N. G. 2004. Mutations in the slow skeletal muscle fiber myosin heavy chain gene (MYH7) cause laing early-onset distal myopathy (MPD1). *Am J Hum Genet,* 75**,** 703-8.

Messerli, M., Aaldijk, D., Haberthür, D., Röss, H., García-Poyatos, C., Sande-Melón, M., Khoma, O. Z., Wieland, F. a. M., Fark, S. & Djonov, V. 2020. Adaptation mechanism of the adult zebrafish respiratory organ to endurance training. *PLoS One,* 15**,** e0228333.

Miao, K. Z., Kim, G. Y., Meara, G. K., Qin, X. & Feng, H. 2021. Tipping the Scales With Zebrafish to Understand Adaptive Tumor Immunity. *Frontiers in Cell and Developmental Biology,* 9.

Millay, D. P., O'rourke, J. R., Sutherland, L. B., Bezprozvannaya, S., Shelton, J. M., Bassel-Duby, R. & Olson, E. N. 2013. Myomaker is a membrane activator of myoblast fusion and muscle formation. *Nature,* 499**,** 301-5.

Millay, D. P., Sutherland, L. B., Bassel-Duby, R. & Olson, E. N. 2014. Myomaker is essential for muscle regeneration. *Genes Dev,* 28**,** 1641-6.

Mills, C. D., Kincaid, K., Alt, J. M., Heilman, M. J. & Hill, A. M. 2000. M-1/M-2 macrophages and the Th1/Th2 paradigm. *J Immunol,* 164**,** 6166-73.

Mishra, P., Varuzhanyan, G., Pham, A. H. & Chan, D. C. 2015. Mitochondrial Dynamics is a Distinguishing Feature of Skeletal Muscle Fiber Types and Regulates Organellar Compartmentalization. *Cell Metab,* 22**,** 1033-44.

Monaco, A. P., Neve, R. L., Colletti-Feener, C., Bertelson, C. J., Kurnit, D. M. & Kunkel, L. M. 1986. Isolation of candidate cDNAs for portions of the Duchenne muscular dystrophy gene. *Nature,* 323**,** 646-50.

Montandon, M., Currie, P. D. & Ruparelia, A. A. 2021. Examining Muscle Regeneration in Zebrafish Models of Muscle Disease. *J Vis Exp*.

Moore, C. A., Parkin, C. A., Bidet, Y. & Ingham, P. W. 2007. A role for the Myoblast city homologues Dock1 and Dock5 and the adaptor proteins Crk and Crk-like in zebrafish myoblast fusion. *Development,* 134**,** 3145-3153.

Moore, F. E., Reyon, D., Sander, J. D., Martinez, S. A., Blackburn, J. S., Khayter, C., Ramirez, C. L., Joung, J. K. & Langenau, D. M. 2012. Improved Somatic Mutagenesis in Zebrafish Using Transcription Activator-Like Effector Nucleases (TALENs). *PLOS ONE,* 7**,** e37877.

Moretti, A., Fonteyne, L., Giesert, F., Hoppmann, P., Meier, A. B., Bozoglu, T., Baehr, A., Schneider, C. M., Sinnecker, D., Klett, K., Fröhlich, T., Rahman, F. A., Haufe, T., Sun, S., Jurisch, V., Kessler, B., Hinkel, R., Dirschinger, R., Martens, E., Jilek, C., Graf, A., Krebs, S., Santamaria, G., Kurome, M., Zakhartchenko, V., Campbell, B., Voelse, K., Wolf, A., Ziegler, T., Reichert, S., Lee, S., Flenkenthaler, F., Dorn, T., Jeremias, I., Blum, H., Dendorfer, A., Schnieke, A., Krause, S., Walter, M. C., Klymiuk, N., Laugwitz, K. L., Wolf, E., Wurst, W. & Kupatt, C. 2020. Somatic gene editing ameliorates skeletal and cardiac muscle failure in pig and human models of Duchenne muscular dystrophy. *Nature Medicine,* 26**,** 207-214.

Moretti, I., Ciciliot, S., Dyar, K. A., Abraham, R., Murgia, M., Agatea, L., Akimoto, T., Bicciato, S., Forcato, M., Pierre, P., Uhlenhaut, N. H., Rigby, P. W. J., Carvajal, J. J., Blaauw, B., Calabria, E. & Schiaffino, S. 2016. MRF4 negatively regulates adult skeletal muscle growth by repressing MEF2 activity. *Nature Communications,* 7**,** 12397.

Mounier, R., Théret, M., Arnold, L., Cuvellier, S., Bultot, L., Göransson, O., Sanz, N., Ferry, A., Sakamoto, K., Foretz, M., Viollet, B. & Chazaud, B. 2013. AMPKα1 Regulates Macrophage Skewing at the Time of Resolution of Inflammation during Skeletal Muscle Regeneration. *Cell Metabolism,* 18**,** 251-264.

Muelas, N., Hackman, P., Luque, H., Garcés-Sánchez, M., Azorín, I., Suominen, T., Sevilla, T., Mayordomo, F., Gómez, L., Martí, P., María Millán, J., Udd, B. & Vílchez, J. J. 2010. MYH7 gene tail mutation causing myopathic profiles beyond Laing distal myopathy. *Neurology,* 75**,** 732.

Murphy, M. M., Lawson, J. A., Mathew, S. J., Hutcheson, D. A. & Kardon, G. 2011. Satellite cells, connective tissue fibroblasts and their interactions are crucial for muscle regeneration. *Development,* 138**,** 3625-3637.

Na, S. J., Kim, W. K., Kim, T. S., Kang, S. W., Lee, E. Y. & Choi, Y. C. 2006. Comparison of clinical characteristics between congenital fiber type

disproportion myopathy and congenital myopathy with type 1 fiber predominance. *Yonsei Med J,* 47**,** 513-8.

Nabeshima, Y., Hanaoka, K., Hayasaka, M., Esuml, E., Li, S., Nonaka, I. & Nabeshima, Y.-I. 1993. Myogenin gene disruption results in perinatal lethality because of severe muscle defect. *Nature,* 364**,** 532-535.

Nadeau, J. H. & Sankoff, D. 1997. Comparable Rates of Gene Loss and Functional Divergence After Genome Duplications Early in Vertebrate Evolution. *Genetics,* 147**,** 1259-1266.

Naganawa, Y. & Hirata, H. 2011. Developmental transition of touch response from slow muscle-mediated coilings to fast muscle-mediated burst swimming in zebrafish. *Developmental Biology,* 355**,** 194-204.

Nakamura, F., Stossel, T. P. & Hartwig, J. H. 2011. The filamins: organizers of cell structure and function. *Cell Adh Migr,* 5**,** 160-9.

Nakayama, T., Blitz, I. L., Fish, M. B., Odeleye, A. O., Manohar, S., Cho, K. W. & Grainger, R. M. 2014. Cas9-based genome editing in Xenopus tropicalis. *Methods Enzymol,* 546**,** 355-75.

Nance, J. R., Dowling, J. J., Gibbs, E. M. & Bönnemann, C. G. 2012. Congenital myopathies: an update. *Curr Neurol Neurosci Rep,* 12**,** 165-74.

Nasevicius, A. & Ekker, S. C. 2000. Effective targeted gene 'knockdown' in zebrafish. *Nature Genetics,* 26**,** 216-220.

Nave, R., Fürst, D. O. & Weber, K. 1990. Interaction of alpha-actinin and nebulin in vitro. Support for the existence of a fourth filament system in skeletal muscle. *FEBS Lett,* 269**,** 163-6.

Nicolas, H. A., Hua, K., Quigley, H., Ivare, J., Tesson, F. & Akimenko, M.-A. 2022. A CRISPR/Cas9 zebrafish lamin A/C mutant model of muscular laminopathy. *Developmental Dynamics,* 251**,** 645-661.

Nicot, A. S., Toussaint, A., Tosch, V., Kretz, C., Wallgren-Pettersson, C., Iwarsson, E., Kingston, H., Garnier, J. M., Biancalana, V., Oldfors, A., Mandel, J. L. & Laporte, J. 2007. Mutations in amphiphysin 2 (BIN1) disrupt interaction with dynamin 2 and cause autosomal recessive centronuclear myopathy. *Nat Genet,* 39**,** 1134-9.

Nishimune, H. & Shigemoto, K. 2018. Practical Anatomy of the Neuromuscular Junction in Health and Disease. *Neurol Clin,* 36**,** 231-240.

Nordgaard, C., Vind, A. C., Stonadge, A., Kjøbsted, R., Snieckute, G., Antas, P., Blasius, M., Reinert, M. S., Del Val, A. M., Bekker-Jensen, D. B., Haahr, P., Miroshnikova, Y. A., Mazouzi, A., Falk, S., Perrier-Groult, E., Tiedje, C., Li, X., Jakobsen, J. R., Jørgensen, N. O., Wojtaszewski, J. F., Mallein-Gerin, F., Andersen, J. L., Pennisi, C. P., Clemmensen, C., Kassem, M., Jafari, A., Brummelkamp, T., Li, V. S., Wickström, S. A., Olsen, J. V., Blanco, G. & Bekker-Jensen, S. 2022. ZAKβ is activated by cellular compression and mediates contraction-induced MAP kinase signaling in skeletal muscle. *The EMBO Journal,* n/a**,** e111650.

North, K. N., Laing, N. G. & Wallgren-Pettersson, C. 1997. Nemaline myopathy: current concepts. The ENMC International Consortium and Nemaline Myopathy. *J Med Genet,* 34**,** 705-13.

North, K. N., Wang, C. H., Clarke, N., Jungbluth, H., Vainzof, M., Dowling, J. J., Amburgey, K., Quijano-Roy, S., Beggs, A. H., Sewry, C., Laing, N. G. & Bönnemann, C. G. 2014. Approach to the diagnosis of congenital myopathies. *Neuromuscul Disord,* 24**,** 97-116.

Norton, N., Li, D., Rieder, Mark j., Siegfried, Jill d., Rampersaud, E., Züchner, S., Mangos, S., Gonzalez-Quintana, J., Wang, L., Mcgee, S., Reiser, J., Martin, E., Nickerson, Deborah a. & Hershberger, Ray e. 2011. Genome-wide Studies of Copy Number Variation and Exome Sequencing Identify Rare Variants in BAG3 as a Cause of Dilated Cardiomyopathy. *The American Journal of Human Genetics,* 88**,** 273-282.

Nowak, K. J., Wattanasirichaigoon, D., Goebel, H. H., Wilce, M., Pelin, K., Donner, K., Jacob, R. L., Hübner, C., Oexle, K., Anderson, J. R., Verity, C. M., North, K. N., Iannaccone, S. T., Müller, C. R., Nürnberg, P., Muntoni, F., Sewry, C., Hughes, I., Sutphen, R., Lacson, A. G., Swoboda, K. J., Vigneron, J., Wallgren-Pettersson, C., Beggs, A. H. & Laing, N. G. 1999. Mutations in the skeletal muscle alpha-actin gene in patients with actin myopathy and nemaline myopathy. *Nat Genet,* 23**,** 208-12.

Nyati, S., Chator, A., Schinske, K., Gregg, B. S., Ross, B. D. & Rehemtulla, A. 2016. A Requirement for ZAK Kinase Activity in Canonical TGF-β Signaling. *Translational Oncology,* 9**,** 473-481.

Oates, E. C., Jones, K. J., Donkervoort, S., Charlton, A., Brammah, S., Smith, J. E., 3rd, Ware, J. S., Yau, K. S., Swanson, L. C., Whiffin, N., Peduto, A. J., Bournazos, A., Waddell, L. B., Farrar, M. A., Sampaio, H. A., Teoh, H. L., Lamont, P. J., Mowat, D., Fitzsimons, R. B., Corbett, A. J., Ryan, M. M., O'grady, G. L., Sandaradura, S. A., Ghaoui, R., Joshi, H., Marshall, J. L., Nolan, M. A., Kaur, S., Punetha, J., Töpf, A., Harris, E., Bakshi, M., Genetti, C. A., Marttila, M., Werlauff, U., Streichenberger, N., Pestronk, A., Mazanti, I., Pinner, J. R., Vuillerot, C., Grosmann, C., Camacho, A., Mohassel, P., Leach, M. E., Foley, A. R., Bharucha-Goebel, D., Collins, J., Connolly, A. M., Gilbreath, H. R., Iannaccone, S. T., Castro, D., Cummings, B. B., Webster, R. I., Lazaro, L., Vissing, J., Coppens, S., Deconinck, N., Luk, H. M., Thomas, N. H., Foulds, N. C., Illingworth, M. A., Ellard, S., Mclean, C. A., Phadke, R., Ravenscroft, G., Witting, N., Hackman, P., Richard, I., Cooper, S. T., Kamsteeg, E. J., Hoffman, E. P., Bushby, K., Straub, V., Udd, B., Ferreiro, A., North, K. N., Clarke, N. F., Lek, M., Beggs, A. H., Bönnemann, C. G., Macarthur, D. G., Granzier, H., Davis, M. R. & Laing, N. G. 2018. Congenital Titinopathy: Comprehensive characterization and pathogenic insights. *Ann Neurol,* 83**,** 1105-1124.

Obermann, W. M., Gautel, M., Steiner, F., Van Der Ven, P. F., Weber, K. & Fürst, D. O. 1996. The structure of the sarcomeric M band: localization of defined domains of myomesin, M-protein, and the 250-kD carboxy-terminal region of titin by immunoelectron microscopy. *J Cell Biol,* 134**,** 1441-53.

Oginuma, M., Nishida, M., Ohmura-Adachi, T., Abe, K., Ogamino, S., Mogi, C., Matsui, H. & Ishitani, T. 2022. Rapid reverse genetics systems for Nothobranchius furzeri, a suitable model organism to study vertebrate aging. *Scientific Reports,* 12**,** 11628.

Okamoto, R., Ali, Y., Hashizume, R., Suzuki, N. & Ito, M. 2019. BNP as a Major Player in the Heart-Kidney Connection. *Int J Mol Sci,* 20.

Okuda, T., Nishimura, M., Nakao, M. & Fujitaa, Y. 2001. RUNX1/AML1: A Central Player in Hematopoiesis. *International Journal of Hematology,* 74**,** 252-257.

Oliver, D., Yuan, S., Mcswiggin, H. & Yan, W. 2015. Pervasive Genotypic Mosaicism in Founder Mice Derived from Genome Editing through Pronuclear Injection. *PLOS ONE,* 10**,** e0129457.

Olsen, L. A., Nicoll, J. X. & Fry, A. C. 2019. The skeletal muscle fiber: a mechanically sensitive cell. *Eur J Appl Physiol,* 119**,** 333-349.

Ortolano, S., Tarrío, R., Blanco-Arias, P., Teijeira, S., Rodríguez-Trelles, F., García-Murias, M., Delague, V., Lévy, N., Fernández, J. M., Quintáns, B., Millán, B. S., Carracedo, Á., Navarro, C. & Sobrido, M.-J. 2011. A novel MYH7 mutation links congenital fiber type disproportion and myosin storage myopathy. *Neuromuscular Disorders,* 21**,** 254-262.

Ott, M. O., Bober, E., Lyons, G., Arnold, H. & Buckingham, M. 1991. Early expression of the myogenic regulatory gene, myf-5, in precursor cells of skeletal muscle in the mouse embryo. *Development,* 111**,** 1097-107.

Ottenheijm, C. A., Witt, C. C., Stienen, G. J., Labeit, S., Beggs, A. H. & Granzier, H. 2009. Thin filament length dysregulation contributes to muscle weakness in nemaline myopathy patients with nebulin deficiency. *Hum Mol Genet,* 18**,** 2359-69.

Pagola-Lorz, I., Vicente, E., Ibáñez, B., Torné, L., Elizalde-Beiras, I., Garcia-Solaesa, V., García, F., Delfrade, J. & Jericó, I. 2019. Epidemiological study and genetic characterization of inherited muscle diseases in a northern Spanish region. *Orphanet J Rare Dis,* 14**,** 276.

Paillard, T. 2017. Relationship between Muscle Function, Muscle Typology and Postural Performance According to Different Postural Conditions in Young and Older Adults. *Front Physiol,* 8**,** 585.

Pan, Q., Shai, O., Lee, L. J., Frey, B. J. & Blencowe, B. J. 2008. Deep surveying of alternative splicing complexity in the human transcriptome by high-throughput sequencing. *Nat Genet,* 40**,** 1413-5.

Papadimas, G. K., Xirou, S., Kararizou, E. & Papadopoulos, C. 2020. Update on Congenital Myopathies in Adulthood. *Int J Mol Sci,* 21.

Parichy, D. M., Elizondo, M. R., Mills, M. G., Gordon, T. N. & Engeszer, R. E. 2009. Normal table of postembryonic zebrafish development: staging by externally visible anatomy of the living fish. *Dev Dyn,* 238**,** 2975-3015.

Patton, E. E., Zon, L. I. & Langenau, D. M. 2021. Zebrafish disease models in drug discovery: from preclinical modelling to clinical trials. *Nat Rev Drug Discov,* 20**,** 611-628.

Pearson, G., Robinson, F., Beers Gibson, T., Xu, B. E., Karandikar, M., Berman, K. & Cobb, M. H. 2001. Mitogen-activated protein (MAP) kinase pathways: regulation and physiological functions. *Endocr Rev,* 22**,** 153-83.

Peng, J. 2019. Gene redundancy and gene compensation: An updated view. *Journal of Genetics and Genomics,* 46**,** 329-333.

Perdiguero, E., Ruiz-Bonilla, V., Gresh, L., Hui, L., Ballestar, E., Sousa-Victor, P., Baeza-Raja, B., Jardí, M., Bosch-Comas, A., Esteller, M., Caelles, C., Serrano, A. L., Wagner, E. F. & Muñoz-Cánoves, P. 2007. Genetic analysis of p38 MAP kinases in myogenesis: fundamental role of p38alpha in abrogating myoblast proliferation. *The EMBO journal,* 26**,** 1245-1256.

Peter, A. K., Cheng, H., Ross, R. S., Knowlton, K. U. & Chen, J. 2011. The costamere bridges sarcomeres to the sarcolemma in striated muscle. *Prog Pediatr Cardiol,* 31**,** 83-88.

Peter, J. B., Barnard, R. J., Edgerton, V. R., Gillespie, C. A. & Stempel, K. E. 1972. Metabolic profiles of three fiber types of skeletal muscle in guinea pigs and rabbits. *Biochemistry,* 11**,** 2627-33.

Pette, D. & Staron, R. S. 2000. Myosin isoforms, muscle fiber types, and transitions. *Microsc Res Tech,* 50**,** 500-9.

Pierson, C. R., Agrawal, P. B., Blasko, J. & Beggs, A. H. 2007. Myofiber size correlates with MTM1 mutation type and outcome in X-linked myotubular myopathy. *Neuromuscul Disord,* 17**,** 562-8.

Pinedo-Villanueva, R., Westbury, L. D., Syddall, H. E., Sanchez-Santos, M. T., Dennison, E. M., Robinson, S. M. & Cooper, C. 2019. Health Care Costs Associated With Muscle Weakness: A UK Population-Based Estimate. *Calcif Tissue Int,* 104**,** 137-144.

Porter, J. D., Merriam, A. P., Leahy, P., Gong, B. & Khanna, S. 2003. Dissection of temporal gene expression signatures of affected and spared muscle groups in dystrophin-deficient (mdx) mice. *Hum Mol Genet,* 12**,** 1813-21.

Porter, K. R. & Palade, G. E. 1957. Studies on the endoplasmic reticulum. III. Its form and distribution in striated muscle cells. *J Biophys Biochem Cytol,* 3**,** 269-300.

Porteus, M. H. & Carroll, D. 2005. Gene targeting using zinc finger nucleases. *Nature Biotechnology,* 23**,** 967-973.

Postlethwait, J. H., Woods, I. G., Ngo-Hazelett, P., Yan, Y. L., Kelly, P. D., Chu, F., Huang, H., Hill-Force, A. & Talbot, W. S. 2000. Zebrafish comparative genomics and the origins of vertebrate chromosomes. *Genome Res,* 10**,** 1890-902.

Pourghadamyari, H., Rezaei, M., Ipakchi-Azimi, A., Eisa-Beygi, S., Basiri, M., Tahamtani, Y. & Baharvand, H. 2019. Establishing a new animal model for muscle regeneration studies. *Mol Biol Res Commun,* 8**,** 171-179.

Poznyak, A. V., Nikiforov, N. G., Markin, A. M., Kashirskikh, D. A., Myasoedova, V. A., Gerasimova, E. V. & Orekhov, A. N. 2020. Overview of OxLDL and Its Impact on Cardiovascular Health: Focus on Atherosclerosis. *Front Pharmacol,* 11**,** 613780.

Purslow, P. P. 2020. The Structure and Role of Intramuscular Connective Tissue in Muscle Function. *Front Physiol,* 11**,** 495.

Quinlivan, R. M., Muller, C. R., Davis, M., Laing, N. G., Evans, G. A., Dwyer, J., Dove, J., Roberts, A. P. & Sewry, C. A. 2003. Central core disease: clinical, pathological, and genetic features. *Archives of Disease in Childhood,* 88**,** 1051.

Rabai, A., Reisser, L., Reina-San-Martin, B., Mamchaoui, K., Cowling, B. S., Nicot, A.-S. & Laporte, J. 2019. Allele-Specific CRISPR/Cas9 Correction of a Heterozygous DNM2 Mutation Rescues Centronuclear Myopathy Cell Phenotypes. *Molecular Therapy - Nucleic Acids,* 16**,** 246-256.

Radev, Z., Hermel, J. M., Elipot, Y., Bretaud, S., Arnould, S., Duchateau, P., Ruggiero, F., Joly, J. S. & Sohm, F. 2015. A TALEN-Exon Skipping Design for a Bethlem Myopathy Model in Zebrafish. *PLoS One,* 10**,** e0133986.

Radley, H. G. & Grounds, M. D. 2006. Cromolyn administration (to block mast cell degranulation) reduces necrosis of dystrophic muscle in mdx mice. *Neurobiology of Disease,* 23**,** 387-397.

Rafay, M. F., Halliday, W. & Bril, V. 2005. Hyaline Body Myopathy: Adulthood Manifestations. *Canadian Journal of Neurological Sciences / Journal Canadien des Sciences Neurologiques,* 32**,** 253-256.

Ramaswamy, K. S., Palmer, M. L., Van Der Meulen, J. H., Renoux, A., Kostrominova, T. Y., Michele, D. E. & Faulkner, J. A. 2011. Lateral transmission of force is impaired in skeletal muscles of dystrophic mice and very old rats. *J Physiol,* 589**,** 1195-208.

Ran, F. A., Hsu, P. D., Wright, J., Agarwala, V., Scott, D. A. & Zhang, F. 2013. Genome engineering using the CRISPR-Cas9 system. *Nature Protocols,* 8**,** 2281-2308.

Rasheed, K., Sethi, P. & Bixby, E. 2013. Severe vitamin d deficiency induced myopathy associated with rhabydomyolysis. *N Am J Med Sci,* 5**,** 334-6.

Ratnayake, D., Nguyen, P. D., Rossello, F. J., Wimmer, V. C., Tan, J. L., Galvis, L. A., Julier, Z., Wood, A. J., Boudier, T., Isiaku, A. I., Berger, S., Oorschot, V., Sonntag, C., Rogers, K. L., Marcelle, C., Lieschke, G. J., Martino, M. M., Bakkers, J. & Currie, P. D. 2021. Macrophages provide a transient muscle stem cell niche via NAMPT secretion. *Nature,* 591**,** 281-287.

Ravenscroft, G., Bryson-Richardson, R. J., Nowak, K. J. & Laing, N. G. 2018. Recent advances in understanding congenital myopathies. *F1000Res,* 7.

Rawls, A., Valdez, M. R., Zhang, W., Richardson, J., Klein, W. H. & Olson, E. N. 1998. Overlapping functions of the myogenic bHLH genes MRF4 and MyoD revealed in double mutant mice. *Development,* 125**,** 2349-2358.

Renshaw, S. A., Loynes, C. A., Trushell, D. M. I., Elworthy, S., Ingham, P. W. & Whyte, M. K. B. 2006. A transgenic zebrafish model of neutrophilic inflammation. *Blood,* 108**,** 3976-3978.

Reumers, S. F. I., Erasmus, C. E., Bouman, K., Pennings, M., Schouten, M., Kusters, B., Duijkers, F. a. M., Van Der Kooi, A., Jaeger, B., Verschuuren-Bemelmans, C. C., Faber, C. G., Van Engelen, B. G., Kamsteeg, E. J., Jungbluth, H. & Voermans, N. C. 2021. Clinical, genetic, and histological features of centronuclear myopathy in the Netherlands. *Clin Genet,* 100**,** 692-702.

Rexed, B. 1954. A cytoarchitectonic atlas of the spinal coed in the cat. *Journal of Comparative Neurology,* 100**,** 297-379.

Rhodes, S. J. & Konieczny, S. F. 1989. Identification of MRF4: a new member of the muscle regulatory factor gene family. *Genes Dev,* 3**,** 2050-61.

Riedl, J., Crevenna, A. H., Kessenbrock, K., Yu, J. H., Neukirchen, D., Bista, M., Bradke, F., Jenne, D., Holak, T. A., Werb, Z., Sixt, M. & Wedlich-Soldner, R. 2008. Lifeact: a versatile marker to visualize F-actin. *Nat Methods,* 5**,** 605-7.

Rief, M., Gautel, M., Oesterhelt, F., Fernandez, J. M. & Gaub, H. E. 1997. Reversible Unfolding of Individual Titin Immunoglobulin Domains by AFM. *Science,* 276**,** 1109-1112.

Rios, E. & Brum, G. 1987. Involvement of dihydropyridine receptors in excitation–contraction coupling in skeletal muscle. *Nature,* 325**,** 717-720.

Rivas-Pardo, J. A., Eckels, E. C., Popa, I., Kosuri, P., Linke, W. A. & Fernández, J. M. 2016. Work Done by Titin Protein Folding Assists Muscle Contraction. *Cell Rep,* 14**,** 1339-1347.

Robinson, K. S., Toh, G. A., Rozario, P., Chua, R., Bauernfried, S., Sun, Z., Firdaus, M. J., Bayat, S., Nadkarni, R., Poh, Z. S., Tham, K. C., Harapas, C. R., Lim, C. K., Chu, W., Tay, C. W. S., Tan, K. Y., Zhao, T., Bonnard, C., Sobota, R., Connolly, J. E., Common, J., Masters, S. L., Chen, K. W., Ho, L., Wu, B., Hornung, V. & Zhong, F. L. 2022. ZAKα-driven ribotoxic stress response activates the human NLRP1 inflammasome. *Science,* 377**,** 328-335.

Rochlin, K., Yu, S., Roy, S. & Baylies, M. K. 2010. Myoblast fusion: when it takes more to make one. *Dev Biol,* 341**,** 66-83.

Rodgers, K. & Mcvey, M. 2016. Error-Prone Repair of DNA Double-Strand Breaks. *Journal of cellular physiology,* 231**,** 15-24.

Romero, N. B., Lehtokari, V. L., Quijano-Roy, S., Monnier, N., Claeys, K. G., Carlier, R. Y., Pellegrini, N., Orlikowski, D., Barois, A., Laing, N. G., Lunardi, J., Fardeau, M., Pelin, K. & Wallgren-Pettersson, C. 2009. CORE-

ROD MYOPATHY CAUSED BY MUTATIONS IN THE NEBULIN GENE. *Neurology,* 73**,** 1159.

Romero, N. B., Monnier, N., Viollet, L., Cortey, A., Chevallay, M., Leroy, J. P., Lunardi, J. & Fardeau, M. 2003. Dominant and recessive central core disease associated with RYR1 mutations and fetal akinesia. *Brain,* 126**,** 2341-2349.

Rommel, C., Bodine, S. C., Clarke, B. A., Rossman, R., Nunez, L., Stitt, T. N., Yancopoulos, G. D. & Glass, D. J. 2001. Mediation of IGF-1-induced skeletal myotube hypertrophy by PI(3)K/Akt/mTOR and PI(3)K/Akt/GSK3 pathways. *Nature Cell Biology,* 3**,** 1009-1013.

Rosenblatt, J. D. & Parry, D. J. 1992. Gamma irradiation prevents compensatory hypertrophy of overloaded mouse extensor digitorum longus muscle. *Journal of Applied Physiology,* 73**,** 2538-2543.

Rossi, A., Kontarakis, Z., Gerri, C., Nolte, H., Hölper, S., Krüger, M. & Stainier, D. Y. R. 2015. Genetic compensation induced by deleterious mutations but not gene knockdowns. *Nature,* 524**,** 230-233.

Roux, J. & Robinson-Rechavi, M. 2011. Age-dependent gain of alternative splice forms and biased duplication explain the relation between splicing and duplication. *Genome Res,* 21**,** 357-63.

Roy, S., Wolff, C. & Ingham, P. W. 2001. The u-boot mutation identifies a Hedgehog-regulated myogenic switch for fiber-type diversification in the zebrafish embryo. *Genes Dev,* 15**,** 1563-76.

Rudnicki, M. A., Braun, T., Hinuma, S. & Jaenisch, R. 1992. Inactivation of MyoD in mice leads to up-regulation of the myogenic HLH gene Myf-5 and results in apparently normal muscle development. *Cell,* 71**,** 383-390.

Rudnicki, M. A., Schnegelsberg, P. N. J., Stead, R. H., Braun, T., Arnold, H.-H. & Jaenisch, R. 1993. MyoD or Myf-5 is required for the formation of skeletal muscle. *Cell,* 75**,** 1351-1359.

Ruggiero, L., Fiorillo, C., Gibertini, S., De Stefano, F., Manganelli, F., Iodice, R., Vitale, F., Zanotti, S., Galderisi, M., Mora, M. & Santoro, L. 2015. A rare mutation in MYH7 gene occurs with overlapping phenotype. *Biochemical and Biophysical Research Communications,* 457**,** 262-266.

Ruiz-Bonilla, V., Perdiguero, E., Gresh, L., Serrano, A. L., Zamora, M., Sousa-Victor, P., Jardí, M., Wagner, E. F. & Muñoz-Cánoves, P. 2008. Efficient adult skeletal muscle regeneration in mice deficient in p38beta, p38gamma and p38delta MAP kinases. *Cell Cycle,* 7**,** 2208-14.

Ruparelia, A. A., Mckaige, E. A., Williams, C., Schulze, K. E., Fuchs, M., Oorschot, V., Lacene, E., Meregalli, M., Lee, C., Serrano, R. J., Baxter, E. C., Monro, K., Torrente, Y., Ramm, G., Stojkovic, T., Lavoie, J. N. & Bryson-Richardson, R. J. 2021. Metformin rescues muscle function in BAG3 myofibrillar myopathy models. *Autophagy,* 17**,** 2494-2510.

Ruparelia, A. A., Zhao, M., Currie, P. D. & Bryson-Richardson, R. J. 2012. Characterization and investigation of zebrafish models of filamin-related myofibrillar myopathy. *Human Molecular Genetics,* 21**,** 4073-4083.

Ryan, M. M., Schnell, C., Strickland, C. D., Shield, L. K., Morgan, G., Iannaccone, S. T., Laing, N. G., Beggs, A. H. & North, K. N. 2001. Nemaline myopathy: a clinical study of 143 cases. *Ann Neurol,* 50**,** 312-20.

Sabha, N., Volpatti, J. R., Gonorazky, H., Reifler, A., Davidson, A. E., Li, X., Eltayeb, N. M., Dall'armi, C., Di Paolo, G., Brooks, S. V., Buj-Bello, A., Feldman, E. L. & Dowling, J. J. 2016. PIK3C2B inhibition improves function and prolongs survival in myotubular myopathy animal models. *The Journal of Clinical Investigation,* 126**,** 3613-3625.

Sabourin, L. A. & Rudnicki, M. A. 2000. The molecular regulation of myogenesis. *Clinical Genetics,* 57**,** 16-25.

Sagar, S., Liu, P. P. & Cooper, L. T. 2012. Myocarditis. *The Lancet,* 379**,** 738-747.

Saint-Amant, L. & Drapeau, P. 1998. Time course of the development of motor behaviors in the zebrafish embryo. *Journal of neurobiology,* 37 4**,** 622-32.

Salpeter, M. M. & Harris, R. 1983. Distribution and turnover rate of acetylcholine receptors throughout the junction folds at a vertebrate neuromuscular junction. *J Cell Biol,* 96**,** 1781-5.

Sam, C. & Bordoni, B. 2022. Physiology, Acetylcholine. *StatPearls.* Treasure Island (FL): StatPearls Publishing

.

Sambasivan, R., Yao, R., Kissenpfennig, A., Van Wittenberghe, L., Paldi, A., Gayraud-Morel, B., Guenou, H., Malissen, B., Tajbakhsh, S. & Galy, A. 2011. Pax7-expressing satellite cells are indispensable for adult skeletal muscle regeneration. *Development,* 138**,** 3647-3656.

Sandri, M., Sandri, C., Gilbert, A., Skurk, C., Calabria, E., Picard, A., Walsh, K., Schiaffino, S., Lecker, S. H. & Goldberg, A. L. 2004. Foxo transcription factors induce the atrophy-related ubiquitin ligase atrogin-1 and cause skeletal muscle atrophy. *Cell,* 117**,** 399-412.

Sanoudou, D. & Beggs, A. H. 2001. Clinical and genetic heterogeneity in nemaline myopathy – a disease of skeletal muscle thin filaments. *Trends in Molecular Medicine,* 7**,** 362-368.

Santoriello, C. & Zon, L. I. 2012. Hooked! Modeling human disease in zebrafish. *J Clin Invest,* 122**,** 2337-43.

Santos, D. P., Kiskinis, E., Eggan, K. & Merkle, F. T. 2016a. Comprehensive Protocols for CRISPR/Cas9-based Gene Editing in Human Pluripotent Stem Cells. *Current protocols in stem cell biology,* 38**,** 5B.6.1-5B.6.60.

Santos, D. P., Kiskinis, E., Eggan, K. & Merkle, F. T. 2016b. Comprehensive Protocols for CRISPR/Cas9-based Gene Editing in Human Pluripotent Stem Cells. *Curr Protoc Stem Cell Biol,* 38**,** 5b.6.1-5b.6.60.

Savage, A. M., Kurusamy, S., Chen, Y., Jiang, Z., Chhabria, K., Macdonald, R. B., Kim, H. R., Wilson, H. L., Van Eeden, F. J. M., Armesilla, A. L., Chico, T. J. A. & Wilkinson, R. N. 2019. tmem33 is essential for VEGF-mediated endothelial calcium oscillations and angiogenesis. *Nature Communications,* 10**,** 732.

Scacheri, P. C., Hoffman, E. P., Fratkin, J. D., Semino–Mora, C., Senchak, A., Davis, M. R., Laing, N. G., Vedanarayanan, V. & Subramony, S. H. 2000. A novel ryanodine receptor gene mutation causing both cores and rods in congenital myopathy. *Neurology,* 55**,** 1689.

Scarpini, G., Valentino, M. L., Giannotta, M., Ragni, L., Torella, A., Columbaro, M., Nigro, V. & Pini, A. 2021. BAG3-related myofibrillar myopathy: a further observation with cardiomyopathy at onset in pediatric age. *Acta Myol,* 40**,** 177-183.

Schessl, J., Medne, L., Hu, Y., Zou, Y., Brown, M. J., Huse, J. T., Torigian, D. A., Jungbluth, H., Goebel, H.-H. & Bönnemann, C. G. 2007. MRI in DNM2-related centronuclear myopathy: Evidence for highly selective muscle involvement. *Neuromuscular Disorders,* 17**,** 28-32.

Schiavo, G., Matteoli, M. & Montecucco, C. 2000. Neurotoxins Affecting Neuroexocytosis. *Physiological Reviews,* 80**,** 717-766.

Schleip, R., Findley, T. W., Chaitow, L. & Huijing, P. 2021. *Fascia: The Tensional Network of the Human Body - E-Book: The science and clinical applications in manual and movement therapy*, Elsevier Health Sciences.

Schmalbruch, H. 1974. The sarcolemma of skeletal muscle fibres as demonstrated by a replica technique. *Cell Tissue Res,* 150**,** 377-87.

Schmalbruch, H. 1976. The morphology of regeneration of skeletal muscles in the rat. *Tissue and Cell,* 8**,** 673-692.

Schneider, M. F. & Chandler, W. K. 1973. Voltage Dependent Charge Movement in Skeletal Muscle: a Possible Step in Excitation–Contraction Coupling. *Nature,* 242**,** 244-246.

Schoenauer, R., Bertoncini, P., Machaidze, G., Aebi, U., Perriard, J.-C., Hegner, M. & Agarkova, I. 2005. Myomesin is a Molecular Spring with Adaptable Elasticity. *Journal of Molecular Biology,* 349**,** 367-379.

Schoenauer, R., Lange, S., Hirschy, A., Ehler, E., Perriard, J. C. & Agarkova, I. 2008. Myomesin 3, a novel structural component of the M-band in striated muscle. *J Mol Biol,* 376**,** 338-51.

Schuermann, A., Helker, C. S. M. & Herzog, W. 2015. Metallothionein 2 regulates endothelial cell migration through transcriptional regulation of vegfc expression. *Angiogenesis,* 18**,** 463-475.

Schultz, E., Gibson, M. C. & Champion, T. 1978. Satellite cells are mitotically quiescent in mature mouse muscle: an EM and radioautographic study. *J Exp Zool,* 206**,** 451-6.

Schwander, M., Leu, M., Stumm, M., Dorchies, O. M., Ruegg, U. T., Schittny, J. & Müller, U. 2003. β1 Integrins Regulate Myoblast Fusion and Sarcomere Assembly. *Developmental Cell,* 4**,** 673-685.

Scoto, M., Cullup, T., Cirak, S., Yau, S., Manzur, A. Y., Feng, L., Jacques, T. S., Anderson, G., Abbs, S., Sewry, C., Jungbluth, H. & Muntoni, F. 2013. Nebulin (NEB) mutations in a childhood onset distal myopathy with rods and cores uncovered by next generation sequencing. *European Journal of Human Genetics,* 21**,** 1249-1252.

Scott, W., Stevens, J. & Binder–Macleod, S. A. 2001. Human Skeletal Muscle Fiber Type Classifications. *Physical Therapy,* 81**,** 1810-1816.

Seale, P., Sabourin, L. A., Girgis-Gabardo, A., Mansouri, A., Gruss, P. & Rudnicki, M. A. 2000. Pax7 Is Required for the Specification of Myogenic Satellite Cells. *Cell,* 102**,** 777-786.

Seebacher, F. & James, R. S. 2019. Increased physical activity does not improve obesity-induced decreases in muscle quality in zebrafish (Danio rerio). *J Appl Physiol (1985),* 127**,** 1802-1808.

Segalés, J., Perdiguero, E. & Muñoz-Cánoves, P. 2016. Regulation of Muscle Stem Cell Functions: A Focus on the p38 MAPK Signaling Pathway. *Front Cell Dev Biol,* 4**,** 91.

Sei, Y., Sambuughin, Nyamkhishig n., Davis, Edward j., Sachs, D., Cuenca, Phil b., Brandom, Barbara w., Tautz, T., Rosenberg, H., Nelson, Thomas e. & Muldoon, Sheila m. 2004. Malignant Hyperthermia in North America: Genetic Screening of the Three Hot Spots in the Type I Ryanodine Receptor Gene. *Anesthesiology,* 101**,** 824-830.

Selcen, D. 2011. Myofibrillar myopathies. *Neuromuscul Disord,* 21**,** 161-71.

Selcen, D., Muntoni, F., Burton, B. K., Pegoraro, E., Sewry, C., Bite, A. V. & Engel, A. G. 2009. Mutation in BAG3 causes severe dominant childhood muscular dystrophy. *Annals of Neurology,* 65**,** 83-89.

Selders, G. S., Fetz, A. E., Radic, M. Z. & Bowlin, G. L. 2017. An overview of the role of neutrophils in innate immunity, inflammation and host-biomaterial integration. *Regen Biomater,* 4**,** 55-68.

Serrano, N., Colenso-Semple, L. M., Lazauskus, K. K., Siu, J. W., Bagley, J. R., Lockie, R. G., Costa, P. B. & Galpin, A. J. 2019. Extraordinary fast-twitch fiber abundance in elite weightlifters. *PLoS One,* 14**,** e0207975.

Sewry, C. A., Laitila, J. M. & Wallgren-Pettersson, C. 2019. Nemaline myopathies: a current view. *J Muscle Res Cell Motil,* 40**,** 111-126.

Shang, E. H., Yu, R. M. & Wu, R. S. 2006. Hypoxia affects sex differentiation and development, leading to a male-dominated population in zebrafish (Danio rerio). *Environ Sci Technol,* 40**,** 3118-22.

Sharp, N. J., Kornegay, J. N., Van Camp, S. D., Herbstreith, M. H., Secore, S. L., Kettle, S., Hung, W. Y., Constantinou, C. D., Dykstra, M. J., Roses, A. D. & Et Al. 1992. An error in dystrophin mRNA processing in golden retriever muscular dystrophy, an animal homologue of Duchenne muscular dystrophy. *Genomics,* 13**,** 115-21.

Shatunov, A., Olivé, M., Odgerel, Z., Stadelmann-Nessler, C., Irlbacher, K., Van Landeghem, F., Bayarsaikhan, M., Lee, H.-S., Goudeau, B., Chinnery, P. F., Straub, V., Hilton-Jones, D., Damian, M. S., Kaminska, A., Vicart, P., Bushby, K., Dalakas, M. C., Sambuughin, N., Ferrer, I., Goebel, H. H. & Goldfarb, L. G. 2009. In-frame deletion in the seventh immunoglobulin-like repeat of filamin C in a family with myofibrillar myopathy. *European Journal of Human Genetics,* 17**,** 656-663.

Shenkman, B. S. 2016. From Slow to Fast: Hypogravity-Induced Remodeling of Muscle Fiber Myosin Phenotype. *Acta Naturae,* 8**,** 47-59.

Shi, H., Scheffler, J. M., Zeng, C., Pleitner, J. M., Hannon, K. M., Grant, A. L. & Gerrard, D. E. 2009. Mitogen-activated protein kinase signaling is necessary for the maintenance of skeletal muscle mass. *American Journal of Physiology-Cell Physiology,* 296**,** C1040-C1048.

Shichiji, M., Biancalana, V., Fardeau, M., Hogrel, J. Y., Osawa, M., Laporte, J. & Romero, N. B. 2013. Extensive morphological and immunohistochemical characterization in myotubular myopathy. *Brain Behav,* 3**,** 476-86.

Shilagardi, K., Li, S., Luo, F., Marikar, F., Duan, R., Jin, P., Kim, J. H., Murnen, K. & Chen, E. H. 2013. Actin-propelled invasive membrane protrusions promote fusogenic protein engagement during cell-cell fusion. *Science,* 340**,** 359-63.

Shimomura, C. & Nonaka, I. 1989. Nemaline myopathy: Comparative muscle histochemistry in the severe neonatal, moderate congenital, and adult-onset forms. *Pediatric Neurology,* 5**,** 25-31.

Shingde, M. V., Spring, P. J., Maxwell, A., Wills, E. J., Harper, C. G., Dye, D. E., Laing, N. G. & North, K. N. 2006. Myosin storage (hyaline body) myopathy: A case report. *Neuromuscular Disorders,* 16**,** 882-886.

Shy, G. M., Engel, W. K., Somers, J. E. & Wanko, T. 1963. NEMALINE MYOPATHY. A NEW CONGENITAL MYOPATHY. *Brain,* 86**,** 793-810.

Sicinski, P., Geng, Y., Ryder-Cook, A. S., Barnard, E. A., Darlison, M. G. & Barnard, P. J. 1989. The molecular basis of muscular dystrophy in the mdx mouse: a point mutation. *Science,* 244**,** 1578-80.

Sidhu, S. & Marine, J. E. 2020. Evaluating and managing bradycardia. *Trends in Cardiovascular Medicine,* 30**,** 265-272.

Sidow, A. 1996. Gen(om)e duplications in the evolution of early vertebrates. *Current Opinion in Genetics & Development,* 6**,** 715-722.

Silva, J., Alkan, F., Ramalho, S., Snieckute, G., Prekovic, S., Garcia, A. K., Hernández-Pérez, S., Van Der Kammen, R., Barnum, D., Hoekman, L., Altelaar, M., Zwart, W., Suijkerbuijk, S. J. E., Bekker-Jensen, S. & Faller, W. J. 2022. Ribosome impairment regulates intestinal stem cell identity via ZAKα activation. *Nature Communications,* 13**,** 4492.

Simeone, A., Daga, A. & Calabi, F. 1995. Expression of runt in the mouse embryo. *Dev Dyn,* 203**,** 61-70.

Skobo, T., Benato, F., Grumati, P., Meneghetti, G., Cianfanelli, V., Castagnaro, S., Chrisam, M., Di Bartolomeo, S., Bonaldo, P., Cecconi, F. & Valle, L. D. 2014. Zebrafish ambra1a and ambra1b Knockdown Impairs Skeletal Muscle Development. *PLOS ONE,* 9**,** e99210.

Slater, C. R. 2017. The Structure of Human Neuromuscular Junctions: Some Unanswered Molecular Questions. *Int J Mol Sci,* 18.

Smith, L., Fabian, L., Al-Maawali, A., Noche, R. R., Dowling, J. J. & Dowling, J. J. 2020. De novo phosphoinositide synthesis in zebrafish is required for triad formation but not essential for myogenesis. *PLoS One,* 15**,** e0231364.

Snieckute, G., Genzor, A. V., Vind, A. C., Ryder, L., Stoneley, M., Chamois, S., Dreos, R., Nordgaard, C., Sass, F., Blasius, M., López, A. R., Brynjólfsdóttir, S. H., Andersen, K. L., Willis, A. E., Frankel, L. B., Poulsen, S. S., Gatfield, D., Gerhart-Hines, Z., Clemmensen, C. & Bekker-Jensen, S. 2022. Ribosome stalling is a signal for metabolic regulation by the ribotoxic stress response. *Cell Metab,* 34**,** 2036-2046.e8.

Snijders, T., Nederveen, J. P., Mckay, B. R., Joanisse, S., Verdijk, L. B., Van Loon, L. J. C. & Parise, G. 2015. Satellite cells in human skeletal muscle plasticity. *Frontiers in Physiology,* 6.

Söllner, T., Bennett, M. K., Whiteheart, S. W., Scheller, R. H. & Rothman, J. E. 1993. A protein assembly-disassembly pathway in vitro that may correspond to sequential steps of synaptic vesicle docking, activation, and fusion. *Cell,* 75**,** 409-418.

Soukup, S. W. 1974. Evolution by gene duplication. S. Ohno. Springer-Verlag, New York. 1970. 160 pp. *Teratology,* 9**,** 250-251.

Spielmann, M., Kakar, N., Tayebi, N., Leettola, C., Nürnberg, G., Sowada, N., Lupiáñez, D. G., Harabula, I., Flöttmann, R., Horn, D., Chan, W. L., Wittler, L., Yilmaz, R., Altmüller, J., Thiele, H., Van Bokhoven, H., Schwartz, C. E., Nürnberg, P., Bowie, J. U., Ahmad, J., Kubisch, C., Mundlos, S. & Borck, G. 2016. Exome sequencing and CRISPR/Cas genome editing identify mutations of ZAK as a cause of limb defects in humans and mice. *Genome Res,* 26**,** 183-91.

Spiro, A. J., Shy, G. M. & Gontas, N. K. 1966. Myotubular Myopathy: Persistence of Fetal Muscle in an Adolescent Boy. *Archives of Neurology,* 14**,** 1-14.

Spudich, J. A. 2001. The myosin swinging cross-bridge model. *Nat Rev Mol Cell Biol,* 2**,** 387-92.

Steffen, L. S., Guyon, J. R., Vogel, E. D., Howell, M. H., Zhou, Y., Weber, G. J., Zon, L. I. & Kunkel, L. M. 2007. The zebrafish runzel muscular dystrophy is linked to the titin gene. *Dev Biol,* 309**,** 180-92.

Stickney, H. L., Barresi, M. J. F. & Devoto, S. H. 2000. Somite development in zebrafish. *Developmental Dynamics,* 219**,** 287-303.

Stifani, N. 2014a. Motor neurons and the generation of spinal motor neuron diversity. *Front Cell Neurosci,* 8**,** 293.

Stifani, N. 2014b. Motor neurons and the generation of spinal motor neurons diversity. *Frontiers in Cellular Neuroscience,* 8.

Story, B. D., Miller, M. E., Bradbury, A. M., Million, E. D., Duan, D., Taghian, T., Faissler, D., Fernau, D., Beecy, S. J. & Gray-Edwards, H. L. 2020. Canine Models of Inherited Musculoskeletal and Neurodegenerative Diseases. *Front Vet Sci,* 7**,** 80.

Straussberg, R., Schottmann, G., Sadeh, M., Gill, E., Seifert, F., Halevy, A., Qassem, K., Rendu, J., Van Der Ven, P. F. M., Stenzel, W. & Schuelke, M. 2016. Kyphoscoliosis peptidase (KY) mutation causes a novel congenital myopathy with core targetoid defects. *Acta Neuropathologica,* 132**,** 475-478.

Street, S. F. 1983. Lateral transmission of tension in frog myofibers: a myofibrillar network and transverse cytoskeletal connections are possible transmitters. *J Cell Physiol,* 114**,** 346-64.

Su, Z., Wang, J., Yu, J., Huang, X. & Gu, X. 2006. Evolution of alternative splicing after gene duplication. *Genome Res,* 16**,** 182-9.

Sunagawa, Genshiro a., Sumiyama, K., Ukai-Tadenuma, M., Perrin, D., Fujishima, H., Ukai, H., Nishimura, O., Shi, S., Ohno, R.-I., Narumi, R., Shimizu, Y., Tone, D., Ode, Koji l., Kuraku, S. & Ueda, Hiroki r. 2016. Mammalian Reverse Genetics without Crossing Reveals Nr3a as a Short-Sleeper Gene. *Cell Reports,* 14**,** 662-677.

Suzuki, T., Kusakabe, M., Nakayama, K. & Nishida, E. 2012. The protein kinase MLTK regulates chondrogenesis by inducing the transcription factor Sox6. *Development,* 139**,** 2988.

Sztal, T. E., Zhao, M., Williams, C., Oorschot, V., Parslow, A. C., Giousoh, A., Yuen, M., Hall, T. E., Costin, A., Ramm, G., Bird, P. I., Busch-Nentwich, E. M., Stemple, D. L., Currie, P. D., Cooper, S. T., Laing, N. G., Nowak, K. J. & Bryson-Richardson, R. J. 2015. Zebrafish models for nemaline myopathy reveal a spectrum of nemaline bodies contributing to reduced muscle function. *Acta Neuropathol,* 130**,** 389-406.

Sztretye, M., Szabó, L., Dobrosi, N., Fodor, J., Szentesi, P., Almássy, J., Magyar, Z. É., Dienes, B. & Csernoch, L. 2020. From Mice to Humans: An Overview of the Potentials and Limitations of Current Transgenic Mouse Models of

Major Muscular Dystrophies and Congenital Myopathies. *International Journal of Molecular Sciences,* 21**,** 8935.

Tagliavini, F., Sardone, F., Squarzoni, S., Maraldi, N. M., Merlini, L., Faldini, C. & Sabatelli, P. 2013. Ultrastructural changes in muscle cells of patients with collagen VI-related myopathies. *Muscles, ligaments and tendons journal* [Online], 3. [Accessed 2013/10//].

Tajsharghi, H., Oldfors, A., Macleod, D. P. & Swash, M. 2007. Homozygous mutation in MYH7 in myosin storage myopathy and cardiomyopathy. *Neurology,* 68**,** 962.

Tajsharghi, H., Thornell, L.-E., Lindberg, C., Lindvall, B., Henriksson, K.-G. & Oldfors, A. 2003. Myosin storage myopathy associated with a heterozygous missense mutation in MYH7. *Annals of Neurology,* 54**,** 494-500.

Takafuta, T., Wu, G., Murphy, G. F. & Shapiro, S. S. 1998. Human β-Filamin Is a New Protein That Interacts with the Cytoplasmic Tail of Glycoprotein Ibα*. *Journal of Biological Chemistry,* 273**,** 17531-17538.

Takahashi, K. & Hattori, A. 1989. Alpha-actinin is a component of the Z-filament, a structural backbone of skeletal muscle Z-disks. *J Biochem,* 105**,** 529-36.

Talbot, J. & Maves, L. 2016. Skeletal muscle fiber type: using insights from muscle developmental biology to dissect targets for susceptibility and resistance to muscle disease. *Wiley Interdiscip Rev Dev Biol,* 5**,** 518-34.

Tan, J., Kuang, W., Jin, Z., Jin, F., Xu, L., Yu, Q., Kong, L., Zeng, G., Yuan, X. & Duan, Y. 2009. Inhibition of NFkappaB by activated c-Jun NH2 terminal kinase 1 acts as a switch for C2C12 cell death under excessive stretch. *Apoptosis,* 14**,** 764-70.

Tanjore, R., Rangaraju, A., Vadapalli, S., Remersu, S., Narsimhan, C. & Nallari, P. 2010. Genetic variations of β-MYH7 in hypertrophic cardiomyopathy and dilated cardiomyopathy. *Indian J Hum Genet,* 16**,** 67-71.

Tanner, S. M., Laporte, J., Guiraud-Chaumeil, C. & Liechti-Gallati, S. 1998. Confirmation of prenatal diagnosis results of X-linked recessive myotubular myopathy by mutational screening, and description of three new mutations in the MTM1 gene. *Hum Mutat,* 11**,** 62-8.

Taylor, J. S., Braasch, I., Frickey, T., Meyer, A. & Van De Peer, Y. 2003. Genome duplication, a trait shared by 22000 species of ray-finned fish. *Genome Res,* 13**,** 382-90.

Taylor., A. W., Essén, B. & Saltin, B. 1974. Myosin ATPase in Skeletal Muscle of Healthy Men. *Acta Physiologica Scandinavica,* 91**,** 568-570.

Teixeira, C. F. P., Zamunér, S. R., Zuliani, J. P., Fernandes, C. M., Cruz-Hofling, M. A., Fernandes, I., Chaves, F. & Gutiérrez, J. M. 2003. Neutrophils do not contribute to local tissue damage, but play a key role in skeletal muscle regeneration, in mice injected with Bothrops asper snake venom. *Muscle & Nerve,* 28**,** 449-459.

Telfer, W. R., Nelson, D. D., Waugh, T., Brooks, S. V. & Dowling, J. J. 2012. Neb: a zebrafish model of nemaline myopathy due to nebulin mutation. *Dis Model Mech,* 5**,** 389-96.

Terrill, J. R., Duong, M. N., Turner, R., Le Guiner, C., Boyatzis, A., Kettle, A. J., Grounds, M. D. & Arthur, P. G. 2016. Levels of inflammation and oxidative stress, and a role for taurine in dystropathology of the Golden Retriever Muscular Dystrophy dog model for Duchenne Muscular Dystrophy. *Redox Biology,* 9**,** 276-286.

Theadom, A., Rodrigues, M., Poke, G., O'grady, G., Love, D., Hammond-Tooke, G., Parmar, P., Baker, R., Feigin, V., Jones, K., Te Ao, B., Ranta, A. & Roxburgh, R. 2019. A Nationwide, Population-Based Prevalence Study of Genetic Muscle Disorders. *Neuroepidemiology,* 52**,** 128-135.

Thompson, T. G., Chan, Y. M., Hack, A. A., Brosius, M., Rajala, M., Lidov, H. G., Mcnally, E. M., Watkins, S. & Kunkel, L. M. 2000. Filamin 2 (FLN2): A muscle-specific sarcoglycan interacting protein. *J Cell Biol,* 148**,** 115-26.

Tilgen, N., Zorzato, F., Halliger-Keller, B., Muntoni, F., Sewry, C., Palmucci, L. M., Schneider, C., Hauser, E., Lehmann-Horn, F., Müller, C. R. & Treves, S. 2001. Identification of four novel mutations in the C-terminal membrane spanning domain of the ryanodine receptor 1: association with central core disease and alteration of calcium homeostasis. *Human Molecular Genetics,* 10**,** 2879-2887.

Tonelotto, V., Consorti, C., Facchinello, N., Trapani, V., Sabatelli, P., Giraudo, C., Spizzotin, M., Cescon, M., Bertolucci, C. & Bonaldo, P. 2022. Collagen VI ablation in zebrafish causes neuromuscular defects during developmental and adult stages. *Matrix Biology,* 112**,** 39-61.

Tonino, P., Kiss, B., Strom, J., Methawasin, M., Smith, J. E., Kolb, J., Labeit, S. & Granzier, H. 2017. The giant protein titin regulates the length of the striated muscle thick filament. *Nature Communications,* 8**,** 1041.

Tonino, P., Pappas, C. T., Hudson, B. D., Labeit, S., Gregorio, C. C. & Granzier, H. 2010. Reduced myofibrillar connectivity and increased Z-disk width in nebulin-deficient skeletal muscle. *J Cell Sci,* 123**,** 384-91.

Topaloglu, H. 2020. Core myopathies - a short review. *Acta Myol,* 39**,** 266-273.

Tosti, E., Waldbaum, L., Warshaw, G., Gross, E. A. & Ruggieri, R. 2004. The stress kinase MRK contributes to regulation of DNA damage checkpoints through a p38gamma-independent pathway. *J Biol Chem,* 279**,** 47652-60.

Toyoshima, Y. Y., Kron, S. J., Mcnally, E. M., Niebling, K. R., Toyoshima, C. & Spudich, J. A. 1987. Myosin subfragment-1 is sufficient to move actin filaments in vitro. *Nature,* 328**,** 536-539.

Tskhovrebova, L., Trinick, J., Sleep, J. A. & Simmons, R. M. 1997. Elasticity and unfolding of single molecules of the giant muscle protein titin. *Nature,* 387**,** 308-312.

Tumaneng, K., Schlegelmilch, K., Russell, R. C., Yimlamai, D., Basnet, H., Mahadevan, N., Fitamant, J., Bardeesy, N., Camargo, F. D. & Guan, K. L. 2012. YAP mediates crosstalk between the Hippo and PI(3)K–TOR pathways by suppressing PTEN via miR-29. *Nat Cell Biol,* 14**,** 1322-9.

Turko, A. J., Kültz, D., Fudge, D., Croll, R. P., Smith, F. M., Stoyek, M. R. & Wright, P. A. 2017. Skeletal stiffening in an amphibious fish out of water is a response to increased body weight. *Journal of Experimental Biology,* 220**,** 3621-3631.

Uchida, D., Yamashita, M., Kitano, T. & Iguchi, T. 2004. An aromatase inhibitor or high water temperature induce oocyte apoptosis and depletion of P450 aromatase activity in the gonads of genetic female zebrafish during sex-reversal. *Comp Biochem Physiol A Mol Integr Physiol,* 137**,** 11-20.

Ulbricht, A., Eppler, F. J., Tapia, V. E., Van Der Ven, P. F., Hampe, N., Hersch, N., Vakeel, P., Stadel, D., Haas, A., Saftig, P., Behrends, C., Fürst, D. O., Volkmer, R., Hoffmann, B., Kolanus, W. & Höhfeld, J. 2013. Cellular mechanotransduction relies on tension-induced and chaperone-assisted autophagy. *Curr Biol,* 23**,** 430-5.

Umansky, K. B., Gruenbaum-Cohen, Y., Tsoory, M., Feldmesser, E., Goldenberg, D., Brenner, O. & Groner, Y. 2015. Runx1 Transcription Factor Is Required for Myoblasts Proliferation during Muscle Regeneration. *PLoS genetics,* 11**,** e1005457-e1005457.

Valenzano, Dario r., Benayoun, Bérénice a., Singh, Param p., Zhang, E., Etter, Paul d., Hu, C.-K., Clément-Ziza, M., Willemsen, D., Cui, R., Harel, I., Machado, Ben e., Yee, M.-C., Sharp, Sabrina c., Bustamante, Carlos d., Beyer, A., Johnson, Eric a. & Brunet, A. 2015. The African Turquoise Killifish Genome Provides Insights into Evolution and Genetic Architecture of Lifespan. *Cell,* 163**,** 1539-1554.

Valenzano, D. R., Terzibasi, E., Genade, T., Cattaneo, A., Domenici, L. & Cellerino, A. 2006. Resveratrol Prolongs Lifespan and Retards the Onset of Age-Related Markers in a Short-Lived Vertebrate. *Current Biology,* 16**,** 296-300.

Valiyil, R. & Christopher-Stine, L. 2010. Drug-related myopathies of which the clinician should be aware. *Curr Rheumatol Rep,* 12**,** 213-20.

Van Der Pijl, R., Strom, J., Conijn, S., Lindqvist, J., Labeit, S., Granzier, H. & Ottenheijm, C. 2018. Titin-based mechanosensing modulates muscle hypertrophy. *J Cachexia Sarcopenia Muscle,* 9**,** 947-961.

Van Der Ven, P. F. M., Obermann, W. M. J., Lemke, B., Gautel, M., Weber, K. & Fürst, D. O. 2000. Characterization of muscle filamin isoforms suggests a possible role of gamma-filamin/ABP-L in sarcomeric Z-disc formation. *Cell motility and the cytoskeleton,* 45 2**,** 149-62.

Van Putten, M., Lloyd, E. M., De Greef, J. C., Raz, V., Willmann, R. & Grounds, M. D. 2020. Mouse models for muscular dystrophies: an overview. *Dis Model Mech,* 13.

Van Raamsdonk, W., Van't Veer, L., Veeken, K., Heyting, C. & Pool, C. W. 1982. Differentiation of muscle fiber types in the teleost Brachydanio rerio, the zebrafish. *Anatomy and Embryology,* 164**,** 51-62.

Van Rooijen, E., Fazio, M. & Zon, L. I. 2017. From fish bowl to bedside: The power of zebrafish to unravel melanoma pathogenesis and discover new therapeutics. *Pigment Cell & Melanoma Research,* 30**,** 402-412.

Vasli, N., Harris, E., Karamchandani, J., Bareke, E., Majewski, J., Romero, N. B., Stojkovic, T., Barresi, R., Tasfaout, H., Charlton, R., Malfatti, E., Bohm, J., Marini-Bettolo, C., Choquet, K., Dicaire, M. J., Shao, Y. H., Topf, A., O'ferrall, E., Eymard, B., Straub, V., Blanco, G., Lochmüller, H., Brais, B., Laporte, J. & Tétreault, M. 2017. Recessive mutations in the kinase ZAK cause a congenital myopathy with fibre type disproportion. *Brain,* 140**,** 37-48.

Velleman, S. G. & Mcfarland, D. C. 2015. Chapter 16 - Skeletal Muscle. *In:* SCANES, C. G. (ed.) *Sturkie's Avian Physiology (Sixth Edition).* San Diego: Academic Press.

Venereau, E., Casalgrandi, M., Schiraldi, M., Antoine, D. J., Cattaneo, A., De Marchis, F., Liu, J., Antonelli, A., Preti, A., Raeli, L., Shams, S. S., Yang, H., Varani, L., Andersson, U., Tracey, K. J., Bachi, A., Uguccioni, M. & Bianchi, M. E. 2012. Mutually exclusive redox forms of HMGB1 promote cell recruitment or proinflammatory cytokine release. *Journal of Experimental Medicine,* 209**,** 1519-1528.

Verdijk, L. B., Koopman, R., Schaart, G., Meijer, K., Savelberg, H. H. C. M. & Loon, L. J. C. V. 2007. Satellite cell content is specifically reduced in type II skeletal muscle fibers in the elderly. *American Journal of Physiology-Endocrinology and Metabolism,* 292**,** E151-E157.

Verdonschot, J. a. J., Vanhoutte, E. K., Claes, G. R. F., Helderman-Van Den Enden, A. T. J. M., Hoeijmakers, J. G. J., Hellebrekers, D. M. E. I., De Haan, A., Christiaans, I., Lekanne Deprez, R. H., Boen, H. M., Van Craenenbroeck, E. M., Loeys, B. L., Hoedemaekers, Y. M., Marcelis, C., Kempers, M., Brusse, E., Van Waning, J. I., Baas, A. F., Dooijes, D., Asselbergs, F. W., Barge-Schaapveld, D. Q. C. M., Koopman, P., Van Den Wijngaard, A., Heymans, S. R. B., Krapels, I. P. C. & Brunner, H. G. 2020. A mutation update for the FLNC gene in myopathies and cardiomyopathies. *Human Mutation,* 41**,** 1091-1111.

Vind, A. C., Snieckute, G., Blasius, M., Tiedje, C., Krogh, N., Bekker-Jensen, D. B., Andersen, K. L., Nordgaard, C., Tollenaere, M. a. X., Lund, A. H., Olsen, J. V., Nielsen, H. & Bekker-Jensen, S. 2020. ZAKα Recognizes Stalled Ribosomes through Partially Redundant Sensor Domains. *Mol Cell*.

Viswanathan, M. C., Tham, R. C., Kronert, W. A., Sarsoza, F., Trujillo, A. S., Cammarato, A. & Bernstein, S. I. 2017. Myosin storage myopathy mutations yield defective myosin filament assembly in vitro and disrupted myofibrillar structure and function in vivo. *Human Molecular Genetics,* 26**,** 4799-4813.

Vry, J., Gramsch, K., Rodger, S., Thompson, R., Steffensen, B. F., Rahbek, J., Doerken, S., Tassoni, A., Beytía, M. D. L. A., Guergueltcheva, V., Chamova, T., Tournev, I., Kostera-Pruszczyk, A., Kaminska, A., Lusakowska, A., Mrazova, L., Pavlovska, L., Strenkova, J., Vondráček, P., Garami, M., Karcagi, V., Herczegfalvi, Á., Bushby, K., Lochmüller, H. & Kirschner, J. 2016. European Cross-Sectional Survey of Current Care Practices for Duchenne Muscular Dystrophy Reveals Regional and Age-Dependent Differences. *Journal of Neuromuscular Diseases,* 3**,** 517-527.

Wakamatsu, Y., Ogino, K. & Hirata, H. 2019. Swimming capability of zebrafish is governed by water temperature, caudal fin length and genetic background. *Scientific Reports,* 9**,** 16307.

Wallgren-Pettersson, C. & Laing, N. G. 2000. Report of the 70th ENMC International Workshop: nemaline myopathy, 11-13 June 1999, Naarden, The Netherlands. *Neuromuscul Disord,* 10**,** 299-306.

Walston, J. D. 2012. Sarcopenia in older adults. *Curr Opin Rheumatol,* 24**,** 623-7.

Wang, C. H., Dowling, J. J., North, K., Schroth, M. K., Sejersen, T., Shapiro, F., Bellini, J., Weiss, H., Guillet, M., Amburgey, K., Apkon, S., Bertini, E., Bonnemann, C., Clarke, N., Connolly, A. M., Estournet-Mathiaud, B., Fitzgerald, D., Florence, J. M., Gee, R., Gurgel-Giannetti, J., Glanzman, A. M., Hofmeister, B., Jungbluth, H., Koumbourlis, A. C., Laing, N. G., Main, M., Morrison, L. A., Munns, C., Rose, K., Schuler, P. M., Sewry, C., Storhaug, K., Vainzof, M. & Yuan, N. 2012. Consensus statement on standard of care for congenital myopathies. *J Child Neurol,* 27**,** 363-82.

Wang, H., Melton, D. W., Porter, L., Sarwar, Z. U., Mcmanus, L. M. & Shireman, P. K. 2014. Altered macrophage phenotype transition impairs skeletal muscle regeneration. *Am J Pathol,* 184**,** 1167-1184.

Wang, J. 2018. Neutrophils in tissue injury and repair. *Cell and Tissue Research,* 371**,** 531-539.

Wang, J. & Conboy, I. 2010. Embryonic vs. Adult Myogenesis: Challenging the 'Regeneration Recapitulates Development' Paradigm. *Journal of Molecular Cell Biology,* 2**,** 1-4.

Wang, K. & Williamson, C. L. 1980. Identification of an N2 line protein of striated muscle. *Proc Natl Acad Sci U S A,* 77**,** 3254-8.

Wang, K. & Wright, J. 1988. Architecture of the sarcomere matrix of skeletal muscle: immunoelectron microscopic evidence that suggests a set of parallel inextensible nebulin filaments anchored at the Z line. *J Cell Biol,* 107**,** 2199-212.

Wang, X., Blagden, C., Fan, J., Nowak, S. J., Taniuchi, I., Littman, D. R. & Burden, S. J. 2005a. Runx1 prevents wasting, myofibrillar disorganization, and autophagy of skeletal muscle. *Genes & development,* 19**,** 1715-1722.

Wang, X., Mader, M. M., Toth, J. E., Yu, X., Jin, N., Campbell, R. M., Smallwood, J. K., Christe, M. E., Chatterjee, A., Goodson, T., Jr., Vlahos, C. J., Matter, W. F. & Bloem, L. J. 2005b. Complete inhibition of anisomycin and UV radiation but not cytokine induced JNK and p38 activation by an aryl-substituted dihydropyrrolopyrazole quinoline and mixed lineage kinase 7 small interfering RNA. *J Biol Chem,* 280**,** 19298-305.

Wang, X., Sun, S., Cao, X. & Gao, J. 2020. Quantitative Phosphoproteomic Analysis Reveals the Regulatory Networks of Elovl6 on Lipid and Glucose Metabolism in Zebrafish. *Int J Mol Sci,* 21.

Wang, Y., Fu, Z., Li, X., Liang, Y., Pei, S., Hao, S., Zhu, Q., Yu, T., Pei, Y., Yuan, J., Ye, J., Fu, J., Xu, J., Hong, J., Yang, R., Hou, H., Huang, X., Peng, C., Zheng, M. & Xiao, Y. 2021. Cytoplasmic DNA sensing by KU complex in aged CD4+ T cell potentiates T cell activation and aging-related autoimmune inflammation. *Immunity,* 54**,** 632-647.e9.

Wang, Z., Grange, M., Pospich, S., Wagner, T., Kho, A. L., Gautel, M. & Raunser, S. 2022. Structures from intact myofibrils reveal mechanism of thin filament regulation through nebulin. *Science,* 375**,** eabn1934.

Weinberg, E. S., Allende, M. L., Kelly, C. S., Abdelhamid, A., Murakami, T., Andermann, P., Doerre, O. G., Grunwald, D. J. & Riggleman, B. 1996. Developmental regulation of zebrafish MyoD in wild-type, no tail and spadetail embryos. *Development,* 122**,** 271-80.

White, R. B., Biérinx, A.-S., Gnocchi, V. F. & Zammit, P. S. 2010. Dynamics of muscle fibre growth during postnatal mouse development. *BMC Developmental Biology,* 10**,** 21.

Widrick, J. J., Alexander, M. S., Sanchez, B., Gibbs, D. E., Kawahara, G., Beggs, A. H. & Kunkel, L. M. 2016. Muscle dysfunction in a zebrafish model of Duchenne muscular dystrophy. *Physiol Genomics,* 48**,** 850-860.

Williams, B. A. & Ordahl, C. P. 1994. Pax-3 expression in segmental mesoderm marks early stages in myogenic cell specification. *Development,* 120**,** 785-96.

Wilson, P. D. 2014. Anatomy of Muscle. *Reference Module in Biomedical Sciences.* Elsevier.

Witting, N., Werlauff, U., Duno, M. & Vissing, J. 2017. Phenotypes, genotypes, and prevalence of congenital myopathies older than 5 years in Denmark. *Neurol Genet,* 3**,** e140.

Wolff, C., Roy, S. & Ingham, P. W. 2003. Multiple muscle cell identities induced by distinct levels and timing of hedgehog activity in the zebrafish embryo. *Curr Biol,* 13**,** 1169-81.

Wong, J., Smith, L. B., Magun, E. A., Engstrom, T., Kelley-Howard, K., Jandhyala, D. M., Thorpe, C. M., Magun, B. E. & Wood, L. J. 2013. Small molecule kinase inhibitors block the ZAK-dependent inflammatory effects of doxorubicin. *Cancer Biol Ther,* 14**,** 56-63.

Wood, A. J., Lin, C. H., Li, M., Nishtala, K., Alaei, S., Rossello, F., Sonntag, C., Hersey, L., Miles, L. B., Krisp, C., Dudczig, S., Fulcher, A. J., Gibertini, S., Conroy, P. J., Siegel, A., Mora, M., Jusuf, P., Packer, N. H. & Currie, P. D. 2021. FKRP-dependent glycosylation of fibronectin regulates muscle pathology in muscular dystrophy. *Nature Communications,* 12**,** 2951.

Woods, I. G., Kelly, P. D., Chu, F., Ngo-Hazelett, P., Yan, Y. L., Huang, H., Postlethwait, J. H. & Talbot, W. S. 2000. A comparative map of the zebrafish genome. *Genome Res,* 10**,** 1903-14.

Wright, W. E., Sassoon, D. A. & Lin, V. K. 1989. Myogenin, a factor regulating myogenesis, has a domain homologous to MyoD. *Cell,* 56**,** 607-17.

Wu, C. C., Peterson, A., Zinshteyn, B., Regot, S. & Green, R. 2020. Ribosome Collisions Trigger General Stress Responses to Regulate Cell Fate. *Cell,* 182**,** 404-416.e14.

Wu, S., Ibarra, M. C. A., Malicdan, M. C. V., Murayama, K., Ichihara, Y., Kikuchi, H., Nonaka, I., Noguchi, S., Hayashi, Y. K. & Nishino, I. 2006. Central core disease is due to RYR1 mutations in more than 90% of patients. *Brain,* 129**,** 1470-1480.

Xie, S.-J., Li, J.-H., Chen, H.-F., Tan, Y.-Y., Liu, S.-R., Zhang, Y., Xu, H., Yang, J.-H., Liu, S., Zheng, L.-L., Huang, M.-B., Guo, Y.-H., Zhang, Q., Zhou, H. & Qu, L.-H. 2018. Inhibition of the JNK/MAPK signaling pathway by myogenesis-associated miRNAs is required for skeletal muscle development. *Cell Death & Differentiation,* 25**,** 1581-1597.

Xu, W., Roos, A., Schlagwein, N., Woltman, A. M., Daha, M. R. & Van Kooten, C. 2006. IL-10-producing macrophages preferentially clear early apoptotic cells. *Blood,* 107**,** 4930-7.

Yablonka-Reuveni, Z., Rudnicki, M. A., Rivera, A. J., Primig, M., Anderson, J. E. & Natanson, P. 1999. The Transition from Proliferation to Differentiation Is Delayed in Satellite Cells from Mice Lacking MyoD. *Developmental Biology,* 210**,** 440-455.

Yadavalli, V. K., Forbes, J. G. & Wang, K. 2009. Nanomechanics of full-length nebulin: an elastic strain gauge in the skeletal muscle sarcomere. *Langmuir,* 25**,** 7496-505.

Yogev, Y., Perez, Y., Noyman, I., Madegem, A. A., Flusser, H., Shorer, Z., Cohen, E., Kachko, L., Michaelovsky, A., Birk, R., Koifman, A., Drabkin, M., Wormser, O., Halperin, D., Kadir, R. & Birk, O. S. 2017. Progressive hereditary spastic paraplegia caused by a homozygous KY mutation. *European Journal of Human Genetics,* 25**,** 966-972.

Yoon, M.-S. 2017. mTOR as a Key Regulator in Maintaining Skeletal Muscle Mass. *Frontiers in Physiology,* 8.

Yoshimura, T. & Takahashi, M. 2007. IFN-gamma-mediated survival enables human neutrophils to produce MCP-1/CCL2 in response to activation by TLR ligands. *J Immunol,* 179**,** 1942-9.

Young, P., Ehler, E. & Gautel, M. 2001. Obscurin, a giant sarcomeric Rho guanine nucleotide exchange factor protein involved in sarcomere assembly. *J Cell Biol,* 154**,** 123-36.

Yu, M., Zhu, Y., Lu, Y., Lv, H., Zhang, W., Yuan, Y. & Wang, Z. 2020. Clinical features and genotypes of Laing distal myopathy in a group of Chinese patients, with in-frame deletions of MYH7 as common mutations. *Orphanet Journal of Rare Diseases,* 15**,** 344.

Yucel, N., Chang, A. C., Day, J. W., Rosenthal, N. & Blau, H. M. 2018. Humanizing the mdx mouse model of DMD: the long and the short of it. *npj Regenerative Medicine,* 3**,** 4.

Yüceyar, N., Ayhan, Ö., Karasoy, H. & Tolun, A. 2015. Homozygous MYH7 R1820W mutation results in recessive myosin storage myopathy: Scapuloperoneal and respiratory weakness with dilated cardiomyopathy. *Neuromuscular Disorders,* 25**,** 340-344.

Yuen, M. & Ottenheijm, C. a. C. 2020. Nebulin: big protein with big responsibilities. *J Muscle Res Cell Motil,* 41**,** 103-124.

Zang, L., Torraca, V., Shimada, Y. & Nishimura, N. 2022. Editorial: Zebrafish Models for Human Disease Studies. *Frontiers in Cell and Developmental Biology,* 10.

Zayia, L. C. & Tadi, P. 2022. Neuroanatomy, Motor Neuron. *StatPearls.* Treasure Island (FL): StatPearls Publishing

.

Zhang, Q., Vashisht, A. A., O'rourke, J., Corbel, S. Y., Moran, R., Romero, A., Miraglia, L., Zhang, J., Durrant, E., Schmedt, C., Sampath, S. C. & Sampath, S. C. 2017. The microprotein Minion controls cell fusion and muscle formation. *Nat Commun,* 8**,** 15664.

Zhou, H., Jungbluth, H., Sewry, C. A., Feng, L., Bertini, E., Bushby, K., Straub, V., Roper, H., Rose, M. R., Brockington, M., Kinali, M., Manzur, A., Robb, S., Appleton, R., Messina, S., D'amico, A., Quinlivan, R., Swash, M., Müller, C. R., Brown, S., Treves, S. & Muntoni, F. 2007. Molecular mechanisms and phenotypic variation in RYR1-related congenital myopathies. *Brain,* 130**,** 2024-2036.

Zhou, H., Liu, B., Weeks, D. P., Spalding, M. H. & Yang, B. 2014. Large chromosomal deletions and heritable small genetic changes induced by CRISPR/Cas9 in rice. *Nucleic acids research,* 42**,** 10903-10914.

Zhu, X., Xu, Y., Yu, S., Lu, L., Ding, M., Cheng, J., Song, G., Gao, X., Yao, L., Fan, D., Meng, S., Zhang, X., Hu, S. & Tian, Y. 2014. An Efficient Genotyping Method for Genome-modified Animals and Human Cells Generated with CRISPR/Cas9 System. *Scientific Reports,* 4**,** 6420.

Zhu, X., Yeadon, J. E. & Burden, S. J. 1994. AML1 is expressed in skeletal muscle and is regulated by innervation. *Mol Cell Biol,* 14**,** 8051-7.

Ziemkiewicz, N., Hilliard, G., Pullen, N. A. & Garg, K. 2021. The Role of Innate and Adaptive Immune Cells in Skeletal Muscle Regeneration. *Int J Mol Sci,* 22.

Zou, J., Tran, D., Baalbaki, M., Tang, L. F., Poon, A., Pelonero, A., Titus, E. W., Yuan, C., Shi, C., Patchava, S., Halper, E., Garg, J., Movsesyan, I., Yin, C., Wu, R., Wilsbacher, L. D., Liu, J., Hager, R. L., Coughlin, S. R., Jinek, M., Pullinger, C. R., Kane, J. P., Hart, D. O., Kwok, P. Y. & Deo, R. C. 2015. An internal promoter underlies the difference in disease severity between N- and C-terminal truncation mutations of Titin in zebrafish. *Elife,* 4**,** e09406.